Trabajo Fin de Máster
Máster en Ingeniería Industrial

Computational Fluid Dynamics modelling and simulation of a fuel cell: Influence of the Gas Diffusion Layer design on the water management and cell performance

Autor: Laura González Morán

Tutor: José Alfredo Iranzo Paricio

Dpto. de Ingeniería Energética
Escuela Técnica Superior de Ingeniería
Universidad de Sevilla

Sevilla, 2021

Proyecto Fin de Máster
Máster en Ingeniería Industrial

Computational Fluid Dynamics modelling and simulation of a fuel cell: Influence of the Gas Diffusion Layer design on the water management and cell performance

Autor:

Laura González Morán

Tutores:

José Alfredo Iranzo Paricio

Dpto. de Ingeniería Energética

Escuela Técnica Superior de Ingeniería

Universidad de Sevilla

Sevilla, 2021

Trabajo Fin de Máster: Computational Fluid Dynamics modelling and simulation of a fuel cell: Influence of the Gas Diffusion Layer design on the water management and cell performance

Autor: Laura González Morán
Tutor: José Alfredo Iranzo Paricio

El tribunal nombrado para juzgar el Proyecto arriba indicado, compuesto por los siguientes miembros:

Presidente:

Vocales:

Secretario:

Acuerdan otorgarle la calificación de:

Sevilla, 2021

El Secretario del Tribunal

Acknowledgements

The theoretical introduction was obtained from the course “Electrochemical energy conversion and storage”, imparted by Andrea Casalegno in Politecnico di Milano. The pandemic has impeded more lively exchanges and collaborations, but I have to thank that my tutor has made possible different exchanges in this strange new normality. A special thanks to my family and everyone that had kept me sane doing this work during these confinements and semiconfinement madness.

Resumen

El objetivo principal de este trabajo ha sido estudiar la influencia que tienen distintos parámetros de la capa de difusión de gases (GDL) en la rendimiento y operación de una pila de combustible de membrana de intercambio protónico (PEMFC). Para ellos se han desarrollado una serie de simulaciones CFD con el modelo ANSYS-Fluent PEMFC, comparando GDLs comerciales con diferentes propiedades, observando su influencia en el desempeño final. Se ha estudiado el efecto de la presencia de la capa microporosa (MPL), simulando las GDL con y sin ella. Todas las GDLs estudiadas se encuentran en el mismo rango de grosor 285±30μm, siendo este uno de los criterios para su elección. Se han considerado cuatro GDLs comerciales (AvCarb P-75, SIGRACET 34BC, SIGRACET 34BA y TORAY TGP-H-090), donde los dos primeros incluyen MPL, creando un total de 6 casos. Se ha hecho también un estudio de los datos base que aportaba ANSYS con y sin MPL para comprobar que todo funcionara adecuadamente, añadiendo dos casos más. Las simulaciones se llevaron a cabo variando los voltajes entre 1.05 y 0.35V para tener una serie de ocho puntos IV representativos para crear la curva de polarización.

El análisis de los resultados se basó en cuatro tipos diferentes de curvas. El primer tipo se obtuvo directamente de los datos proporcionados por la simulación, creando las curvas de polarización (voltaje vs. densidad de corriente), potencia y eficiencia eléctrica; todas ellas contra la densidad de corriente para todos los casos. La siguiente serie de curvas se obtuvo para todas las GDLs comerciales, midiendo para cada voltaje el contenido el agua, saturación del líquida, fracción másica de oxígeno, temperaturas máximas y medias en el volumen de ciertos componentes de la célula, como son la membrana, GDL, MPL y capa catalítica. Fueron agrupadas en propiedades afines para simplificar la representación. Otra serie de curvas fue creada estudiando la evolución de diferentes variables a lo largo de la coordenada axial de la PEMFC, dibujando dichas líneas en 12 puntos estratégicos, obteniendo la evolución longitudinal de la temperatura, fracción másica de oxígeno, saturación líquida y contenido de agua a lo largo de la célula. Esto fue estudiado para los casos de las GDLs con MPL y sus variaciones sin ésta, para voltaje bajo (0.45V) y medio (0.65V). Finalmente, se crearon una serie de mapas de contorno, creado en plano medio (en la dirección a través del plano) in la PEMFC, representando las distribuciones de temperatura, contenido de agua y el flujo de corriente a través del plano.

Se puede concluir que altas conductividades eléctricas y térmicas llevan a un mejor comportamiento de la célula. La MPL contiene permeabilidades más bajas, resultando en una peor actuación, pero su ausencia lleva a problemas de hidratación y degradación.

Abstract

The main objective of this work is to study the influence of different parameters of the Gas Diffusion Layer (GDL) on the performance and operation of a Proton-Exchange Polymer Electrolyte Fuel Cell (PEMFC). In order to do so, several CFD simulations have been carried out with the ANSYS-Fluent PEMFC model, comparing real commercial GDLs with different properties, and observing their influence on their performance. The effect of the presence of the Microporous Layer (MPL) has been studied by simulating the same GDL with and without the MPL. All the GDLs studied had approximately the same thickness range of 285± 30μm. Four commercial GDLs have been singled out (AvCarb P-75, SIGRACET 34BC, SIGRACET 34BA and Toray TGP-H-090), two of them including MPL, with a total of 6 cases. The simulations were carried out varying the voltage between 1.05 and 0.35V to a have a set of eight representative IV points to obtain the polarization curve.

The analysis of the results was carried out based on four different kind of curves. The first set of curves was obtained directly from the simulation data, obtaining the polarization curves (voltage vs. current density), power and electrical efficiency; all against the current density for all the 6 cases. Secondly, the next set of curves was obtained for all the commercial GDLs, measuring for each voltage the water content, liquid saturation, O2 mass fraction, average and maximum temperatures in the volume of certain cell components (membrane, catalyst layer, GDL, MPL). They were grouped in sets of similar properties to simplify them. For an additional set of results, the evolution of different variables along the axial coordinate of the PEMFC was drawn in 12 strategic locations, obtaining the longitudinal evolution of temperature, O2 mass fraction, liquid saturation and water content along the cell. This was studied for the cases of the GDLs with and without MPL, and for low voltage (0.45V) and medium voltage (0.65V). Finally, contour plots were created at the membrane mid-plane (through-plane direction) on the PEMFC representing the distributions of temperature, water content and through-plane current flux.

It can be concluded that higher electrical conductivity and higher permeability lead to a better cell performance. The MPL features a lower permeability, and therefore results in a worse performance, but the lack of it may create cell hydration and degradation issues.

Index

TABLE INDEX

FIGURE INDEX

Notation

δ_m	Membrane thickness [m]
σ_{mem}	Membrane electrical conductivity [S/m]
σ_{sol}	Solid electrical conductivity[S/m]
R_{el}	Electrolyte resistance [Ω*m^2]
a_{O2}	Oxygen activity [-]
$a_{O2,ch}$	Oxygen activity in the channel [-]
τ	Tortuosity [-]
ε	Porosity [-]
C_{nom}	Nominal capacity [Ah]
N_{cycles}	Number of cycles [-]
t_{cycles}	Hours in which the electrolyser is operating [h]
P_{nom}	Nominal power [W]
$\eta_{round\text{-}trip}$	Round-trip efficiency [-]
R	Ideal gases constant, 8.314 $\frac{J}{mol*K}$
T	Temperature [K]
Ƒ	Faraday's constant: 96485.3329 s A / mol
β	Coefficient dependent on α the transfer coefficient; if it is an oxidation, $\alpha=\beta_o$; but if it is a reduction, $(1-\alpha)=\beta_r$
E^-	Anode potential [V]
j	Current density [A/m^2]
ΔV/V	Voltage [V]
K_r	Kinetic coefficient [-]
i*	Exchange current density [A/m^2 of Pt]
$E^+ + \eta^+$	Cathode potential [V]
η_{el}	Membrane Ohmic losses [V]
j_{lim}	Limiting current [A/m^2]
ρ	Electrical resistance [Ω*m]

Q	Volumetric flow [m^3/s]
A	Area [m^2]
k	Absolute permeability [m^2]
Δp	Pressure [Pa]
μ	Viscosity [Pa*s]
Δx	Longitude or thickness [m]
v	Velocity [m/s]
σ_{sup}	Superficial tension in the gas-liquid interphase [N/m]
θ_c	Hydrophobic angle [º]
φ	Electric potential [V]
R_{mem}	Membrane volumetric transfer current [A/m^3] (when there is a subindex it is the volumetric transfer current and not the ideal gases constant)
$\zeta_{an/cat}$	Anode/cathode specific active surface area [1/m]
$\eta_{an/cat}$	Anode/cathode surface overpotential [V]
$\gamma_{an/cat}$	Anode/cathode concentration dependence [-]
$\alpha_{an/cat}$	Anode/cathode transfer coefficients [-]
$[A]$, $[A]_{ref}$	Anode local molar species concentration and reference value of the species upon which the reaction rate depends: H_2 [$kmol/m^3$]
$[C]$, $[C]_{ref}$	Cathode local molar species concentration and reference value of the species upon which the reaction rate depends: O_2 [$kmol/m^3$]
$j_{an/cat}(T)$	Reference exchange current density dependent on the local temperature
T_{ref}	Anode/cathode user-specified reference temperature [K]
$E_{an/cat}$	Anode/cathode user-specified activation energy [J/kmol]
j_{ref}	Anode/cathode reference exchange current density at a specified reference temperature [K]
μ_l	Liquid dynamic viscosity [Pa*s]
ρ_l	Liquid water density [kg/m^3]
K	Absolute permeability [m^2]
K_r	Relative permeability [m^2]
s	Water saturation [-]
S_{gl}	Rate of mass change between gas and liquid phases
S_{ld}	Rate of mass change between liquid and dissolved phases
p_l	Liquid pressure [Pa]
EW	Equivalent weight of the membrane [g]
$M_{w,H2O}$	Molecular mass of water [g/mol]
λ	Water content [-]
$\lambda_{s=1}$	User-defined water content at a water saturation of 100%
γ_e	Evaporation rate coefficient [-]
γ_c	Condensation rate coefficient [-]
p_{wv}	Water vapour partial pressure [Pa]
p_{sat}	Saturation pressure [Pa]
D_{gl}	Gas-liquid diffusion coefficient [-]
R_j'	Corrected volumetric transfer current of layer j [A/m^3]
γ_j	User-specified reduction coefficient [-]
D_{liq}	Liquid water diffusion coefficient in the gas channel
$\overrightarrow{v_l}$	Liquid velocity [m/s]
$\vec{v}_g$	Gas velocity [m/s]

χ	Liquid to gas velocity ratio [-]
A_{mem}	Membrane active area [$0.0001m^2=1cm^2$]
P	Power [W]
$\dot{m}_{H_2}$	Fuel (hydrogen) mass flow [kg/s]
LHV_{H2}	Fuel (hydrogen) low heating value [J/kg]

1 SCOPE AND OBJECTIVES

The main objective of this work is to study the influence of different parameters on the performance and operation of Proton-Exchange Polymer Electrolyte Membrane Fuel Cell (PEMFC). In order to do so, several CFD (Computational Fluid Dynamics) simulations will be carried out. First, the ANSYS-Fluent model will be simulated with and without microporous layer (MPL), to have an initial basis and check that the model and CFD solver is working smoothly, and later real commercial Gas Diffusion Layers (GDLs) will be simulated. The effect that the GDL and MPL have will be studied having different commercial GDLs with different properties, analysing the influence of those variables on the performance. It is not very common that the companies provide full information of their products, so the selected ones are the ones that provided the relevant information and where on the range of 285± 30μm. Four commercial GDLs have been singled out (AvCarb P-75, SIGRACET 34BC, SIGRACET 34BA and Toray TGP-H-090), two of them including MPL. The cases where there was also an MPL, have been also simulated in a modified version without them, to isolate their effect. A total of eight different GDLs have been analysed.

As an additional study a patterned wettability simulation will be done, in order to obtain a beneficial effect modifying the GDL properties from under- rib to under- channel by changing the mesh. This is a novel study that in CFD modelling has not been done yet, providing something additional to the bulk of the work since modelling the effect of the properties has been done repeatedly. [1] [2] [3] [4] [5] [6]

The outline of this project and what will be developed in the following chapters will be:

- Chapter 1 Scope and objectives: the current chapter where the main objectives, the scope of the project and the composition of the Master thesis are described.
- Chapter 2 Theoretical introduction: The description of the PEMFC, its principles and components are explained. The problematics they face, and their applications will be briefly discussed. The influence of the different components on the polarization curve will be described to have a background when analysing them on Chapter 5.
- Chapter 3 Methodology: The process followed to select the GDLs, the methodology to calculate the properties and the methodology to develop the simulations, while detailing the troubles encountered.
- Chapter 4 CFD PEMFC model description: The different equations and variables the Computational Fluid Dynamics model considers will be described.

- Chapter 5 Simulations: The polarization curves obtained from the different simulations will be explained and stated.
- Chapter 6 Analysis of the results: An in-depth analysis of the results will be carried. Not only polarization curves but also a power vs. current density and an electrical efficiency vs. current density curves will be obtained and discussed. The effect of the GDL properties on different variables relevant for the operation and final performance of the cell, such as water content, water saturation, temperature, or oxygen concentration, will be analysed. The spatial distributions of such variables will be also represented and discussed.
- Chapter 7 Conclusions: The main conclusion obtained after the analysis of the results and their postprocessing will be outlined.

Summarizing, the main objectives of this work, considering the above, are:

- Technological review of fuel cells and the influence of the components and operation conditions. It must include the fundamental concepts, components, principles and operation.
- Review on CFD fuel cell modelling.
- Introduction to the simulation tool ANSYS-Fluent and its fuel cell module.
- Development of the CFD modelling and execution of the simulations for a single cell for different components and operation conditions.
- Analysis of the results of the simulations, indicating the observations made and discussing the results obtained.
- Preparation and redaction of the Master thesis.

2 THEORETICAL INTRODUCTION

The main concepts concerning a PEMFC will be explained, introducing its different components, the operating principles, issues and applications. The influence of the different parameters will be stated in order to understand its changes on the polarization curve and briefly discuss its different components.

2.1. PEMFC

The proton-exchange/polymer electrolyte membrane fuel cell (PEMFC) directly converts the fuel into electric energy, not going through heat (a typical thermodynamic cycle) direct cycle. It is composed by an anode and a cathode, being fed the fuel (H_2) and an oxidant (air) respectively. Hydrogen arrives to the anode catalyst that will allow a hydrogen oxidation reaction: [7]

$$H_2 \rightarrow 2H^+ + 2e^- \quad \text{Anode (2-1)}$$

H^+ can move to the electrolyte, while the electrons cannot pass, moving outside of the system. The load will consume the electrical power that is generated. The electron flow is the direct electrical current. On the cathode we have oxygen (present in air). Having on its catalyst oxygen, H+ and electrons producing water, having an oxygen reduction reaction:

$$2H^+ + \frac{1}{2}O_2 + 2e^- \rightarrow H_2O \quad \text{Cathode (2-2)}$$

Obtaining an overall reaction of oxidation of hydrogen [8]:

$$H_2 + \frac{1}{2}O_2 \rightarrow H_2O \quad \text{Overall (2-3)}$$

On the Figure 2-1 it can be seen the different phenomena that occur in a PEMFC, clearly noting the entrance and exit of the fuel and oxidant.

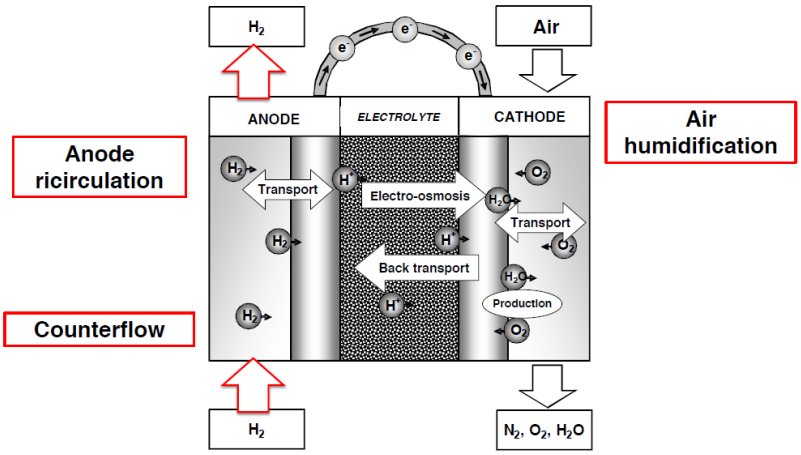

Figure 2-1 Diagram of a PEMFC functioning. **Source:** [9]**,** [8]

If the reaction went in the opposite direction it would be an electrolyser, not a fuel cell. The aim of electrolysis is to produce hydrogen and oxygen, splitting water into H_2 and O_2. It is a process similar to charging a battery and that is why it is used for storage. [10] [11]

The power of the system depends on the size of the fuel cell. It is independent from the energy, that depends on the tank of hydrogen. It is an advantage because power and energy can be decoupled and Li-ion batteries cannot. The reaction can occur at relatively low temperatures, between the ambient temperature and 100ºC.

Some of the more important features of this technology are it is needs pure hydrogen (CO<10p.p.m.) because at low temperatures it is susceptible of poisoning. It has very high-power density, higher than 3kW/dm^3. This technology works at low temperatures, giving fast dynamics and start-up. Water needs to be carefully managed to avoid drying and flooding, where the formation of liquid water blocks the GDL or the catalyst layer (CL). [7] [12] This technology has secure access to raw materials (Pt) and can be completely manufactured in Europe, in contrast with Li-ion batteries which materials and technology are Asiatic. [13] The main issues of this technology are its cost and durability, affected by degradation. [8]

2.2. Components

This technology is characterized by its membrane, which is a very thin solid electrolyte to permit the transfer of protons, being the active layer and where the electrochemical reaction occurs. The actual working temperature is around 40-90ºC, because of the membrane it cannot be higher. These temperatures require a very effective catalyst such as platinum or platinum alloys on both sides. On top of the CL there is a diffusion layer which is necessary to have a uniform distribution of the reactant on the CL. Then there are some gaskets to prevent leakages. After them, there are the flowfields, that are where the channels to feed the reactants are cut. Finally, they are sandwiched in a symmetrical way as seen on Figure 2-2:

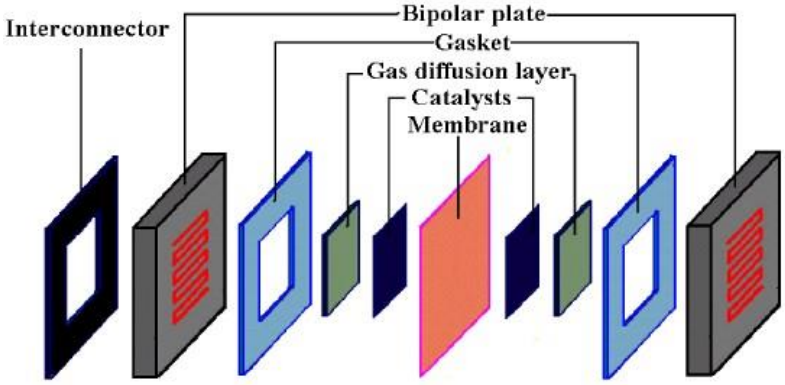

Figure 2-2 Exploded view of PEMFC components. **Source:** [14]

2.2.1 Catalyst layer

It is the core of the technology, where the reaction occurs. Typically its thickness is about 10-15μm. It has a high surface of platinum (ECSA) compared to the real surface of the fuel cell, having improved kinetics because there is more active area, improving the reactions. It is a compact system. Platinum is very expensive, so there is a need to achieve a high ECSA with a low load, done by maximizing the surface and minimizing the volume and mass of the particles. It is done with small diameters, but there is an optimum of 2-5nm because smaller ones will incur in degradation phenomena. The only effective platinum nanoparticles are the ones connected with carbon, ionomer and membrane at the same time. This means there is a need to optimize platinum utilization, which tells us how much of what is introduced is really in a condition in which it can operate. The larger the diameter, the higher the utilization.

This layer has a good proton (H^+) and electron conductivity, which depends on the carbon and ionomer in the distribution. It needs to have a sufficiently controlled pore size, of at least 10nm in order to have a good gas transport, so H_2 and O_2 can flow freely. The CL needs to have a certain durability because it will have to survive driving cycles with cycling operations and an acidic condition. [8] [12]

2.1.2. Membrane

It has a polymeric structure backbone, similar to Teflon, based on fluorine, modified introducing some SO_3H groups. H^+ movement is promoted by water, whereas its absence makes it and SO_3 attached to the backbone. It is very thin, typically 20-25μm because the electrolyte losses are proportional to its thickness, being paramount its reduction:

$$R_{el} = \frac{\downarrow \delta_m}{\uparrow \sigma_m} \quad (2\text{-}4)$$

It has a low gas permeability because we need to ensure minimal gas crossover (no mixture of hydrogen and oxygen). Some hydrogen can go through the membrane, producing crossovers, so at the cathode side there is H2 and O2 at the catalyst, having at the same time HOR and ORR. There is an internal current while hydrogen is oxidized, dissipated as heat. This small current is due to ORR crossovers, which affects the polarization curve by creating an overpotential η^+, mainly near the open circuit voltage (~0.15V loss at OCV), whereas at high currents it is negligible.

It needs good mechanical and chemical stability in order to mitigate and avoid any degradation of the membrane. It has a high proton conductivity, which depends on the water content of the membrane, so it is important to keep it hydrated, and then it will give a limitation in the maximum temperature. It needs to have a minimal electron conductivity to have minimal short circuits because a null one cannot be achieved. Even if there is no crossover, there will be a small shortcircuit current due to electrons passing, giving the same effect as the former.

The membrane can be also referred as Membrane Electrode Assembly (MEA), which not only includes the membrane, but also the CL and the GDL (and MPL if there is one). [8] [12]

2.1.3. Gas diffusion layer

It has a high electronic conductivity since it is carbon based. It has large pores in order to give a high gas transport assistance to the H_2 and O_2 flows. As the rest of the components, it needs to have mechanical and chemical stability.

At the cathode side, water is being produced. The temperature is below 100ºC and pressure is 1-3atm, propitiating the formation of water droplets, which hinder diffusion, blocking the passage of O_2. For this reason, the GDL needs a high hydrophobicity for the purpose of avoiding pore obstruction caused by liquid water.

The GDL is made by carbon fibers, often covered by PTFE (Polytetrafluoroethylene), a very hydrophobic and stable element. The diffusion layer is often composed by the GDL and the MPL, which is a layer added the GDL and the CL. This layer is even more hydrophobic that the GDL, because it has higher amounts of PTFE. The liquid water would move outside and go to the channel. [8] [12] [15]

The microporous layer has not been considered as a separate component because not all commercial GDLs possess them. There is quite a debate on whether the MPL is useful or not because it is more hydrophobic, nonetheless it has a lower permeability and porosity, hindering the water transport, but also the gas transport. [3] It has a beneficial effect when working at high RH, as stated on [2].

2.1.4. Flowfield

On the flowfield the thermofluidodynamics have a more prominent weight because the geometry needs to be optimized in order to have a controlled transport of reactants and remove water. The geometry will determine an advection effect through the diffusion layer because it searches a uniform distribution, keeping a low pressure drop and favouring water removal. This is the reason why it also needs good electron conductivity and chemical stability. Coated metal sheets are commonly used because they can be very thin (<0.3mm) and hence cheaper, but they have corrosion issues. Graphite composites are very expensive, thicker (~0.8mm) and more fragile but they are more stable. The stacks are fed in parallel, trying to keep a uniform temperature. The flowfields need to be counterflow because of water flooding issues detailed on 2.3.2.Water management [8] [12] [16]

2.3. Operating principles

The operation and some of its issues will be explained with more detail, focusing on the triple phase boundary and the water management.

2.3.1. Triple phase boundary

On the triple phase boundary a reaction is occurring, going towards the membrane H^+ and electrons on the other direction, which need an electrical contact so they can flow. This means the CL must therefore be electrically conductive, same as the GDL and flowfield. There needs to be something to separate the CL from the current collector to have diffusion. The thicker that layer, the simpler will diffusion be, being the reason the GDL is needed.

The catalysts are very small nanoparticles, within a carbon support which is electrically conductive. There needs to be a material that allows electrons to flow and other that also permits H^+ flow, which must be before the membrane where the protons move freely. [8] [12] An ionomer is introduced, which is "a polymer composed of macromolecules in which a significant but small proportion of the constitutional units have ionizable or ionic groups or both." [17] It creates a contact between the catalyst and the membrane itself.

The triple phase boundary is created by a catalyst that is supported, permitting electron transport, a polymer electrolyte to have a pathway for the protons and some void with a porosity to permit reactant flow or hydrogen in the active side of the nanoparticles to reach the catalyst layer. It is shown a detailed sight on Figure 2-3 and the process is the following, where $2H^+$ corresponds to the ionomer and $2e^-$ to the carbon:

$$H_2 \rightarrow 2H^+ + 2e^- \quad (2\text{-}5)$$

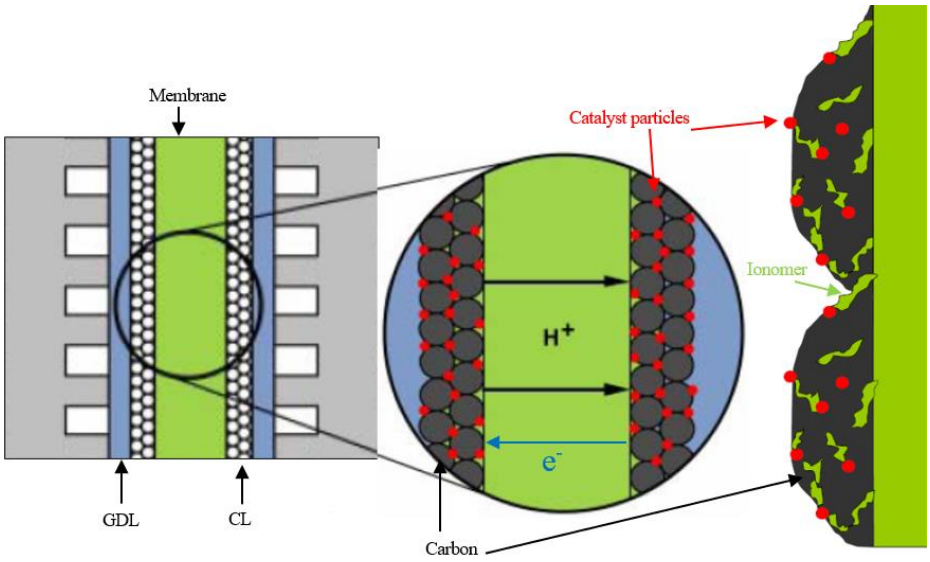

Figure 2-3 Triple phase boundary detailed. **Source:** [8]

The decrease on platinum content is of orders of magnitudes but still dealing with microtechnologies. [8] [12]

2.3.2. Water management

There is a channel where air is flowing and oxygen is consumed along, starting with high concentration and therefore high O_2 activity on the air inlet. Then there is a diffusion and a gradient of the activity because the reaction is occurring in the catalyst. This decrease makes that at the end of the channel a_{O2} is very low, leading to a high overpotential. The low O_2 content might be due to the oxygen consumption or the water production, which dilutes the O_2 and reduces its concentration. To solve this issue, it is fed an air flow, that is twice the needed amount (stoichiometry ~2) to mitigate the overpotential produced by low concentrations.

Ideally there would be a high-water content on the membrane and avoid liquid water on the CL. Along the cathode water is being produced, having an electro-osmosis, so when water moves it drags H^+. There is also back transport, where water is able to diffuse back because there is a higher water content on the cathode side. In addition, there is also water transport from the diffusion layers to the membrane. To avoid liquid water in the GDL, while still having the membrane hydrated air humidification and anode recirculation plus a counterflow scheme configuration are introduced. On the cathode air with a 30-50% RH is introduced, exiting with a ~100% RH because there is production and electro-osmosis. On the anode the opposite happens, H_2 is fed with a 30-50% RH, exiting with high humidity. Water is transported in that direction because it goes where it is less hydrated. H2 is consumed and water will remain there and be transported to the other side.

There is an internal circulation of water that is controlling the air humidification and H_2 recirculation, controlling the humidity of the whole system. For these reasons, the flowfields must be counterflow. All these mechanisms can be seen in Figure 2-1. [8] [12] [9]

2.4. Issues

The main PEMFC issues are performance, degradation and cost. Today efficiency is limited by cost. [8] [18] [12] [19]

2.4.1. Degradation

Electrochemical devices have a progressive degradation of the components; a decay, deterioration of the materials, gradually decreasing the performance. The unexpected degradation is bigger than the expected one. Once the origin is known, it can be counteracted. Several effects are combined, and it is the cause of most of the issues. Degradation depends on the cycle you are performing. [18] [12]

2.4.2. Platinum dissolution

Platinum can go from its metal form to, dissolving into ions and producing electrons.

$$Pt \rightarrow Pt^2 + 2e^- \quad (2\text{-}6)$$

The ionomer permits the transport of Pt ions and the carbon support does the same for the electrons. A reaction that consumes these ions and electrons is needed, which is favoured by this acidic environment. Oxidation is enhanced by high potential, leading to high overpotential, which happens in the cathode side. Two different mechanisms can occur.

- **Pt band formation or Pt loading loss**: There is a platinum dissolution, having partially disappeared, having Pt^{2+} ions flowing that will arrive to the membrane, reacting with H_2 that appeared due to crossover.

  $$Pt^2 + H_2 \rightarrow Pt + 2H^+ \quad (2\text{-}7)$$

  There will be deposition of platinum inside the membrane, close to the cathode side, losing Pt loading. There is a Pt band, a range where Pt is deposited, which is not active anymore because though it is in contact with the ionomer it is not in contact with the carbon structure, reducing the ECSA. H+ will cross from the membrane to the cathode CL (CCL) to react with the electrons and probable with O2, occurring the ORR. [20] [18] [12]

- **Ostwald's ripening or redeposition/size growth:** The backwards reaction of equation (2-6) above takes place, creating bigger nanoparticles.

  $$Pt^2 + 2e^- \rightarrow Pt \quad (2\text{-}8)$$

  A small nanoparticle is less stable than a larger one because on the later there can be dissolution and on the other one redeposition. Platinum ions will move from the smaller to the bigger nanoparticles and electrons will do the same in the opposite direction. The radius will impact on the thermodynamic equilibrium. This phenomenon is called Ostwald's ripening and it determines the growth of the size.

  Nanoparticles smaller than a certain radius will tend to become smaller and the ones bigger than that radius will become even larger. Assuming the volume is fixed, the ratio surface volume will decrease because the radius is increasing, therefore reducing the ECSA.

  The Pt band effect will be close to the interface and at the same time Ostwald's ripening will be happening, both contributing to reduce the ECSA. This is enhanced by cycling from low to high potential. [20] [18] [12]

2.4.3. Effect of cathode ECSA loss

It mainly affects the polarization curve, shifting it vertically, which means voltage is lost. This effect is mainly produced by degradation. [18] [12]

2.4.4. GDL/MPL decay

There are changes on the structure given by mechanical stress. Warming and cooling the system during shutdown and start-up will have an effect on the humidity, increasing the size of the membrane which introduces mechanical stress in the structure, inducing fatigue.

There can also be a change in the hydrophobicity, a reduction of the properties of the GDL and MPL, that can be caused by erosion. There is gas and water flowing, which might detach the PTFE that is present in the MPL or GDL. There can also be a chemical attack due to a formation of radicals that can corrode carbon and detach PTFE from the surface of carbon. Once this happens, the flooding effect can be more severe. [18] [12]

2.4.5. GDL/MPL diffusivity decrease

At high current density there is a high-water production therefore it is expected a decrease in diffusivity because some of the pores are flooded. There is a decrease on the maximum current density it reaches or j_{lim} on the aged ones where the oxygen transport is more relevant, at high current density. The impedance increases at low frequency for high current density. [18] [12]

2.4.6. Membrane decay

From the mechanical point of view, wet and dry cycles can induce fatigue stress, that generally determine a thinning phenomenon of the membrane, increasing the crossover. Crossover is the transport phenomena that allows the chemical attack. H_2 and O_2 will arrive at the cathode side, producing free radicals. This happens also during operation. It gives a chain break of the membrane polymer, having a conductivity loss and a further increase on the crossover. The chemical and mechanical degradation interact, whereas individually the effect is not very dangerous, generally the happen simultaneously. [18] [12]

2.4.7. Membrane resistance increase

It can be introduced as an increase on the membrane loss, as seen on Equation (2-4) above, which is linear. It is smaller but still present at low current density and increases gradually with current. There is a decrease in the OCV that is related to an increase on the crossover. There is an increase on the membrane conductivity, so the ionomer is deteriorated. The impedance translates at every current. [18] [12]

2.4.8. CL Proton conductivity decrease

The ionomer on the catalyst layer is supposed to follow the same mechanism as seen on the membrane, so there might be a decrease of the proton conductivity on the CL. There is a change on the distribution of the reaction rate because ion transport is hindered below proton conductivity, squeezing the reaction in a smaller domain, moving the active domain closer to the membrane. This effect is more evident at high current density. [18] [12]

2.4.9. Carbon corrosion

It is a corrosion mechanism of the carbon support of the CL, which can react with water present in the system at the cathode side, mainly giving O_2, protons and electrons.

$$C + 2H_2O \rightarrow CO_2 + 4H^+ + 4e^- \quad (2\text{-}9)$$

The carbon support is being oxidized, which generally occurs when there is a H_2/O_2 front that happens during startup and shutdown of the fuel cell, where O_2 enters during the inactive period. After 1500 startups, a decrease on the cathode thickness will be observed, while the anode side will not have any change. This is because there is a corrosion of carbon and the structure will collapse as it has become more fragile, applying a compression on the fuel cell. The collapse will determine a decrease on the diffusivity of the CL. The morphology structure will change in terms of porosity and the diffusivity will be hindered. Some Pt nanoparticles will detach from the structure, not being anymore in contact with the carbon, additionally losing some ECSA.

The HOR and ORR can happen simultaneously on the anode side. Carbon corrosion can occur when there is a very high potential (higher than 1V). At the beginning the system is shutdown, having O_2 in both sides. Then is started-up, feeding H_2 inside. It is identified a front between the domain of the anode channel in which there is hydrogen and the domain of the cathode side in which there is oxygen. There is a similar situation at the shutdown, where there is H_2 in the anode and O_2 in the cathode, introducing air on the anode side. During standard operation there is no carbon corrosion, but at shutdown on the cathode ΔV=1-1.5V can be reached. A counter measure will be avoiding the H_2/O_2 fronts on the anode side, or to have a very fast start-up, decreasing the time and therefore the damage. [18] [12] [21]

2.4.10. CL Diffusivity decrease

The change in diffusivity can be determined by the carbon corrosion. The diffusivity is higher closed to the GDL because there is a higher O_2 activity, having the reacting domain moved closer to the GDL since near the membrane it is hindered. The impedance decreases at low frequency and the voltage decreases at medium-high current density. It is difficult to consider it because the O_2 transport to the CL layer must be accounted and it is rather complex.

2.5. Sensitivity analysis parameters

Some of the more relevant model parameters while doing a sensitivity study will be stated here, having a notion of what parameters might affect more the results:

- Tortuosity of the cathode GDL
- Electrical conductivity of the CCL
- Tortuosity of the CCL
- K_r or reduction constant depending on the temperature of the CCL
- Tortuosity of the cathode MPL
- Electrical conductivity of the membrane
- K_o or oxidation constant depending on the temperature of the anode CL
- Electrical conductivity of the anode CL
- Tortuosity of the anode MPL
- Tortuosity of the anode GDL [22]

The tortuosity can be defined depending on the porosity:

$$\tau = \varepsilon^{-0.5} \text{ [23]} \quad (2\text{-}10)$$

This model could be run under different operation conditions, whose variation affects the transport phenomena and properties:

- Gas pressure
- Temperature
- Oxygen partial pressure
- Fuel/oxidant flow rate (stoichiometry)
- Fuel composition (pure hydrogen or reformate)
- Gas relative humidity [22]

2.6. Applications

2.6.1. Automotive application

Fuel cell electric vehicles (FCEV) are composed by a high-pressure tank (70MPa), a fuel cell stack (~80kW), a drive battery (1-5kWh), the electrical traction motor, power control unit and boost converter as shown on Figure 2-4:

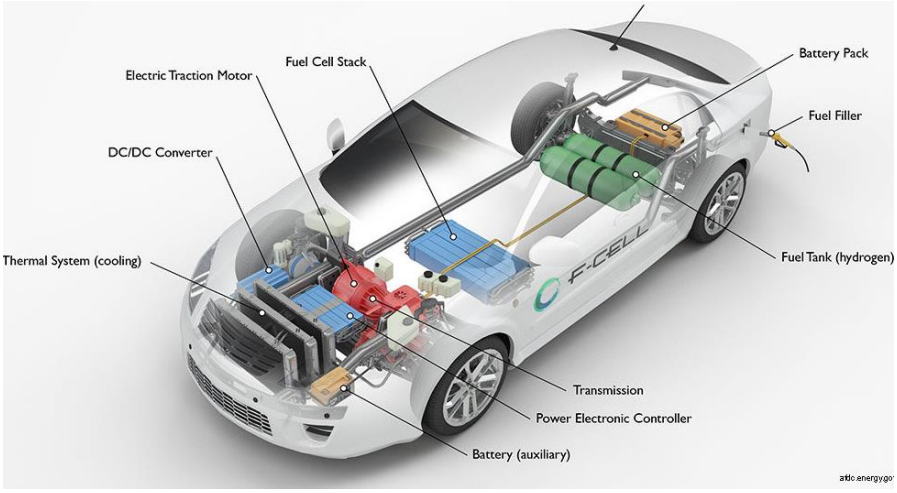

Figure 2-4 Fuel cell vehicle. **Source:** [24]

The number of FCEV produced and bought is limited (around 10^3 globally). Their range is limited compared to gasoline cars but considerably higher than battery electric vehicles (650 vs. 200-300km). The main cons are the cost and the consumption of hydrogen, increasing the expenditure. It needs 0.8kg of H_2 every 100km. Its cost is around 75k€ for segments C/D (sedan), being more expensive than gasoline or hybrid vehicles on the same segment. [25] [26]

Depending on the size of the vehicle and the daily range in km, it will be more or less suitable for each application. FCEV are better than hybrid vehicles when there is a very high use and better than electric ones when there is a long range, making it appropriate for SUVs and D private segments for that use, taxis, utility, military vehicles, passenger ships, long-haul trucks, mining and international road masters trucks. [26] [13]

2.6.2. Energy storage applications

As mentioned in 2.1 PEMFC, to store energy, an electrolyser would be needed, not a PEMFC. In theory it could be possible a reversible PEMFC or electrolyser, but in reality is not yet feasible, but it is starting to be developed for reversible Solid Oxide Fuel Cell (SOFC), commercially [27] and experimentally through European development projects [28]. Energy is stored in form of H_2 and then it is converted to electricity with the fuel cell. There is not a storage capacity, but it depends on the amount of hydrogen produced. Energy from renewable sources could be stored, so it is not lost, but there is a loss from e.g. eolic to H_2 and then another loss from H_2 to electric energy. The electric energy stored (EES) depends on the power times the hours of operation; the higher this number, the higher the energy stored:

$$EES_{cost} = \frac{EES_{power,cost} * P_{nom} + EES_{capacity,cost} * C_{nom}}{N_{cycles} * C\_nom * \eta_{round-trip}} \approx \frac{EES_{power,cost} * P_{nom}}{N_{cycles} * P_{nom} * t_{cycles} * \eta_{round-trip}} = \frac{EES_{power,cost}}{N_{cycles} * t_{cycles} * \eta_{round-trip}} \quad (2\text{-}11)$$

This means that in the electrolyser, the cost of electricity is not affected by the number of cycles, but by the hours of operation, therefore being suitable for long term storage, something that does not happen for other technologies. [29] [10] [12]

2.6.3. Distributed electric energy

The search for energetic efficiency and zero emissions has led to the deployment of fuel cell technology for generating electric energy for large-scale stationary applications. The company AkzoNobel installed a chlorine electrolysis 70kW [30] plant in Delfzijl, where PEMFC consume the H_2 generated, producing electric energy. [31] Distributed power decentralized generation has been boosted in South Korea and Japan [32], nonetheless the biggest fuel cell plant is a 50MW in Seosan [33], with 114 units of 440kW [34]. There is no comparison with other power plants considered big, such as the four 2.8MW Daegu (South Korea) [35] plants, the 1MW PEMFC Martinique plant [36] or the 2MW chemical plant in Yingkou (similar to AkzoNobel's and also built by them) [37]. Japan has mainly developed fuel cells for gas-turbine combined power cycles [30].

2.6.4. Micro combined Heat and Power

Combined heat and power (CHP) systems are being employed in banks, hospitals or telecom companies requiring reliable power to maintain operation. In hospitals it produces hot water (at the operating temperature ~80-90ºC) and electricity [32]. The Japanese residential fuel cell systems fleet is huge and is highly spread with the Panasonic 700W PEMFC based or the Aisin Seiki 700W SOFC (solid oxide fuel cell) based EneFarms, which have been traditionally below 1kW, but units around 5-10kW are coming around. This technology has reached anecdotally Europe, mainly Germany [33].

2.7. Polarization curve

On the simulations, the voltage is varied, obtaining the corresponding current density. In this section, the basics that govern it will be seen, to understand what happens from one curve to another and what loses may intervene each term of the voltage difference equation has a meaning:

$$\Delta V = -b * \ln\left(\frac{j}{i^* * ECSA}\right) + b * \ln\left[a_{O_2,ch} * \left(1 - \frac{j}{j_{lim}}\right)\right] - \left(\frac{\delta_m}{\sigma_m}\right) * j - E^- \quad (2\text{-}12)$$

Where b is the Taefel slope, depending on the temperature, the ideal gas constant, the Faraday's constant and a transfer coefficient:

$$b = \frac{R*T}{\beta*F} \quad (2\text{-}13)$$

i* is a rate of reaction in term of electrons, the exchange current density, Faraday's law for reactants:

$$i^* = 4F * K_r \quad (2\text{-}14)$$

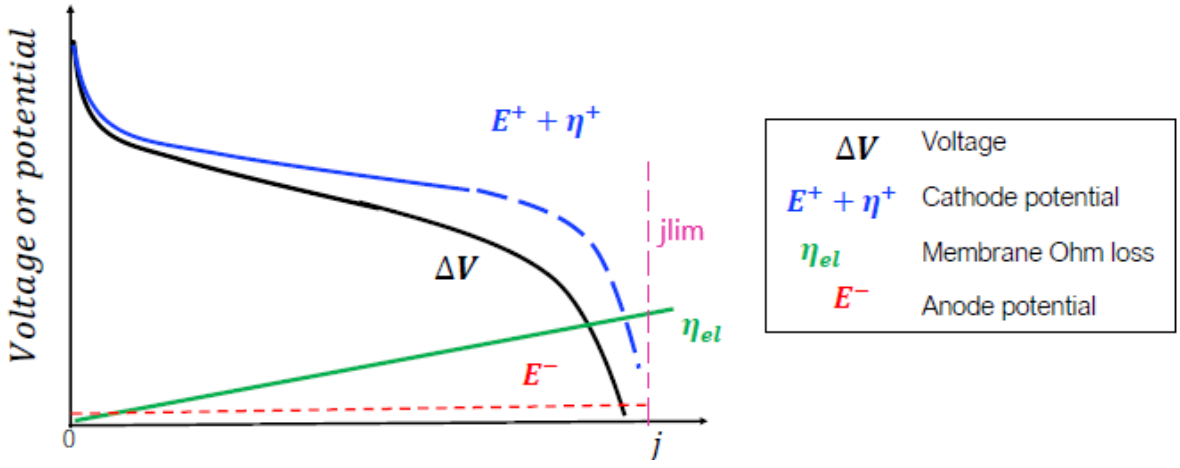

Figure 2-5 Polarization curve parts. **Source:** [38]

The first term of the equation (2-12) above corresponds to the ORR kinetics and the low current region of the cathode potential ($E^+ + \eta^+$), first part of the curve on Figure 2-5. Here the activation losses take place, it is quite a sluggish reaction with a logarithmic behaviour.

Then there is an Ohmic part of the curve on the intermediate part where the link between the voltage and current density is almost linear, corresponding to the third term on equation (2-12) above. The dominant loss here is due to membrane ionic resistance, following the Ohmic law. When charged protons move inside the membrane, to enhance it a certain loss in potential is required because of the interaction between ions and the medium.

The last part of the curve corresponds to the second term on equation (2-12) above, it is related to problems with oxygen transport. It is where the concentration losses of the polarization curve and the transport limitations of O_2 inside the GDL are.

A limiting condition is defined, j_{lim}, which is the maximum current that the system can draw, that will occur in the case where the limiting current will depend on the oxygen there is in the channel and the transport resistance of the GDL medium, depending on its properties. [38] [12]

3. METHODOLOGY

In this section it will be commented the selection of the GDLs, the methodology to calculate the different properties from the information supplied by the datasheets, and the methodology to develop the simulations and the case studies obtained.

3.1. GDL selection

The ANSYS-Fluent PEMFC model had a certain dimensions and properties. Since the dimensions of the model could not be modified, in order to approach it and be able to compare the results, the measures of the GDLs must be similar to the ones in the model. The ensemble composed by the GDL and the MPL is 285μm and just the GDL is 180μm, leaving a 105μm MPL. It has been considered a 285±30μm[1] range (between 255 and 315μm). It could be available GDL or GDL+MPL, on both cases the dimensions must be on the range necessary. On the cases where both layers are present, they will be simulated with and without the MPL to isolate its effect. The suppliers did not provide all the information necessary, so the criterion for the selection was not exclusively determined by size but also by usefulness of the properties available. Some necessary properties were calculated from the ones provided as explained on 3.2 Method for properties calculation.

3.1.1. Study cases

Four different commercial GDLs have been selected, half of them including a MPL, so including the base case and the cases where it was simulated with and without the MPL, makes a total of eight cases. The commercial GDLs selected are AvCarb P-75, SIGRACET 34BC, SIGRACET 34BA and TORAY TGP-H-090, having MPL the two first. The properties and the model parameters used on the simulation can be seen in Table 3-1.

[1] It was later found out that the actual dimensions were 255μm and not 285μm.

	Base case	Base case w/o MPL	AvCarb [39] [40]		SIGRACET [41]			TORAY [42]
			P-75	P-75 w/o MPL	34 BA	34 BC	34 BC w/o MPL	TGP-H-090
GDL Porosity %	60	60	85	85	83	75	75	78
MPL Porosity %	30	60	40	85	83	40	75	78
GDL H-phobic contact angle (°)	110	110	107 [43]	107	104	104 [43]	104	138 [43]
MPL H-phobic contact angle (°)	130	110	126 [43]	107	104	126	104	138
GDL Absolut permeability (m2)	3.00E-12	3.00E-12	5.70E-12	5.70E-12	8.71E-12	8.71E-12	8.71E-12	4.53E-12 [43]
MPL Absolut permeability (m2)	1.00E-12	3.00E-12	9.70E-14	5.70E-12	8.71E-12	7.62E-14	8.71E-12	4.53E-12
GDL Density (kg/m3)	2719	2719	2719	2719	307.14	444.44	444.44	440
GDL Electrical conductivity (S/m)	5000	5000	1250	1250	254.55	286.36	286.36	1250
GDL Thermal conductivity (W/m*K)	10	10	1.7	1.7	0.533 [44]	0.467 [44]	0.467 [44]	1.7
Thickness (µm)	285	285	275	275	280	315[2]	315	280
¿MPL?	YES	NO	YES	NO	NO	YES	NO	NO
PTFE %	-	-	YES	YES	5	15	15	5

Table 3-1 CFD model parameters

The parameters used on the base case are the ones that appear on the ANSYS-Fluent PEMFC model. The AvCarb data was obtained from articles where it was simulated [39] [40], not specifying the model, just pertaining to the series P-75, so the amount of PTFE is also missing but it says it does contain it. The model in the articles is from 2010 and it does not coincide with any current model, but it had all the pertinent information. Since the suppliers just provided information of the GDL and [39] provided information of the AvCarb MPL it has been taken as basis for the rest of the cases. The material properties of the GDL and the MPL are the same (density, electrical and thermal conductivity).

3.2. Method for properties calculation

All the necessary parameters of the AvCarb GDL were already provided, so no calculations were needed.

The hydrophobic angle was calculated with the following formula in all the real cases:

$$\sigma_{sup} * cos\theta_c = 0.0006 * \%PTFE - 0.0274 \text{ [45] (3-1)}$$

Where σ_{sup} is the superficial tension in the liquid-gas interphase having a typical value of 0.062-0.065N/m at 80-90ºC and θ_c is the hydrophobic angle. The equation provided by Kumbur led to results that had no sense. It is seen on [1] [23] that an increase on the PTFE leads to an increase on the contact angle and a reduction on the water saturation. Whereas if the equation was negative as it was suggested on one of the graphs on [46] the contact angles would be smaller than 90º, being hydrophilic instead of hydrophobic, which could not be possible. Since the angles and the results obtained with them had no sense, the hydrophobic contact angles were obtained from the measurements in [43]. Since the SIGRACET 34BC and SIGRACET 34BA are very similar, one possessing MPL and the other not, and it was only provided one angle, it was supposed that the used for the 34BC was the one of the MPL and the one for the 34BA was the one of the GDL. That value of the MPL hydrophobic angle was used also for the AvCarb case considering it was provided only for the GDL.

[2] As mentioned in the previous footnote, the actual dimensions were 255µm, which means that the SIGRACET 34BC would not be in the range, nonetheless it was still considered.

As it can be seen in Table 3-2, the angles calculated with Table 3-2 Actual angles used vs. the previous ones calculated with decrease with the amount of PTFE, as opposite as found in [1] and [23]. The rest of the angles were obtained from [43], where it says that the hydrophobic contact angle depends on the pression, porosity (and therefore on its PTFE amount), permeability and conductivity, whereas Kumbur [46] considers only the PTFE on equation (3-1).

In the case of AvCarb without MPL both angles were really similar (107º vs. 110º), dismissing a redo. This also happened for SIGRACET 34BC without MPL (104º vs. 106.71º) and SIGRACET 34BA (104º vs. 112.41º).

	AvCarb [39] [40]		SIGRACET [41]			TORAY [42]
	P-75	P-75 w/o MPL	34 BA	34 BC	34 BC w/o MPL	TGP-H-090
GDL H-phobic contact angle (°) [43]	107	107	104	104	104	138
MPL H-phobic contact angle (°) [43]	126	107	104	126	104	138
GDL H-phobic contact angle (°) [46]	110	110	112.41	106.71	106.71	112.41
MPL H-phobic contact angle (°) [46]	102	110	112.41	102	106.71	112.41
PTFE %	YES	YES	5	15	15	5

Table 3-2 Actual angles used [43] vs. the previous ones calculated with [46]

The SIGRACET thermal conductivities were obtained from [44]. The electrical conductivity was not provided, but the electrical resistance through plane in mΩcm^2 [41]. Since the electrical resistance is the inverse of the electrical conductivity, it was necessary to divide it between the thickness to obtain the desired units (S/m).

$$\sigma = \frac{1}{\rho} = \left(11 m\Omega * cm^2 * \frac{1\Omega}{10^3 m\Omega} * \frac{1m^2}{10^{2^2} cm^2} * \frac{10^6 \mu m}{1m} * \frac{1}{275 \mu m}\right)^{-1} = 254.55 \text{ S/m} \quad (3\text{-}2)$$

The absolute permeability was not given in m^2, but in cm^3/(cm^2*s) being a velocity, so to transform it Darcy's Law is needed, changing the volumetric flow (Q) into a velocity by dividing it between the area, solving for the permeability:

$$Q = \frac{A*k*\Delta p}{\mu*\Delta x} \rightarrow v = \frac{k*\Delta p}{\mu*\Delta x} \rightarrow k[m^2] = \frac{v[\frac{m}{s}]*\mu[Pa*s]*\Delta x[m]}{\Delta p[Pa]} \quad [4] \ (3\text{-}3)$$

The pressure is the one at which the test was done with the Gurley model [41], 304 Pa; the longitude is the thickness and the viscosity is the one at the working temperature of the cell (T=80ºC → $\mu_{H_2O} = 2.1 * 10^{-5}$).

The permeabilities calculated had significative differences. The SIGRACET 34BC contained a MPL and since it is considerably smaller than the GDL permeability, it would be dominant, meaning the permeability provided corresponds to the MPL. It is two orders of magnitude smaller than the SIGRACET 34BA, corresponding to the differences between the MPL and the GDL (7.62E-14 vs. 8.71E-12 m^2). Being the two GDLs almost the same model but one with MPL and other without it, it has been assumed that the GDL permeability is the SIGRACET 34BA one and the MPL permeability is the SIGRACET 34BC one. In this way both GDLs have the same permeability but the MPLs have a different one.

The density was given as an aerial weight in g/m^2, so to obtain a density it was needed to divide between the thickness to obtain it in kg/m^3.

The TORAY absolute permeability was given in strange units needing a transformation (mL*mm/(cm^2*h*mmH_2O)):

$$1700 * \frac{mL*mm}{cm^2*h*mmH_2O} * \frac{1m^3}{10^{3^2} mL} * \frac{1m}{10^3 mm} * \frac{10^{2^2} cm^2}{1m^2} * \frac{1h}{60s} * \frac{1mmH_2O}{9.8Pa} * \frac{1Pa*m*s^2}{kg} = 2.891 * 10^{-5} m^3 * s/kg \quad (3\text{-}4)$$

Following the units and Darcy's law [4] it needs to be multiplied by the viscosity to end up with the absolute permeability. Given that the permeability obtained was several orders of magnitude bigger than the rest, it was opted for the one measured in [43].

The thermal resistivity trough-plane was given at room temperature, which has an error because it should be at the operation temperature (25 vs. 80ºC), but the other case is the in-plane resistivity at 100ºC, closer to the working range but the through-plane properties are needed [6], or it could have been done a conversion where the in-plane properties are ten times the value of the through-plane ones [6]. The transformation is following above Equation (3-2).

3.3. Method for simulations

A simulation for each case is carried out varying the voltages between 1.05 and 0.35V, with a 0.1V interval, obtaining a total of eight points to form the polarization curve. A problem appeared while calculating the lower voltages simulations when there was no MPL: a floating-point error emerged impeding the continuation of the simulations. It happened when the current density went above 2.39A/cm^2 and analysing it, there was an error on the water content variable, being one order of magnitude higher than with MPL. This happened in the following cases: base case without MPL at 0.35V, AvCarb P-75 without MPL 0.35V, SIGRACET 34BC without MPL at 0.35V and TORAY TGP-H-090 at 0.35V, missing a total of four points. In the TORAY case there was not a floating-point error, but it did not converge, having considerable oscillations. This means that the solver is facing difficulties when simulating the cases without MPL at higher loads (thus higher water generation). The results have been analysed (Chapter 6) in order to determine possible reasons for this behaviour.

The AvCarb model had a very low MPL absolute permeability compared to the ANSYS-Fluent model (1e-12 vs. 9.7e-14m^2) but since the former was a real commercial one, the value of the Fluent model was considered not realistic. It was confirmed by the SIGRACET 34BA and 34BC permeabilities, being the in the same order of magnitude than the AvCarb.

The parameters corresponding to the membrane electrolyte and the CL have remained constant because the objective of the study is to analyse the effect of the GDL and the MPL, so the rest of the variables must remain the same, as control variables.

While simulating without a MPL, since the programme allows to introduce properties for the both MPL and GDL, the properties introduced must be in both the same, being those of the GDL.

4. CFD PEMFC MODEL DESCRIPTION

The main equations the ANSYS-Fluent model uses, the cell, mesh, geometry, boundary conditions and operational conditions will be described in this chapter.

4.1. The geometry

First it is shown in the Figure 4-1 the complete geometry of the ANSYS-Fluent PEMFC module on the YZ plane. Its full length is of 10cm on the X coordinate.

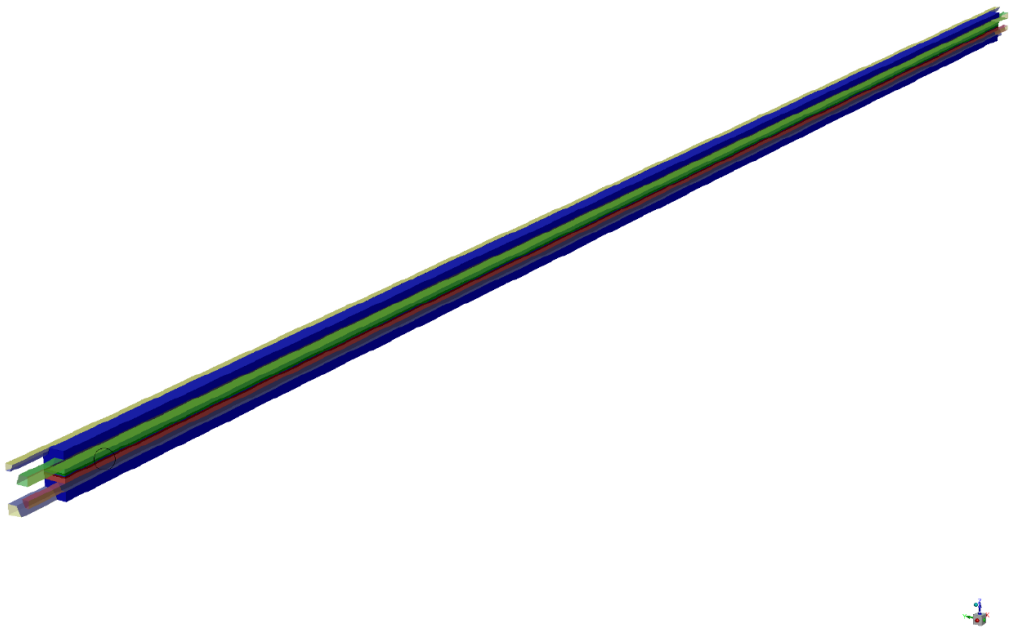

Figure 4-1 PEMFC full length mesh. **Source:** [47]

To show with more detail the geometry and structure of the cell, the Figure 4-1 will be zoomed. In Figure 4-2 it can be seen differentiated the cathode and anode side and the fuel, oxidant and cooling channels, all of them on the YZ plane.

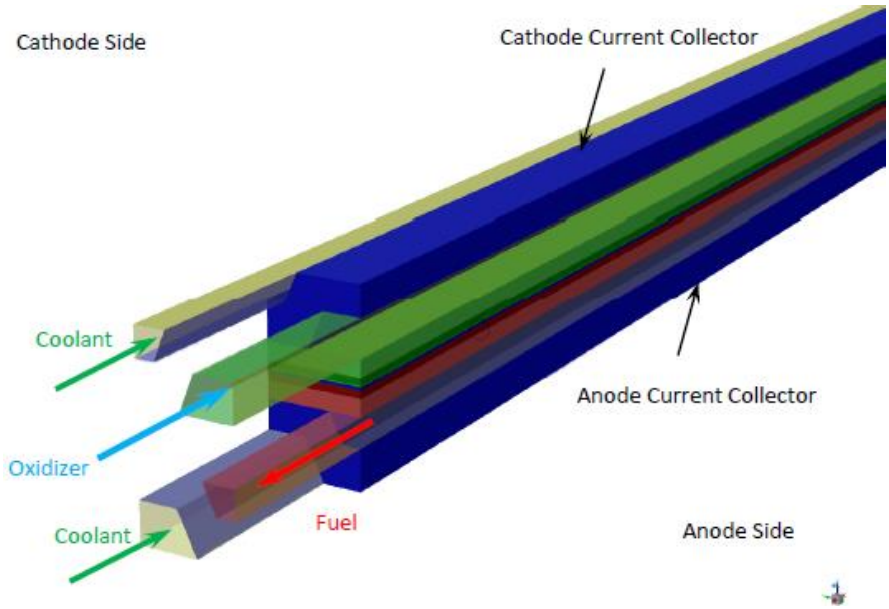

Figure 4-2 PEMFC fuel, oxidant and cooling channels. **Source:** [47]

Zooming even more the previous images, the different layers that form the PEMFC can be distinguished in Figure 4-3. There is the cathode GDL, followed by the cathode MPL and the cathode CL. The membrane is separating the cathode layers from the anode ones. Following the direction as before, going down on the Z axis, there is the anode CL, then the anode MPL and finally the anode GDL.

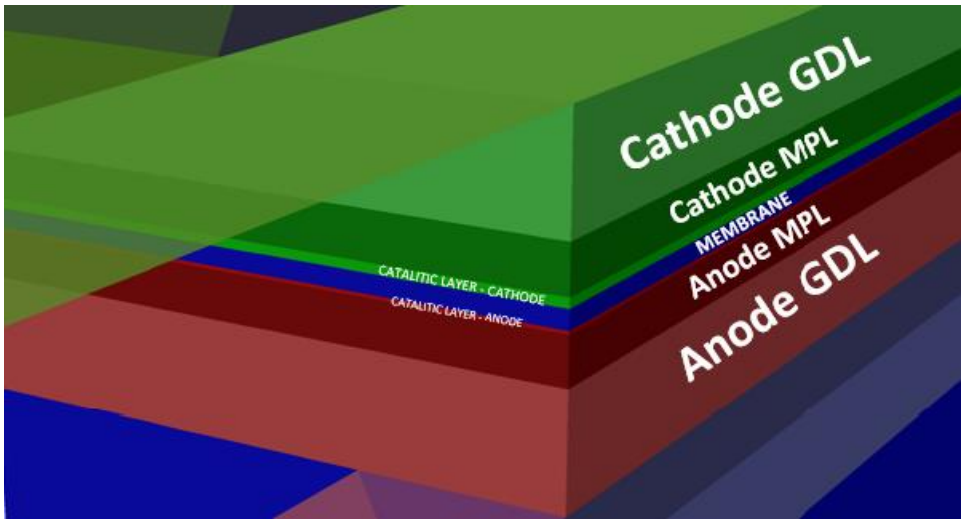

Figure 4-3 PEMFC porous layers and MEA. **Source:** [47]

On Figure 4-4, the most relevant dimensions of the PEMFC geometry can be seen on the ZY plane. Most of the measurements are in micrometres, being the total width of 2000µm and the height of 1000µm. Some of the most relevant dimensions are the thickness of the GDL and MPL, which are 180µm and 75µm respectively, making the total thickness of the assembly of 255µm.

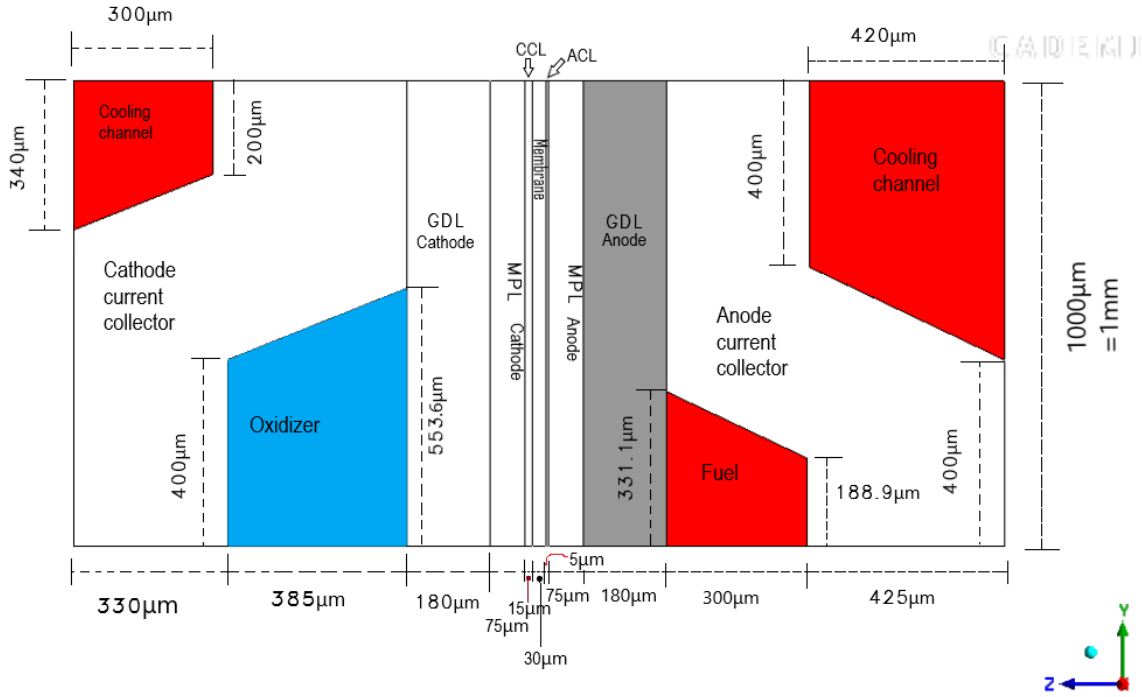

Figure 4-4 ZY plane PEMFC dimensions

4.2. The mesh

The mesh has hexahedral elements, where its number of cells, faces, nodes and partitions, as well as some relevant properties will be shown in Table 4-1. The number of cells corresponds to the total number of elements.

Cells	101070
Faces	318917
Nodes	124461
Partitions	1
Cell zones	13
Face zones	95
Maximum Face Angle (°)	129.6
Minimum Face Angle (°)	49.04
Edge/Length ratio Max	2602.2
Edge/Length ratio Min	10.7
Maximum Connectivity Number	8
Maximum Element/Volume Ratio	3.4

Table 4-1 Mesh properties

The maximum and minimum face angle are a range, where in each case the minimum or maximum respectively is 90º. The connectivity number and element volume ratio are also ranges, starting from 1. Length scales range from µm in the catalytic layer to cm along the channel length.

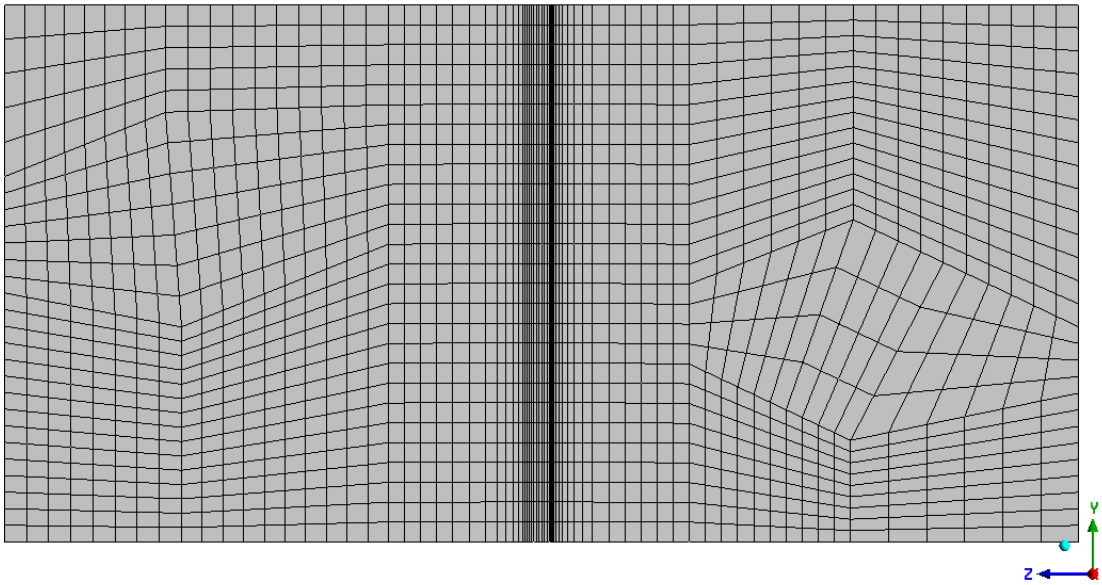

Figure 4-5 CFD PEMFC model mesh

In Figure 4-5 it can be seen the mesh that the CFD PEMFC model presents, where it has a gradual expansion from the catalytic layers into the GDLs and MPLs.

4.3. Material properties

The following properties are the default values in the CFD PEMFC model and were not changed, so it could be considered they are fixed parameters. Even if in [39] it specified the CL and electrolyte membrane properties, the original ones were kept because the objective is to study the influence of different parameters of the GDL and the MPL (and its presence) on the performance and operation of a PEMFC. Having properties change, that are not the one of interest would only smudge the results and make it more difficult to discern the actual effect of GDL and MPL. The properties that appear in Table 3-1 CFD model parametersTable 3-1 were the ones that changed from one GDL to another.

CL	Porosity %	20
	Absolute Permeability (m^2)	2E-13
	H-phobic contact angle (°)	95
	Surface/volume ratio (1/m)	200000
	Reference Temperature (K)	343
	Reference Activation Energy (J/kmol)	8314340
	Density (kg/m^3)	2719
	Specific heat (c_p) (J/kg*K)	871
	Thermal conductivity (W/m*K)	10
	Electrical conductivity (S/m)	5000
	Equivalent weight (kg/kmol)	1100
MEMBRANE	Absolute Permeability (m^2)	1E-18
	Density (kg/m^3)	1980
	Specific heat (Cp) (J/kg*K)	2000
	Thermal conductivity (W/m*K)	2
	Electrical conductivity (S/m)	1E-16
GDL	Specific heat (c_p) (J/kg*K)	871

Table 4-2 Material properties

In Table 4-2 are shown the different properties that the materials had in each layer. The surface/volume ratio was the same in anode and cathode, contrary to what was shown in [39]. As in Table 3-1, the GDL properties are the same for the MPL.

There were difficulties when trying to identify the properties given by the CFD model and actual materials. The CL is composed by platinum particles (catalyst) embed in a carbon support, intermingled with polymeric nanoparticles (ionomer). It is composed by three very different materials, being complicated point to a single material, being the properties a mixture of them, e.g. the electrical conductivity is closer to the one of the carbon (same order of magnitude while platinum is several orders above), which makes sense since its particles are bigger compared to the other compounds. This can also be applied to the other layers and materials that compose it. Something that could strike strange is that the properties of CL, GDL and MPL in the CFD PEMFC model are all the same. In the other cases, the GDL and MPL are differentiated from the CL.

4.4. Electrochemistry modelling

The thin electrolyte material is between the anode and cathode sides, separating them. In this CFD PEMFC model, the outer walls of both anode and cathode current collectors are adiabatic. The fuel and oxidizer progress through the porous anode and cathode mediums toward the catalysts, where the electrochemical reactions take place. Fuel is being reduced in the anode side:

$$H_2 \rightarrow 2H^+ + 2e^- \quad (4\text{-}1)$$

The hydrogen ions advance across the membrane towards the cathode catalyst where the oxidation takes place:

$$O_2 + 2e^- \rightarrow O^- \quad (4\text{-}2)$$
$$2H^+ + O^- \rightarrow H_2O \quad (4\text{-}3)$$

The CFD PEMFC model is used for the calculation of the current density, voltage, species, temperature and potential, among others, distributions throughout the fuel cell. [47]

The driving force behind the anodic and cathodic reactions is the surface overpotential, the difference between the phase potential of the solid and the electrolyte/membrane. The following equations account for the electrons/protons transport respectively through the solid conductive materials:

$$\nabla \cdot (\sigma_{sol} \cdot \nabla \varphi_{sol}) + R_{sol} = 0 \quad (4\text{-}4)$$

$$\nabla \cdot (\sigma_{mem} \cdot \nabla \varphi_{mem}) + R_{mem} = 0 \quad (4\text{-}5)$$

Where σ is the electrical conductivity, ϕ the electric potential and R the volumetric transfer current, corresponding the sol and mem subindex to solid conductive material and membrane respectively. For the potential equation in the solid phase, R_{sol}= -R_{an} (<0) on the anode side and R_{sol}= +R_{cat} (>0) on the cathode side. For the potential equation in the membrane phase, R_{mem}= +R_{an} (>0) on the anode side and R_{mem}= -R_{cat} (<0), where the cat and a subindex correspond to the cathode and anode side. Then volumetric transfer current equations are obtained for anode and cathode:

$$R_{an} = \zeta_{an} \cdot j_{an}(T) \cdot \left(\frac{[A]}{[A]_{ref}}\right)^{\gamma_{an}} \cdot \left(e^{\alpha_{an} \cdot F \cdot \frac{\eta_{an}}{RT}}\right) \quad (4\text{-}6)$$

$$R_{cat} = \zeta_{cat} \cdot j_{cat}(T) \cdot \left(\frac{[C]}{[C]_{ref}}\right)^{\gamma_{cat}} \cdot \left(e^{\alpha_{cat} \cdot F \cdot \frac{\eta_{cat}}{RT}}\right) \quad (4\text{-}7)$$

Where [A] and [C] represent the molar local species concentration and their reference value that mark the reaction rates of anode and cathode, symbolizing H_2 and O_2. ζ is the specific active surface area, γ the concentration dependence, α the anode and cathode transfer coefficients and η the overpotential.

The reference exchange current density of anode and cathode are dependent on the local temperature and as they are one of the main outputs obtained from the CFD simulations, it is relevant to show how they are calculated. It is considered a simulation has converged when anode and cathode current density have reached

the same value.

$$j_{an}(T) = j_{an}^{ref} \cdot e^{-\frac{E_{an}}{R \cdot T \cdot \left(1 - \frac{T}{T_{an}^{ref}}\right)}} \quad (4\text{-}8)$$

$$j_{cat}(T) = j_{cat}^{ref} \cdot e^{-\frac{E_{cat}}{R \cdot T \cdot \left(1 - \frac{T}{T_{cat}^{ref}}\right)}} \quad (4\text{-}9)$$

Where E is the user-specified activation energy, T_{ref} the user-specified reference temperature and j_{ref} the reference exchange current density at a specified reference temperature.

The following parameters were defined in order to calculate a series of properties later specified: reference temperature [K] and pressure [N/m^3], concentration dependence exponents (γ_p, γ_t) and pore blockage (r_s).

- p_0=101325 N/m3
- T_0=300K
- γ_p = 1.0
- γ_t = 1.5
- r_s=2.5

These reference values are used to calculate: gas phase species diffusivity, electrolyte phase ionic conductivity, diffusivity of water content, osmotic drag coefficient and saturation pressure. [48]

4.5. Water transport

4.5.1. Water transport in GDL, MPL and membrane

The driving force of the water transport is liquid pressure gradient ∇p_l:

$$\frac{\partial}{\partial t}(\varepsilon \cdot \rho_l \cdot s) = \nabla\left(\frac{\rho_l \cdot K \cdot K_r}{\mu_l} \cdot \nabla p_l\right) + S_{gl} - S_{ld} \quad (4\text{-}10)$$

Where μ_l and ρ_l are the liquid dynamic viscosity and density, K and Kr are the absolute and relative permeability, ε the porosity, s the liquid saturation, S_{ld} the rate of mass change between liquid and dissolved phases and S_{gl} the rate of mass change between gas and liquid phases. It is considered that the liquid pressure is equivalent to the sum of the capillary pressure p_c and the gas pressure p_g, which are function of saturation:

$$p_l = p_c + p_g \quad (4\text{-}11)$$

In the membrane, the relative permeability can be expressed as:

$$K_r = \left(\frac{\left(\frac{M_{w,H_2O}}{\rho_l}\right) \cdot \lambda_{s=1} + \left(\frac{EW}{\rho_l}\right)}{\left(\frac{M_{w,H_2O}}{\rho_l}\right) \cdot \lambda + \left(\frac{EW}{\rho_i}\right)} \cdot \left(\frac{\lambda}{\lambda_{s=1}}\right)\right)^2 \quad (4\text{-}12)$$

Where EW is the equivalent weight, M_{w,H_2O} is the molecular mass of water and λ the water content.

In the GDL and MPL, the relative permeability is defined as:

$$K_r = s^b \quad (4\text{-}13)$$

Where b is a user-defined constant.

The mass transfer rate between the gas and liquid phases follows the unidirectional diffusion theory:

$$S_{gl} = \begin{cases} \gamma_e \cdot \varepsilon \cdot s \cdot D_{gl} \cdot \frac{M_{w,H_2O}}{R \cdot T} \cdot p \cdot \ln\left(\frac{p - p_{sat}}{p - p_{wv}}\right); & p_{wv} \leq p_{sat} \\ \gamma_c \cdot \varepsilon \cdot (1-s) \cdot D_{gl} \cdot \frac{M_{w,H_2O}}{R \cdot T} \cdot p \cdot \ln\left(\frac{p - p_{sat}}{p - p_{wv}}\right); & p_{wv} > p\_sat \end{cases} \quad (4\text{-}14)$$

Where γ_e is the evaporation rate coefficient, γ_c is the condensation rate coefficient, p_{sat} the saturation pressure, p_{wv} is the water vapour partial pressure and D_{gl} has a different expression depending if it is on the cathode or anode:

$$D_{gl} = \begin{cases} 0.365 \cdot 10^{-4} \cdot \left(\frac{T}{343}\right)^{2.334} \cdot \left(\frac{10^5}{p}\right); cathode \\ 1.79 \cdot 10^{-4} \cdot \left(\frac{T}{343}\right)^{2.334} \cdot \left(\frac{10^5}{p}\right); anode \end{cases} \quad (4\text{-}15)$$

Liquid water reduces the effective active surface area in the catalyst layers, modifying the transfer current, modelling it as a function of the saturation and the user-specified constant γ_j:

$$R_j' = (1-s)^{\gamma_j} \cdot R_j \quad (4\text{-}16)$$

4.5.2. Water transport in gas channels

Liquid water is created in the electrode, diffusing first to the GDL, MPL and later entering the gas channels. The following equation is used to predict the pressure drop increase produced:

$$\frac{\partial}{\partial t}(\rho_l \cdot s) + \nabla \cdot (\rho_l \overrightarrow{v_l} \cdot s) = \nabla \cdot (D_{liq} \cdot \nabla s) \quad (4\text{-}17)$$

Where D_{liq} is the liquid water diffusion coefficient in the gas channel and $\overrightarrow{v_l}$ is the liquid velocity, which is a fraction of the gas velocity $\overrightarrow{v_g}$:

$$\overrightarrow{v_l} = \chi \cdot \overrightarrow{v_g} \quad (4\text{-}18)\ [48]^3$$

4.6. Operating conditions

The following variables are kept constant throughout the simulations in the different locations mentioned, which will be later developed:

- Anode inlet: H_2 mass flow and relative humidity
- Cathode inlet: Air mass flow and relative humidity
- Coolant inlets: Mass flow and temperature

The simulations were done for voltages between 1.05 and 0.35V with 0.1V intervals. This made a total of 8 points to create the polarization curves. The cell voltages were always the same for all the cases, in order to obtain the current densities.

The anode inlet is fed with 10^{-7}kg/s of humidified hydrogen at 343.15K, with a 60% mass fraction against the water vapour 40%, making it a $6*10^{-8}$kg/s of H_2. The cathode inlet is fed with $1.4*10^{-6}$kg/s of air at 343.15K, being its composition: 21% of O_2, 5% of water vapour and 74% of nitrogen.

The flux is treated as laminar, gases as ideal and the simulations are in steady state.

[3] For more information, consult the ANSYS Fluent Theory User's Guide [48]

5. SIMULATIONS RESULTS

In this chapter the results obtained in the simulations will be commented and compared. The direct result from them is the polarization curve since the current density is obtained without any postprocessing. The set of curves shown will be:

- The polarization curves.
- The power vs. current density curves
- The electric efficiency vs. current density curves.

All of them have been considered as direct results because there was no need for a postprocessing tool, even though they needed intermediate calculations. The ANSYS base case is used as a reference, verifying everything works adequately. The voltage was varied between 1.05 and 0.35V with a 0.1V interval, obtaining a total of 8 points.

5.1. Curves generation

- Polarization curve: The voltage [V] is dependent variable while the current density [A/cm^2] is the independent one, even though its value is obtained as a result from the simulation.
- Power vs. current density curves: The power [W] is the dependent variable while the current density [A/cm^2] is the independent one. It needs some calculations:

$$P = V \cdot j \cdot A_{mem} \quad (5\text{-}1)$$

The voltage is multiplied by the current density and the superficial area of the membrane, which is 1cm^2 or 0.0001m^2.

- Electric efficiency vs. current density: The electric efficiency (dimensionless) is the dependent variable while the current density [A/cm^2] is again the independent variable. The electric efficiency was calculated as the ratio between the actual power produced and the power the fuel contained, given

by its Low Heating Value (LHV) and its mass flow. In this case the fuel is hydrogen.

$$\eta_e = \frac{P}{\dot{m}_{H_2} \cdot LHV_{H_2}} \quad (5\text{-}2)$$

The cases where there was a MPL were compared with themselves without a MPL. All the cases appear in final graphs comparing the different curves of all of them.

5.2. Base case with and without MPL

The base case was done in order to check than everything ran smoothly. Its results were compared with the ones provided by ANSYS in the tutorial [47]. In the simulation the results were obtained with 6 decimals precision and the results given by ANSYS had a 3 decimals precision, having to round up, as seen in Table 5-1.

Current density [A/cm²]		Voltage [V]	Relative error [%]
ANSYS	Base case		
0.006	0.006	1.05	0
0.075	0.075	0.95	0
0.294	0.294	0.85	0
0.824	0.824	0.75	0
1.530	1.531	0.65	0.065
2.029	2.029	0.55	0
2.170	2.167	0.45	0.138
2.192	2.191	0.3	0.274

Table 5-1 ANSYS tutorial and the base case results comparison

As it can be seen in Table 5-1 the relative error that appeared between both values was so small that could be negligible, where only in 3 cases the values differed and in the rest was lower than 0.3%. Taking into account the difference in precision the error might be different, but it mixes with the rounding.

Where the properties of the MPL should be introduced, the GDL properties were introduced, duplicating it, as if both layers were the GDL. This is a way to try to isolate the MPL behaviour, by seeing the performance with and without it. This procedure took place for the other two cases where there were MPLs. Both curves with and without MPL will be shown together to compare the effect that the presence of the MPL have.

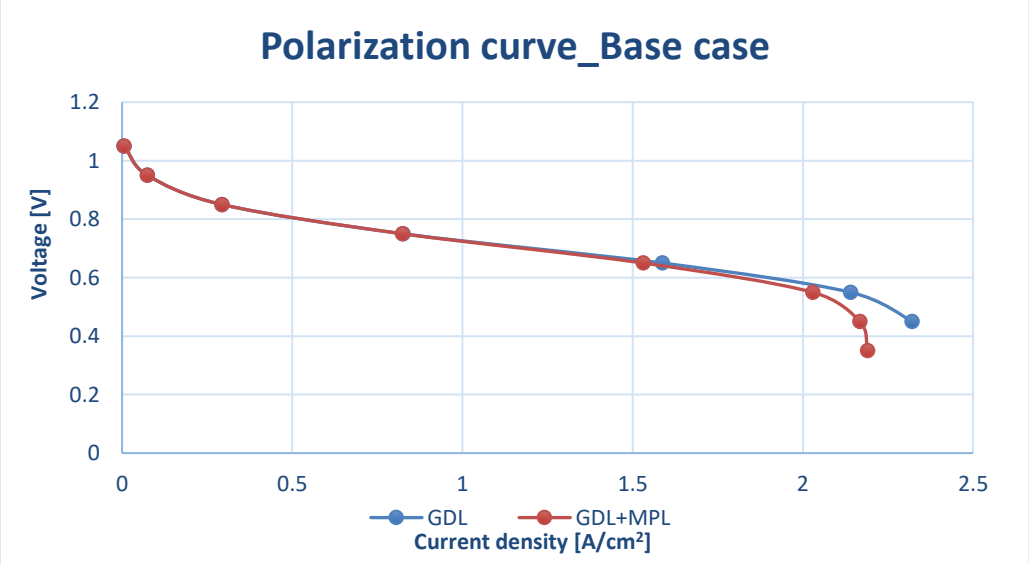

Figure 5-1 Base case polarization curve with and without MPL

In Figure 5-1 it can be seen a comparison between the polarization curves of the base case with and without

MPL, including all the parts mentioned in chapter 2.7. It has a first part with slight increases in the current density, where the ORR kinetics take place slowly, until it reaches a zone with a constant slope due to membrane ionic resistances and materials electronic resistances. Then there is sudden drop of the cell voltage, being affected by limitations in the oxygen transport.

The case without MPL has a larger zone influenced by the membrane ionic resistance, leading to think it has a better performance. Nonetheless there was a point where the simulations could not continue due to the water content error mentioned in 3.3 Method for simulations, not having completely that last zone where the current density values are almost constant. The MPL is a highly hydrophobic layer and it makes sense that without it there is too much water, having opposed effects. The values of both simulations are the same until 0.65V, where the behaviours of the curves start to differ, so it could be said that the effect of the presence of MPL is only seen at high voltages. There is a 5.6% difference among the maximum current density values achieved in both cases. There is apparently a better performance without MPL because the higher porosity and permeability present in the GDL means there are less hindrances for the O_2 diffusion, which can be supported by the oxygen mass fraction that can be seen in the postprocessing. It means the oxygen can diffuse better, but also the water, having flooding and hydration problems, since it is not where it should be. There are opposed effects to the MPL presence.

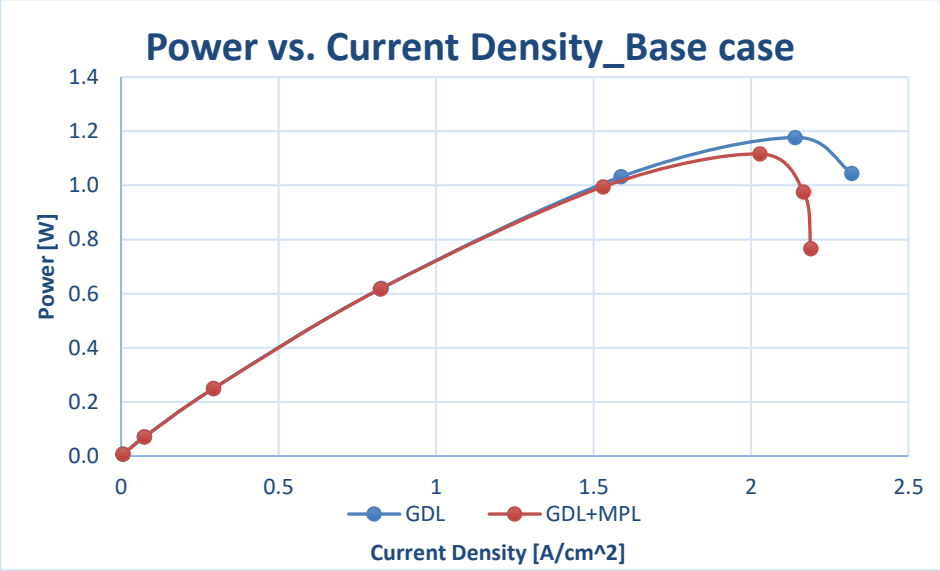

Figure 5-2 Base case power- current density curve with and without MPL

In Figure 5-2 it the power vs. current density curves comparison of the base case with and without MPL. The power suffers an increase until it reaches a maximum at 2.03A/cm^2 (0.55V) with a value of 1.12W and then it starts to abruptly decrease, being the value almost constant and vertical in the case with MPL. The case without MPL has a higher maximum power of 1.18W, a 5.2% difference with respect to having MPL. Since the complete behaviour has been hindered, the power does not reach the point where it decreases abruptly with an almost constant current density. As on the polarization curve, the behaviours start to differ at 0.65V.

If Figure 5-2 and Figure 5-3 are compared, they have a very similar behaviour, reaching the maximum at the same point, with a value of 15.1% for the case with MPL, decreasing again abruptly. This is due to the fact that the efficiency has a direct relationship with the power, as seen in Equation 5-2. In Figure 5-3 it can be seen the electric efficiency vs. current density curves comparison of the base case with and without MPL. The maximum efficiency in the case without MPL is achieved at 16.4%, being again the difference with respect to having a MPL a 5.2% due to the power dependency. As on the polarization curve, both behaviours start to differ at 0.65V. It does not present a zone where the efficiency decreases abruptly, it is smoother than in the case with MPL, but again, it has been hindered.

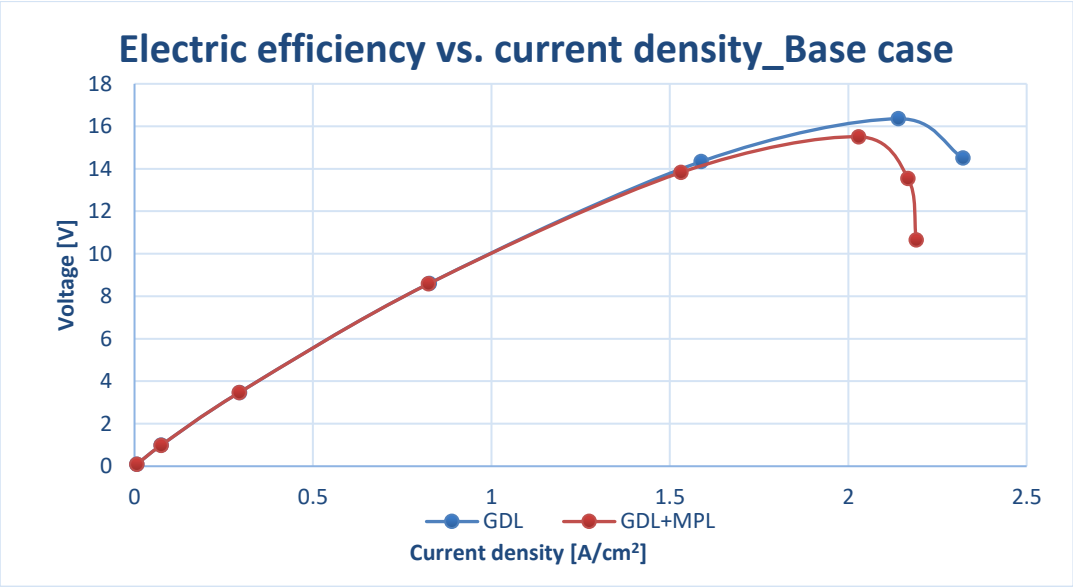

Figure 5-3 Base case electric efficiency- current density curve with and without MPL

The electrical efficiency of a PEMFC can be up to 40% for distributed power and 60% for transportation, where SOFC and MCFC are the fuel cells with higher efficiencies and in stationary and portable applications it goes down to 26-30%, according to [32]. This would mean that the efficiency would highly depend in the application and the power output, having smaller units or stacks a higher efficiency. According to [43] the practical fuel cell efficiency can be up to 65%, not specifying to which type of fuel cell it refers. Nevertheless, [30] states that PEMFC efficiency can be between 60 and 40%, depending on the purity of the hydrogen used. [3] states that the PEMFC efficiency can be up to around 55%, while [33] says is 57%.

In [49] an experimental analysis of the efficiencies is performed with an ElectroChem PEMFC, finding that the maximum was located around 46% at low currents. At very low currents the efficiencies are very low because there is a minimum H_2 mass flow, which was higher than needed. This problem that can be seen, it appears clearly in Figure 5-3 because the hydrogen mass flow was kept constant. In [49] is seen that not adequate H_2 flows act in detriment of the efficiency and since through out all the simulations the efficiency was kept constant, it would not have adjusted to what it is needed affecting seriously the maximum efficiency. It was opted to keep the H_2 mass flow constant because its variation would have added another independent variable, not seeing clearly the effect of the different GDL and MPL properties and presence have on the behaviour.

5.3. AvCarb P-75 with and without MPL

AvCarb P-75 includes a MPL, so this subsection will include and compare the results obtained of this case with and without MPL, being simulated as explained before. A comparison with the original case will give a sense of the relevance of the MPL on its behaviour, but a definite answer will only be obtained when analysing each variable individually in a more thorough postprocessing. It will also tell if the base case is a completely irreal and ideal model or if it had something to do with the AvCarb P-75 with MPL case. This will be confirmed or refuted by later GDLs. At 0.35V in the case without MPL appeared a floating-point error due to the water content, not being able to finish the simulations.

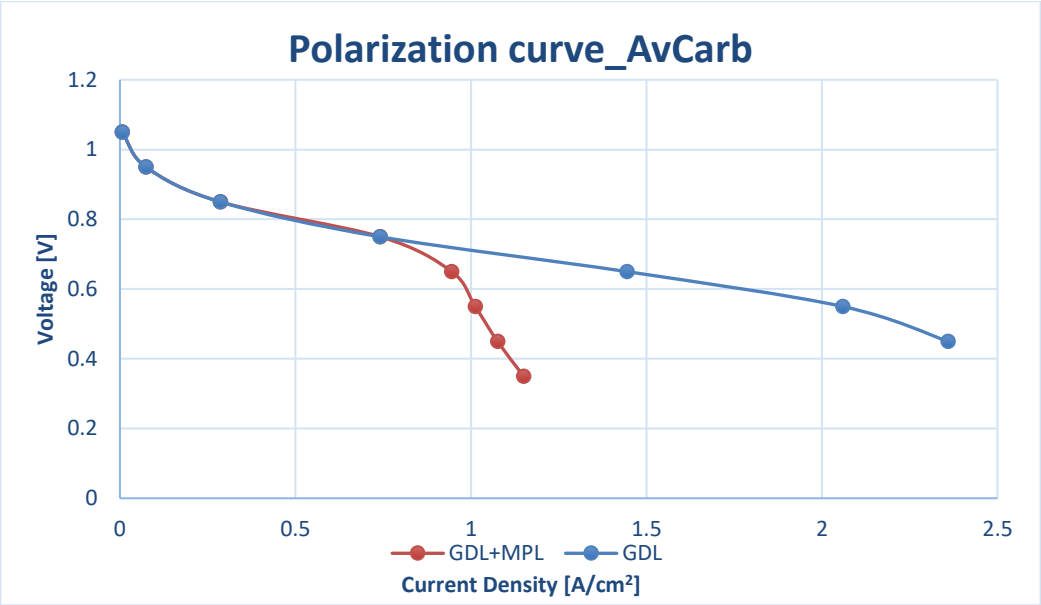

Figure 5-4 AvCarb P-75 polarization curve with and without MPL

In Figure 5-4 it is shown a comparison between the polarization curves of AvCarb P-75 with and without MPL. Observing the case with MPL, the current density values are smaller than in the base case, maybe indicating than in reality not so higher values could be achieved (before seeing other commercial GDLs). The maximum current value is roughly half (1.15A/cm^2) of the base case value. The membrane ionic resistance zone is smaller and instead of decreasing abruptly, it has a more gradual slope. While on the base case the curve started to lose its horizontality at 0.55V, here it happens at 0.65V, reducing its growth phase. When the rest of GDLs are available, it will be possible to discern if this is a bad behaviour or if it is how commercial GDLs behave, being far for the ideality.

The case without MPL has a completely different behaviour from the one with a MPL. The horizontal zone due to the ionic membrane resistance is prolonged until a 2 A/cm^2 current density at 0.55V, being larger its growth. At that point it starts to slowly decrease, but it is not abrupt, as seen on Figure 5-1, being its behaviour quite similar to the base case without a MPL seen in **¡Error! No se encuentra el origen de la referencia.**. Its behaviour is again hindered when not having a MPL due to problems with the water content in the simulation, not been able to finish for all the points. There is a 51.2% difference among the maximum current density values with and without MPL, significantly higher than the 5.6% difference in the base case. The behaviour is almost twice the one with MPL, what would imply just looking at these results that the presence of a MPL is harmful for its development, but while analysing thoroughly the rest of variables in the postprocessing, such as the oxygen amount or liquid saturation, it will be seen if this is true or if there are opposed effects.

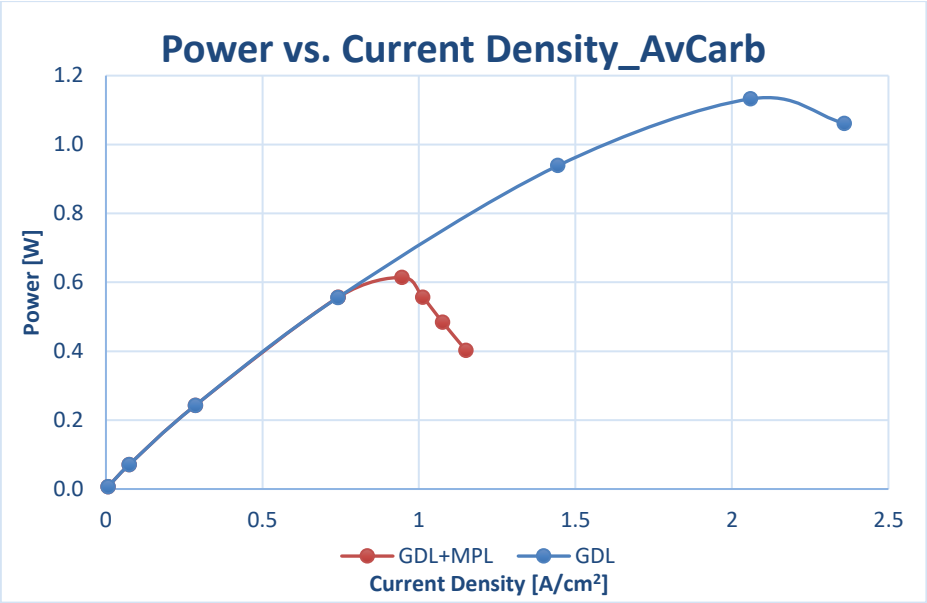

Figure 5-5 AvCarb P-75 Power-current density curve with and without MPL

In Figure 5-5 it is seen the comparison between the power vs. current density curves of AvCarb P-75 with and without MPL. The maximum power is 0.614W in the case with MPL. As in the polarization curve, the decrease it faces is gradual and not as abrupt as it has been seen in **¡Error! No se encuentra el origen de la referencia.**, also starting it before. The limitations in the polarization curve highly affect the development of the power. The maximum power is achieved at 0.65V, translating the X axis to the left, limiting its maximum, which later affects the maximum electric efficiency.

Similar to what is seen in the polarization curve, there is a huge difference between having a MPL or not. The curve development of the case without MPL suits the polarization curves seen in Figure 5-5, it keeps growing until it reached its maximum, slowly decreasing. The soft decrease on the zone where the oxygen transport problems are present, is reflected on the soft decrease when the maximum is reached. The maximum power is 1.13W, achieved at 0.55V, more similar to what happened in the base case than with MPL. The difference between the maximum powers with and without MPL is a 45.6%, while its difference with the base case is of just between 1.5 and 4%.

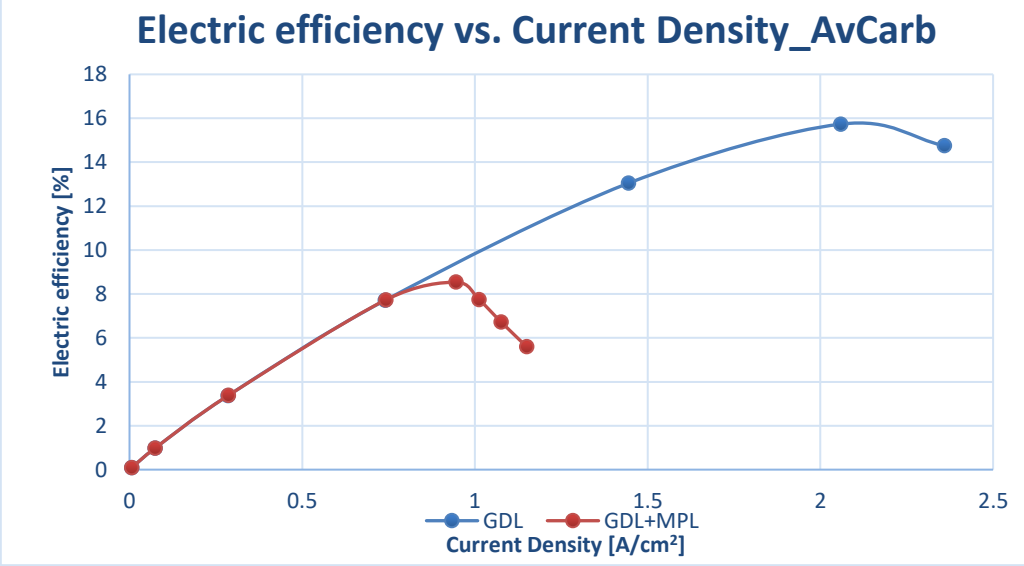

Figure 5-6 AvCarb P-75 Electric efficiency-current density curve with and without MPL

In Figure 5-6 it is shown the comparison between the electric efficiency vs. current density curves of AvCarb

P-75 with and without MPL. It is heavily dependent on the power, showing almost the same behaviour as in Figure 5-5. The decrease happens again before than in Figure 5-3 and it does not decrease so abruptly. Its maximum value is achieved at 0.65V with a value of 8.5% in the case with MPL. Again, it has shown more similarities with the base case without MPL than with its original version with MPL, being the percentual differences between them the same as with the power. Its maximum value is 15.7% for the case without MPL.

5.4. SIGRACET 34BA

SIGRACET 34BA does not include a MPL. It has not been modification, so there might be notable differences with respect to the SIGRACET 34BC without MPL even if both had similar properties. All the SIGRACET cases have low electric conductivity.

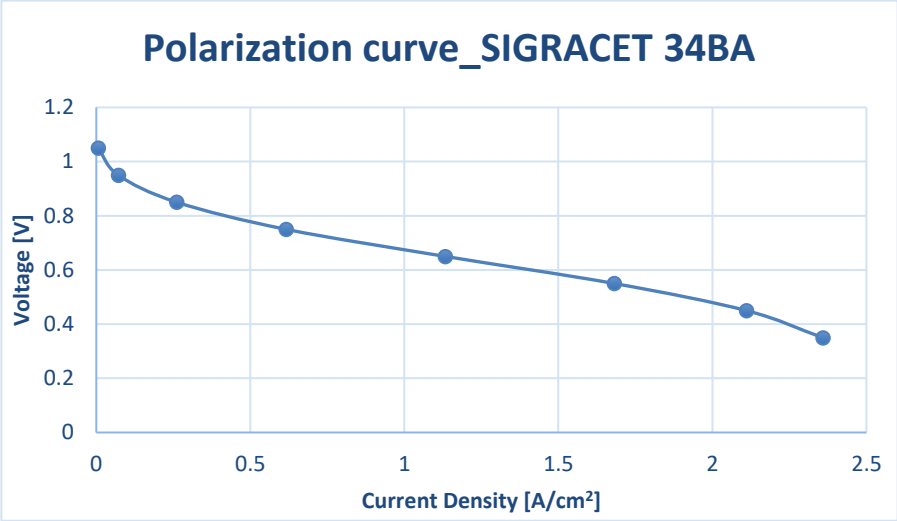

Figure 5-7 SIGRACET 34BA polarization curve

In Figure 5-7 it can be seen the SIGRACET 34BA polarization curve. If it is compared with Figure 2-5, which is an example on a standard polarization curve and its parts, or with Figure 5-1 since the base case is considered the standard result obtained from the CFD model, it has clear differences with both. The central part where the relation between voltage and current density is almost horizontal and is mainly affected by the membrane ionic resistance, here it presents a more notable linearity. The different zones are not as differentiated, the transitions are smoother. It cannot be seen the zone where the curve shows an abrupt decrease, having a constant current density. This last part is similar to Figure 5-1 without MPL, as if its development is hindered, even though the simulations were not stopped due to water content problems and were able to finish, as in Figure 5-1 and Figure 5-4. Its behaviour is quite similar to the other cases seen without MPL in Figure 5-1 and Figure 5-4, being their maximum values apart in just between a 0.02 and 1.6%. The main difference is that while SIGRACET 34BA achieved this value at 0.35V, while the other cases did it at 0.45V.

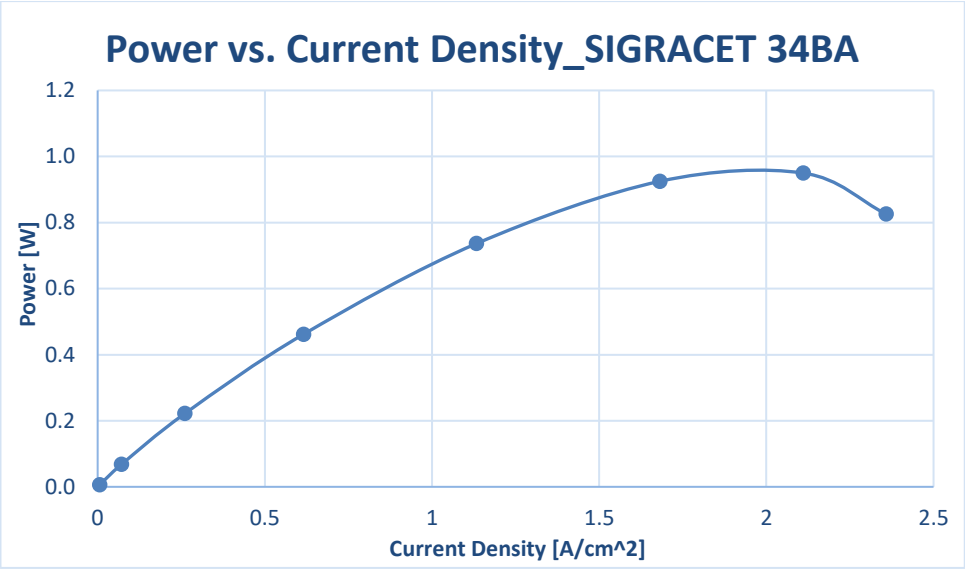

Figure 5-8 SIGRACET 34BA Power-current density curve

In Figure 5-8 is can be seen the power vs. current density curve of SIGRACET 34BA. As on the polarization curve, the behaviour of this curve has not abrupt changes and a strong behaviour as on Figure 5-2 and Figure 5-5. The curve is smooth, decreasing slowly. The maximum point in the other cases without MPL was found in 0.55V, whereas here is found at 0.45V as if everything was delayed and the decrease has not happened yet. The maximum power is 0.95W, it is lower than in the other cases without MPL between 17.5 and 19.2%, but this is due to its displacement on the X axis, having the maximum value at a lower voltage.

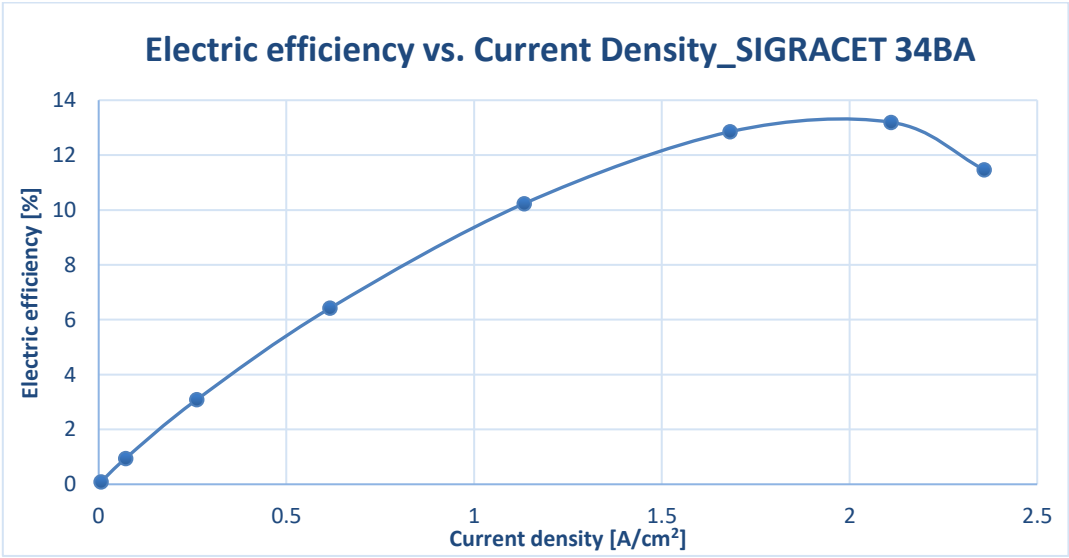

Figure 5-9 SIGRACET 34BA Electric efficiency-current density curve

In Figure 5-9 it can be seen the electric efficiency vs. current density curve of the SIGRACET 34BA. Again, its behaviour is strongly linked to the power curve due to it dependency. Its maximum point is delayed to 0.45V, with a value of 13.2%. It is comparatively smaller than in the other cases without an MPL, having the same difference as in the power, since they are linked. This reduction in the efficiency is due to the reduction of maximum power because of its translation in the X axis to the right.

5.5. SIGRACET 34BC with and without MPL

This case has a MPL but simulated with and without it, enlarging the GDL to where the MPL should be in the latter case. As the previous case it has a low electric conductivity. Their properties are very similar with slight

differences in the electrical conductivity. At 0.35V in the case without MPL appeared a floating error due to problems with the water content, not finishing the curve.

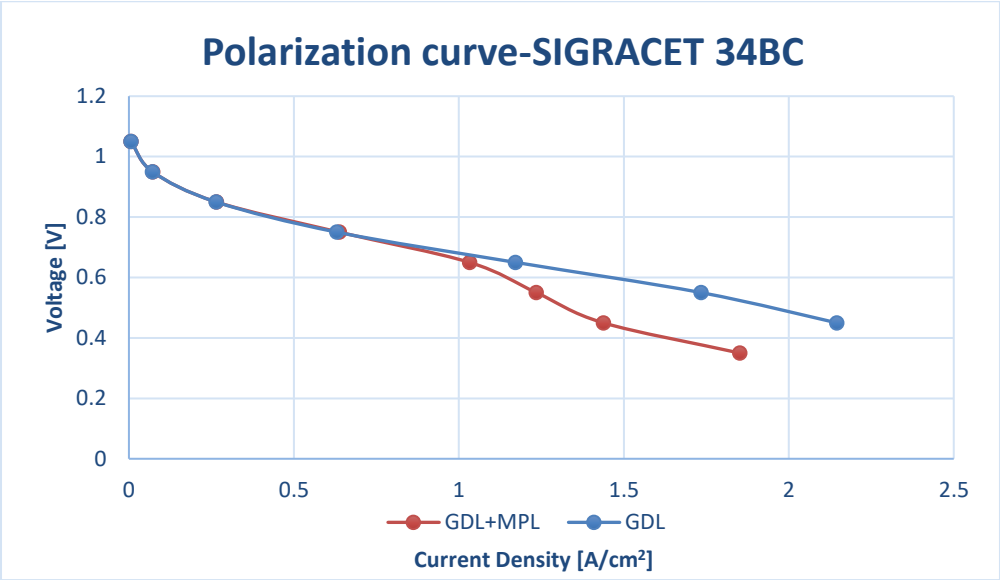

Figure 5-10 SIGRACET 34BC polarization curve with and without MPL

In Figure 5-10 it is seen a comparison between the polarization curves of the SIGRACET 34BC case with and without MPL. The curve corresponding to the case with MPL has an irregular form, quite different form the ones seen in Figure 2-5 or Figure 5-1. The middle zone mainly affected by the membrane ionic resistance seems to be shortened, starting the sudden decrease at 0.65V, as the AvCarb P-75 case seen in Figure 5-4. However, the change on the slope does not lead to an abrupt decrease, but to a smooth one, continuing its growth along the X axis. When it reaches 0.45V there is another change on the slope, leading to an even smoother decrease.

The difference between both curves is not as steep as the one seen in Figure 5-4 between the AvCarb P-75 cases. There is not such a great difference among the maximum current density they reach, while in Figure 5-4**¡Error! No se encuentra el origen de la referencia.** the difference was of 51.3%, in Figure 5-10 was of 13.7%. This case is very similar to other cases without a MPL, as seen in Figure 5-4 and Figure 5-7.

In the case without MPL the zone affected by the membrane ionic resistance has a not so horizontal behaviour, but a more marked decrease than in other cases. It reaches appoint where this zone is clearly differenced with the zone affected by the oxygen transport by a sudden decrease, which could be seen in Figure 5-1, Figure 5-4 and Figure 5-10, the cases with MPL. In Figure 5-4 and Figure 5-7 the decrease is smoother and seems to be hindered. In Figure 5-10 the difference in the slope (if there is), is so subtle that cannot be clearly distinguished. Taking into account that the simulations of this case could not be completed due to errors, it is possible that its behaviour was hindered, taking place subsequently. Figure 5-10 implies that the behaviour of the case without MPL is better than with it, but observing the oxygen mass fraction and liquid saturations in the posterior postprocessing it would be seen probably that they are opposed effects.

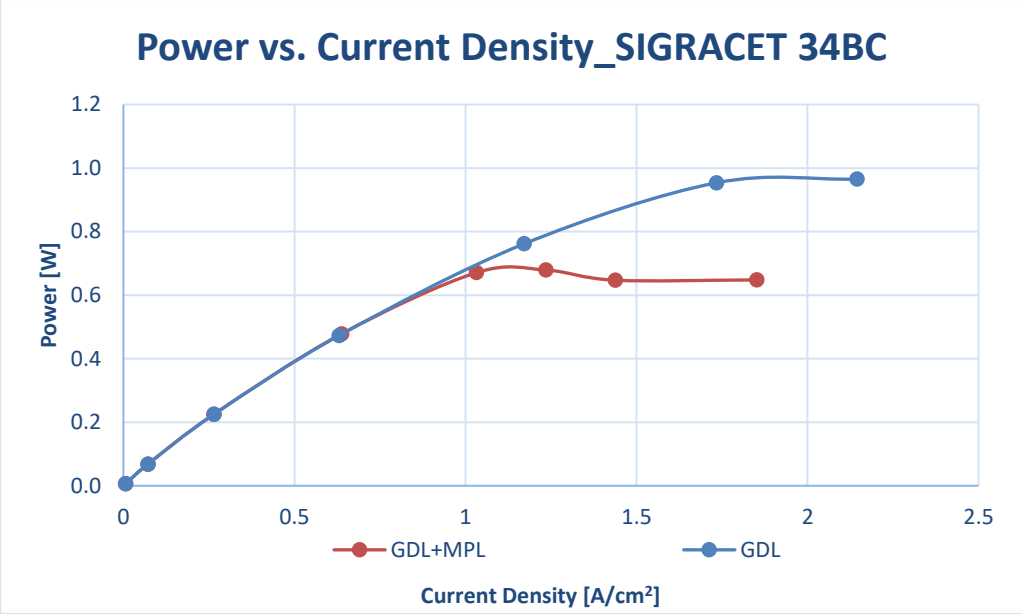

Figure 5-11 SIGRACET 34BC Power- current density curve with and without MPL

In Figure 5-11 it is shown a comparison between the power vs. the current density curves for the SIGRACET 34BC case with and without MPL. The behaviour in the case with MPL is different from the one seen on previous cases. The power increases with the current density until it reaches its maximum at 0.68W. This value is relatively similar to the one found in Figure 5-5, with a 9.6% difference, while the difference with the other SIGRACEET case in Figure 5-8 has a 39.9% difference, more considerable. Looking to the behaviour before the maximum, it has more similitudes to the other case with a MPL (AvCarb P-75) than with the other SIGRACET case (34BA). Then there is slight decrease, with a very smooth slope, leading to an almost horizontal zone, staying the power constant with the current density but it is slowly increasing again. In other cases when it reached the maximum, it only decreased, but here there is an anomaly.

The difference in the axis makes the SIGRACET 34BC with MPL case seem almost constant when it reaches its maximum. The behaviour the case without MPL shows in Figure 5-11, could be described similar to those without MPL shown in Figure 5-2, Figure 5-5 or Figure 5-8, nonetheless the last three experience a decrease when they arrived to the maximum. In Figure 5-11 the case without MPL reaches its maximum at the end of its simulation range, which makes it seem like it is obstructed or cut. The maximum is achieved at 0.45V, making it seem it displaced in the X axis if it is compared with other cases, being its value 0.97W, which is a 29.6% difference between the curves seen in Figure 5-11. It has a 1.6% difference with the SIGRACET 34BA case seen in Figure 5-8, being both SIGRACET cases with really similar properties where the mayor difference was the hydrophobic contact angle, which remained unchanged due to a previous error (even if the difference was a 7.5%, it was deemed negligible) and the electrical conductivity with a 12.5% difference. Compared to other cases without MPL such as the AvCarb P-75, there is a bigger difference, of 17.3%.

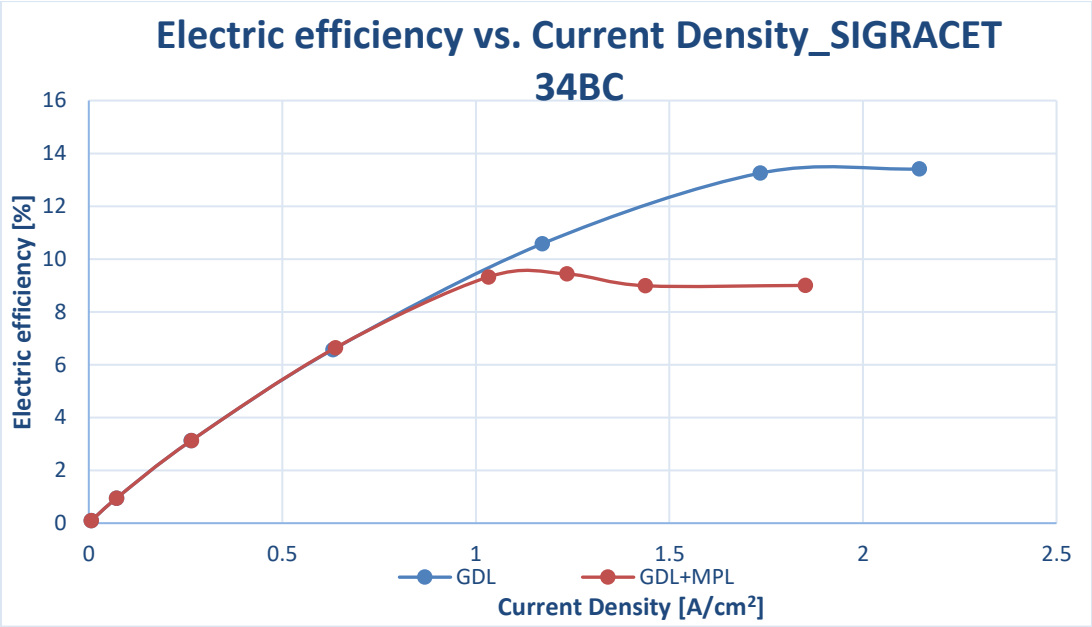

Figure 5-12 SIGRACET 34BC Electric efficiency- current density curve with and without MPL

In Figure 5-12 it is represented the comparison between the electric efficiency vs. current density curves for the SIGRACET 34BC case with and without MPL. As seen before, the efficiency curve is heavily linked to the power one, having almost the exact behaviour. The maximum of the case with MPL is achieved also at 0.65V with a 9.4% value, which has the same difference respect the AvCarb P75 and SIGRACET 34BA cases seen in Figure 5-6 and Figure 5-9 respectively as seen in the power curve. Contrary to what was seen before, the electric efficiency increases with the current until it reaches a maximum, without decreasing. In the case with MPL it slightly decreases to remain constant, while in the one without MPL it reaches to a plateau. I the latter, the maximum is achieved at 0.45V with a value of 13.4%, having the same difference with the other cases as the one seen on the power curves. Figure 5-10 SIGRACET 34BC polarization curve

5.6. TORAY TGP-H-090

This case did not have a MPL originally, so it is not a modification. It has a high electric conductivity, which will be appreciated when it is compared to the other cases. At 0.35V there was a convergency problem, where the values of the current density oscillated up to a 45% from one iteration to another, considering that for that point there was no solution.

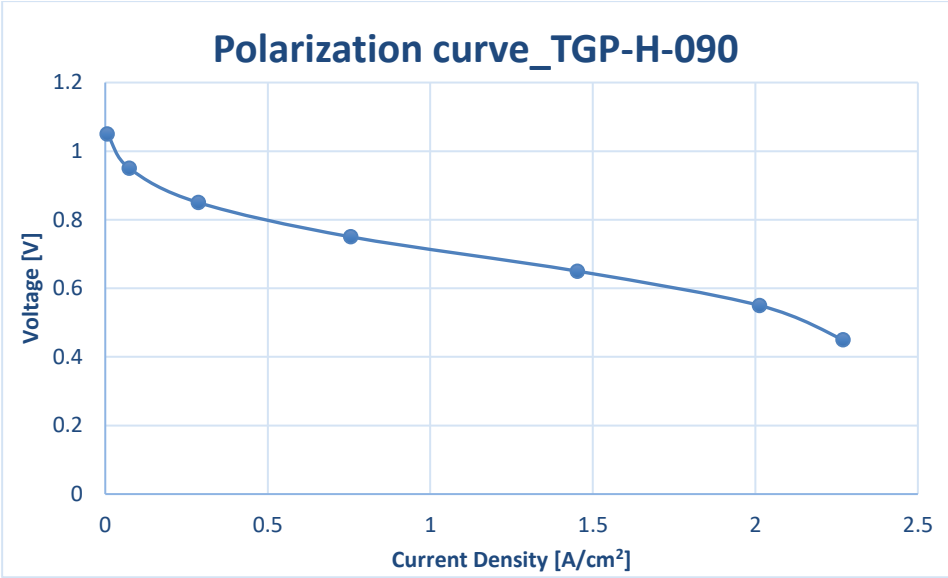

Figure 5-13 TORAY TGP-H-090 polarization curve

In Figure 5-13 it can be seen the polarization curve of the TORAY TGP-H-090 case. If it is compared with other cases without MPL, as in Figure 5-1, Figure 5-4 or Figure 5-7, it can be seen they all have a similar behaviour. The zone affected by the membrane ionic resistance in the central part has a smooth slope, not being completely horizontal. The sudden decrease due to oxygen transport problems is not as pronounced and almost vertical as on the cases with MPL seen in Figure 5-1, Figure 5-4 or Figure 2-5. It seems like the behaviour has been hindered, which makes sense since it is missing its last point.

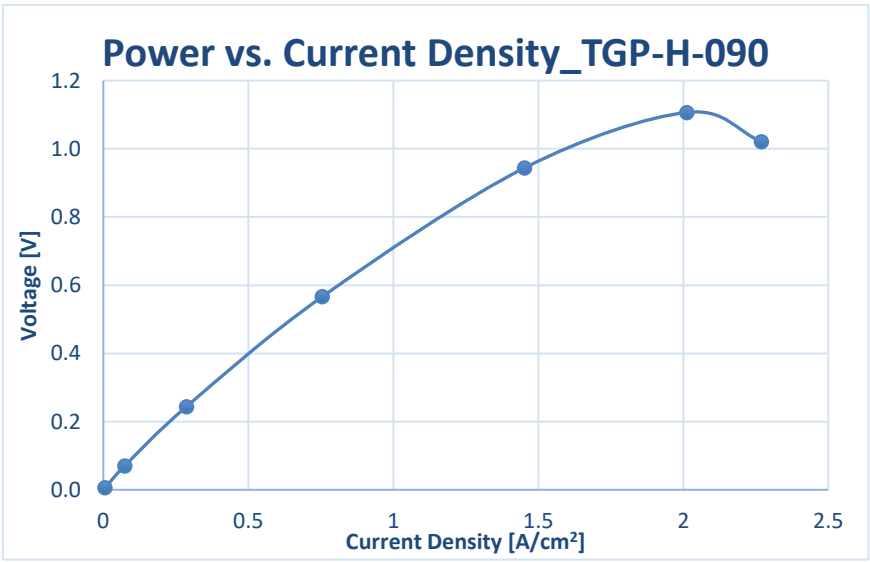

Figure 5-14 TORAY TGP-H-090 Power vs. current density curve

In Figure 5-14 it is shown the power vs. the current density for the TORAY TGP-H-090 case. The power increases with the current density until it reaches its maximum, starting a smooth decrease. This behaviour bears similarities with the one seen in other cases without MPL such as Figure 5-2, Figure 5-5, Figure 5-8 or Figure 5-11Figure 5-8. The maximum is achieved at 0.55V as in Figure 5-2 and Figure 5-4. Comparing the maximum with other cases without MPL there can be seen similarities mainly with the ones with higher electrical conductivities. AvCarb P-75 case has the same electrical conductivity and there is just a 2.3% difference among their maximum values. The base case has similar values with a 6.4% difference even if the conductivity is 3 times bigger, they both belong to the high conductivity range. There is a bigger difference with the SIGRACET cases, of between 12.8% and 14.2%, which may be linked to the difference in their electrical conductivities, being 5 times smaller.

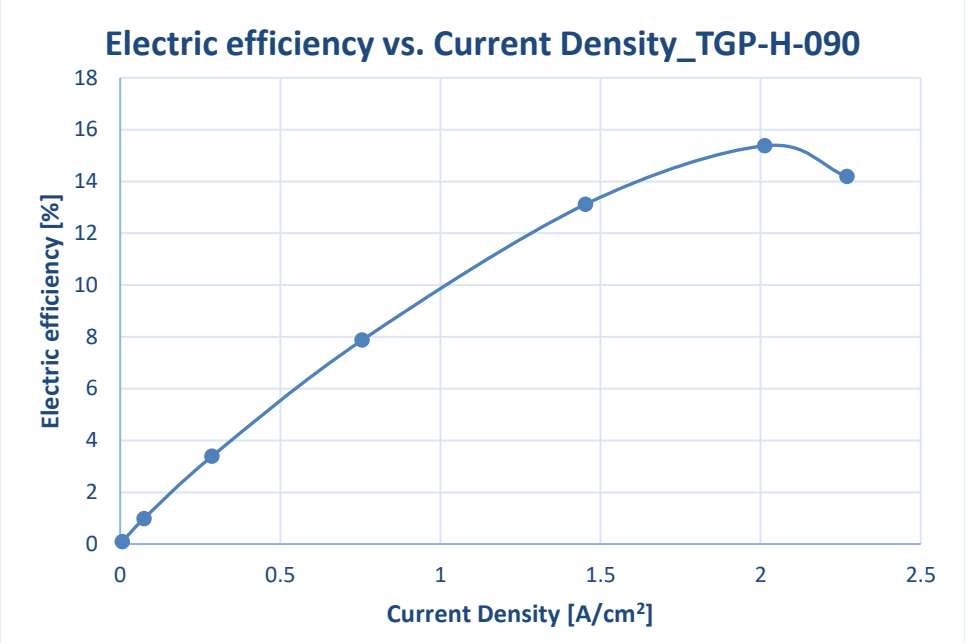

Figure 5-15 TORAY TGP-H-090 Electric efficiency vs. current density curve

In Figure 5-15 it is shown the electrical efficiency vs. the current density for the TORAY TGP-H-090 case. The efficiency increases with the current density, until it reaches its maximum, where it starts to slowly decrease. Its behaviour is heavily linked to the one seen in the power curve due to its dependency. Its maximum value is achieved at a 15.4%, having the same differences with other cases as the ones seen in the power curves.

5.7. Comparative study

The values obtained in the simulations will be shown in this subchapter, grouping all the polarization curves cases in one single graph with the same axis and scale, in order to compare the curves between them. This will also be done for the power vs. current density curves and the electric efficiency curves. It will serve as a summary before proceeding to a more detailed postprocessing. As mentioned before, the different values obtained in the simulations to create the different three graphs, will be shown in this subsection. Showing all the graphs in the same axis allow a better understanding and comparison.

I								V
Base case	Base case No MPL	AvCarb (GDL+MPL)	AvCarb (GDL)	SIGRACET 34BC (GDL+MPL)	SIGRACET 34BC (GDL)	SIGRACET 34BA (GDL)	TGP-H-090 (GDL)	
0.00628	0.00628	0.00628	0.00628	0.00625	0.00625	0.00624	0.00628	1.05
0.0747	0.0748	0.0741	0.0741	0.0718	0.0718	0.0714	0.0742	0.95
0.294	0.294	0.286	0.285	0.265	0.264	0.261	0.287	0.85
0.824	0.826	0.742	0.740	0.637	0.631	0.616	0.756	0.75
1.531	1.588	0.945	1.444	1.032	1.172	1.133	1.452	0.65
2.029	2.140	1.012	2.059	1.235	1.734	1.682	2.012	0.55
2.167	2.321	1.076	2.359	1.438	2.145	2.112	2.270	0.45
2.191	-	1.150	-	1.851	-	2.359	-	0.35

Table 5-2 Current densities obtained for each study case

The data that appears in Table 5-2 is used to create Figure 5-16, where I is representing the current density and V the voltage. In order to analyse the different curves obtained, the properties they possess (Table 3-1) have to be taken into account. The base case is represented in blue, the base case without MPL is in orange, AvCarb P-75 is in grey, AvCarb P-75 without MPL is in yellow, SIGRACET 34BC is in red, SIGRACET 34BC without MPL is in green, SIGRACET 34BA is in indigo and TORAY TGP-H-090 is in pink. This colour code will be

kept for the three graphs represented.

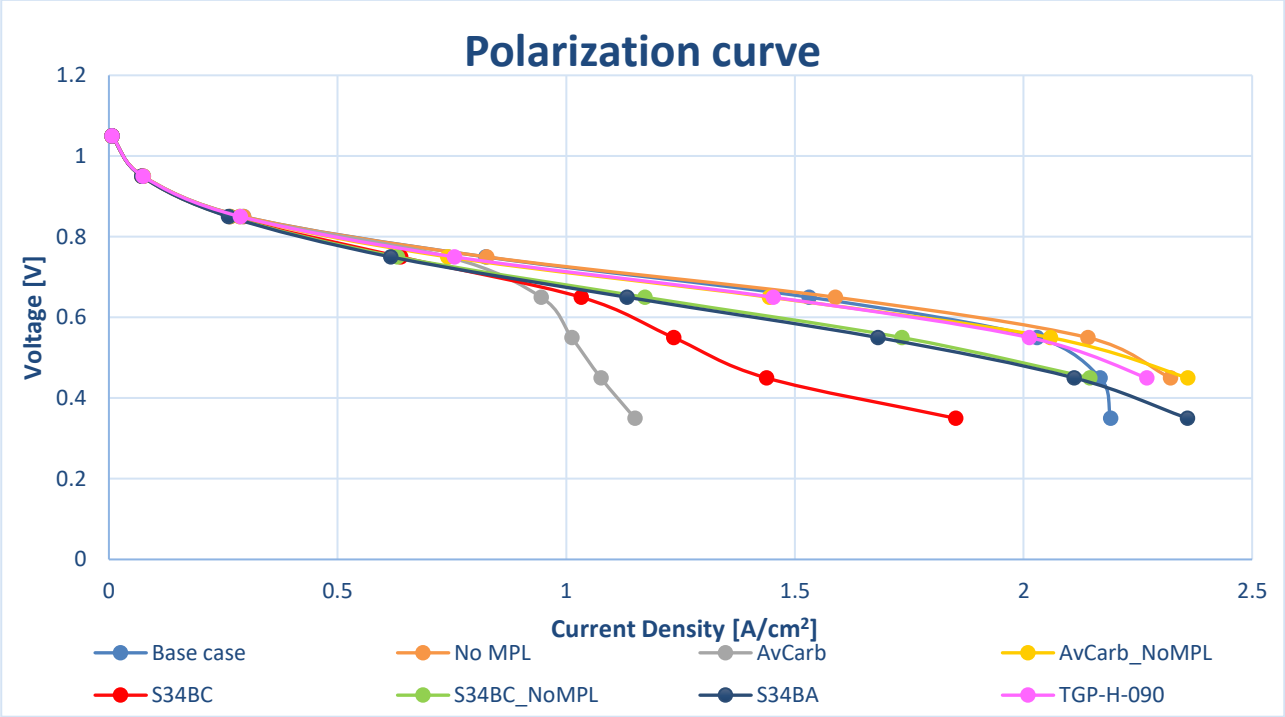

Figure 5-16 Compilation of all the study cases polarization curves

The AvCarb P-75 with MPL is an exception and compared to the rest of the curves it has a strange behaviour, which could be due the problematics that existed while looking to which exact GDL it corresponded. The properties were obtained from [40], a 11-year-old article. The actual AvCarb product version did not appear in current catalogues, being an old GDL, which is why its behaviour could be deemed worse that the others.

The graph can be divided in two zones of high and low electric conductivity. The SIGRACET are the lower conductivity GDLs, seeing clearly that they are below the other curves. Their conductivities are at least 4.4 times smaller than the other curves. The SIGRACET curves have the same permeability, differing a 11.1% their electrical conductivities, a 12.4% their thermal conductivities and a 10.7% their porosities. The differences are very small, but in they can be appreciated in the graph, having the SIGRACET 34BC slightly better behaviour than the SIGRACET 34BA, being above it. This main difference could correspond to the higher conductivity that the SIGRACET 34BC has. The cases with MPL have a worse behaviour than the ones without it, however the apparently better performance is hindered by the water content problems they face.

Above these curves can be seen the base case, TORAY TGP-H-090 and AvCarb P-75 without MPL. The two commercial GDLs have the same electrical and thermal conductivity of 1250 S/m and 1.7 W/m*K. Even if the difference between their permeabilities is of a 33.8%, they are on the same order of magnitude. The TORAY has apparently a slightly worse performance than the AvCarb without MPL. It could seem that the difference in permeability could affect it but since TORAY has a higher one, there must be other property that affects it, such as the porosity. TORAY has a 9% lower porosity, that seems to affect the behaviour, since the other properties were the same and the permeability was better. It is slightly below the AvCarb without MPL, also ending with a lower current density value. The base case is slightly above them. It has an electrical conductivity three times bigger, but its porosity is between 30 and 41.7% smaller than those other two cases, which seems to be detrimental, compensating the positive effect produced by the electrical conductivity.

Taking into account that small differences in the porosity seem to highly affect the behaviour, the lower porosity of the MPL can explain what seems a poorer behaviour when that layer is present.

P								V
Base case	Base case No MPL	AvCarb (GDL+MPL)	AvCarb (GDL)	SIGRACET 34BC (GDL+MPL)	SIGRACET 34BC (GDL)	SIGRACET 34BA (GDL)	TGP-H-090 (GDL)	
0.0066	0.0066	0.0066	0.0066	0.0066	0.0066	0.0066	0.0066	1.05
0.071	0.071	0.070	0.070	0.068	0.068	0.068	0.070	0.95
0.25	0.25	0.24	0.24	0.23	0.22	0.22	0.24	0.85
0.62	0.62	0.56	0.56	0.48	0.47	0.46	0.57	0.75
1.00	1.03	0.61	0.94	0.67	0.76	0.74	0.94	0.65
1.12	1.18	0.56	1.13	0.68	0.95	0.92	1.11	0.55
0.98	1.04	0.48	1.06	0.65	0.97	0.95	1.02	0.45
0.77	-	0.40	-	0.65	-	0.83	-	0.35

Table 5-3 Power obtained for each study case

The values obtained in Table 5-3 were used to create Figure 5-17, P representing the power and V the voltage.

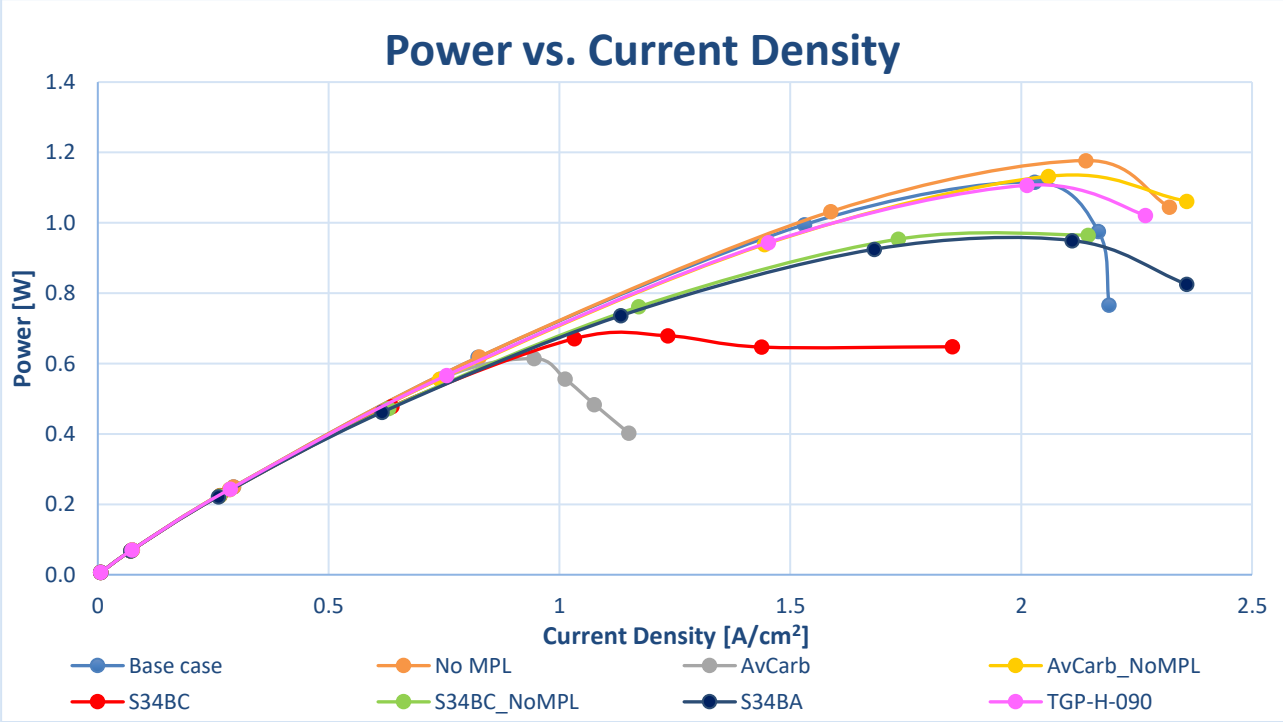

Figure 5-17 Compilation of all the study cases power-current density curves

The changes and differences mentioned in Figure 5-16 can also be seen in Figure 5-17. The differences between the polarization curves were more subtle, being able to see clearly which curve has a higher power such as between SIGRACET 34BC without MPL and SIGRACET 34BA, with just a 1.6% difference, and TORAY TGP-H-090 and AvCarb P-75 without MPL, with a 2.3% difference that was not assessed. The cases without MPL have a smoother decrease, leading to think their behaviour was stopped by the water content problems they faced.

The differences between the low and high electrical conductivity cases are seen clearly, where there is between a 14.7 and 23.9% difference, being ones around 0.95W and the others around 1.12W. The curves without MPL have a less steep decrease when they reach the maximum.

η_{el}								V
Base case	Base case No MPL	AvCarb (GDL+MPL)	AvCarb (GDL)	SIGRACET 34BC (GDL+MPL)	SIGRACET 34BC (GDL)	SIGRACET 34BA (GDL)	TGP-H-090 (GDL)	
0.09	0.09	0.09	0.09	0.09	0.09	0.09	0.09	1.05
1.0	1.0	1.0	1.0	0.9	0.9	0.9	1.0	0.95
3.5	3.5	3.4	3.4	3.1	3.1	3.1	3.4	0.85
8.6	8.6	7.7	7.7	6.6	6.6	6.4	7.9	0.75
13.8	14.3	8.5	13.0	9.3	10.6	10.2	13.1	0.65
15.5	16.4	7.7	15.7	9.4	13.3	12.9	15.4	0.55
13.6	14.5	6.7	14.7	9	13.4	13.2	14.2	0.45
10.7	-	5.6	-	9	-	11.5	-	0.35

Table 5-4 Electric efficiency obtained for each study case

The values of electric efficiency obtained in Table 5-4 were used to build Figure 5-18. V represents the voltage and η_{el} the electrical efficiency. The values obtained are too small because the hydrogen mass flow was kept constant, which is highly affected by it when the flow is not the adequate, as seen in [49].

As it has been said before, the behaviour seen in the electric efficiency curves is almost the same as the one seen on the power curves due to its heavy dependency. The differences between the cases were perceptually the same.

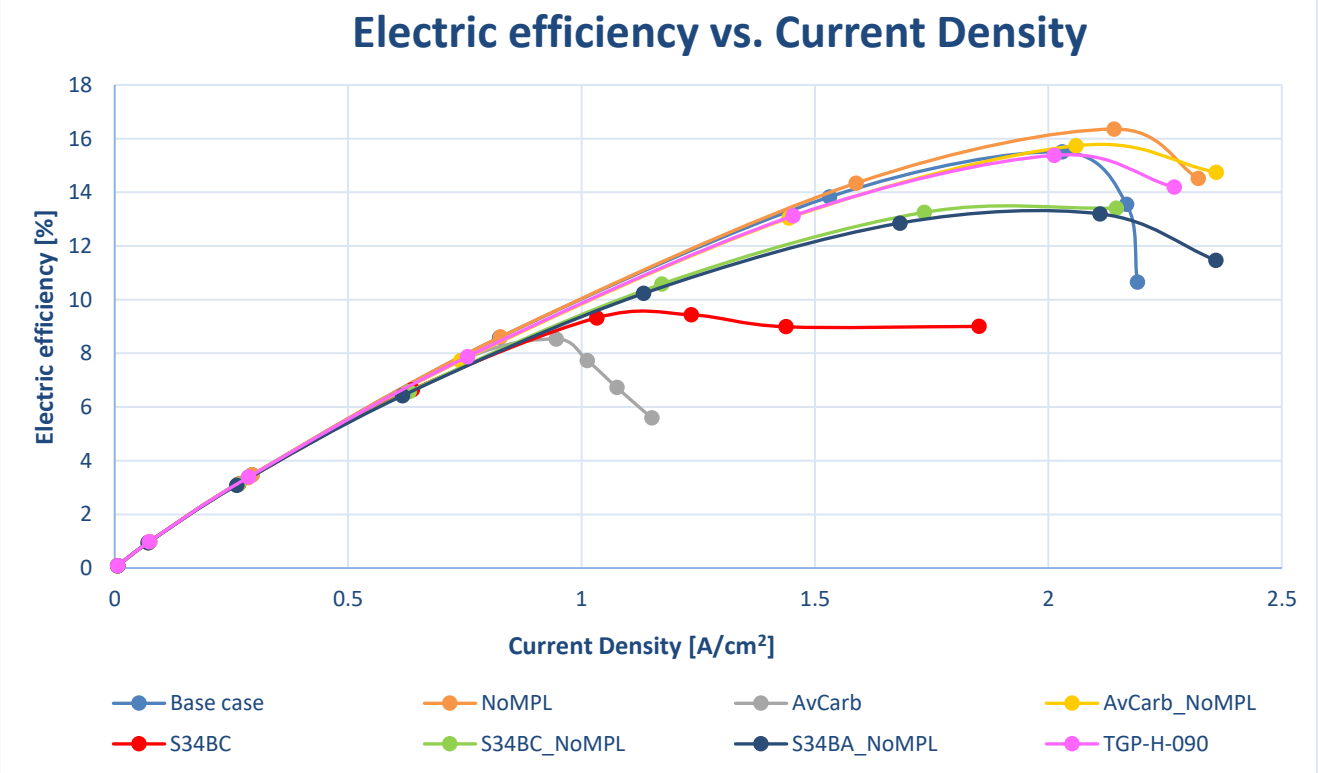

Figure 5-18 Compilation of all study cases electric efficiency-current density curves

The separation seen between the low and high electrical conductivities translates in efficiencies around 13.4% and 15.5% respectively, which does not seem a big difference.

5.8. Discussion of the results

A higher GDL electrical conductivity leads to higher power. This is not a direct relation since 4-5 times higher conductivity leads to 15-20% higher power but just in the case without MPL. The AvCarb P-75 had a strange behaviour, values 2 times smaller than its case without MPL. The SIGRACET 34BC case showed lower

values than the modification without MPL, but they were 42% smaller, not a difference as big as the other case.

The permeability and porosity seem to have an effect on the performance and output power. The TORAY TGP-H-090 and AvCarb P-75 without MPL only differences are the porosity, permeability and hydrophobic angle. Since it was stated in [1], [40] and [23] that an increase on the hydrophobic angle leads to better performance and water saturation, and the TORAY has a higher one, what leads to a lower power is the permeability and porosity. A permeability 20.5% higher and a porosity 8.2% higher lead to 2.5% increases of the power. Both cases were compared without MPL.

The SIGRACET cases had similar electrical and thermal conductivities but the permeability was the same. The SIGRACET 34BC has an electrical conductivity 11.1% higher, a thermal conductivity 12.4% lower and a porosity 10.7% lower than the SIGRACET 34BA. Nonetheless, the first one has an output power 1.6% higher, being able to conclude that the electrical conductivity is dominant over the other two properties. It could be possible that the porosity has no effect on the power since here is lower and in the permeability is the same, being possible that just the permeability affects it, or it has a bigger effect. Carcadea et al. [5] indicated that the porosity improved the performance but affected negatively the water saturation and structure. This could mean that the increase porosity effect is irrelevant compared to a lower electrical conductivity, being dominant.

6. ANALYSIS OF THE RESULTS

The results were later analysed closely with a postprocessing tool. Only the commercial GDLs were studied because the base ANSYS model was not the real behaviour they would have, but it was used a reference to see that the simulations worked smoothly, having no point a more thorough study. There were produced graphs of the average in the volume of a certain layer of a series of variables, where the points were obtained from each of the current densities studied (corresponding to a voltage of study). Then graphs of the evolution of some variables along lines created in given points were produced. Finally contour plots were created to show the evolution of variables in a mid-plane created.

6.1. Types of postprocessing

6.1.1. Average in the volume

They were done for all the commercial GDL cases. It was obtained the average in the volume of a variable in a layer for each voltage (and therefore for each current density), being the calculated variable the independent variable and the current density the independent variable [A/cm^2]. In this way the evolution could be compared to the one of the polarization curves.

The variables and the regions where they were studied are:

- Water saturation in the anode MPL [-].
- Water saturation in the anode GDL [-].
- Water saturation in the cathode MPL [-].
- Water saturation in the cathode GDL [-].
- Water saturation in the anode channels [-].
- Water saturation in the cathode channels [-].
- Oxygen mass fraction in the cathode MPL [-].

- Oxygen mass fraction in the cathode GDL [-].
- Oxygen mass fraction in the cathode CL [-].
- Maximum temperature in the membrane [K].
- Average temperature in the membrane [K].
- Water content (λ) in the membrane [-].

All of these variables were grouped between the ones with higher affinity to avoid overload of graphs. The water saturation in the anode was shown with the water saturation in the channels, where the first one appeared in the main axis and the later in the secondary axis. The water saturation in the cathode was graphed with the oxygen mass fraction, where the first one appeared in the main axis and the last one in the secondary axis. The variables measured in the membrane were all graphed together, were the water content appeared in the main axis and the temperatures in the secondary axis.

6.1.2. Evolution along a line

In Figure 6-1it can be seen the same image as in Figure 4-4, but in the foremost the locations of the points are clearly shown. On the points were created lines along the X coordinate, where the evolution of certain variables was studied.

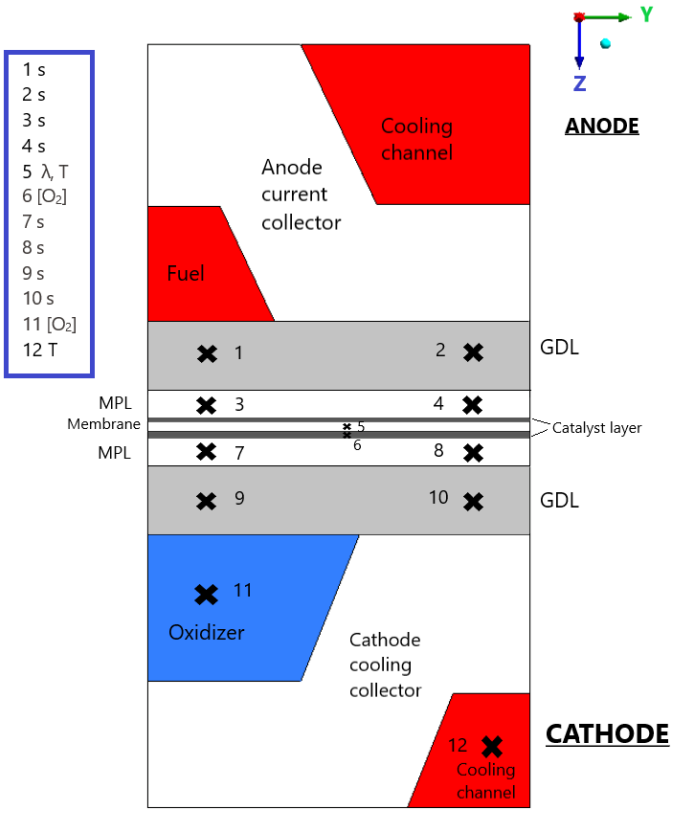

Figure 6-1 ZY plane PEMFC and the points position

On the porous layers there are 2 points in each, corresponding to under-rib and under-channel location. There are points in the middle of the membrane and the cathode CL. The others are in line with what quarter to the edge of the PEMFC in the Y axis in the positive and negative direction (on each side).

The variables studied are different in each point:

- [1]: water saturation [-] in the anode GDL under-channel.
- [2]: water saturation [-] in the anode GDL under-rib.

- [3]: water saturation [-] in the anode MPL under-channel.
- [4]: water saturation [-] in the anode MPL under-rib.
- [5]: water content (λ) [g of H_2O/kg of air] and temperature [K] in the membrane.
- [6]: oxygen mass fraction [-] in the cathode catalyst layer.
- [7]: water saturation [-] in the cathode GDL under-channel.
- [8]: water saturation [-] in the cathode GDL under-rib.
- [9]: water saturation [-] in the cathode MPL under-channel.
- [10]: water saturation [-] in the cathode MPL under-rib.
- [11]: oxygen mass fraction [-] in the oxidizer channel.
- [12]: temperature [K] in the cathode cooling channel.

This kind of postprocessing was only done for the cases where there was a MPL: AvCarb P-75 with and without MPL and SIGRACET 34BC with and without MPL; having a total of 4 cases studied here. The studied variables were the dependent variable and the X coordinate was the independent variable, taking measurements from 0 to 0.1m with a 0.001m interval, having a total of 100 points.

To not overcrowd memoir and see the evolution clearly, there were some groupings. A graph was produced with all the evolutions of the water saturation in the anode (1, 2, 3 and 4) and another separated one with the same but in the cathode (7, 8, 9 and 10). Another graph containing the oxygen mass fraction was created (6 and 11). Last was manufactured a graph including the water content and the temperatures (5 and 12), where the first one appeared in the main axis and the other ones in the secondary axis.

It must be studied at a certain voltage or current density, opting for medium (0.65V) and low (0.45V) voltages, obtaining two sets of each graph. It is intended to compare the low with the medium voltage and the case with MPL with the case without it.

6.1.3. Mid-plane contours

An in-plane in the membrane has been constructed along the X coordinate. In this way it can been seen the evolution of the variables in the membrane. It's a 0.001*0.01m plane in the YX plane, which can be seen in Figure 6-2, where the perpendicular line that appears, represents a plane cutting the PEMFC transversally in the middle of the PEMFC in the X axis.

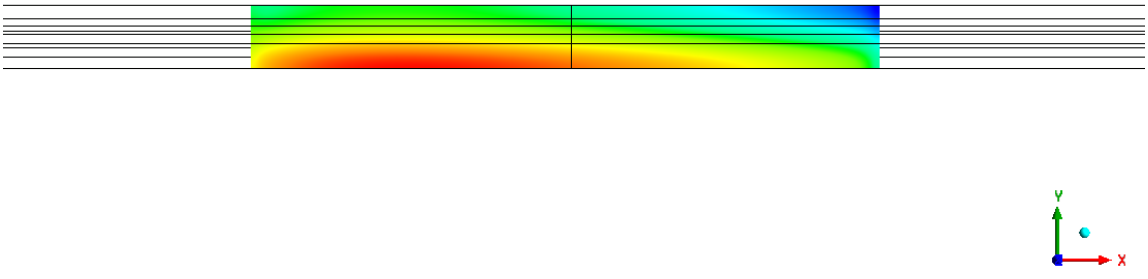

Figure 6-2 YZ view showing the mid-plane

In Figure 6-3, it can be seen another view of the mid- plane, in order to understand more clearly where it is located.

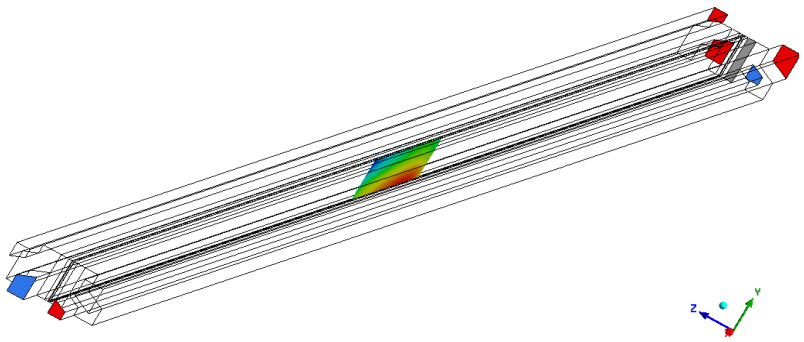

Figure 6-3 Rotated view of the PEMFC

This type of postprocessing was again only performed for the cases where there was a MPL and for low and medium voltages (0.45 and 0.65V) for the purpose of comparing the results between them, as in the evolution along a line analysis.

All the variables were measured in the membrane, since it is where the plane was located:

- Temperature [K].
- Water content (λ) [g of H_2O/kg of air].
- Z Current Flux Density [A/cm^2].

6.2. Average in the volume

All the graphs will have the same axis with the same scale in order to compare them correctly. This might cause that some of the curves that were completely visible with a different axis, are no longer visible because the values were a different order of magnitude.

6.2.1. AvCarb P-75

The water content (λ) is represented in blue, the average temperature in orange and the maximum temperature in grey. The main axis goes from 0 to 10 and the secondary axis from 341 to 376K. This colour scheme and axis scale will be kept for all the cases. In Figure 6-4 it can be seen the temperature and water content vs. the current density of the average in the membrane in the AvCarb P-75 case. Since its polarization curve went until 1.15A/cm^2, as seen in Figure 5-4, and the rest of the cases went further as seen in Figure 5-16, it appears as it has been cut but it is due to all the cases having the same scale.

An increase on the current density produces an increase on the temperature because the reaction is exothermic: the more current density there is, more water is being produced, heating up more. This can be extrapolated to the case of the water content because they are both related: an increase in the current density produces an increase in the water content because more water is being produced. It reaches a point where the water content starts to decrease, which takes place at high currents where the temperature is very high, making the water evaporate.

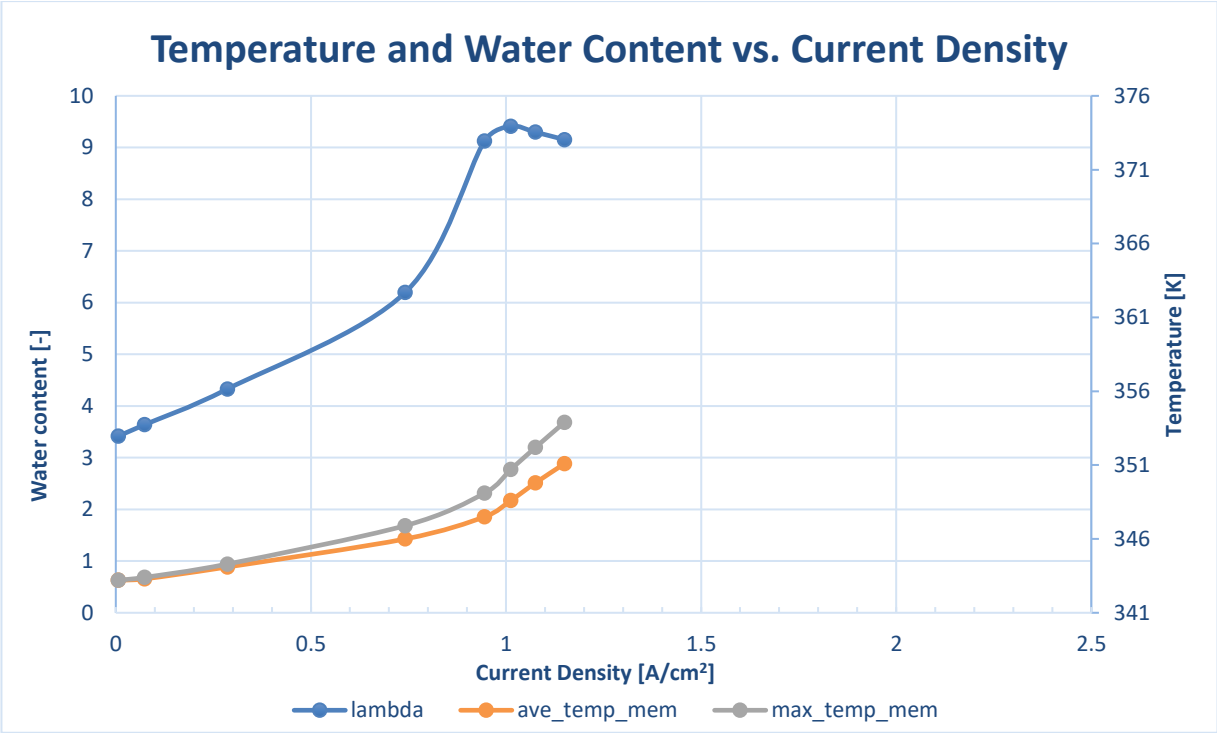

Figure 6-4 AvCarb P-75 temperature and water content vs. current density in the membrane

The maximum water content is produced where the maximum power was produced in Figure 5-5, at 0.65V with 9.41. The maximum temperature is 353.9K at high voltages, which means it will not have degradation problems because they appear at 100ºC. When the temperature gradient is higher than 5ºC, degradation problems appear. This is not a problem because the difference between the maximum and average temperature is of 2.8ºC, only at higher current densities. Both temperatures are the same up until 0.75V, where they start to diverge.

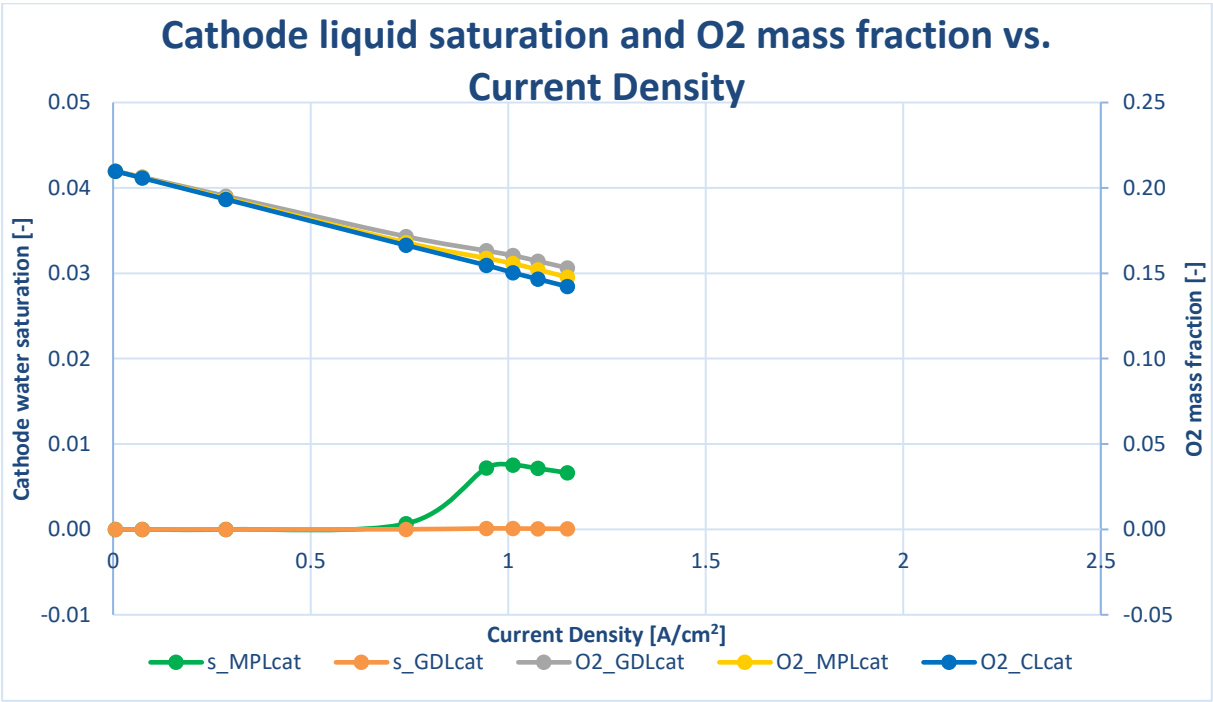

Figure 6-5 AvCarb P-75 liquid saturation and O_2 mass fraction vs. current density in the cathode

The O2 mass fraction is represented grey in the cathode GDL, yellow in the cathode MPL and blue in the cathode CL. The liquid saturation is represented green in the cathode MPL and orange in the cathode GDL.

The main axis goes from -0.01 to 0.05 (5%) and the secondary from -0.05 to 0.25 (25%). This colour scheme and axis scale are kept for all the cases to avoid confusions. In Figure 6-5 it can be seen the cathode liquid saturation and oxygen mass fraction of average in the in the cathode MPL, GDL and CL of the AvCarb P-75 case. As in Figure 6-4, it seems like the have cut, but it is due to the low current densities it achieved in its polarization curve in Figure 5-4.

The oxygen mass fraction is reduced with an increase in the current because more O_2 is being consumed. The layers that are closer to the channel are the ones that have a higher oxygen amount and while the distance from it rises, the oxygen mass fraction decreases due to a diffusion process. So, there is more O_2 in the GDL, then in the MPL and then in CL since it is the furthest from the channel, as it can be seen in Figure 6-5. The O2 mass fraction values oscillate from 0.21to between 0.148 and 0.142.

The liquid saturation increases with the current because more water is being produced. It reaches a point where it is starts to decrease because high temperatures evaporate the water. There is more water closer to the electrode, where it is produced, so the MPL will have a higher liquid saturation. The point where it starts to decrease and is also considered the maximum value is reached at 0.55V with a 0.75% saturation. The GDL liquid saturation is an order of magnitude smaller making it appear as if it is 0 (7.54e-3 vs. 1.75e-4).

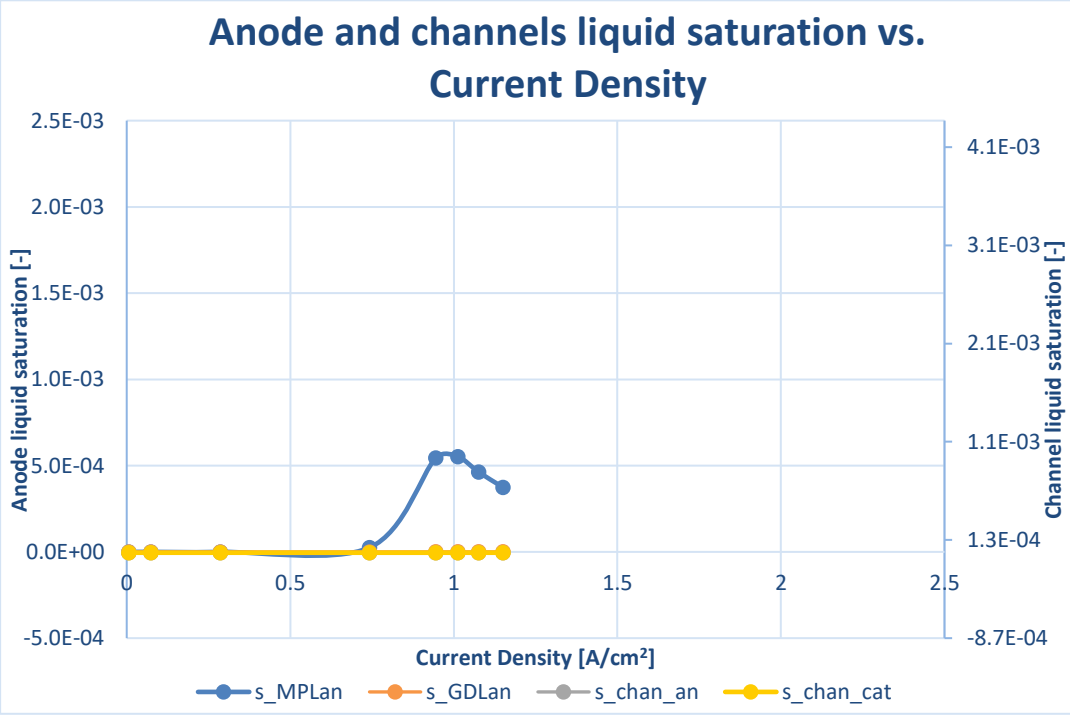

Figure 6-6 AvCarb P-75 liquid saturation vs. current density in the anode and channels

The liquid saturation is represented blue in the anode MPL, orange in the anode GDL, grey in the anode channel and yellow in the cathode channel. The main axis goes from -5e-4 to 2.5e-3 (0.21%) and the secondary axis from -8.7e-4 to 4.4e-3 (0.42%). This colour scheme and axis scale will be kept for all the cases to avoid confusion. In Figure 6-6 can be seen the liquid saturation in the anode MPL and GDL and anode and cathode channels against the current density of the average in the anode and channels. Again, the curves seem to be suddenly cut due to the low current density values obtained in the polarization curve in Figure 5-4.

The liquid saturation increases due to increase in water production with the current, until it reaches a point where high temperatures make the water evaporate, decreasing. In the layer closer to the electrode there will be more water, since it is closer to where it is being produced, having the MPL a higher liquid saturation that the GDL. The GDL liquid saturation is 3 orders of magnitude smaller than the one of the MPL, not being visible due to the smaller scale (4e-4 vs. 3e-7). The maximum point where it starts to decrease is achieved at 0.55V, with a 0.055% of liquid saturation in the MPL.

The liquid saturation in the channels have the same behaviour where they increase with the current until it reaches a point where it starts to decrease because the high temperatures evaporate the water. The liquid saturation is higher in cathode than in the anode channel, but none of them are visible because they have very small values, almost zero, being their maximum values 4e-11 and 5.5e-16.

6.2.2. AvCarb P-75 without MPL

This case does not have an MPL, but the place where it should be in the CFD PEMFC model is also the GDL, so it is made up by two GDLs, one closer to the channels and other to the CL. In Figure 6-7 it is shown the temperature and water content of the average in the membrane vs. the current density for the AvCarb P-75 without MPL case. These curves are not cut like the case with MPL seen in Figure 6-4, which is influenced by the range of their polarization curves seen in **¡Error! No se encuentra el origen de la referencia.**.

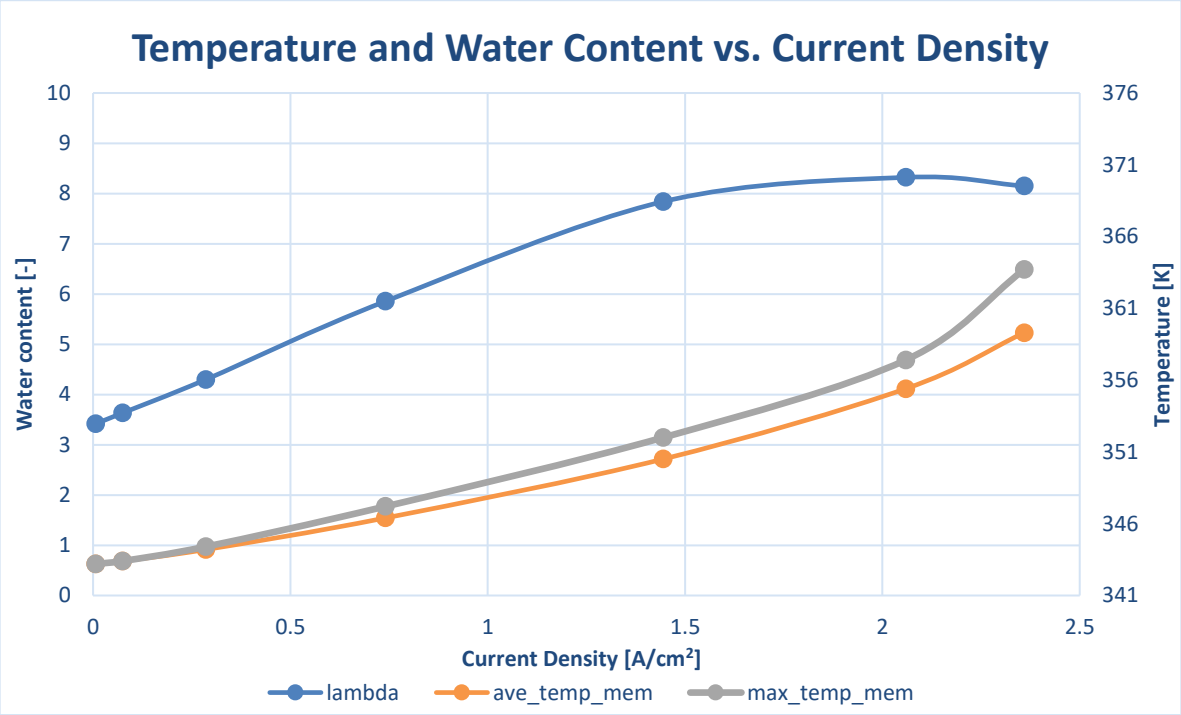

Figure 6-7 AvCarb P-75 without MPL temperature and water content vs. current density in the membrane

These curves have a softer evolution, with changes not so abrupt as in Figure 6-4. The maximum temperature is 363.7K, still below the upper limit where degradation appears, which is 2.7% higher than with MPL. It needs to be taken into account that the simulations could not continue to 0.35V because there were convergence and water content problems, so if both were compared in the same range, the difference would be bigger. The maximum temperature gradient is roughly below the maximum 5ºC, being 4.4ºC, a 36.4% increase with respect to having MPL. While in Figure 6-4 at 0.65V it faced a steepness of the slope, here it is seen at 0.55V and only for the maximum temperature curve and not both temperature curves. Both temperatures start to diverge again at 0.75V.

The maximum seen in the water content, where it starts to decrease due to water evaporation is 8.32, which is a 11.7% smaller than with MPL. In Figure 6-4 is seen that the maximum is achieved at 0.65V, here it is at 0.55V, being the curve displaced, even if had a larger range in the X axis. It has higher temperatures, making that the water evaporates more, decreasing its water content.

In Figure 6-8 it can be seen the liquid saturation of the average and oxygen mass fraction of the average in the cathode GDL and CL vs. the current density for the AvCarb P-75 case without MPL. This figure expands throughout the whole X axis range, contrary to Figure 6-5.

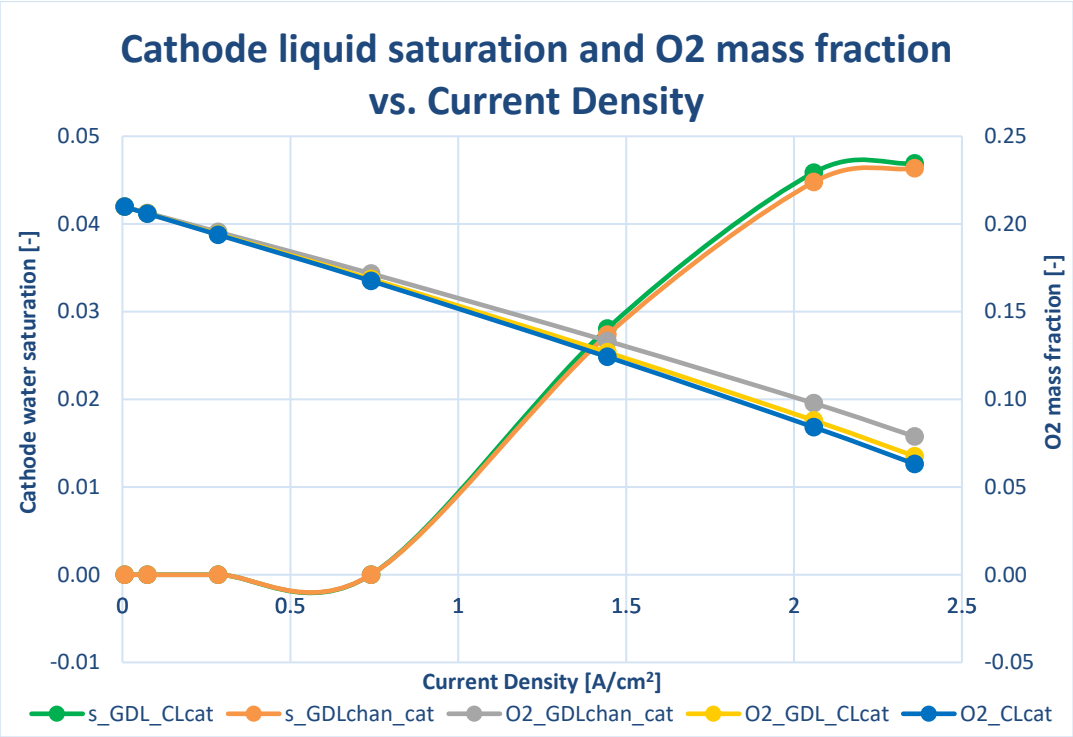

Figure 6-8 AvCarb P-75 without MPL liquid saturation and O_2 mass fraction vs. current density in the cathode

Even if both are part of the GDL, the distance the O2 has to travel still affects it form diffusing. The MPL is a less porous layer, making it more difficult to diffuse, which makes the difference between both layers smaller. In the case been studied right now there is a difference among these layers of 14.2%, while it was of just 3.5% when they were two completely different layers. In Figure 6-5 the minimum values achieved were between 0.153 and 0.142, while in Figure 6-8 those values were between 0.0788 and 0.0632, being less than half than with MPL.

In Figure 6-8 it can be seen clearly the difference between the MPL and GDL (in this case the side closer to the CL and to the channels), where there is more water closer to the electrode, since it is produced there, having both curves almost the same value. The maximum liquid saturation is achieved at 0.45V and since the temperature is getting higher it could be assumed that it would start to decrease there due to water evaporation, being 4.7% for the CL side and 4.6% for the channels side. The difference between both values is almost negligible. These values differ to the ones obtained in Figure 6-5, were having a MPL the maximum liquid saturation was achieved in the MPL with a 0.8% and the GDL was an order of magnitude below. Not having a MPL produced an 84% increase in the CL side, whereas the increment with respect to the channel side is 99.7%. The liquid saturation started to increase at 0.75V.

In Figure 6-9 it can be seen the liquid saturation of the average in the anode GDL and the channels of the AvCarb P-75 case without MPL. It expands throughout the X axis, opposite to what happened in Figure 6-6.

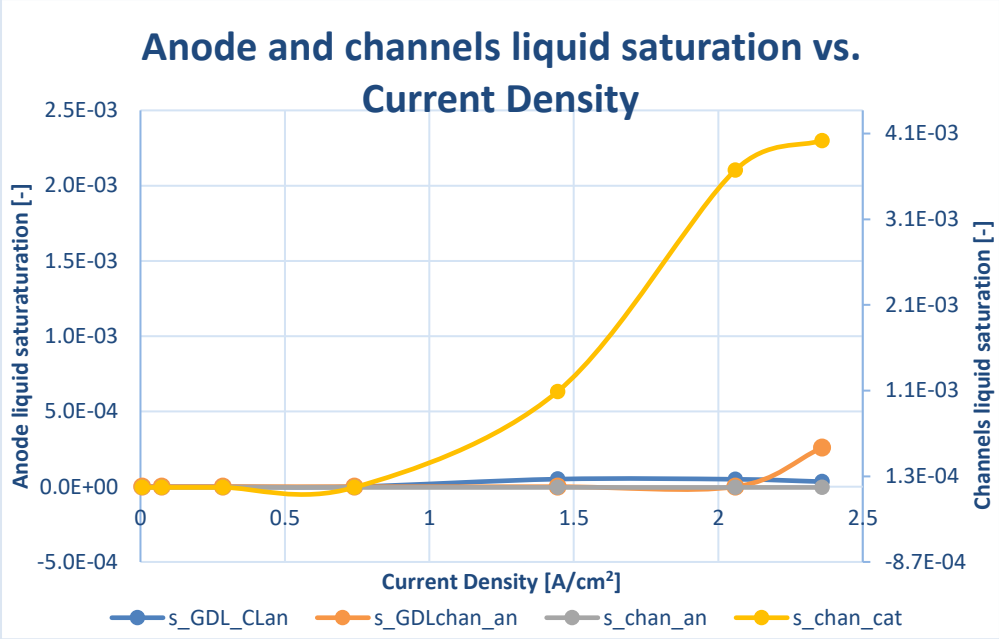

Figure 6-9 AvCarb P-75 without MPL liquid saturation vs. current density in the anode and channels

The GDL is divided in two, the part that previously corresponded to the MPL is the one on the CL side and the other one is the closer to the channel side. The liquid saturation increases with the current, until it reaches a point where it starts to decrease because high temperatures are achieved, which make the water evaporate. In Figure 6-9 the liquid saturation on the CL side of the GDL starts to increase at 0.65V, being its maximum, and then it starts to slowly decrease, but with low values that make the curve almost flat. The maximum liquid saturation achieved in the CL side is 0.005%. On the channel side of the GDL the liquid saturation does not start to increase until 0.45V, being its maximum since it is its last measurement value. It seems like the curve is translated on the X axis, delaying its take off. If it is compared with Figure 6-6 there are clear differences, the liquid saturation in zone closer to the CL has a higher liquid saturation with MPL, occurring its maximum a bit later at 0.55V an order of magnitude higher than without it. The liquid saturation in the zone closer to the channel is raised to the minus eighth power until it takes off with a 0.026% value at the end in the case without MPL. The case with MPL is raised to the minus seventh power, being possible to think that is had not taken off yet or it could be considered simply three orders of magnitude smaller. There is supposed to be more water in the zone closer to the CL, since it is produced there, but the increase on the porosity due to all those layers having the higher porosity of the GDL could highly affect it.

The liquid saturation in the anode channel seems again to be zero, but it reaches a value of raised to the tenth power, contrary to the raised to the sixteenth power in the case with MPL (4.14e-10 vs. 5.48e-16). They could both be considered negligible. The results obtained in the anode channel without MPL are similar to the ones in the cathode channel with MPL (4.14e-10 vs. 7.8e-11). The liquid saturation in the cathode channel has a great increase with respect to having a MPL, it can be seen it increases with the current, reaching its maximum at 0.45V with a 0.4% value. It is an enormous increase, considering before it was considered almost negligible and now it is 8 orders of magnitude higher being the most outstanding curve in Figure 6-9.

6.2.3. SIGRACET 34BA

This case does not have a MPL originally, so it is not a modification of another case. In Figure 6-10 it is shown the temperature and water content average in the membrane vs. the current density for SIGRACET 34BA.

The temperature increases with the current. The maximum temperature seen in Figure 6-10 is 375.4K, which is above 100ºC. This means this GDL will have degradation problems at high current densities. The CFD tool allows to see this, being able to avoid damage to the actual PEMFC. The temperature gradient is also too high for a safe operation, being 6.5ºC, a 30% above safety, leading to degradation problems. Both temperatures start to diverge again at 0.75V. The change in the slope that could be seen in Figure 6-4 at 0.65V and at Figure 6-7

at 0.55V just for the maximum temperature, is seen here in 0.55V mainly in the maximum temperature curve.

There is a 3.1% increase of the temperature with respect to the AvCarb case with no MPL in Figure 6-7, which has more similarities with it since it does not have a MPL. This difference might be related to the difference in the electric conductivity. A low conductivity makes that the PEMFC does not correctly evacuate the heat, warming up. The AvCarb conductivity is almost 4 times the SIGRACET 34BA (1250 vs. 254.6 S/m), leading to roughly a 3% increase in the temperature and approximately a 2.5% increase in the average temperature. If the absolute increments in the temperature where considered, the differences would be even higher.

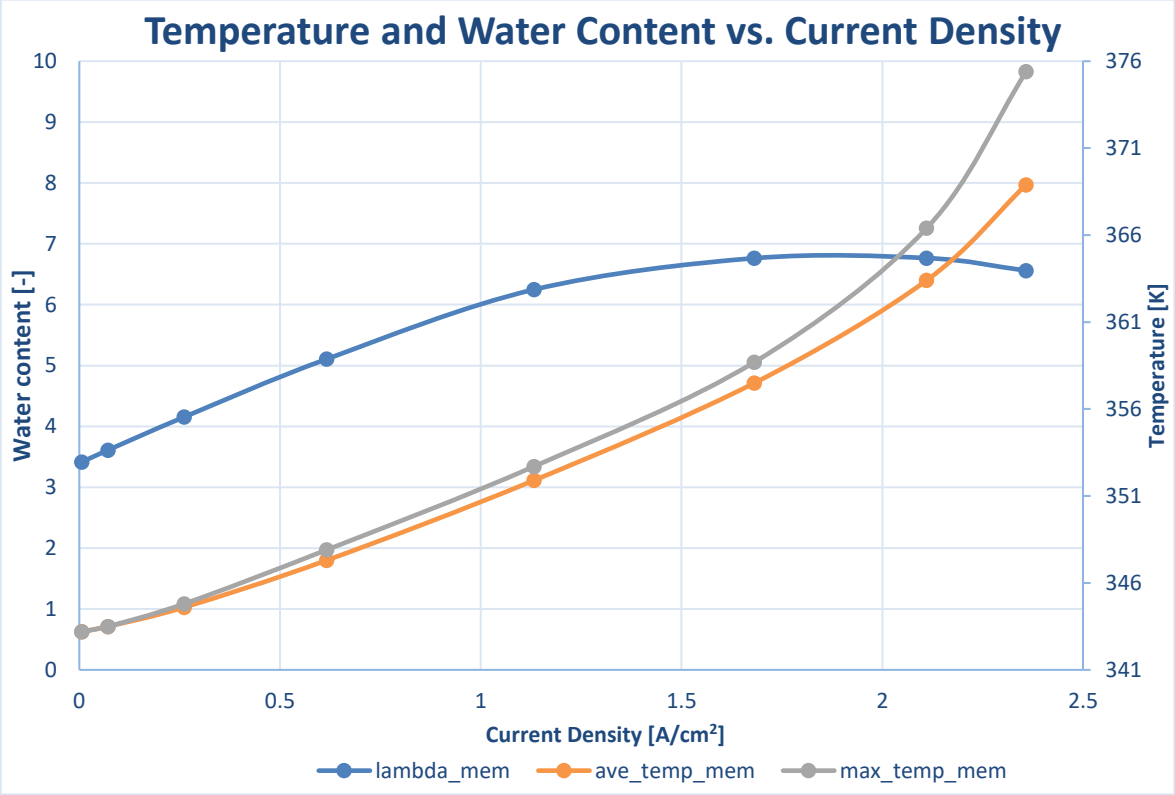

Figure 6-10 SIGRACET 34BA temperature and water content vs. current density in the membrane

The water content increases with the current until it reaches a point where it starts to decrease due to high temperatures evaporating the water. Its maximum is achieved at 0.45V and 6.77. The lower conductivity leads to the heating up of the PEMFC, which makes that due to the higher temperatures, the water evaporates before, obtaining lower water content than in other cases. This difference is even more notable than with the temperature with Figure 6-7, being of up to a 23% decrease. It seems that the maximum is also delayed, since it happens at 0.45V and in Figure 6-7 it was at 0.55V.

In Figure 6-11 it can be seen that oxygen mass fraction decreases with the current since it is being consumed. The layers closer to the channels have more and then it diffuses. The values are very similar to the ones seen in Figure 6-8, barely having a 0.4% difference among them in their minimum, almost negligible. These values differ from Figure 6-5, but as was seen before, the existence of the MPL makes the results completely different.

The liquid saturation starts to increase at 0.75V, as in Figure 6-8, until it reaches it maximum at 0.45V with a 3.1% at the CL side and 3.3% at the channel side. This behaviour seems to be inverted from the one explained on Figure 6-8, but it makes sense. The CL is where the water is being produced, so it should be where there is more, but it has also a higher temperature, since the reaction is taking place, leading to the evaporation of the water. The further from the membrane, the less water there would be, but since the temperature is lower, it is in liquid state, having more. This anomaly is produced by the higher temperatures produced by lower electrical conductivities. The decrease due to high temperatures is seen more clearly in the CL side, because the temperature there is higher, being accentuated at high current densities.

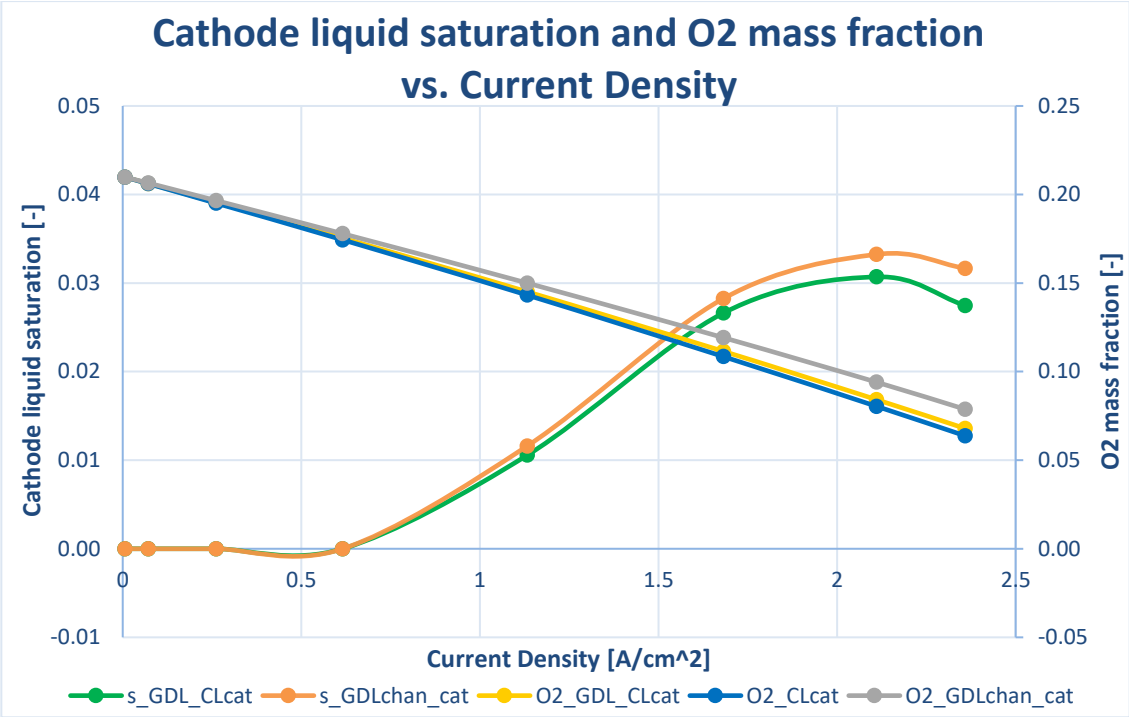

Figure 6-11 SIGRACET 34BA liquid saturation and O_2 mass fraction vs. current density in the cathode

Even if the conductivity is 4 times less than in Figure 6-7, the difference between the maximum values is of just a 1.6% and 1.3% in the CL and channel side respectively.

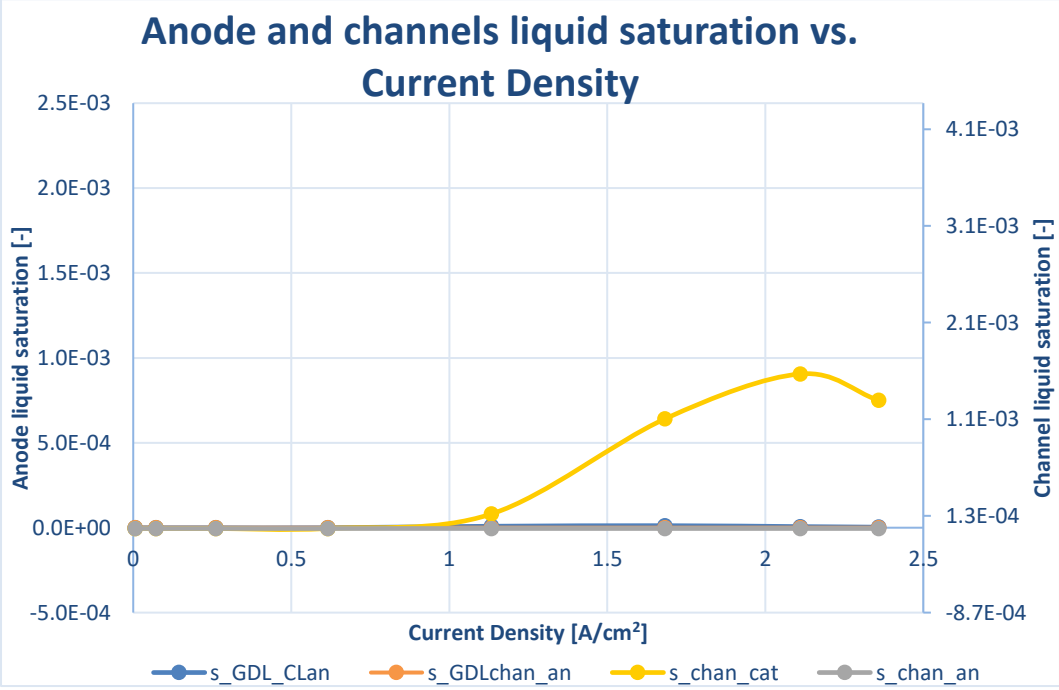

Figure 6-12 SIGRACET 34BA liquid saturation vs. current density in the anode and channels

The only completely appreciable curve in Figure 6-12 is the cathode channel liquid saturation, which increases until it reaches a maximum at 0.45V and 0.16% and then it decreases because due to the high temperatures at high current, the water evaporates. This value is a 60.5% lower from the one in Figure 6-9.

The anode channel liquid saturation could be again considered negligible seeing that its values are raised to the eighteenth power, eight orders of magnitude lower than in Figure 6-9, but on the same range as Figure 6-6, being possible that this curve has not taken off yet, considering that it could be said that most of its parameters were delayed in the X axis with respect to the AvCarb cases.

The CL side of the GDL will have more water than the channel side because the first corresponds to where the MPL would be, being closer to the membrane where water is being produced. It is not very clear, but the CL side curve seems to be slightly separated from the axis, which could be clearly seen in Figure 6-9. Both cases were in the same order of magnitude, but they were raised to the fifth power, against a third power axis, not being seen very clearly. Even if both were the same order of magnitude, Figure 6-9 was a value 4.2 higher than Figure 6-12, the difference being in its reduced visibility.

The liquid saturation in the anode GDL channel side was the same order of magnitude in Figure 6-9 as in Figure 6-12, until the first one suddenly increased up to a 0.024% value. It was been seen that most changes and shapes were delayed in the SIGRACET 34BA, as seen in Figure 5-7 compared to **¡Error! No se encuentra el origen de la referencia.** of AvCarb case, so it could be possible it had not taken off yet.

6.2.4. SIGRACET 34BC

This case includes a MPL and it was later simulated a variant without MPL in order to compare them both and see the effect of its presence. The curves extended through the X axis in current density range seen in Figure 5-10.

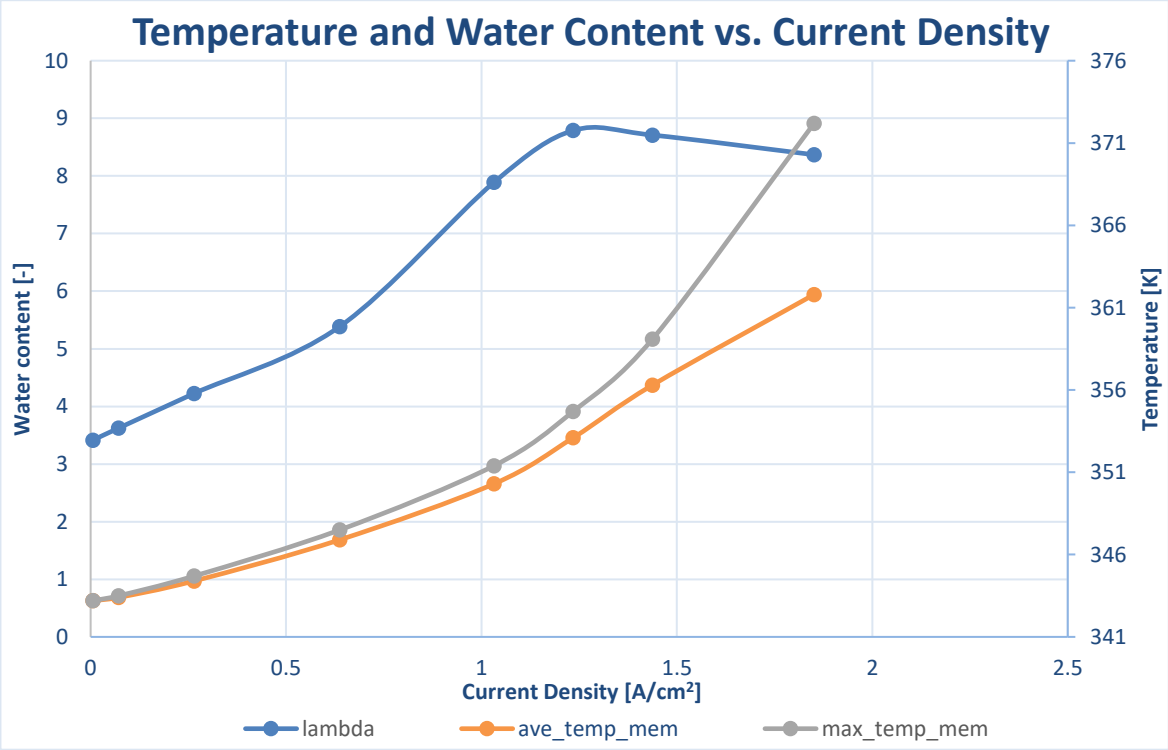

Figure 6-13 SIGRACET 34BC temperature and water content vs. current density in the membrane

In Figure 6-13 it is represented the average in the membrane of the temperature and water content vs. current density for the SIGRACET 34BC case. This case has a low electrical conductivity, leading to the heating up of the PEMFC. The temperature increases with the current density. The maximum temperature achieved is 372.2K, which is too close to the limit temperature of 100ºC where degradation starts being an issue. The temperature gradient is very high at high current densities, while in the previous cases it was 2.8, 4.4 and 6.5K for the AvCarb, AvCarb without MPL and SIGRACET 34BA cases respectively, here it is of 10.4K, a 37.4% higher than the closest case, being more than double than safety. In Figure 6-10 it can be seen that it had problems with its maximum temperature and temperature gradient, whereas in Figure 6-13 there is just trouble the temperature gradient.

Both temperatures start to diverge at 0.75V as in the other cases seen. The change on the slope is seen at 0.65V, been this change stronger in the maximum temperature curve.

The water content increases with the current density until it reaches a maximum, where it starts to decrease due

to the high temperatures achieved, that make the water evaporate. It suffers a change on the slope at 0.75V, something that could not be seen in Figure 6-10, Figure 6-7 or Figure 6-4. Its maximum is 8.79, achieved at 0.55V, as on the previous figures. This value is 23% higher than the one seen on the SIGRACET 34BA case, even if their properties bear similarities. The water content may be directly linked to the average temperature and not the gradient or maximum temperature. While there was a 8% difference between the average temperatures of both SIGRACET cases, there was a 2.8% difference with the AvCarb without MPL case, translating to just a 5.3% differences between their water content. The decrease seen in Figure 6-13 is smoother than the one seen in Figure 6-4, being almost constant, nonetheless still having similar behaviours, while the cases without MPL had in overall a behaviour with no steep slopes and smooth transitions. The reduced porosity of the MPL may contribute to a higher water content, since the water cannot diffuse outwards as easily, being the cases with MPL the ones with the higher values.

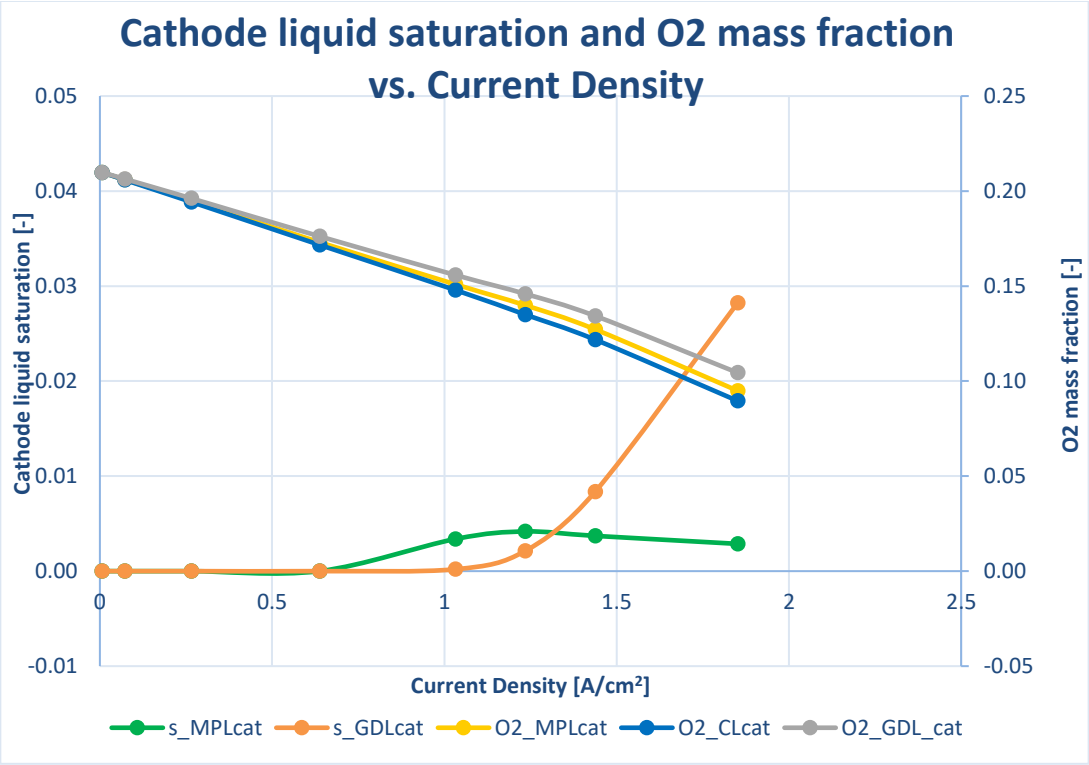

Figure 6-14 SIGRACET 34BC liquid saturation and O_2 mass fraction vs. current density in the cathode

In Figure 6-14 it is represented liquid saturation and oxygen mass fraction of the average in the cathode vs. the current density for the SIGRACET 34BC case.

The oxygen mass fraction decreases with the current density because it is being consumed in the electrode, the closer to it, the smaller the amount will be. In Figure 6-11, Figure 6-8 and Figure 6-5 it can be seen that the oxygen mass fraction evolution is completely lineal, whereas in Figure 6-14 there is a certain curvature. The values go from 0.21 to between 0.104 and 0.09. The cases without MPL had half the amount the AvCarb with MPL case had, but SIGRACET 34BC is situated between both. It is 27.3 and 27.6% higher than the SIGRACET 34BA and AvCarb P-75 without MPL respectively and a 53.6% lower than the AvCarb P-75 case. The MPL has a lower permeability and porosity, not allowing the diffusion of oxygen, lowering its reduction. Taking into account that a higher permeability allows a greater passage of oxygen ions, this explains why SIGRACET 34BC has a lower amount of oxygen than AvCarb P-75, since it has a 52.8% higher permeability.

In Figure 6-14 the GDL cathode liquid saturation increases with the current density due to more water being produced, starting at 0.65V, whereas in Figure 6-11 and Figure 6-8 it started at 0.75V, at 0.45V was there maximum and then they started to decrease. This does not happen here, ending in growing slope, which could mean, as it seems since growth was postponed, that the graph is translated in the X axis. Its maximum is 2.8% of liquid saturation.

The MPL cathode liquid saturation slightly increases due to the production of water, starting at 0.75V, until it reaches its maximum at 0.55V of 0.42%, slowly decreasing due high temperatures that evaporate it. The maximum value is almost seven times smaller than the one found in the GDL. As it was said before, there is supposedly more water in the MPL, since it is closer to the electrode where it is being produced, as seen in Figure 6-8, but it seems that it may have happened what could be seen in Figure 6-11 where both curves were inverted. The MPL is where most water should be, but it is also where there are higher temperatures, being the water in gaseous state, and given there is a lower temperature in the GDL, it condensed, ending up with a higher amount there.

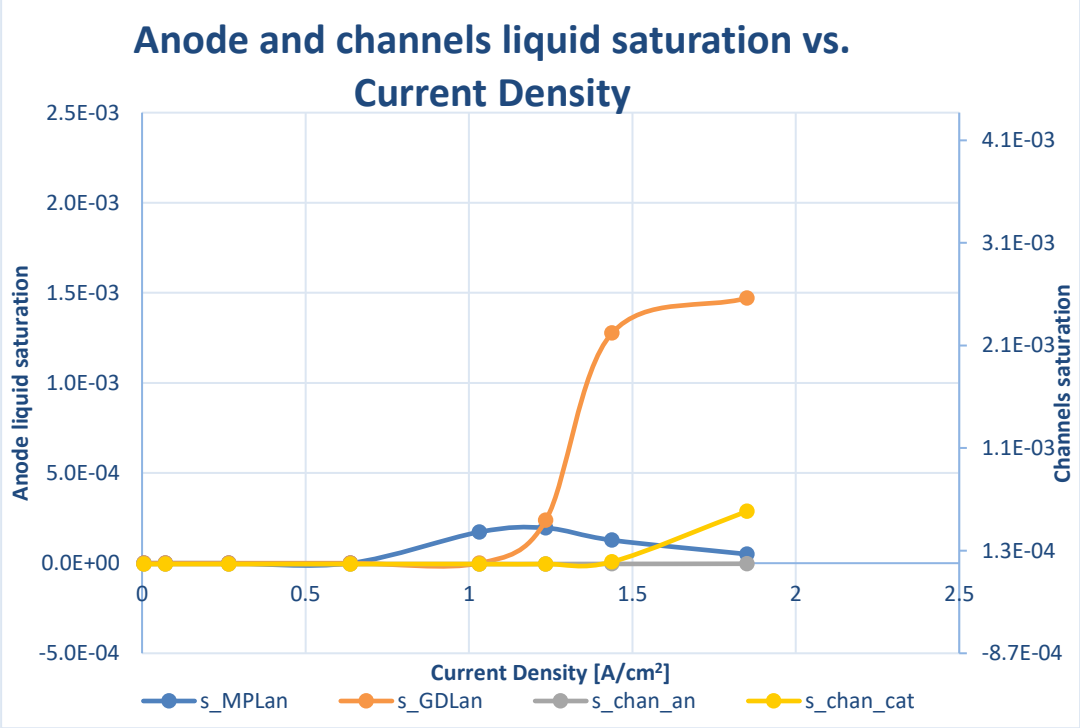

Figure 6-15 SIGRACET 34BC liquid saturation vs. current density in the anode and channels

In Figure 6-15 it is represented the liquid saturation average in the anode and channels vs. the current density for the SIGRACET 34BC case.

The channel cathode liquid saturation starts increasing at 0.45V, ending up with a 0.052% value. In previous cases, such as Figure 6-9 or Figure 6-12, the increase started much sooner and when it arrived at the maximum, it started to decrease due to evaporation caused by the high temperatures at high current densities, being almost one order of magnitude higher. The maximums seen were 3 and 7.9 times higher in the AvCarb P-75 without MPL and SIGRACET 34BA respectively than in the SIGRACET 34BC. I t is possible that the growth was delayed.

The channel anode liquid saturation seems again zero, but it is really raised to the sixth power, not being visible due to the scale of the graph and its axis. It is the highest value for the cases seen so far for this variable, where for AvCarb the values were raised to the sixteenth power, for AvCarb without MPL to the tenth power and for SIGRACET 34BC to the eighteenth power. It is between 4 and 12 orders of magnitude above the previous cases. It has to be taken into account that it has followed the same tendency as seen on the AvCarb without MPL case, where it started with values raised to the eighteenth power, progressing to raised to the tenth and in SIGRACET 34BC case continuing to being raised to the sixth power. It could be possible this evolution was hindered or translated in the X axis for the other cases.

The GDL anode liquid saturation starts increasing at 0.65V with an almost vertical raise, arriving to a horizontal zone around its maximum at 0.15%. The other case where this variable was visible was in Figure 6-9, starting the increase at 0.45V, so it could be possible that the increase was delayed there. It is also the highest value for this variable achieved at the moment. The SIGRACET 34BC maximum value is 5.7 times

higher than the AvCarb without MPL one. The other two cases values were 5 orders of magnitude smaller.

The anode liquid saturation in Figure 6-15 bears more similitudes with Figure 6-9 AvCarb without MPL case. As in Figure 6-12 and Figure 6-9, the MPL anode liquid saturation in Figure 6-15 experienced a slight increase until it reached its maximum, where it starts to decrease due to water evaporation produced by high temperatures. It starts increasing at 0.75V and the maximum is achieved at 0.55V with a value of 0.02%. There are not huge differences between the cases as with the channel liquid saturation, they are all around the same order of magnitude. The values reached in Figure 6-15 are around 4 and 10 times bigger than the ones in AvCarb without MPL and SIGRACET 34BA respectively. The curve in Figure 6-6 was a completely different shape, arriving to higher values, 3 times bigger than in the case in question.

6.2.5. SIGRACET 34BC without MPL

This case is a modification of the SIGRACET 34BC, substituting the MPL by enlarging the GDL, having it divided in two parts, one closer to the CL and another closer to the channels. This case had an error due to water content problems at 0.35V, not being able to complete the simulation range.

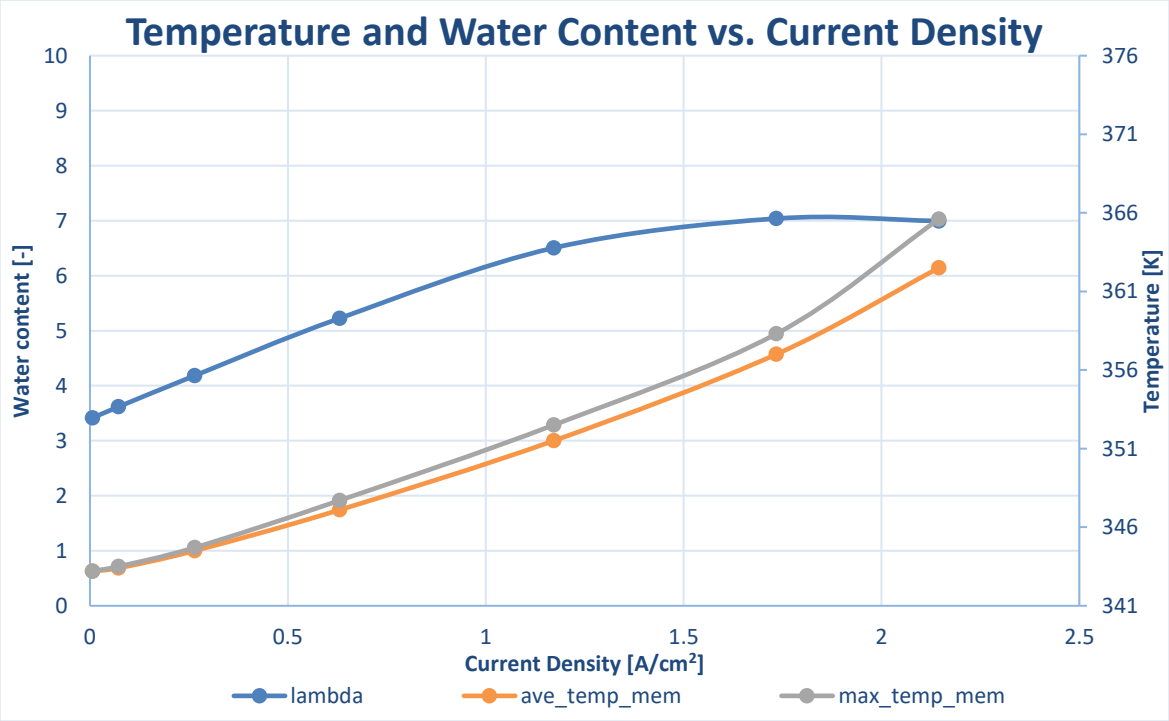

Figure 6-16 SIGRACET 34BC without MPL temperature and water content vs. current density in the membrane

In Figure 6-16 it is represented the average in the membrane of the temperature and water content for the SIGRACET 34BC without MPL case. It has a low electrical conductivity and the same properties as the GDL of the SIGRACET 34BC case.

The maximum temperature is not as high as the other SIGRACET cases, but it has to be taken into account that it misses one point. Both temperatures start to diverge at 0.75V and the slope changes at 0.55V, but only for the maximum temperature curve, similar to what happened in the other cases without a MPL in Figure 6-10 and Figure 6-7. Its maximum value is 365.6K, below the 100ºC upper degradation limit. The temperature gradient is just 3.1K, but if in Figure 6-13 is considered what values it had at 0.45V, they were smaller. Comparing at the same voltage, the maximum temperature was 6.5ºC below and temperature gradient was 2.8ºC. It could be considered that if it could have completed the simulations, the case without MPL would have a higher temperature. It needs also to be taken into account that intense divergence between the curves seen in Figure 6-13 was mainly produced between 0.45 and 0.35V and that the changes were produced at different current densities because the cases had different ranges.

There is just a 0.8% increase of the average temperature with the SIGRACET 34BC with MPL, but a 6.9% increase if it is compared at the same voltage, whereas the maximum temperature suffered a decrease. There is a 7.1 and 10.6% decrease on the maximum temperature compared to Figure 6-13 and Figure 6-10 respectively and a 2.1 and 12.7% increase compared to Figure 6-7 and Figure 6-4 respectively. There are more similarities with the other artificial case without MPL because both ended beforehand, having small differences. The percentage differences were not the same for the average temperature, and in some cases instead of a decrease there was an increase.

The water content increases with the current density, until it reaches a maximum at 0.55V, as in Figure 6-13, Figure 6-7 or Figure 6-4, later decreasing due to water evaporation caused by high temperatures at high current densities. The behaviour and shape are very similar to the other cases without MPL seen in Figure 6-7 and Figure 6-10, even if the last one had its maximum delayed. The maximum is 7.04. This value entails a 34.6, 19 and 25.7% decrease with respect to Figure 6-4, Figure 6-7 and Figure 6-13 respectively, while it is a 3.3% increase to Figure 6-10, being the closer values. Both cases with low electrical conductivity and no MPL had almost the same lower water content values. The low porosity and permeability of the MPL makes it difficult for the water to diffuse and stay and its absence produces the opposite, while the low electrical conductivity heats up the cell leading to additional evaporation, reducing the water content.

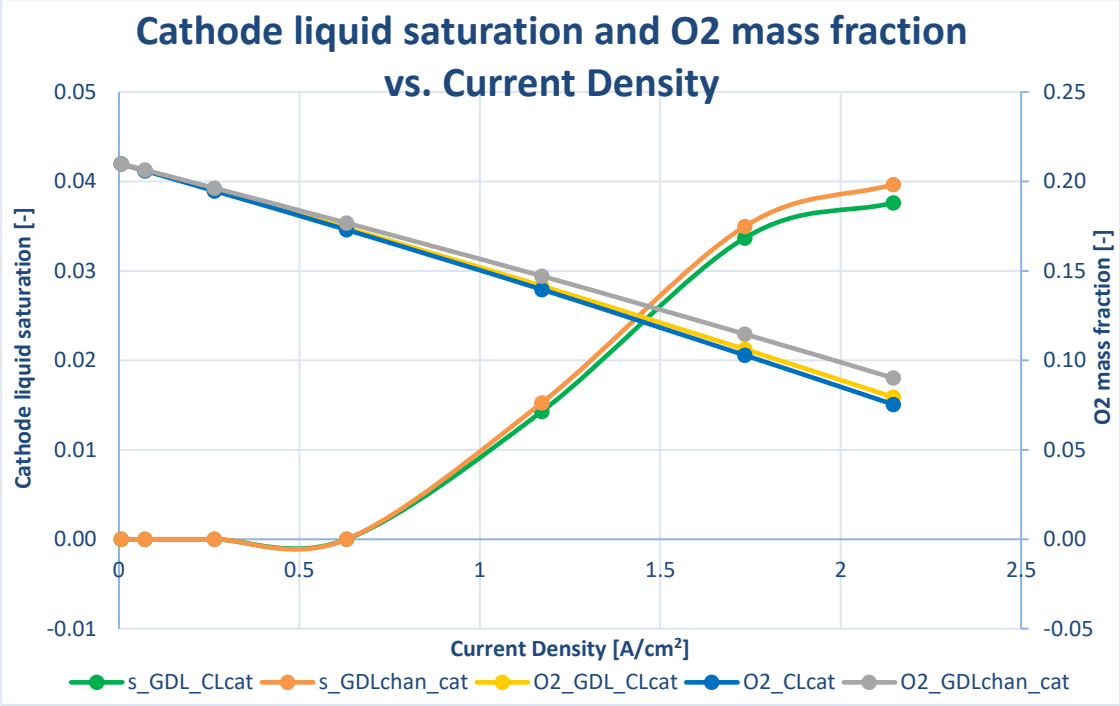

Figure 6-17 SIGRACET 34BC without MPL liquid saturation and O_2 mass fraction vs. current density in the cathode

In Figure 6-17 it is represented the liquid saturation and oxygen mass fraction average in the cathode for the SIGRACET 34BC without MPL case. The oxygen mass fraction goes from 0.21 to between 0.09 and 0.0754. As it was seen before, it is closer to the cases without MPL, showing a 14.6 and 14.2% increase with respect to Figure 6-8 and Figure 6-11. It shows a 81.2 and 18% decrease being compared to Figure 6-5 and Figure 6-13. It should be underlined that while in the AvCarb P-75 case the amount of oxygen reduced to half without MPL, in the SIGRACET 34BC case the difference the difference seen between having MPL or not was 80% smaller than in the AvCarb case. This contrast could be due to the lower porosity the SIGRACET 34BC has, existing a smaller difference between the porosity of the MPL and the GDL.

It can be seen that the oxygen mass fraction decreases with the current density because it is been consumed. The closer to the channels, the higher it would be, since it is further to the consumption point in the electrode.

The GDL liquid saturation curves have a similar shape to the ones seen in Figure 6-8 and Figure 6-11. Both

curves start increasing with the current at 0.75V, arriving to its maximum at 0.45V where there is a plateau. In Figure 6-11 it started to decrease at 0.35V due to evaporation produced by high temperatures but since that point could not be achieved in this case, the behaviour was hindered. In the zone closer to the CL there should be more water since it is produced there and then there would be less due to diffusion. However, the high temperatures produced by lower electrical conductivity make that the closer to the reaction, the hotter it is, evaporating the water and the further from there, the lower the temperature, leading to water condensation. Therefore, apparently the curve closer to the CL and the channels seem to be inverted as in Figure 6-11, which makes sense since the have similar electrical conductivities.

Starting with the zone closer to the CL, which would correspond to the MPL, its maximum value is 3.8%, making it a 24.8% smaller than Figure 6-8 and a 18.4% bigger that Figure 6-14, being in the order of magnitude and closer to those cases, which has no MPL. The cases with MPL differed a bit more from this value, being almost an order of magnitude smaller showing a 80% and 90.1% increase with respect to Figure 6-5 and Figure 6-14.

When looking at the zone closer to the channels, which correspond to the GDL, its maximum is 4%, making it a 16.8% smaller than Figure 6-8 and a 16.2% bigger that Figure 6-14, having a smaller difference with the cases without MPL. The SIGRACET 34BC case in Figure 6-14 does not have a value as distant as in the MPL, but the shape is completely different, delaying the increase up until 0.65V, being possible that the behaviour was delayed with respect to the X axis, being just a 28.8% smaller than the one shown in Figure 6-17. The values in Figure 6-5 were two orders of magnitude smaller, not being appreciable in the graph.

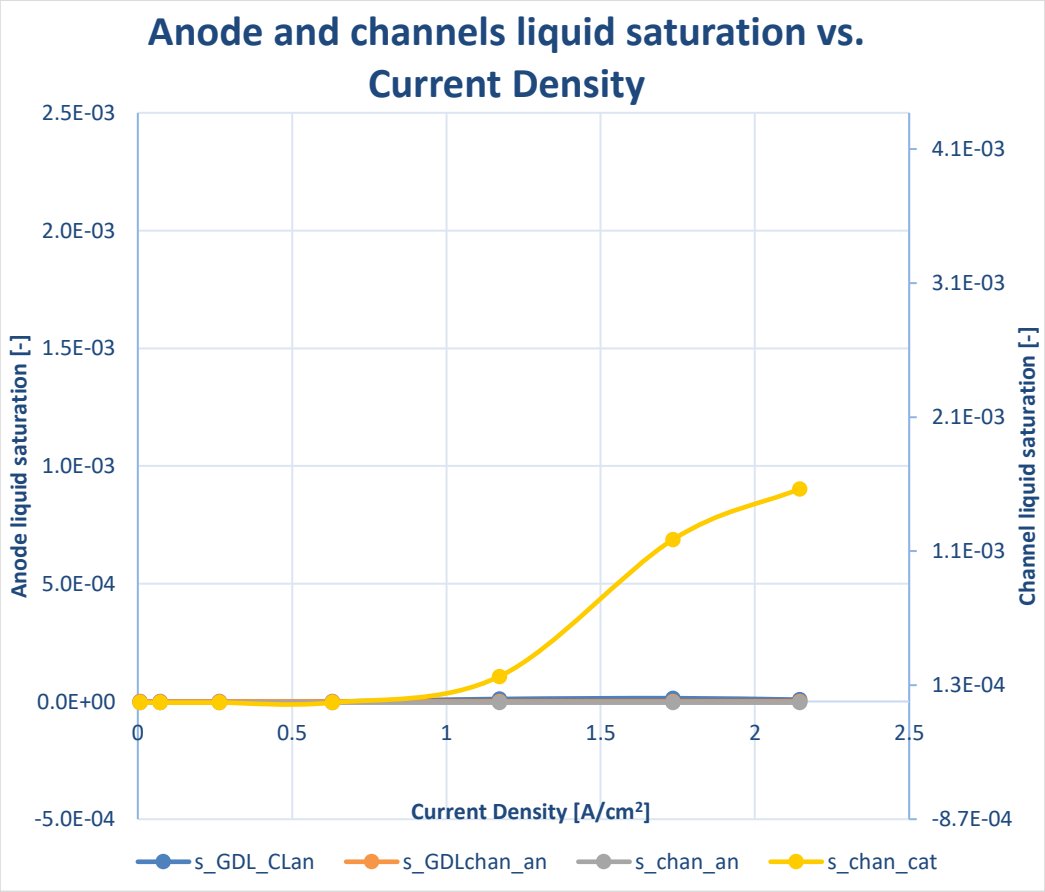

Figure 6-18 SIGRACET 34BC without MPL liquid saturation vs. current density in the anode and channels

In Figure 6-18 it is represented the liquid saturation average in the average in the GDL anode and the channels vs. the current density for the SIGRACET 34BC without MPL case. The only curve that is clearly visible is the cathode channel liquid saturation, it starts growing at 0.75V, until it reaches its maximum of 0.16% in a zone where there is a smaller slope. Its development is more similar to the other cases without MPL, where Figure 6-9 has the same behaviour but arriving to higher values, which could be influenced by the higher

electrical conductivity that would not make the PEMFC hotter, thus the water would be present in liquid form. In Figure 6-12 it can be seen more or less the same values and behaviour but when it reaches its maximum it starts to decrease, due to water evaporation caused by high temperatures produced at high current densities, which could be mainly due to the missing final point of 0.35V implying that if the simulation could be finished it would have continued with that behaviour. It 2.5 times and just a 0.3% smaller than Figure 6-9 and Figure 6-12, proving the first case is just scaled and the second is really similar since they have almost the same properties. Its case with MPL in Figure 6-15 is 67.7% smaller, being almost half. The values seen in Figure 6-6 are seven orders of magnitude smaller, not being in the same range as the rest of them.

Other of the lines that could be slightly differentiated form the axis is the GDL anode liquid saturation on the CL side, which is exactly the same behaviour seen in Figure 6-9 and Figure 6-12, both cases without MPL, and could be seen more clearly in Figure 6-15. It starts increasing around 0.75V, reaches its maximum at 0.55V with a 0.0014% value and starts decreasing due to water evaporation produced by high temperatures. All this behaviour can be seen clearly, it just can be seen that there is a curve that disengages from the X horizontal axis. It bears more resemblance with the cases without MPL, involving just a 14.3% increase from Figure 6-12 and is 3.6 times smaller than Figure 6-9. It makes sense that it is really similar to the other SIGRACET case without MPL, since they their properties have small differences. It is an order of magnitude smaller than the cases with MPL, having less differences with its version with MPL, being 13.9 and 39.3 times smaller than Figure 6-15 and Figure 6-6 respectively.

The anode channel liquid saturation cannot be distinguished, as in all the previous cases, seeming negligible and zero. Its maximum is raised to the eighteenth power, deeming it completely negligible. It bears more similarities with the other SIGRACET case without MPL, being in the same order of magnitude and just half its value. It is 2, 8 and 12 orders of magnitude smaller than Figure 6-6, Figure 6-9 and Figure 6-15 respectively. These cases start at raised to the eighteenth power and then take off leading to higher values and what could have happened is this case has not taken off yet since the simulation had been hindered.

In the liquid saturation in the zone closer to the channels there are really small values, where its maximum is raised to the nineth power, considering it negligible. It is completely opposite to its case with MPL in Figure 6-15, being the one with the bigger difference, being six orders of magnitude smaller. It is closer to the other SIGRACET case without MPL, being just a 35% smaller. It is 38.5 times and 5 orders of magnitude smaller than Figure 6-6 and Figure 6-9 respectively. It is the case with the lowest values for this variable yet seen.

6.2.6. TORAY TGP-H-090

This case originally did not have a MPL, it has a high electrical conductivity and there was a convergence error at 0.35V. There was not a floating-point error due to excessive water content, but did not converge after several iterations, having oscillations of up to a 45%.

In Figure 6-19 it is shown the temperature and water content average in the membrane vs. the current density for the TORAY TGP-H-090 case. The temperature increases with the current density, both curves starting to diverge at 0.75V and changing the slope at 0.55V, mainly the maximum temperature. The maximum temperature is 361.3K, still far from the 100ºC temperature at which degradation starts. It has to be taken into account that case could not finish the simulations and if it was possible, the temperatures would have finished even higher. It makes more sense to compare it to the other cases without MPL that could not end the iterations, since they had the same voltage. It is also where there are less differences, just a 3.3 and 5.9% decrease with respect to Figure 6-7 and Figure 6-16, being closer to the one that had the same electrical conductivity. There is a 10.1% increase and a 19.2 and 14.9% decrease compared to Figure 6-4, Figure 6-10 and Figure 6-13 respectively.

The average temperature ends in 356.9K, leading to a 3.8K gradient, being below the 5ºC degradation limit. Comparing the temperature gradients, it can be seen it is the same as in the AvCarb P-75 without MPL in Figure 6-7. Since AvCArb P-75 has the same electrical conductivity, even if it has a MPL, it is not as further as other cases implying a 36.4% increase from Figure 6-4, whereas there was a 47.7 and 136.4% decrease and a 29.6% increase with respect to Figure 6-10, Figure 6-13 and Figure 6-16 respectively, also showing

similarities with the cases that could not finish the simulation.

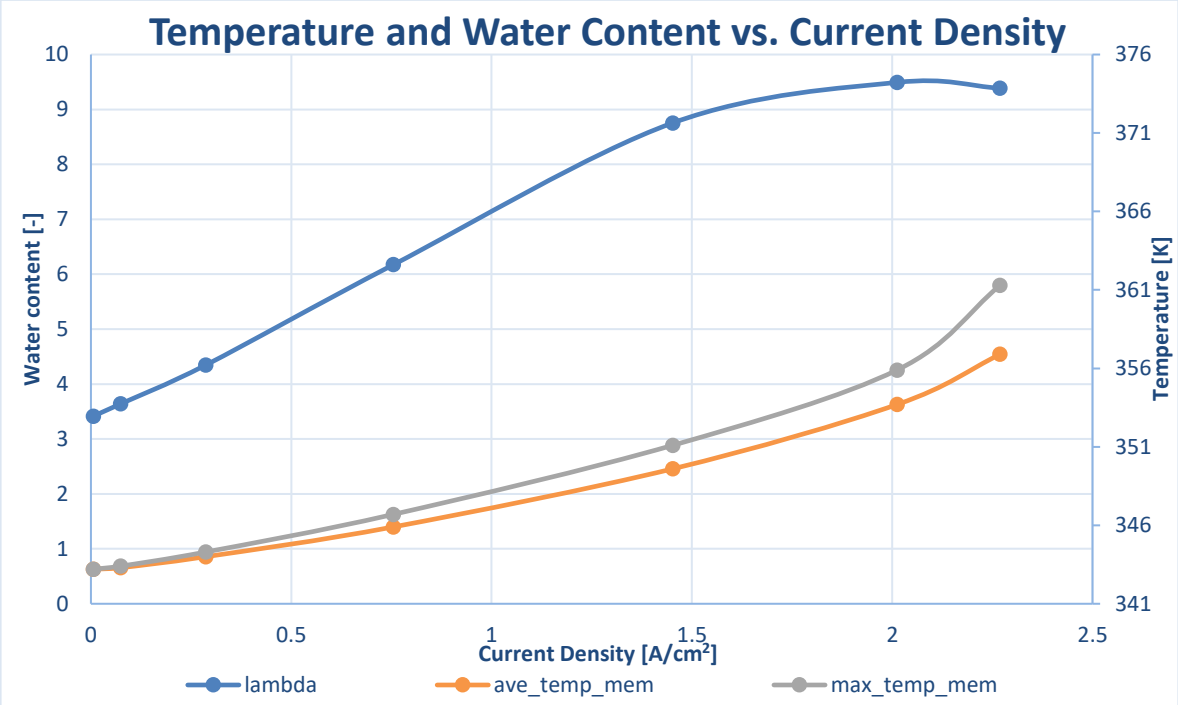

Figure 6-19 TORAY TGP-H-090 temperature and water content vs. current density in the membrane

It has a comparatively low temperature and high-water content, which are directly linked to the electrical conductivity, where having a high value avoid the heating up of the PEMFC and consequently the evaporation of liquid water, reducing its amount. The water content increases with the current density because it is being produced, but when it arrives to the maximum at 0.55V, it starts to slowly decrease. The descending slope is smaller than the one seen in Figure 6-13 because of the difference higher temperatures the second has. Its maximum is achieved at 9.49, which is the highest value seen for all the cases studied.

The AvCarb P-75 case has the same thermal and electrical conductivities as TORAY, which are also higher than the SIGRACET cases. Figure 6-4 has lower temperatures than Figure 6-19, which would not explain why there is more water. The permeability and porosity are 8.7 and 25.8% smaller respectively in the TORAY case, which means that the water being produced in the membrane would have more difficulties diffusing to the outer layers and therefore remaining there, making its value higher.

In Figure 6-20 it is shown the liquid saturation and oxygen mass fraction average in the cathode vs. the current density for the TORAY TGP-H-090 case. The O_2 mass fraction decreases with the current density because it is being consumed. The closer to the channels, the more there would be, later diffusing, being less in the CL, where it is being consumed. The oxygen mass fraction goes from 0.21 to between 0.0851 and 0.0696. Here there are more similarities with the other cases without MPL, having just a 8.5 and 8.1% increase and a 7.1% decrease with respect to Figure 6-8, Figure 6-12 and Figure 6-17 in that order. A smaller porosity than AvCarb P75 without MPL, makes the oxygen more difficult to diffuse, keeping it inside, making the amount bigger even if the other properties were almost the same. The cases with MPL presented a higher oxygen amount, implying a 94.2 and 26.4% decrease referring to Figure 6-5 and Figure 6-14. Taking into account the difference in electrical and thermal conductivities and the fact that the SIGRACET 34BC has a MPL with the porosity difference it implies, it can be concluded the conductivities highly affect the O_2 mass fraction, as well as the porosity of the mediums.

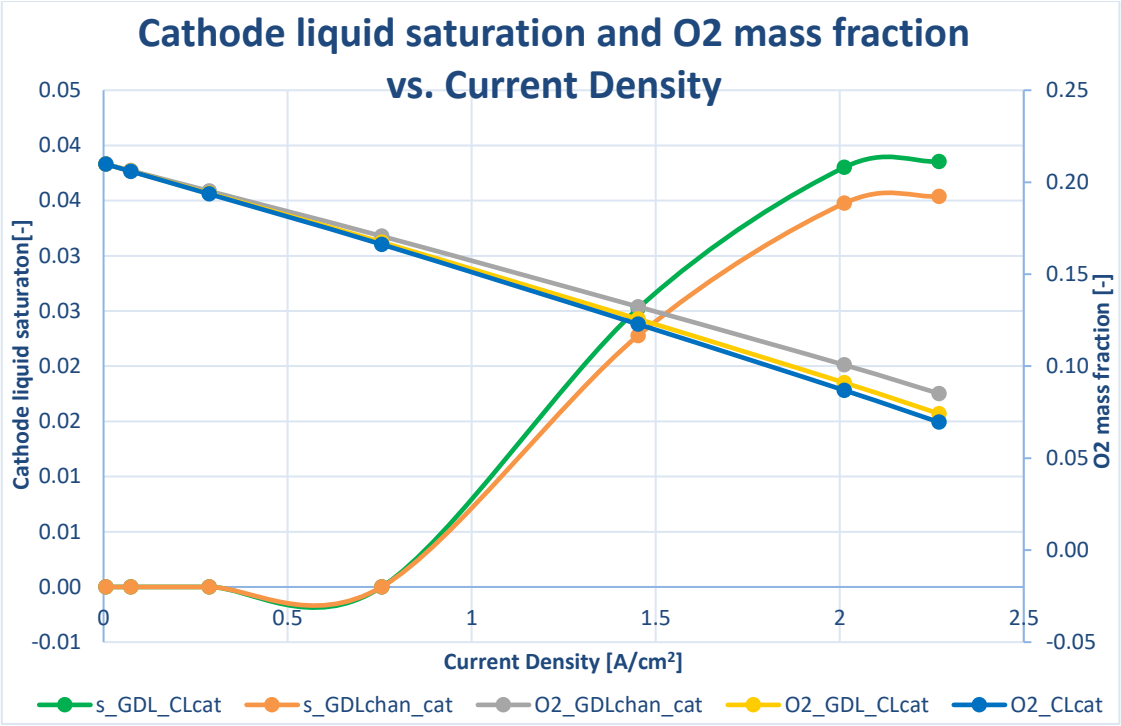

Figure 6-20 TORAY TGP-H-090 liquid saturation and O_2 mass fraction vs. current density in the cathode

The curves corresponding to the liquid saturation in the cathode follow the same behaviour as the one seen in the other cases without MPL, such as Figure 6-8, Figure 6-11 or Figure 6-17, where the water saturation starts to increase at 0.75V, arriving to a plateau at 0.55V, leading to a maximum and then decreasing its value. This decrease it not clearly seen, but it would have been more obvious if the simulation had been finished. At the point where the curves start to increase, they start to diverge leading to a parallel situation at the plateau.

In the zone closer to the CL there should be more water since it is produced there and it diffuses to other layers. This did not happen in Figure 6-11 and Figure 6-17 because the high temperatures evaporated the water closer to the CL, leading to a condensation closer to the channels because of lower temperatures. Here the temperatures are lower, not facing this problem, having the behaviour that was expected.

In the case of the zone closer to the CL, there are smaller differences with the cases that did not have a MPL, meaning a 21.7% decrease and a 20.3 and 2.4% increase to Figure 6-8, Figure 6-11 and Figure 6-17. SIGRACET 34BC without MPL and TORAY TGO-H-090 have very different electrical and thermal conductivities, but they have porosities that have just a 3.8% difference, which could mean that the porosity affects heavily the cathode liquid saturation in the zone closer to the CL. The cases with MPL face higher difference of 80.5% and 89.2% in Figure 6-5 and Figure 6-14.

In the case of the zone closer to the channels, those differences held with other cases without MPL change completely. In the AvCarb P-75 without MPL case, the difference increases to 30.9%, while the SIGRACET 34BA plummets to 6.1% and the SIGRACET 34BC without MPL changes its tendency, implying a decrease and not an increase of 12.1%. These differences may be due to mainly the inversion of both curves seen in the cases with lower conductivities. The differences that maybe seen with the cases with MPL are not as comparable because the shape and behaviour has nothing to do, being 2 orders of magnitude and a 20.23% bigger than Figure 6-5 and Figure 6-14. The SIGRACET 34BC case with MPL seems that its increase has been delayed, since the curve looks displaced in the X axis.

In Figure 6-21 it is shown the liquid saturation average in the anode and channels vs. the current density for the TORAY TGP-H-090 case. If it is compared with the rest of the cases, its behaviour is like Figure 6-9 but some of its variables are magnified.

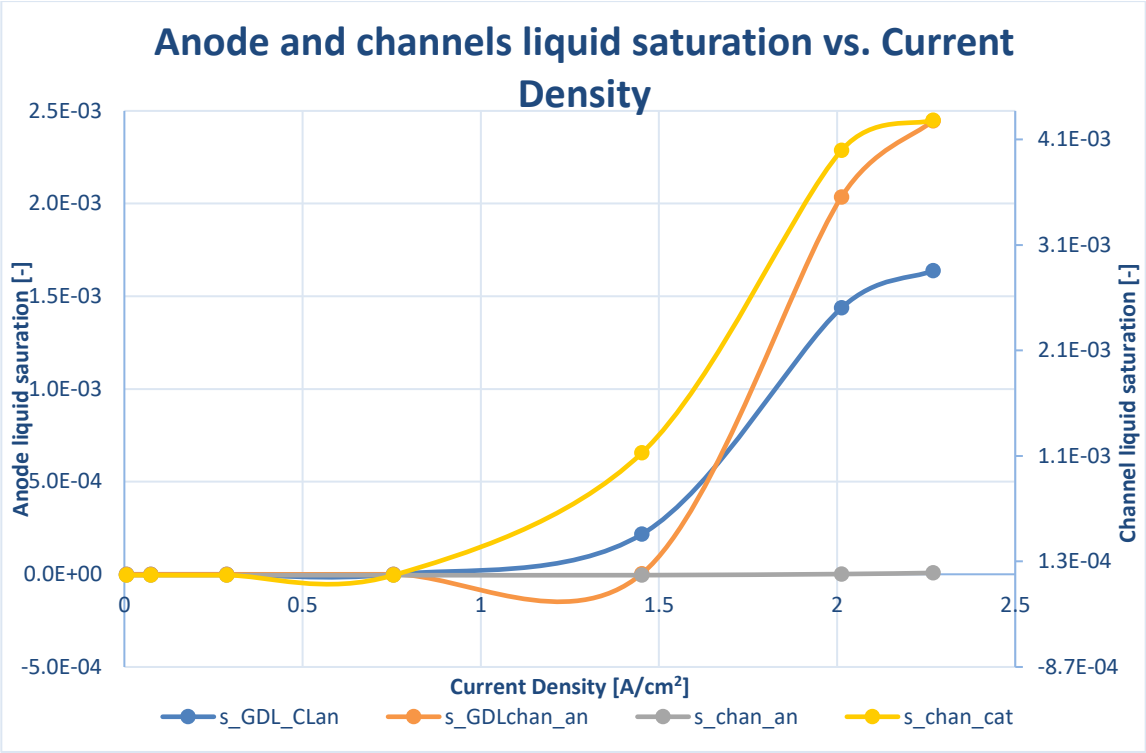

Figure 6-21 TORAY TGP-H-090 liquid saturation vs. current density in the anode and channels

The liquid saturation in the cathode channel starts increasing at 0.75V, until it reaches to its maximum at the end of its range with a 0.43% value, being the highest value achieved of the variable in question for all the study cases. It is safe to assume that if it could have finished the simulation the curve would have started to decrease due to evaporation caused by high temperatures at high current densities, since it has arrived at a plateau. This shape and maximum value are almost the same as the one seen in Figure 6-9 with just a 6.1% difference. The cases without MPL have the closest values, being in the same order of magnitude, where there is a 62.9 and 63% increase with respect to Figure 6-12 and Figure 6-18, having similar differences with both SIGRACET cases without MPL. There is a 88.1% increase to Figure 6-15 since there was not a great difference with the SIGRACET cases without MPL, whereas the AvCarb P-75 case is 8 orders of magnitude smaller. All these makes this case the one with the highest cathode channel liquid saturation of all the cases studied.

The anode channel liquid saturation seems again to be zero. The maximum value achieved is 0.0021%, being the highest value achieved for this variable for all the study cases, though it could be also deemed negligible. The behaviour is as the one seen before, where it starts around a number raised to the eighteenth power, decreasing to raised to the tenth and then to the sixth/fifth power. This happened to Figure 6-15, remaining in raised to the sixth power, being 7.7 times smaller than the case in question, or to Figure 6-9, remaining raised to the tenth power. The other cases seemed they did not take off, since they all started in the same numbers but some of the cases increased and others did not, remaining cases in Figure 6-12 and Figure 6-18 in raised to the eighteenth power and Figure 6-6 raised to the sixteenth power. In the order described the differences were of 1, 5, 13, 13 and 11 orders of magnitude, being clearly the highest value.

The curve corresponding to the liquid saturation in the anode GDL zone closer to the CL, corresponding to the MPL, has only a similar shape to Figure 6-6, where liquid saturation increases with the current but is delayed to 0.75V and it arrives to a maximum, even if here is way bigger. In Figure 6-6 when it arrived at the maximum it started to decrease due to the high temperatures at high current density, but here the behaviour is enlarged, delaying everything. Whereas the behaviour shown on Figure 6-9, Figure 6-12 and Figure 6-18, and more clearly seen in Figure 6-15 was an almost flat curve that had an slight increase, arriving to its maximum and later decreasing, where the slope was smooth, contrary to the steep slope seen on the first part of the growth in Figure 6-21.

The maximum is achieved at 0.16% at 0.45V, making think that if it finished the simulation it would have declined, making it the highest value for this variable of all the study cases. All the cases without MPL were raised to the fifth power, being almost two orders of magnitude smaller, making them 32.5, 136.2 and 116.7 times bigger than Figure 6-9, Figure 6-12 and Figure 6-18. The cases with MPL were around one order of magnitude smaller than this case, being a 66.3 and 88.1% bigger than cases in Figure 6-6 and Figure 6-15. It does not make much sense that it has more similarities with the cases with MPL than with the ones that do not.

The liquid saturation in the GDL anode zone closer to the channels, was only visible for cases completely unrelated, with no similarities in their properties or the presence of the MPL, as in AvCarb P-75 without MPL and SIGRACET 34BC, where this curve looks like neither of them. In Figure 6-9 this curve has just started growing with a short growth leading to a 89.4% difference, while Figure 6-15 increased until it reached the maximum that was almost horizontal. Here it starts growing at 0.65V, as in Figure 6-15, but continues growing, creating a 39.9% difference among them. There is a slight change in the slope, indicating it might be close or in the maximum, being that value 0.25%, being therefore the highest value recorded for all the study cases. This makes that the values for the anode and channel liquid saturations are the highest of all the cases. The other cases were almost negligible, where it is 4, 5 and 6 orders of magnitude bigger than Figure 6-6, Figure 6-12 and Figure 6-18.

6.3. Evolution along a line

The different variables studied will be analysed in the set of curves mentioned before. First the water content and temperature curves will be shown, then the oxygen curves and finally the cathode and anode liquid saturation. First the medium voltage graph of a set of variables will be shown, followed by the low voltage one, to later continue with other set of variables.

6.3.1. AvCarb P-75

The water content in the membrane is represented blue, the temperature in the membrane is grey and the temperature in the cooling channel is orange. It is not mentioned where exactly because those layers had just one point. The main axis goes from 5.3 to 9.8 and the secondary axis goes from 339 to 364K. The X coordinate goes from 0 to 0.12m, where the PEMFC length is 0.1m. The colour scheme and axis have been kept for all the other cases the same in order to facilitate the comparison.

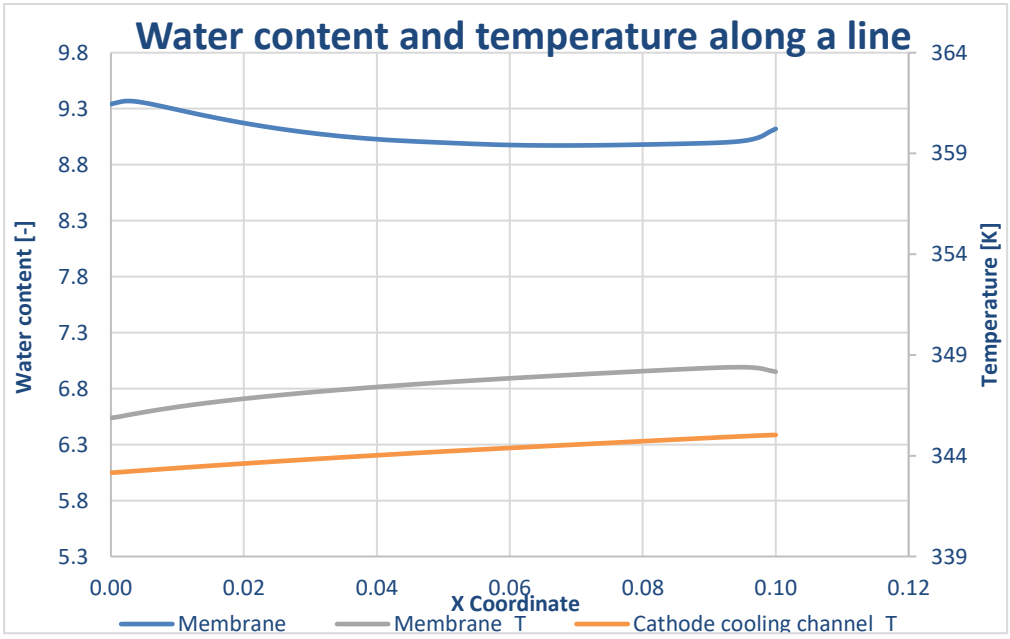

Figure 6-22 AvCarb P-75 medium voltage water content and temperature along a line

In Figure 6-22 is shown the water and temperature in the membrane and cathode cooling channel evolution along the X coordinate at medium voltage for the AvCarb P-75 case. The AvCarb case has a high electrical conductivity, which would lead to higher water content because the fuel cell would not heat up, not causing higher temperatures. The water content ranges from 9.37 to 8.97, just being separated a 4.2%. Therefore, the changes seen are trifling. The curve starts at 9.34, increasing until it reaches the maximum, where it starts to decrease until reaches an almost horizontal zone with constant values around the minimum and later increasing again up to 9.12 just at the end.

The temperature in the membrane ranges between 348.4 and 345.9K, just varying a 0.7%. This low temperature values are due to the high electrical conductivity, that avoids the heating up of the cell. The curve starts at its minimum slowly increasing, until it reaches the maximum almost at the end to decrease later briefly.

The temperature in the cathode cooling channel ranges between 345 and 343.2K, just varying a 0.5%. The curve has a linear behaviour starting at the minimum and ending at its maximum. The differences between the temperatures in the membrane and the cooling channel are between 1 and 0.8%, being both values very close. At the beginning of the line is where the coolant is being introduced.

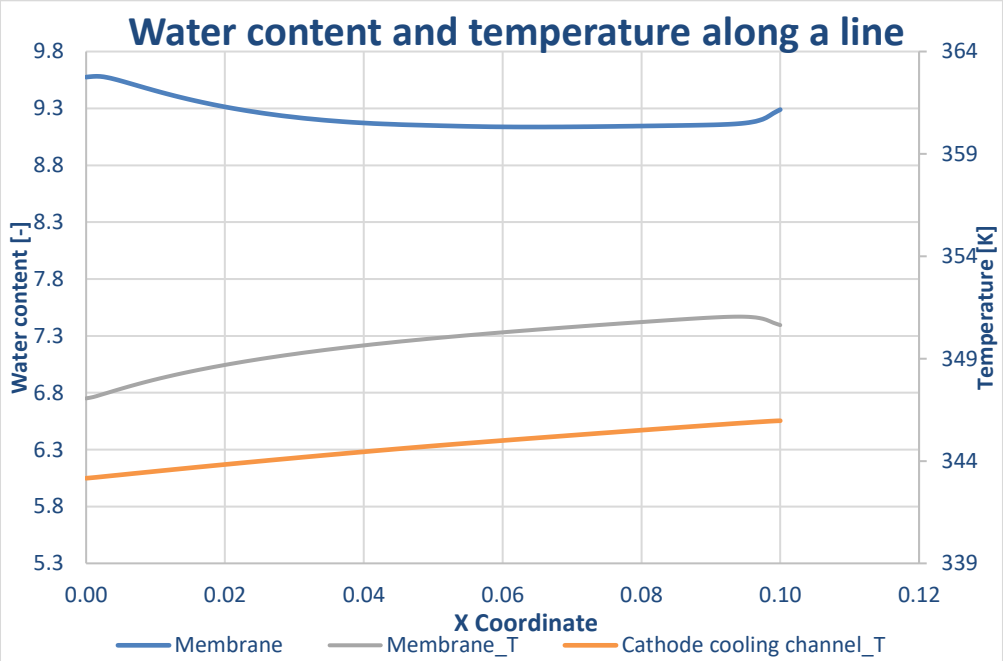

Figure 6-23 AvCarb P-75 low voltage water content and temperature along a line

In Figure 6-23 it can be seen the water and temperature in the membrane and cathode cooling channel evolution along the X coordinate at low voltage for the AvCarb P-75 case. The water content ranges between 9.58 and 9.14, having a 4.6% difference. The difference with the medium voltage case is just between 2.4 and 1.5%. The shapes of the curves are similar, however Figure 6-23 starts already on the maximum, decreasing until it arrives to an almost constant or horizontal zone, at around the minimum, increasing again at the end up to a 9.29 value. The water content is higher because at lower voltages more water is being produced in the reaction.

The temperature in the membrane ranges between 351.1 and 347.1K, varying a 1.1% among them. The curve starts at its minimum, slowly increasing until it reaches the maximum almost at the end, to decrease later briefly to 350.6K. It has almost the same behaviour as the medium voltage case, varying between a 0.3% and 0.8% among them.

The temperature in the cathode cooling channel spans between 346 and 343.2K, just a 0.8% difference. It has a linear behaviour, as the one seen in Figure 6-22, starting at its minimum and ending at its maximum. The differences with the medium voltage are so small that are comprised between a 0.001% and 0.3%. The

difference between the membrane and cooling channel temperatures is between 1.5 and 1.1%. All differences seen are very small. More extreme values would have been obtained if the electrical efficiency was lower. The temperatures are higher at lower voltages because more is being produced and consumed and since the reaction is exothermic, it leads to higher temperatures.

The O_2 mass fraction in the cathode channel is represented red and in the cathode CL is blue. The axis goes from 0 to 0.25. These colour schemes and axis will be kept for all the cases to compare them easily.

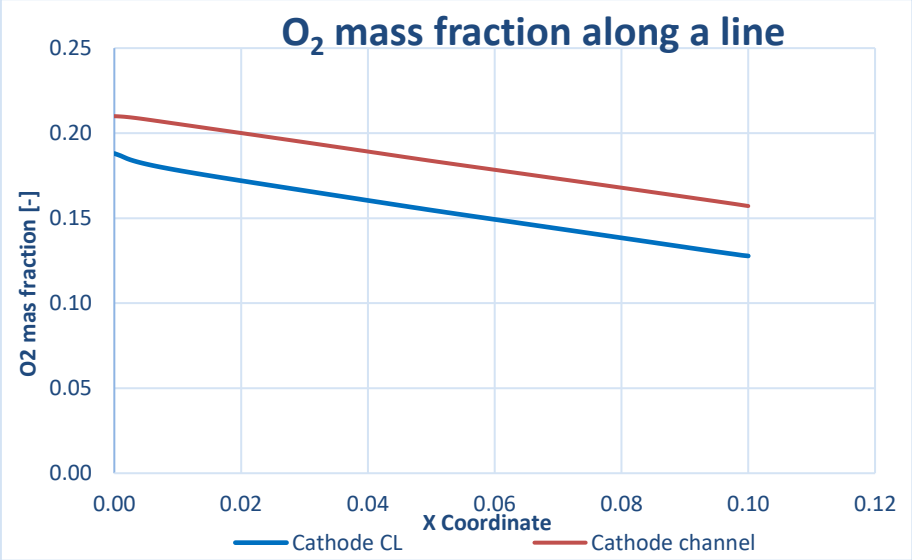

Figure 6-24 AvCarb P-75 medium voltage oxygen mass fraction along a line

In Figure 6-24 it is represented the oxygen mass fraction in the cathode CL and channel evolution along the X coordinate at medium voltage for the AvCarb P-75 case. The O_2 mass fraction in the cathode channel spans from 0.210 to 0.157, which means a 25.2% difference. Its behaviour could be considered almost linear. The O_2 mass fraction in the cathode CL spans from 0.188 to 0.128, implying a 30% difference. Its behaviour is almost linear and parallel to the cathode channel but at the beginning there is a slight change on the slope. This leads to a 10.4% difference among the curves at their maximum and a 18.7% at the minimums, which means that they are diverging from each other. The oxidizer is introduced at the beginning of the line in the cathode channel, which means it will decrease along its length. The cathode CL is where the oxygen is being consumed, reducing amount. The further from the oxidizer channel where it is introduced, the lower its value would be due to diffusion.

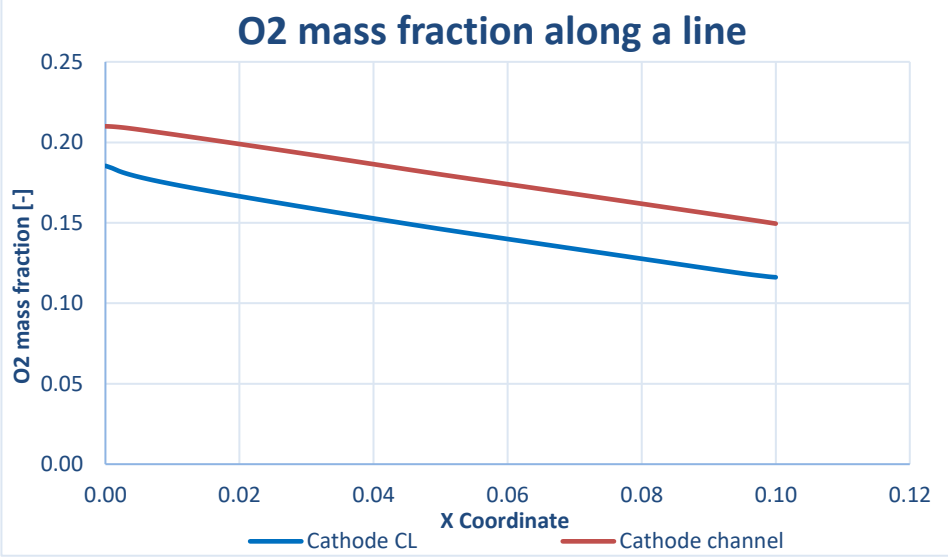

Figure 6-25 AvCarb P-75 low voltage oxygen mass fraction along a line

In Figure 6-25 it is represented the oxygen mass fraction in the cathode CL and channel evolution along the X coordinate at low voltage for the AvCarb P-75 case. The O_2 mass fraction in the cathode channel goes from 0.210 to 0.149, having a 28.8% difference. The behaviour is almost linear. The O2 mass fraction in the cathode CL goes from 0.185 to 0.116, having a 37.3% difference. If these numbers are compared to the ones obtained at medium voltage in Figure 6-24, it can be seen that the differences between the maximum and the minimum increase. If the amounts in the cathode CL and channel are compared, there is a difference between a 22.4 and 11.7%, which corresponds to the difference between the minimums and the maximums respectively, meaning the curves start to diverge from each other even if they seem parallel. These differences are again bigger than the medium voltage ones.

The difference between the O_2 mass fraction in the cathode CL at medium and low voltage is between 10% and 1.4%, seeing the minimum difference at its maximum and the bigger one at the minimum since it diverges more, arriving to lower values. The difference between the O_2 mass fraction in the cathode channel is between 5.4% and 0.0001%, corresponding the bigger difference to the minimum and the lower to the maximum. Again, the difference increases along the X coordinate because at lower current it diverges more. At lower voltages the oxygen mass fraction decreases more because more O_2 is being consumed.

The anode liquid saturation is represented blue in the GDL point 1, orange in the GDL point 2, yellow in the MPL point 3 and grey in the MPL point. The points mentioned are the ones represented in Figure 6-1, corresponding the odd numbers to the under-channel zone and the even to the under-rib. In order for all the cases to have the same axis and see correctly all the changes, the MPL points have been put in the main axis with it going from -5e-5 to 6.5e-4 and the GDL points in the secondary axis going from -4.5e-3 to 5.5e-2. The multiple orders of magnitude difference between the axis means that if they were not separated most of the variables would not be visible and in some cases, nothing would be seen. These colour schemes and axis have been kept for all the cases to facilitate comparison.

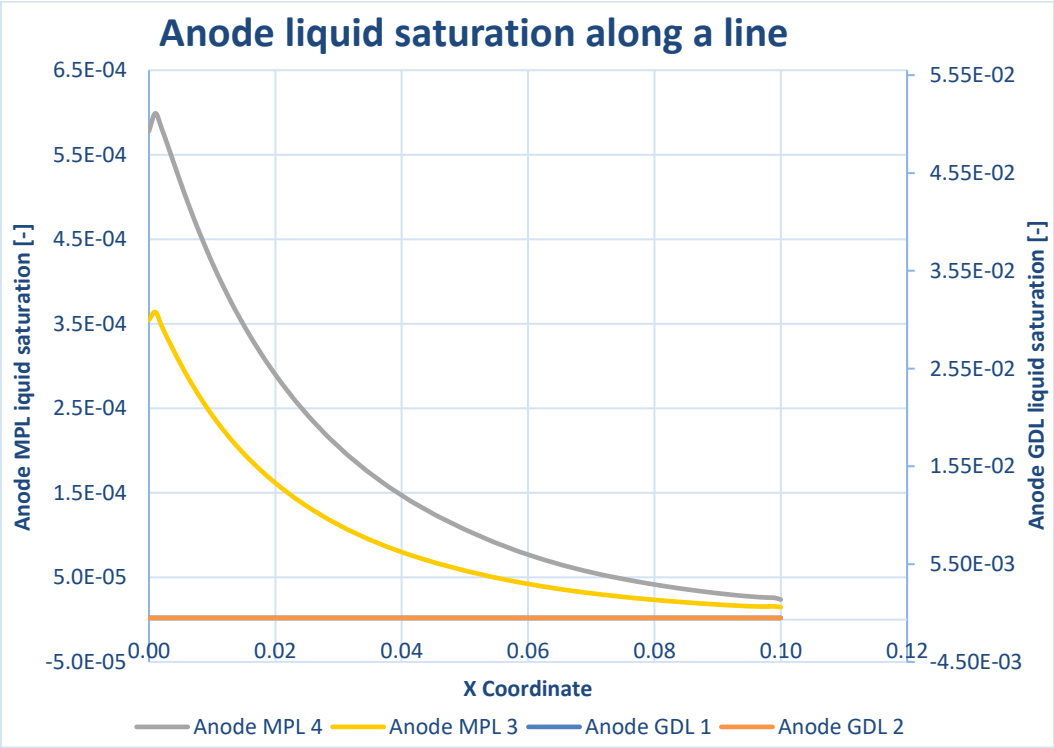

Figure 6-26 AvCarb P-75 medium voltage anode liquid saturation along a line

In Figure 6-26 it can be seen the anode liquid saturation in the different points of the MPL and GDL evolution along the X coordinate at medium voltage for AvCarb P-75 case. The anode GDL liquid saturation cannot be seen because the under-channel is raised to the seventh power and the under-rib one is raised to the sixth power, existing a 76.6% difference among them. This makes sense because in the under-rib there is more water because there are lower temperatures further form the channel that allow that more water condensates.

The anode MPL liquid saturation are visible. Here the curve corresponding to the under-rib has a higher value than the under-channel one. They both start increasing until they reach to the maximum at the beginning of the evolution and then start to decrease approaching asymptotically to zero. The under-channel anode MPL liquid saturation maximum is 0.036% and the under-rib is 0.06%, implying a 39.2% increase. They both have similar behaviours varying perceptually between 38 and 45.7%, which makes the under-rib between 1.6 and 1.9 times bigger than the under-channel. Even if visually the biggest differences are seen at the begging, numerically they are the smallest. The differences between the under-rib and under-channel are bigger in the GDL, which makes sense since it is closer to the channel. In the MPL there is more water because it is closer to the electrode where water is being produced.

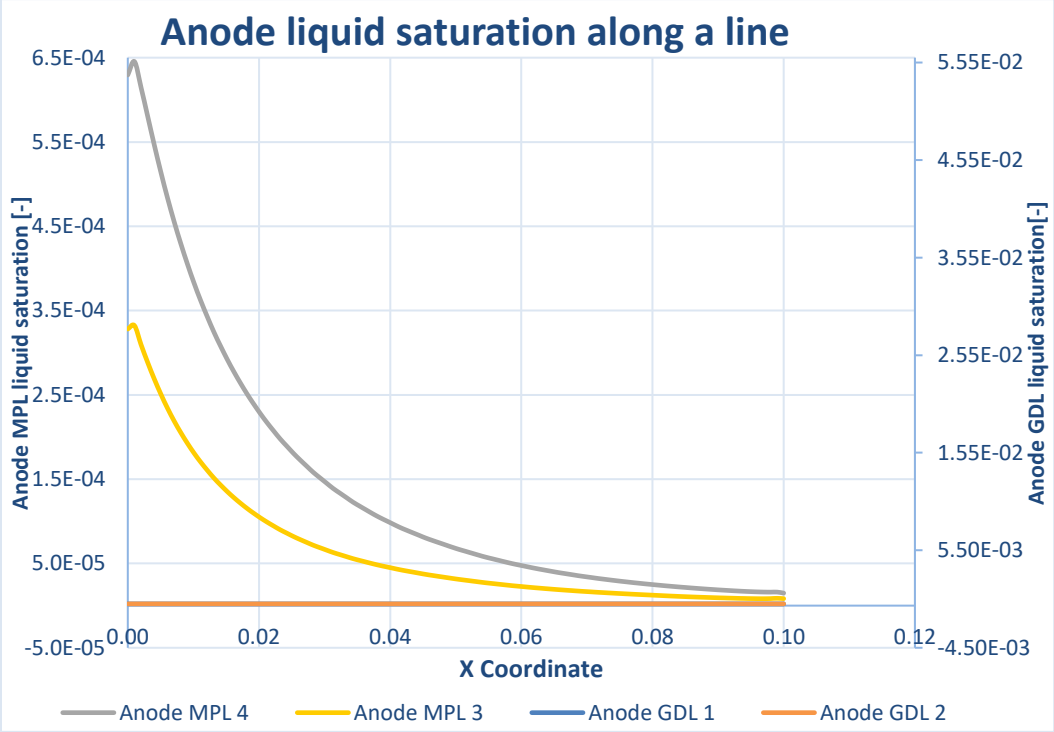

Figure 6-27 AvCarb P-75 low voltage anode liquid saturation along a line

In Figure 6-27 it can be seen the anode liquid saturation in the different points of the MPL and GDL evolution along the X coordinate at low voltage for AvCarb P-75 case. The behaviour seen here is similar to the one seen in Figure 6-26, but the values here are slightly higher because at higher currents more water is being produced. The under-channel anode GDL liquid saturation is raised to the seventh power while the under-rib is raised to the sixth, having a 87.6% difference among them. The under-channel value is smaller than the medium voltage one, while in the under-rib happens the opposite.

The anode MPL liquid saturation starts increasing, arriving to their maximums in the early stages, to later decrease asymptotically. The maximums are 0.065% in the under-rib and 0.033% in the under-channel, existing a 48.5%, that has increased with respect to the medium voltage case. As in the GDL, the under-channel has a lower maximum than the medium voltage case while in the under-rib happens the opposite. There is a 10.4% increase on the maximum of the under-rib liquid saturation with respect to the medium voltage case, while there is a 9.5% decrease in the under-channel case. There is between a 47.9 and 54.7% increase from the under-channel to the under-rib, which is a bigger increase than in the medium voltage case. If the values are compared with the medium voltage ones, the differences oscillate between the ones obtained at the maximums up to more than a 90%, meaning they later diverge. In the under-rib case, after the high values, they become smaller than in the medium voltage case, meaning the decrease is steeper.

The cathode liquid saturation is represented in blue in the point GDL 9, orange in GDL 10, yellow in MPL 7 and grey in MPL8. The points mentioned correspond to ones shown in Figure 6-1, where the odd numbers correspond to the under-channel and the even numbers correspond to the under-rib. It was opted for a single

axis, because contrary to what happened in the anode, here the variables are more or less in the same order of magnitude, going the axis from -4e-3 to 4.6e-2. These colour schemes and axis are kept throughout all the cases studied.

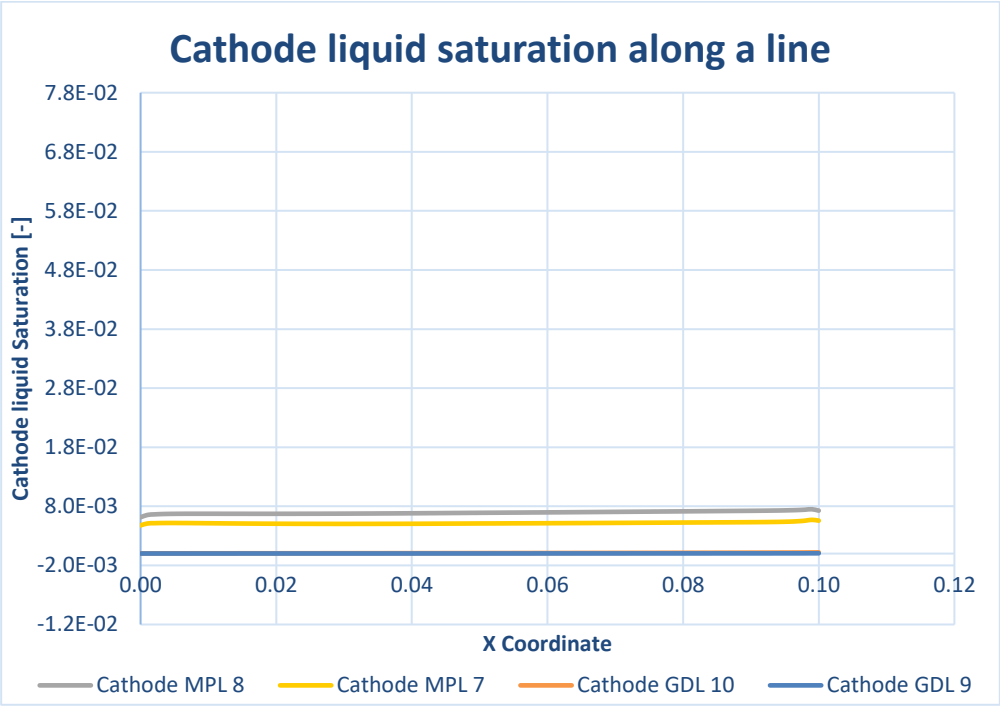

Figure 6-28 AvCarb P-75 medium voltage cathode liquid saturation along a line

In Figure 6-28 it is represented the cathode liquid saturation in different points of the MPL and GDL evolution along the X coordinate at medium voltage for the AvCarb P-75 case. As it was seen in the anode case, the liquid saturation in the MPL is higher than in the GDL, whereas here the difference is not of various orders of magnitude. The cathode MPL under-rib liquid saturation starts to increase suddenly until reaches a plateau and at the middle of the evolution it continues to increase again, arriving to its maximum to decrease briefly. The maximum is achieved at 0.75% and the minimum is 0.62% at the beginning, making it a 18.1% difference, being the range way smaller than the one seen on the anode cases in Figure 6-26 and Figure 6-27, which was 96 and 97.7%

The behaviour of the cathode MPL under-channel liquid saturation is similar to the under-rib one, but when it reaches the plateau after a brief increase, it starts to decrease to later increase to the maximum and then later swift decrease. The maximum is 0.57% and the minimum is 0.48%, ranging a 16.4%, which is again smaller than the ones seen in the anode case, ranges that were the same in the under-rib and under-channel cases. This might mean that their behaviours could be parallel. The increase that the under-rib supposes from the under-channel is a 39.2%, the exact same as the one seen on the anode case in Figure 6-26.

The values of the cathode GDL liquid saturation are around an order of magnitude smaller that the MPL ones, making the curves less visible. It seems to have a linear behaviour, but closely looking to the numbers, there are two slope changes, growing almost vertically towards the end. The liquid saturation in the under-rib is higher than in the under-channel as seen before. The under-rib values go from 0.0036 to 0.021%, being the minimum at the beginning and the maximum at the end, having a 82.4% difference which is again bigger than the one seen on the MPL, as seen in Figure 6-26 and Figure 6-27. The under-channel values go from 0.0013 to 0.0052%, having a 75% difference. The under-rib supposes a 74.8% increase with respect to the under-channel, not exactly the same but almost as seen in the anode medium voltage graph in Figure 6-26.

In Figure 6-29 it is represented the cathode liquid saturation in different points of the MPL and GDL evolution along the X coordinate at low voltage for the AvCarb P-75 case. The behaviour is similar to the one seen in medium voltage in Figure 6-28. The cathode GDL liquid saturation seem again so be linear because their development is barely visible. The under-rib has starts at its minimum continuing to grow with different

slopes, finishing at a maximum value of 0.016% oscillating a 80.8%, being higher than the under-channel, which has the same behaviour with a 0.003% maximum and oscillating a 67.6%, which are both smaller ranges than in the medium voltage case. The under-rib maximum highly differs from the medium voltage value, being its decrease a 74.3%, while the under-channel decrease is not as pronounced, being a 26.8%. At low current more water is being produced, but also there are higher temperatures that would evaporate it, showing more difference between the under-rib and under-channel. The under-rib supposes a 81.7% increase with respect to the under-channel, which means bigger increase than in the medium voltage case in Figure 6-28.

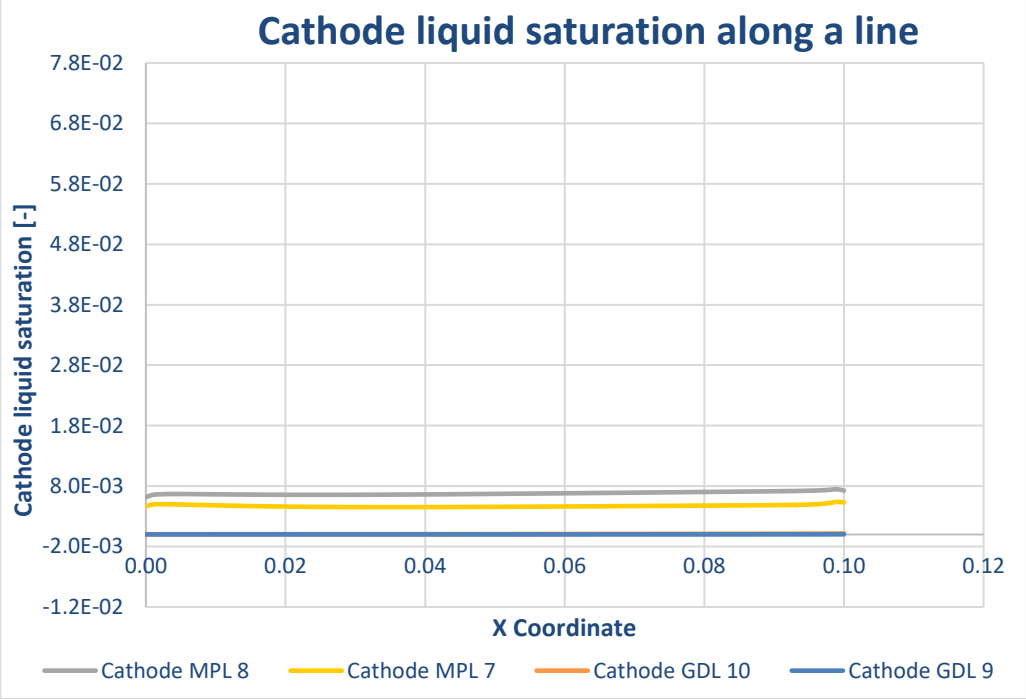

Figure 6-29 AvCarb P-75 low voltage cathode liquid saturation along a line

The cathode MPL liquid saturation has the same behaviour and almost the same values as in Figure 6-28. They start increasing almost vertically and where the plateau was reaches in the medium voltage case, here it clearly decreases to grow towards the last half of the evolution, arriving to the maximum and briefly decreasing. The under-rib liquid saturation goes from 0.62 to 0.75%, being both the maximum and minimum just a 0.3% smaller than the medium voltage case. It oscillates a 17.6%, which is less than the medium case. In the under-channel case, the range obtained goes from 0.42 to 0.54% which is again smaller than the medium case, implying a 5.8% decrease on both maximums and minimums. The oscillation is of a 16.3%, which is again smaller than in the medium voltage case. The under-rib supposes between a 24.2 and 32.1% to the under-channel liquid saturation, which is smaller than in the medium voltage case in Figure 6-28.

6.3.2. AvCarb P-75 without MPL

In Figure 6-30 it can be seen the water content and temperature in the membrane and cathode cooling channel evolution along the X coordinate at medium voltage for the AvCarb P-75 without MPL case. The water content starts increasing with a steep slope, to later smooth it, having several slope changes but continues growing. It goes from its minimum to its maximum between 6.29 to 8.72, having a 27.8% difference, which is bigger than the one seen in Figure 6-22. However, the values are between a 48.4% smaller at the minimum and a 4.6% at the maximum than with a MPL. The GDL has a higher permeability and porosity than the MPL, allowing more water to go through, diffusing to other layers.

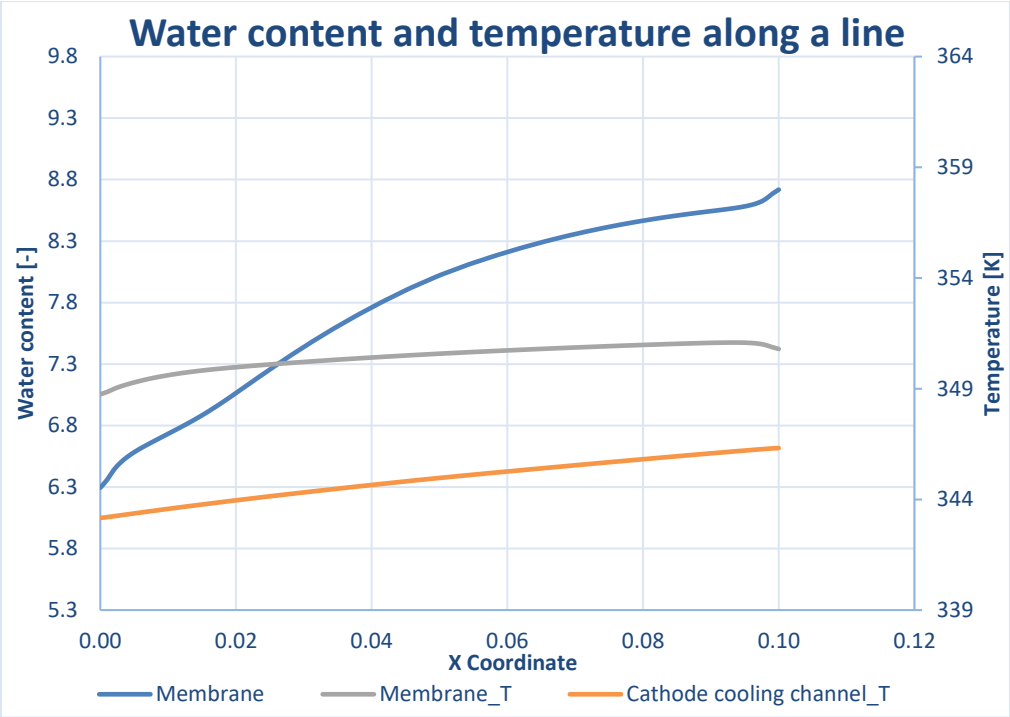

Figure 6-30 AvCarb P-75 without MPL medium voltage water content and temperature along a line

The temperature in the membrane is higher than the one in the cathode cooling channel because the reaction takes place there, leading to higher temperatures. The temperature in the membrane starts to increase until it arrives to an almost constant zone, growing very slowly, to finish with a slight decrease. It values go between 348.8 to 351.1K, ranging only a 0.7%. What was the maximum in the case with MPL, is now the minimum in the case without MPL, meaning an increase on the temperatures. The lower water content in the membrane leads to the heating up of it, which leads to the higher temperatures. There is an 0.8% increase with respect to the case with MPL seen in Figure 6-22, meaning it has the same behaviour, but it is parallel to it, displaced upwards, since the percentage is kept throughout the curve.

The temperature in the cathode cooling channels seems to be linear, growing from 343.2 to 346.3K, varying a 0.9%, which is a bigger variation than in the case with MPL. The minimum is the same, but the maximum is a 0.4% bigger. The differences with Figure 6-22 go from a 0.001% increase at the minimum to 0.9% at the maximum, diverging as it advances along the X coordinate. At the beginning of the length is where the coolant is being introduced, so it is where the lower temperatures are.

In Figure 6-31 it can be seen the water content and temperature in the membrane and cathode cooling channel evolution along the X coordinate at low voltage for the AvCarb P-75 without MPL case. The water content starts with a marked slope, to continue growing linearly, ending with a slight bigger slope. It goes from 7.22 to 8.88, having a 18.8% difference, which is smaller than in the medium voltage in Figure 6-22. The minimum and the maximum suffer a 12.8% and a 1.8% increase respectively with respect to the medium voltage case, being reduced the distance among them. There is more water than in the case with medium voltage in Figure 6-30 because at lower currents more water in being produced. There is between a 32.7 and 4.6% decrease with respect to the case with MPL seen in Figure 6-23, reducing the difference with the distance on the X coordinate.

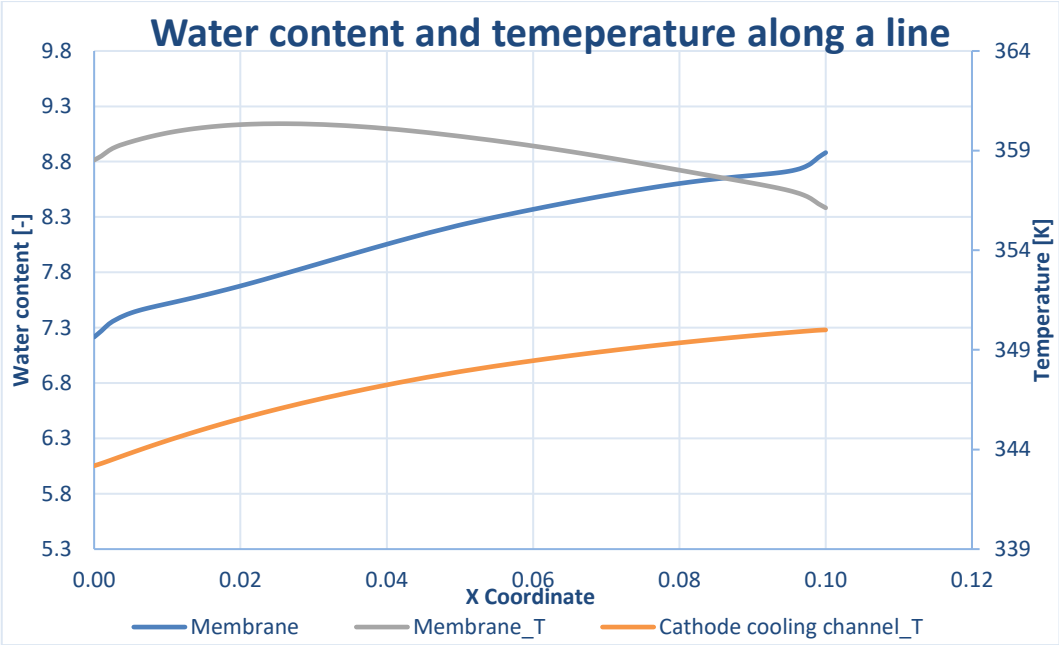

Figure 6-31 AvCarb P-75 without MPL low voltage water content and temperature along a line

The temperature in the membrane has a strange shape, if it is compared with the other cases seen in Figure 6-22, Figure 6-23 or Figure 6-30. The previous ones had almost the same behaviour and shape with the same valleys and lows but displaced upwards or downwards on the Y axis, being parallel. In this case the temperature starts increasing until it arrives at the maximum and continues decreasing until the end, going lower than it started. It minimum is 356.1K and the maximum is 360.4K, ranging a 1.2%, higher than in other cases. It is between a 2.9 and 1.5% increase to the medium voltage case in Figure 6-30 and between 3.3 and 1.5% increase to the case with MPL in Figure 6-23.

In the previous cases the cathode cooling channel temperature was linear, being the adjustment more than 99% precise, while here is just a 95.8%. Even if it keeps its linearity it is not as precise. It starts growing at 343.2K, finishing at its maximum at 350K, with no clear changes in slope. It ranges a 1.9%, higher than in previous cases, below 1%. It is a decrease with respect to the membrane temperature of between 4.4 and 1.7%, which is a higher difference than the one seen in previous cases. There is an increase to the medium voltage case in Figure 6-30 of between 0.007 and 1.1%, going from the minimum to the maximum, meaning it diverges at the end of the length. As the lower voltages have higher temperatures and it increases with length because the coolant is introduced in the beginning, this difference will be worsened as it progresses along the X coordinate. It supposes an increase with the case with MPL in Figure 6-23 of between 0.007 and 1.2%, almost the same as with the medium voltage case.

In Figure 6-32 it is shown the oxygen mass fraction in the cathode CL and channel evolution along the X coordinate at medium voltage for the AvCarb P-75 without MPL case. The oxygen mass fraction in both cathode CL and channel decreases with the length. At the beginning is where the oxidant is introduced, so going along the X coordinate it would be consumed, having less. The oxygen mass fraction in the cathode channel has a linear behaviour, going from 0.21 to 0.127, decreasing 39.7%, which is a higher difference than in Figure 6-25 and Figure 6-24. It is between a 0.001 and 24.1% smaller than the case with MPL in Figure 6-24, which means that the maximums are the same, but the minimums are lower, diverging towards the end and going to lower amounts. The MPL has a low porosity, what would not allow the oxygen to diffuse to other layers, hence its absence would promote the diffusion, having less oxygen.

The O_2 mass fraction in the cathode CL has an abrupt slope but quickly returns to a steadier one parallel to the one in the cathode channel. It goes from 0.178 to 0.088, having a 50.5% decrease, bigger than the one seen in Figure 6-24 and Figure 6-25. It is between a 5.9 and 45.5% smaller than the case with MPL in Figure 6-24, diverging towards the end. It is between 15.4 and 30.6% smaller than the amount present in the cathode channel. In the CL is where the reaction takes place, so more oxygen is consumed there, having a smaller

amount there.

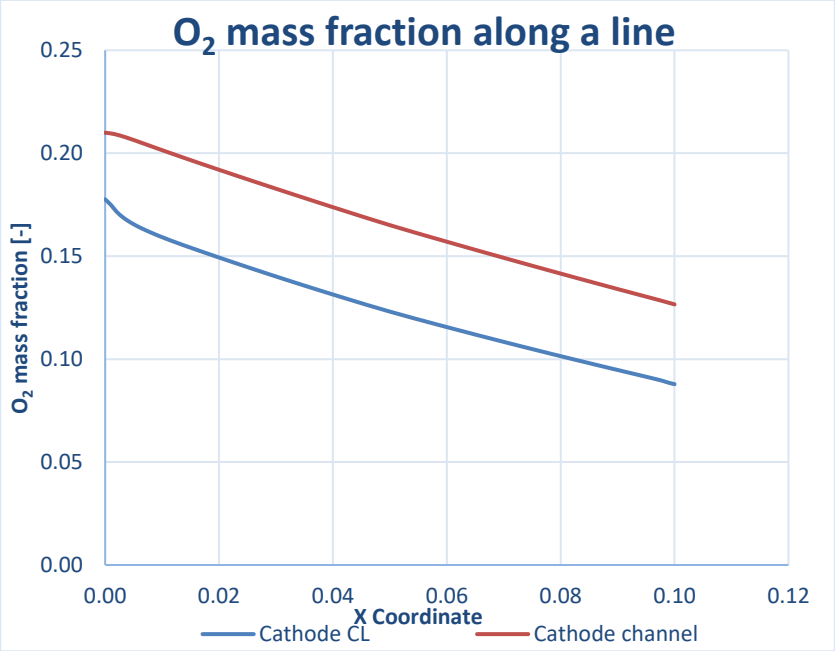

Figure 6-32 AvCarb P-75 without MPL medium voltage oxygen mass fraction along a line

In In Figure 6-32 it is shown the oxygen mass fraction in the cathode CL and channel evolution along the X coordinate at low voltage for the AvCarb P-75 without MPL case. In this case both curves are neither parallel nor linear. The O2 mass fraction in the cathode channel has a steeper decrease than in previous cases, going from 0.21 to 0.072, decreasing a 65.6%, the highest yet seen. It is between a 0.03 and a 75.2% smaller than the medium voltage case in Figure 6-32, going to smaller values. At higher currents, more oxygen is consumed. It is between 0.04% and 2.1 times smaller than the case with MPL in Figure 6-25, going progressively to lower oxygen amounts as it progresses through the X coordinate.

The oxygen amount in the cathode CL decreases harshly to curve more softly. It goes from 0.137 to 0.031, the lower maximums and minimums seen yet, decreasing a 77.5%, also the highest decrease seen yet. It is between 29.3% and 2.8 times smaller than the same case at medium voltage in Figure 6-32. It is between 34.9% and 3.8 times smaller than the case with MPL seen in Figure 6-25. It is between 34.6 and 57.1% smaller than the amount in the cathode channel, which is due to diffusion.

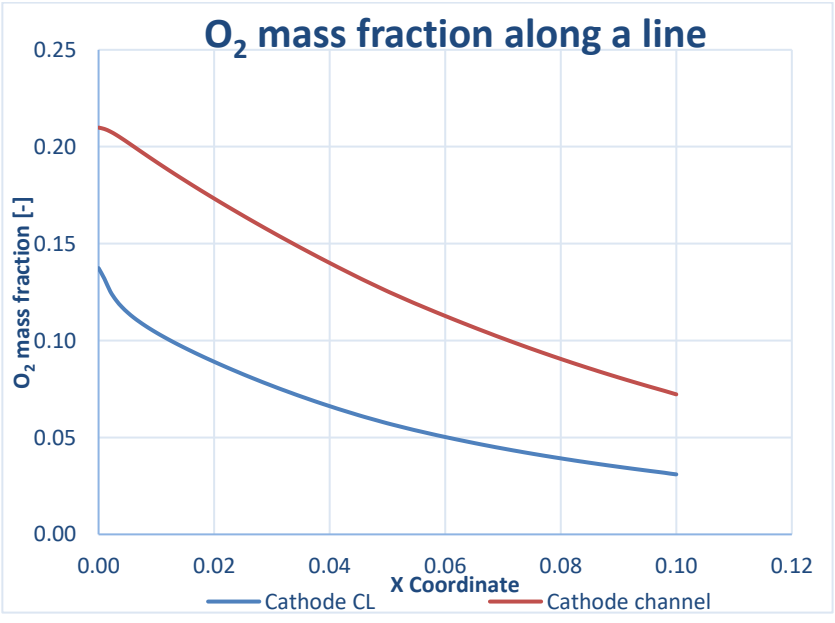

Figure 6-33 AvCarb P-75 without MPL low voltage oxygen mass fraction along a line

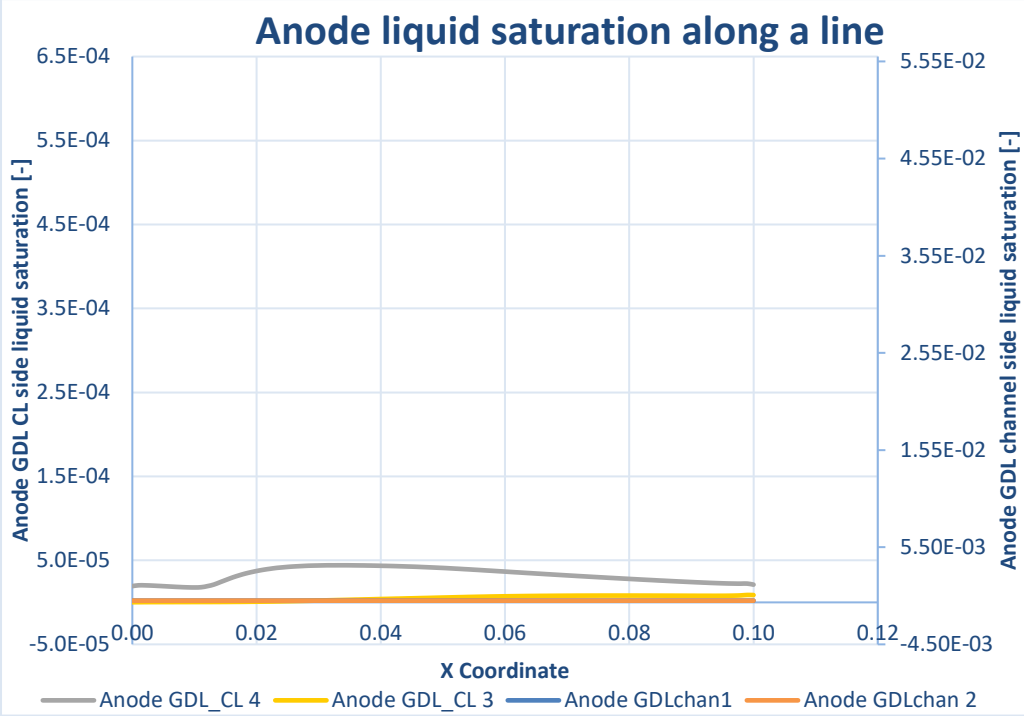

Figure 6-34 AvCarb P-75 without MPL medium voltage anode liquid saturation along a line

In Figure 6-34 it is represented the anode liquid saturation in different points of the GDL evolution along the X coordinate at medium voltage for AvCarb P-75 without MPL case. It is divided in the zone that is closer to the CL (previously the MPL) and other closer to the channels (previously the GDL). The anode GDL channel side liquid saturation is not visible because they are several orders of magnitude smaller. The under-channel one has values of around raised to the nineth power, being smaller than the one in the under-rib, being an order of magnitude higher. Both are two orders of magnitude smaller than the values seen in the case with MPL in Figure 6-26 and Figure 6-27. The under-rib value is higher than the under-channel because it is a colder zone, having more water.

The anode GDL CL side liquid saturation under-channel has a value that is almost not visible, being raised to the seventh power. This zone was previously the MPL, with a lower porosity, but since it has the one of the GDL there is less water because it is allowed to diffuse more freely, explaining the lower values. The higher porosity and permeability are what makes that in all the layers there is less water than with MPL in Figure 6-26 and Figure 6-27 (between three and two orders of magnitude less) because it diffuses elsewhere.

The anode GDL CL side liquid saturation under-rib is the only curve that is completely visible, starting in a constant value, to later increase to its maximum and slowly and asymptotically decrease. It varies between 0.0044 and 0.0018%, varying a 59.8%. The values at the maximum are 30 times smaller than the case with MPL in Figure 6-26, but when they arrive to the asymptotically zone, both converge, being just 12.6% smaller there, meaning they both approaching the same values.

In Figure 6-35Figure 6-34 it is represented the anode liquid saturation in different points of the GDL and MPL evolution along the X coordinate at low voltage for AvCarb P-75 without MPL case. Here is the first time where the anode GDL liquid saturation (in this case closer to the channel) have visible values. In the under-rib it starts at 3.3% to abruptly decrease to an almost zero value that is kept constant throughout the rest of the progress. This is considerably higher than in the previous cases in Figure 6-26, Figure 6-27 and Figure 6-34, where that variable was almost zero since it was raised to the between the sixth and the tenth power.

The GDL under-channel closer to the channel side (previously the GDL) has a maximum raised to the sixth power, which makes it one order of magnitude bigger than the case with MPL in Figure 6-27 and three bigger than the medium voltage case in Figure 6-34. There is more water produced at lower voltages because the reaction is more active, producing more water.

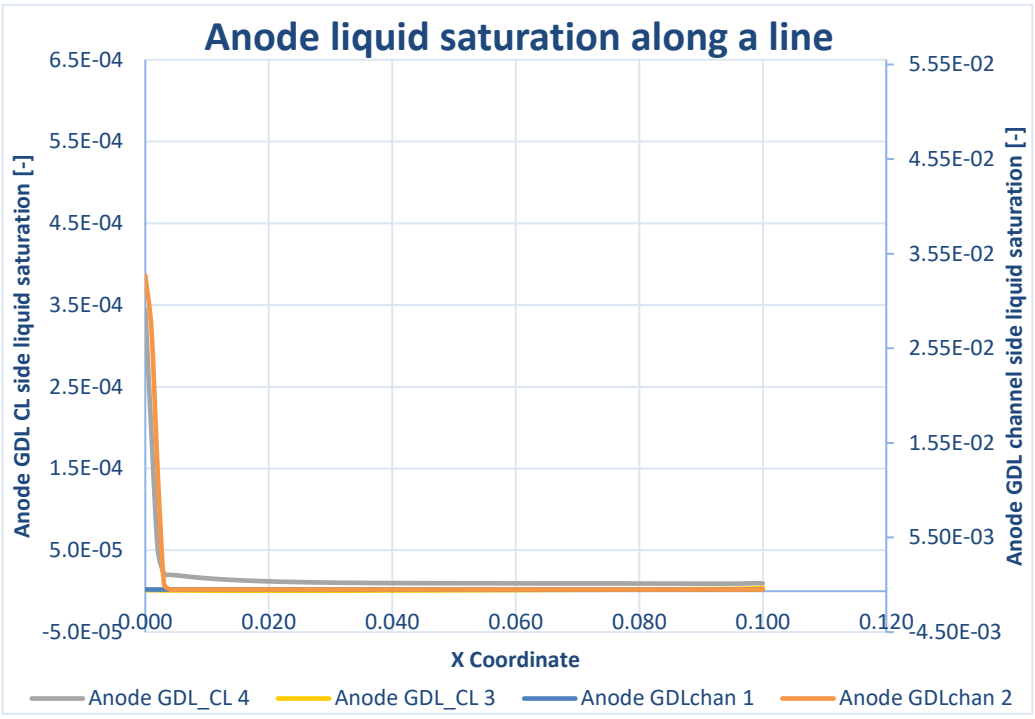

Figure 6-35 AvCarb P-75 without MPL low voltage anode liquid saturation along a line

The anode GDL CL side liquid saturation in the under-rib has a similar shape to the anode GDL channel side under-rib. It starts at 0.034%, to abruptly decrease to almost null values, whereas here it continues with a slow and asymptotical decrease, being not so far to the values reached before. It is 2.2 times smaller than the medium voltage case in Figure 6-34 and 1.6 times smaller than the case with MPL in Figure 6-27.

The anode GDL CL liquid saturation in the under-channel has, as in Figure 6-34, a not visible value, raised to the sixth power, 2.2 times smaller. In the other cases in Figure 6-26 and Figure 6-27, the values were several orders of magnitude higher, so they are comparable. Again, it can be seen that the values found in the under-rib are higher than the ones in the under-channel because the first one is a colder zone, leading to water condensation.

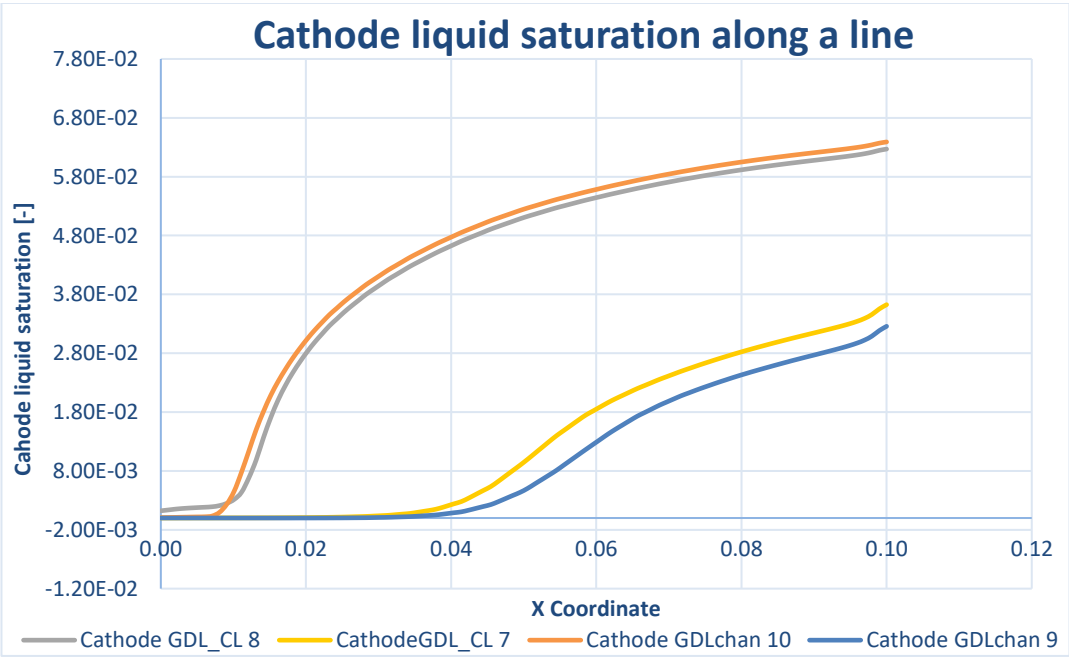

Figure 6-36 AvCarb P-75 without MPL medium voltage cathode liquid saturation along a line

In Figure 6-36 it is represented the cathode liquid saturation in different points of the GDL evolution along the X coordinate at medium voltage for the AvCarb P-75 without MPL case. There are clearly two set of curves differentiated: the ones with higher values are the under-rib (GDL CL side 8 and GDL channel side 10) and the lower ones correspond to the under-channel (GDL CL side 7 and GDL channel side 9). The under-rib has a higher amount of water because it is a colder zone.

The cathode GDL CL side under-rib starts at constant value over zero, taking off higher and later than in the GDL channel side. They both start increasing vertically until 0.02m, where a curvature is formed, leading to a zone with a lower slope. The CL side under-rib goes from its minimum at 0.12% to its maximum at 6.3%, while the channel side goes from 0.007 to 6.4%. Starting at the point where both curves meet, the difference between them is a 30.6% at the beginning to 1.9% at the end, converging asymptotically towards the end. The CL side starts to increase at 0.011 while the channel side does it 0.008.

Both under-channel curves start at values close to zero, starting an irregular growth with several changes on the curvature. They are almost parallel, taking off the CL side first at 0.022m and the channel side at 0.031m. The CL side goes from 0.0006% to 3.6% and the channel side from 0.00002 to 3.3%. The CL side is between a 74.5 and a 10.4% bigger than the channel side, if the values that had taken off are considered, reducing the difference among them as it progresses along the X coordinate. The last part conserved around a 11% difference meaning they were parallel. The side closer to the CL has more water because it is where it is being produced. The temperatures are higher closer to the reaction, which is also where there is more water, evaporating it. The under-ribs are a zone much colder than the other, so where it is hotter this gradient would be more noticeable, having more water in the channel side under-rib because there is more water condensating, creating this anomaly.

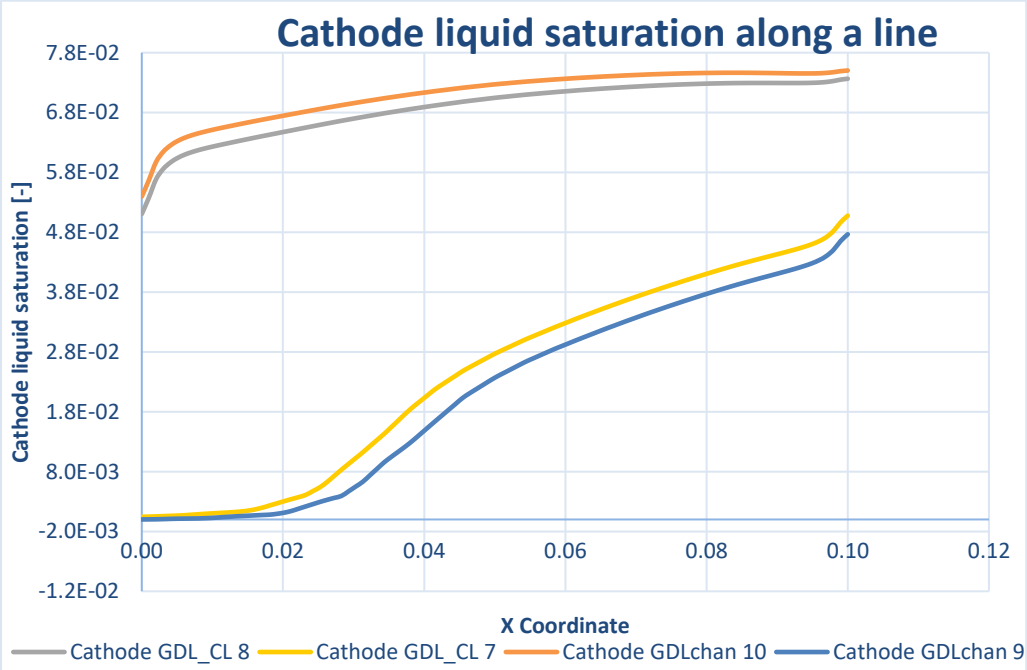

Figure 6-37 AvCarb P-75 without MPL low voltage cathode liquid saturation along a line

In Figure 6-37Figure 6-36 it is represented the cathode liquid saturation in different points of the GDL evolution along the X coordinate at medium voltage for the AvCarb P-75 without MPL case. There is a differentiated zone with higher liquid saturation, corresponding to the under-rib and a lower one, corresponding to the under-channel.

The cathode GDL under-rib liquid saturation start at a certain high value, growing almost vertically, to later continue growing asymptotically. Both curves have the same behaviour, seeming almost parallel. The zone closer to the CL goes from 5.1 to 7.4%, increasing a 30.7%. The zone closer to the channel goes from 5.4 to 7.5%, increasing a 28.1%. The zone closer to the channel implies between a 5.4 and 1.8% increase with

respect to the zone closer to the CL. It is a very small difference that is reduced with the length, converging asymptotically, which could be almost consider parallel. In the medium voltage case in Figure 6-36 these curves started at values close to zero, so they would only be comparable when they took off. Henceforth, in the case closer to the CL there is between a 68.6 and a 14.9% with respect to the medium voltage case mainly because at the beginning they had a very different shape but later they both approached that asymptotically behaviour, while in the case closer to the channel the increase was between a 68.6 and a 14.8%, having the same difference as in the side closer to the CL.

In the under-channel, both curves start at null values, starting a linear growth, first the one closer to the CL at 0.01m and the one closer to the channel at 0.02m. This delay makes that their behaviour is almost parallel. Then they continue growing with continued changes on the curvature. The one closer to the CL goes from 0.044 to 5.1%, while the one closer to the channel goes from 0.0007 to 4.8%. The increase that the one closer to the CL entail to the one closer to the channel, should be considered when they both take off, being between 62.7 and 6.1%, meaning they are approximating to each other. It seems that the shape that the medium voltage in Figure 6-36 has, is the same shape as here, but delayed. The first one takes off later, having less margin to grow, which is why here higher values are achieved, considering the differences after this point. The side closer to the channel has between a 92.2 and 28.6%, while the side closer to the CL is between a 93.5 and a 31.6% bigger than the medium case. The difference is being reduced with the length, mainly because the growth phases started at a different time, approaching to the similar behaviour commented before.

6.3.3. SIGRACET 34BC

The SIGRACET 34BC case has an electrical conductivity which is around five times smaller than the AvCarb P-75 case, which might show considerable differences. In Figure 6-38 it can be seen the water content and temperature in the membrane and cathode cooling channel evolution along the X coordinate at medium voltage for the SIGRACET 34BC case.

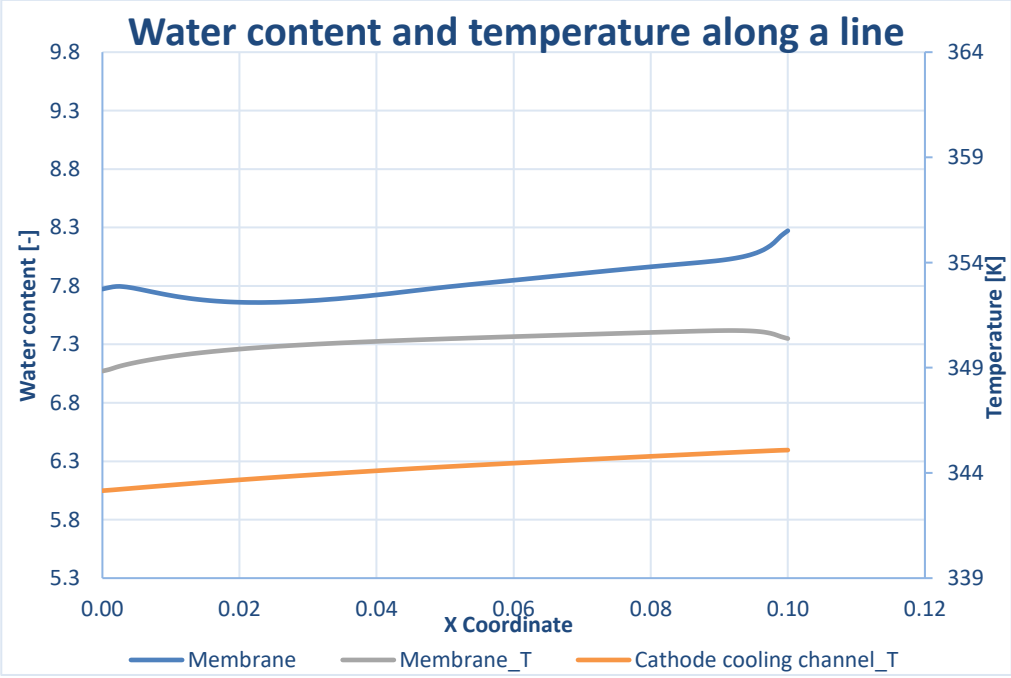

Figure 6-38 SIGRACET 34BC medium voltage water content and temperature along a line

The shape of the water content is very similar to the one seen in Figure 6-22, but here the values are lower, being displaced downwards in the Y axis. It starts growing to soon decrease slightly, continuing later growing with an almost flat slope very slowly, to have an increase on the slope at the end. Its values go between 7.66 and 8.27, being the difference among the values 7.4%, which is a higher difference than in the AvCarb P-75 case in Figure 6-22. Its difference with the AvCarb P-75 is between 20.2 and 10.4%. During almost half of the length a around 20% was kept constant, which confirms that for a period they are parallel, to later reduce their

differences due to the increase Figure 6-38 suffers.

The temperature curves have a similar shape and behaviour to the ones in Figure 6-22, but are a higher, being displaced upwards in the Y axis. The temperature in the membrane starts to increase, reaching a plateau with a slow growth, to decrease briefly at the end. It ranges between 348.8 and 350.8K with a 0.5% difference, slightly smaller than the ones seen in Figure 6-22 and Figure 6-23. The values are higher than in the AvCarb P-75 case, since the minimum is higher than the maximum in Figure 6-22. This happens because of the lower electrical conductivity, which makes that the PEMFC heat up more. There is between a 0.6 and a 0.8% increase between Figure 6-38 and Figure 6-22, which is reduced towards the end.

The temperature in the cathode cooling channel is significantly smaller because the coolant is introduced there. The temperature increases with the length linearly because it is introduced at the beginning of the channel. It goes from 343.2 to 345.1K, varying a 0.5%, being the exact values as the ones seen in Figure 6-22. If the temperature in the membrane has increase with respect to the AvCarb P-75 case and the temperature in the cooling channel has been kept the same, the difference among them has increased, locating between a 1.8 and 1.5%, whereas in Figure 6-22 they were below the unit.Figure 6-38

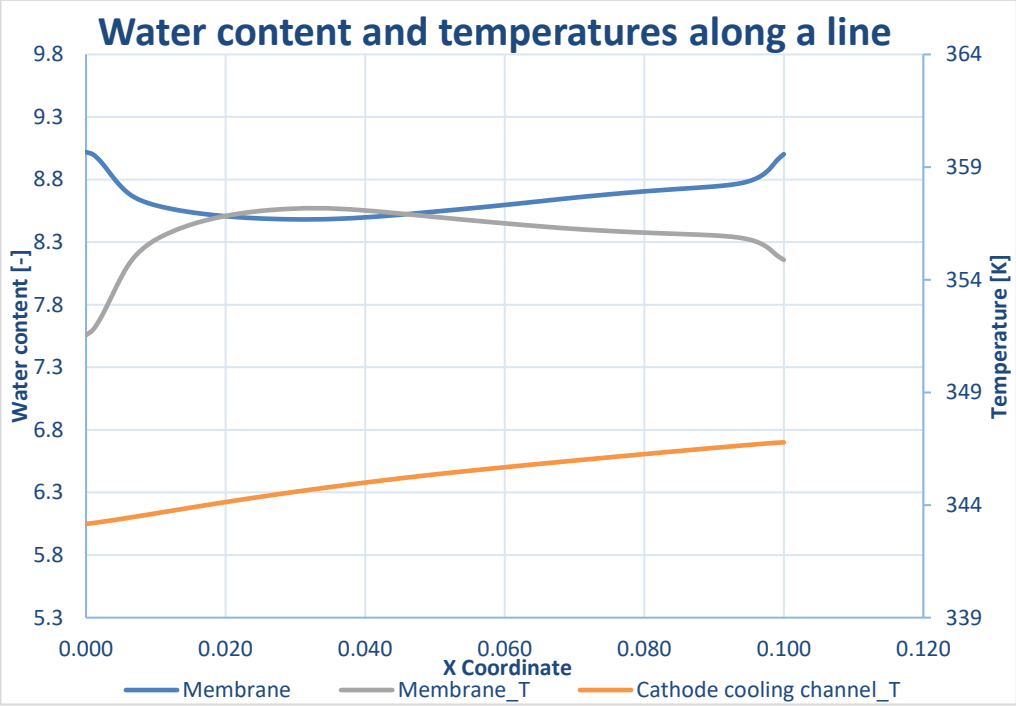

Figure 6-39 SIGRACET 34BC low voltage water content and temperature along a line

In Figure 6-39 it can be seen the temperature and water content in the membrane and cathode cooling channel evolution along the X coordinate at low voltage for the SIGRACET 34BC case. The water content has a similar shape to the medium voltage one in Figure 6-38, but ups and downs have been magnified, similar to what happened between Figure 6-22 and Figure 6-23 in the AvCarb P-75 case. It starts at a maximum, decreasing later, leading to the plateau where growth is slow, to change to a steeper slope at the end. It starts at its maximum at 9.02, because the valley is more pronounced than in the previous cases and the minimum is 8.48, ranging a 6%. It is between a 86.2 and 91.9% higher than the medium voltage case, a considerable increase. At higher currents, more water is being produced and since the PEMFC heats up more due to the low electrical conductivity, it is more accused. The difference between the medium and low voltage AvCarb P-75 cases, was smaller, being between 2.4 and 1.5%. There is between a 3.2 and 10% decrease with respect to the AvCarb P-75 case in Figure 6-23, reducing the difference towards the end. The higher temperatures evaporate the water, having a smaller amount.

The shape of the temperature in the membrane seen, is closer to the AvCarb without MPL low voltage case in Figure 6-31 than any other, even if they do not have many things in common. It starts to increase close to

verticality, to reach a plateau. It later starts decreasing slowly, to change at the end the slope to a steeper one. The changes seen in Figure 6-38 are more exaggerated. It ranges between 351.5 and 357.2K, with have a 1.6% difference, which are the highest difference, maximums and minimums seen yet. The maximums in the medium voltage case are lower than the minimums here. It is between a 0.8 and 2% to the medium voltage curve in Figure 6-38. The difference with the AvCarb P-75 case in Figure 6-23 is between 1.2 and 2.3%, which is almost double of what has been seen before.

The temperature in the cathode cooling channel has a linear growing behaviour, going from 343.2 to 346.8K, which are the same values as the ones seen in AvCarb P-75 in Figure 6-23, even if the properties were completely different. They are different in the case without MPL in Figure 6-31, which means it cannot be concluded that the cathode cooling channel temperature is independent to the GDLs and their properties. The difference with the medium voltage is case is between a 0.001 and 0.5%, diverging towards the end.

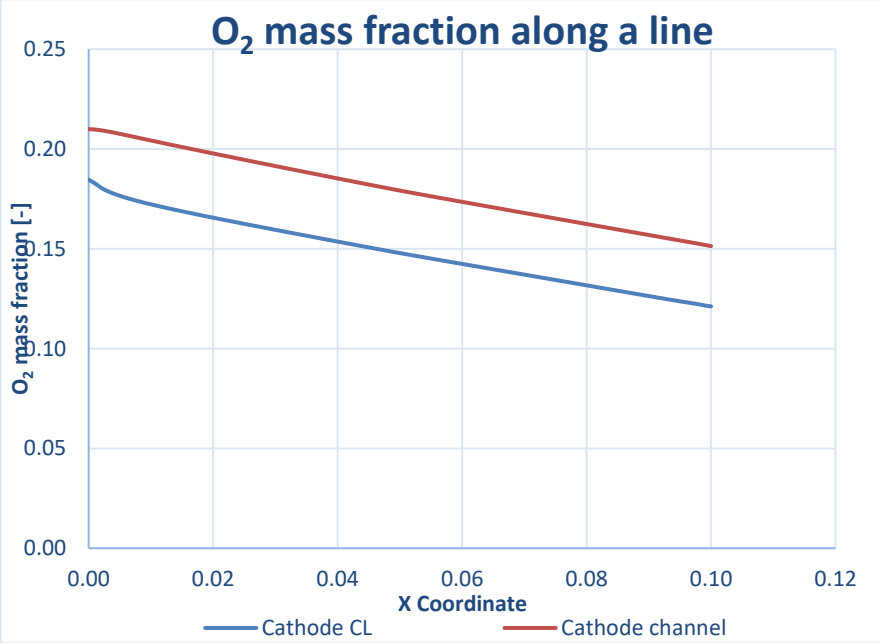

Figure 6-40 SIGRACET 34BC medium voltage oxygen mass fraction along a line

In Figure 6-40 it can be seen the oxygen mass fraction in the cathode CL and channel evolution along the X coordinate at medium voltage for the SIGRACET 34BC case. Both curves decrease with the distance because more oxygen is being consumed, being almost parallel. The cathode CL oxygen mass fraction goes from 0.185 to 0.121, decreasing a 34.4%, having a linear behaviour. It is between a 1.9% smaller at the start and 5.4% bigger at the end than the AvCarb P-75 case in Figure 6-24, having a constant 3% difference to diverge towards the end. The cathode channel oxygen mass fraction goes from 0.21 to 0.151, decreasing a 27.9%. Nevertheless, this curve has lower values than Figure 6-24, being between 0.003 and 3.8% smaller, increasing the difference with the length.

Both curves start having a 12.1% difference that increases to reach a constant value of 20% towards the last half, being parallel, which happens because of a change in the slope in the cathode CL at the beginning, not making it completely linear. The cathode channel has a higher amount because there is where the oxidizer is introduced and at the CL is where it is being consumed. The GDL porosity and MPL permeability of the AvCarb P-75 case are a 11.7 and 21.4% higher respectively, while its GDL permeability is 34.6% smaller. Having a lower permeability in the MPL, the values in the cathode CL are higher because they are not as free to diffuse to other layers, not reducing as much the oxygen amount. However, the GDL permeability is higher, so the oxygen will be able to diffuse more, having less there.

In Figure 6-41 it can be seen the oxygen mass fraction in the cathode CL and channel evolution along the X coordinate at low voltage for the SIGRACET 34BC case. The curves are not as linear as the medium voltage case in Figure 6-40, but the cathode channel keeps mostly its linearity fitting a 99.6 instead of a 99.9% as before. The cathode channel oxygen mass fraction goes from 0.21 to 0.127, decreasing a 39.3%, which is

higher than in the AvCarb P-75 case, being highly affected by the difference in permeability. This increase happens because at high current densities more oxygen is consumed. It is between 0.005 and 17.3% smaller than Figure 6-25. This is why it is between 0.003 and 18.7% smaller than the medium voltage case in Figure 6-40.

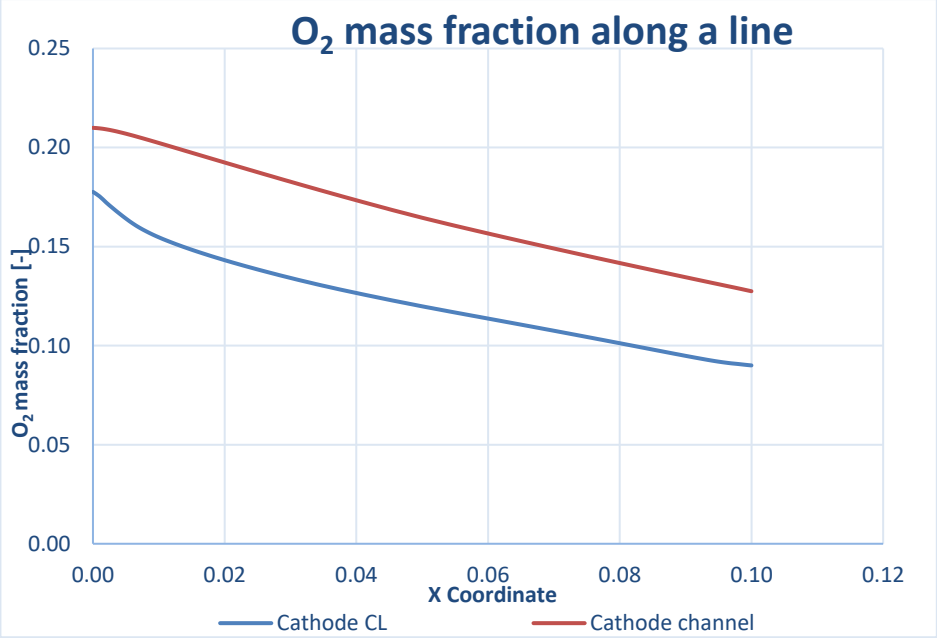

Figure 6-41 SIGRACET 34BC low voltage oxygen mass fraction along a line

The cathode CL oxygen mass fraction goes from 0.178 to 0.09, decreasing 49.3%, again higher than in Figure 6-25. It is between 4.4 and 29% smaller than Figure 6-25. Due to the higher oxygen consumption at low voltages, it is between 3.9 and 34.6% smaller than the medium voltage case. The change on the slope seen in Figure 6-40, happens here later, having a larger zone where both curves are not parallel. The cathode channel has between 15.4 and 29.4% more oxygen than the cathode CL, having a constant value at the end that indicates they are parallel there.

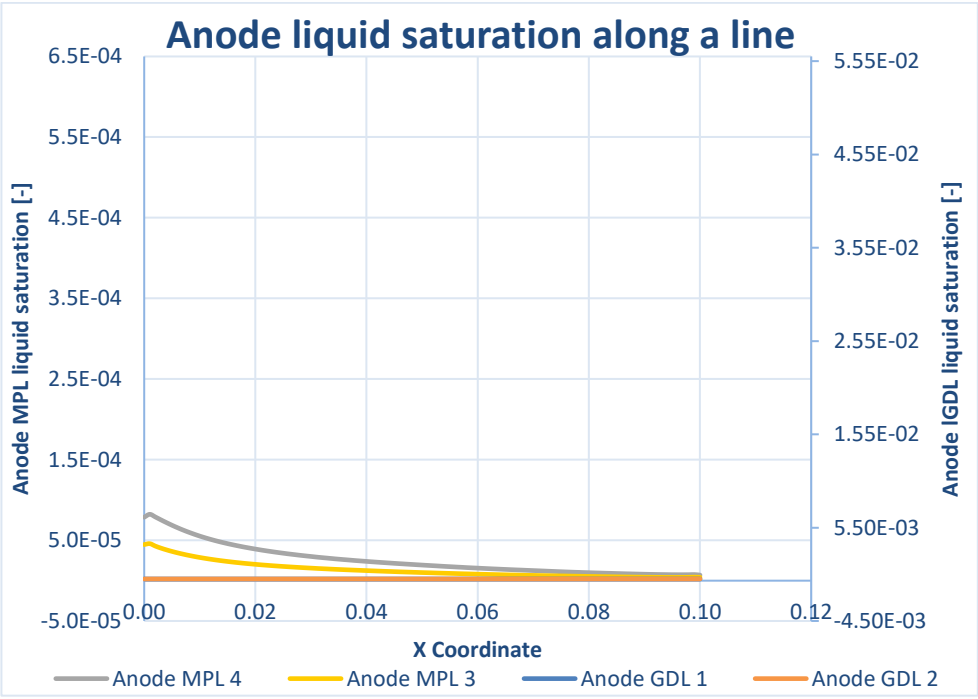

Figure 6-42 SIGRACET 34BC medium voltage anode liquid saturation along a line

In Figure 6-42 it can be seen the anode liquid saturation in different point of the MPL and GDL evolution along the X coordinate at medium voltage for the SIGRACET 34BC case. The GDL curves are not visible because they are several orders of magnitude smaller, being both raised to the eighth power, but the under-rib maximum is 16.5% higher.

The anode MPL liquid saturations both have a similar behaviour but the under-rib one has higher values. They briefly increase to the maximum to later decrease asymptotically. It is a similar behaviour to the one seen in Figure 6-26 and Figure 6-27, but with lower maximums, around seven times smaller. The SIGRACET 34BC has a lower electrical conductivity than the AvCarb P-75, what heats up the PEMFC, evaporating the water, having less in liquid form. The maximum in the under-rib is 0.008%, while at the under-channel is 0.005%, being the first one a 44.3% higher. The minimums are raised to the sixth power, approaching a null value. The under-rib has between 40.4 and 48.1% higher values, what makes their reduction almost constant.

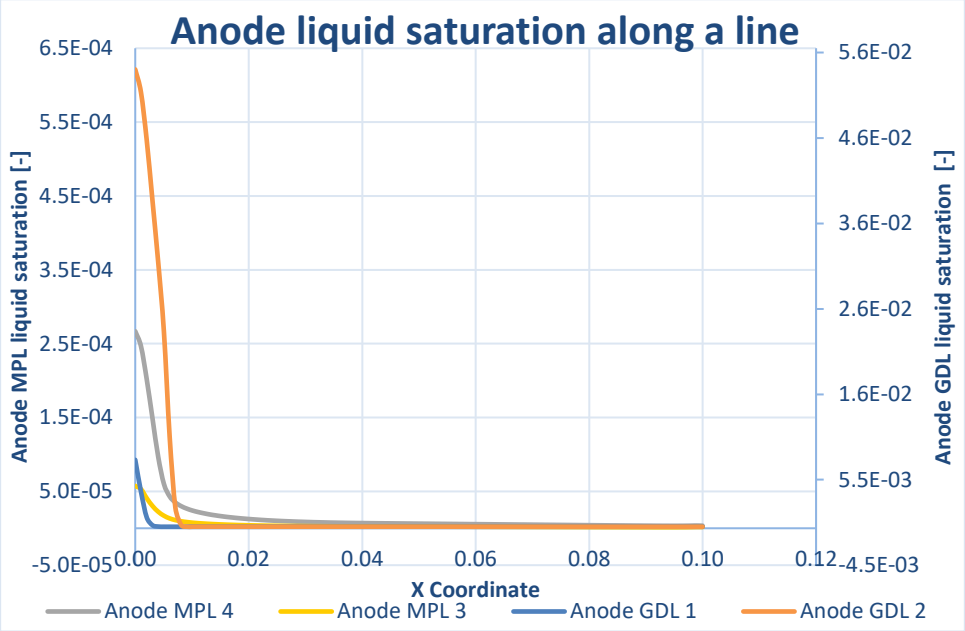

Figure 6-43 SIGRACET 34BC low voltage anode liquid saturation along a line

In Figure 6-43 it can be seen the anode liquid saturation in different points of the MPL and GDL evolution along the X coordinate at low voltage for the SIGRACET 34BC case. The behaviour of the MPL curves is similar to the one in the AvCarb P-75 case in Figure 6-27, but with 3 and 6 times lower maximums. The differences later start to increase because there is a sudden decrease and then it continues asymptotically, while in the previous case was more progressive. The maximum in the under-rib is 0.027% and in the under-channel 0.0057%, having 78.5% difference at beginning that is reduced to a 50.9% with the length. The under-rib is at its maximum 70.5% higher than the medium voltage case but later drops to smaller values. Something similar happens in the under-channel, where the maximums are 22% higher but it later drops to smaller values. At high current densities more water is being produced, but it is opposed to the effect that the higher temperatures have, evaporating the water, reducing its amount as it progresses.

In Figure 6-43 occurs the opposed effect that the high temperatures caused by lower electrical conductivities have, as it could be seen in Figure 6-11 and Figure 6-17. In the GDL supposedly there is less water, however the MPL has higher temperatures due to its closeness to the reaction, which have increase due to the conductivity, evaporating the water. The GDL is colder, condensing that water that was gaseous in the MPL. This would happen just at the beginning, receiving that water from the MPL and then it would plumet to almost null values. The under-channel has a maximum value of 5.4%, descending quickly, where at 0.009m its value is already zero. The under-channel maximum is 0.78%, falling to zero even before, making it a 85.4% smaller. The difference between the under-rib and under-channel is accused because due to the higher temperatures, the effect of a colder zone is magnified. They are not comparable to the medium voltage case or the AvCarb P-75 case because the values were several orders of magnitude smaller, being almost zero.

In Figure 6-44 it is represented the cathode liquid saturation in different points of the GDL and MPL evolution along the X coordinate at medium voltage for SIGRACET 34BC case. The behaviour of the MPL curves is similar to the one seen in the AvCarb P-75 case in Figure 6-28 and Figure 6-29. The values of the GDL were almost zero, but in this case the under-rib takes off.

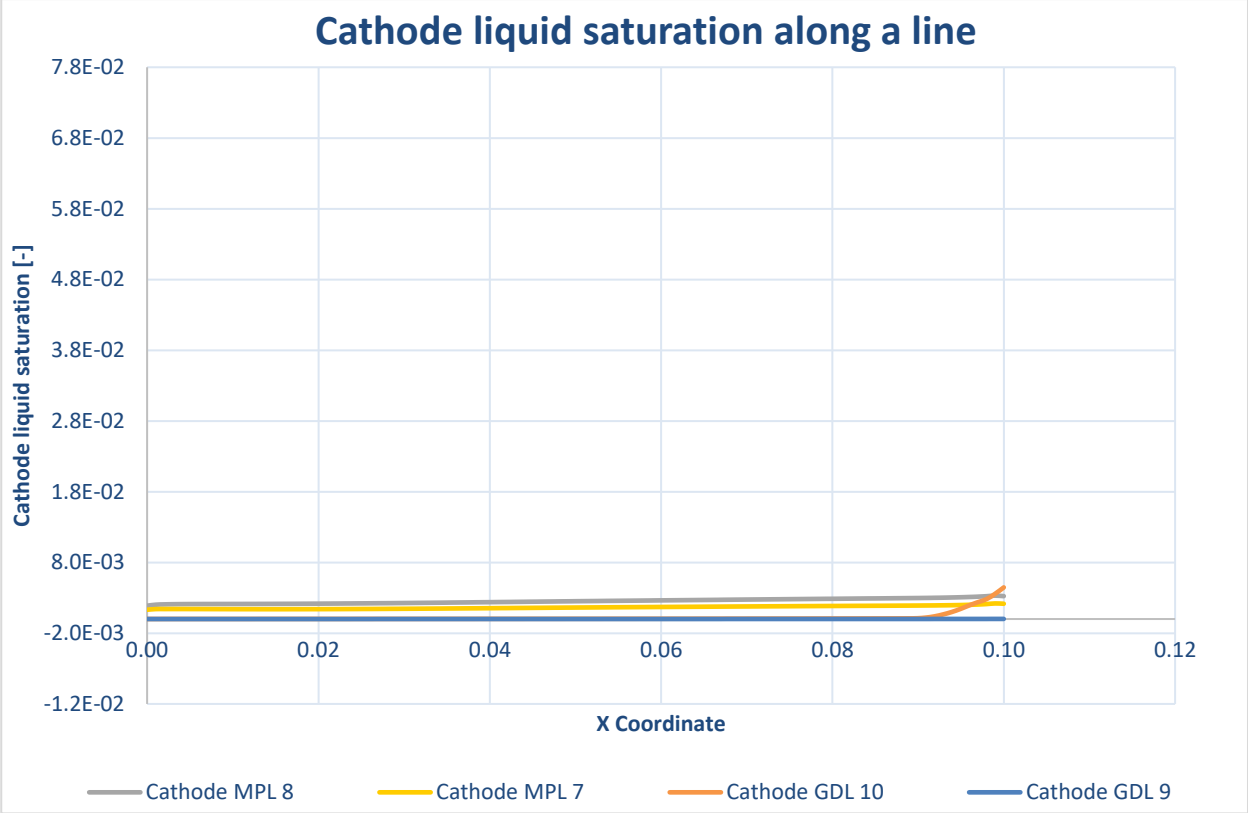

Figure 6-44 SIGRACET 34BC medium voltage cathode liquid saturation along a line

The cathode MPL liquid saturation start growing with a high slope, to arrive to a plateau, later increasing slowly, arriving to the maximum and finally briefly decreasing. The under-rib ranges between 0.19 and 0.33%, with a 43% difference, which is higher than in Figure 6-28 and Figure 6-29. The under-channel oscillates between 0.13 and 0.22%, with a 40.3%. They are both around 3 times smaller than the AvCarb P-75 case. The lower electrical conductivity affects it, heating it up and evaporating the water. There is between 30.2 and 33.2% difference among the under-rib and under-channel, meaning they are almost parallel.

The cathode GDL liquid saturation curves have negligible values, being similar to Figure 2-1Figure 6-28 and Figure 6-29, except where the under-rib one takes off at the end at 0.092m. The under-channel is raised to the sixth power, being one order of magnitude smaller than the AvCarb P-75 case. The under-rib has the same values until the point said, growing vertically to a 0.45% value, which is not comparable to the other cases that remained in low values. The colder zone suddenly has the condensed water that could not be seen before because the high temperatures had evaporated it.

In Figure 6-45 it is represented the cathode liquid saturation in different points of the GDL and MPL evolution along the X coordinate at low voltage for the SIGRACET 34BC case. The evolution in the cathode MPL is similar to the ones seen in previous cases, such as Figure 6-28, Figure 6-29 or Figure 6-44, where it is seen a increase, then a depression that leads to a constant saturation, to slowly increase, arriving at its maximum at the end. These changes are barely appreciable because the values are one order of magnitude smaller than the axis. The under-rib goes between 0.17 to 0.43%, with a 59.6% variation. At its maximum, it is a 23.5% higher than the medium voltage case in Figure 6-44, but it oscillates between that value and 25.4% smaller, because the decrease is more pronounced. At lower voltages, more water is produced, the changes on slope will also be more exaggerated. It is between 2 and 4 times smaller than the AvCarb P-75 case in Figure 6-29.

The under-channel values are between 0.094 and 0.22%, oscillating a 58.7%, being in both cases a bigger difference than in the medium voltage case. It is a 3.3% higher than the medium voltage at its maximum but a 52% smaller at the depression, showing that the stages are magnified but there is a smaller increase than in the under-rib. It is between 2.5 and 5 times smaller than the AvCarb P-75 case in Figure 6-29. Since the SIGRACET 34BC has a lower electrical conductivity and therefore higher temperatures, there is less water because it has already evaporated. It is between 41.8 and 54.7% smaller than the medium voltage case, higher than in the medium voltage case in Figure 6-44 and the AvCarb P-75 case in Figure 6-29.

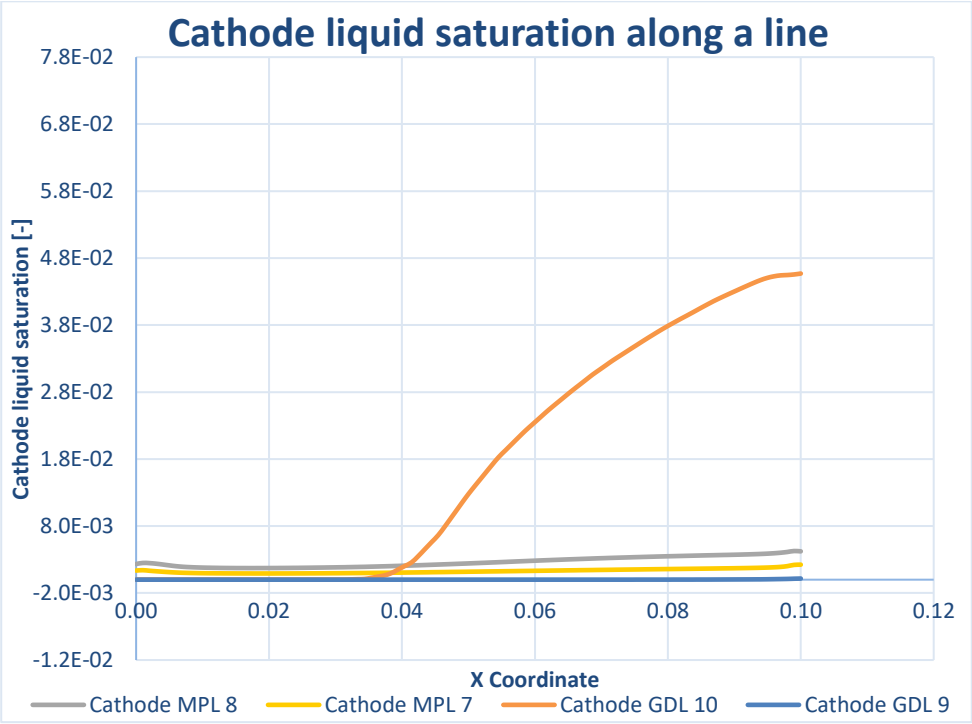

Figure 6-45 SIGRACET 34BC low voltage cathode liquid saturation along a line

The cathode GDL liquid saturation under-channel is almost negligible, starting at values raised to the seventh power and ending with three orders of magnitude more, still being several orders of magnitude smaller than the axis. At its maximum it is 89.5% higher than the medium voltage case and a 82% bigger than the AvCarb P-75 case, even if intermediate values are smaller. The higher temperatures make that there is more water evaporated, but when they reach the GDL, it is colder, condensing and having a higher amount.

The cathode GDL liquid saturation under-rib is completely different to the cases seen before because it does not remain at low and negligible values as in Figure 6-44, Figure 6-28 or Figure 6-29, but there is a point at 0.035m where it takes off, increasing up to a 4.6% value, which is several orders of magnitude higher. The high temperatures in the MPL caused by a lower electrical conductivity make that there is less water in the MPL. The GDL is colder, condensing that water, having a bigger amount than in previous cases. The temperature difference in the under-rib and its colder zone would be magnified, having a higher water amount there due to the condensation that takes place at colder zones. Figure 6-22

6.3.4. SIGRACET 34BC without MPL

This is the SIGRACET 34BC case simulated without its MPL. In Figure 6-46 it is represented the water content and temperature evolution in the membrane and cathode cooling channel evolution along the X coordinate at medium voltage for the SIGRACET 34BC without MPL case. The water content increases with slight changes on the curvature, having approximately the same growth. It starts at 5.41 and ends at 7.6, having a 28.8% increase. It is a higher difference than in the AvCarb P-75 without MPL case, but the values are smaller. It bears similarities mainly with the other case without MPL in Figure 6-30 and Figure 6-31. It is between a 14.7 and 26.3% smaller than Figure 6-30. The lower electrical conductivity makes the PEMFC heat up, having higher temperatures that evaporate the water, having less. Its behaviour has no similitudes to the

case with MPL in Figure 6-38, but it is between 43.6 smaller at the beginning and 8.8% smaller at the end. It is smaller because due to the higher permeability and porosity of the GDL, there are less impediments for the water to diffuse to other layers.

The membrane temperature briefly increases, arriving to a constant value around 351.6K, to decrease slightly at the end. The values are between 350.1 and 351.8K, just varying a 0.5%. It is between a 0.3 and 0.4% higher than the same case with MPL. The presence of the MPL hydrates better the PEMFC, reducing the temperature problems. It is between 0.38 and 0.2% smaller at the beginning and the end than the other case without MPL in Figure 6-30. It has a smaller electrical conductivity which heats up the cell, leading to higher temperatures.

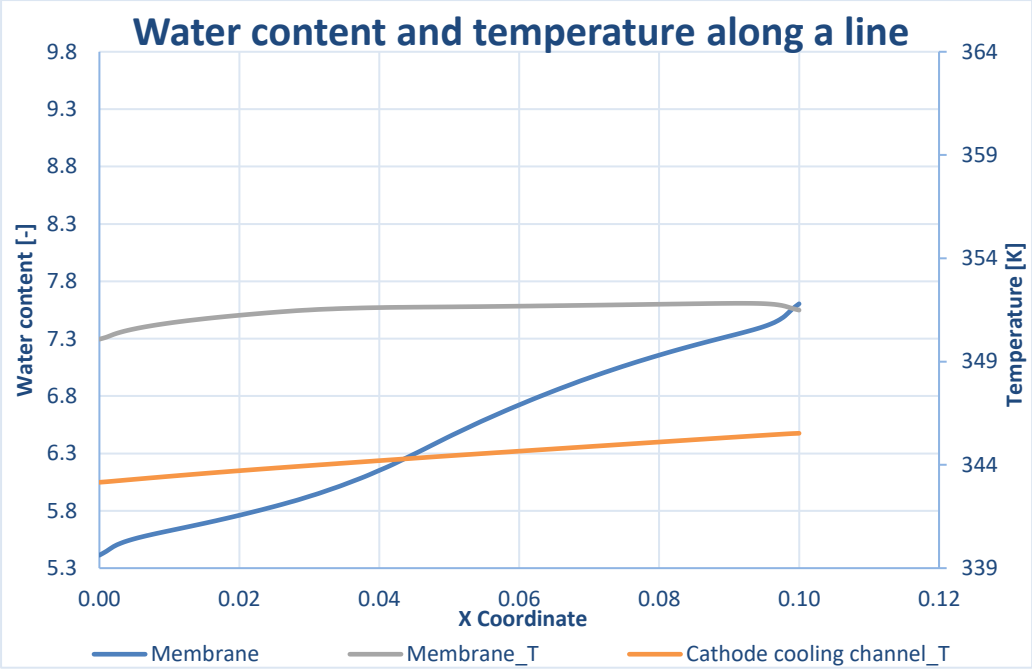

Figure 6-46 SIGRACET 34BC without MPL medium voltage water content and temperature along a line

The cathode cooling channel temperature increases with the length because at the beginning the coolant is introduced, being the coldest zone. It has a linear behaviour going from 343.2 to 345.5K, increasing a 0.7%, being the difference smaller than in the other case without MPL. It is between a 0.002 and 0.1% bigger than with MPL in Figure 6-38 at beginning and at the end respectively, meaning they diverge. It is between a 0.001 and 0.2% smaller than the values in the other case without MPL. It is a 2.1 and 1.7% decrease with respect to the temperature in the membrane, which is a higher difference than the ones seen in the case with MPL.

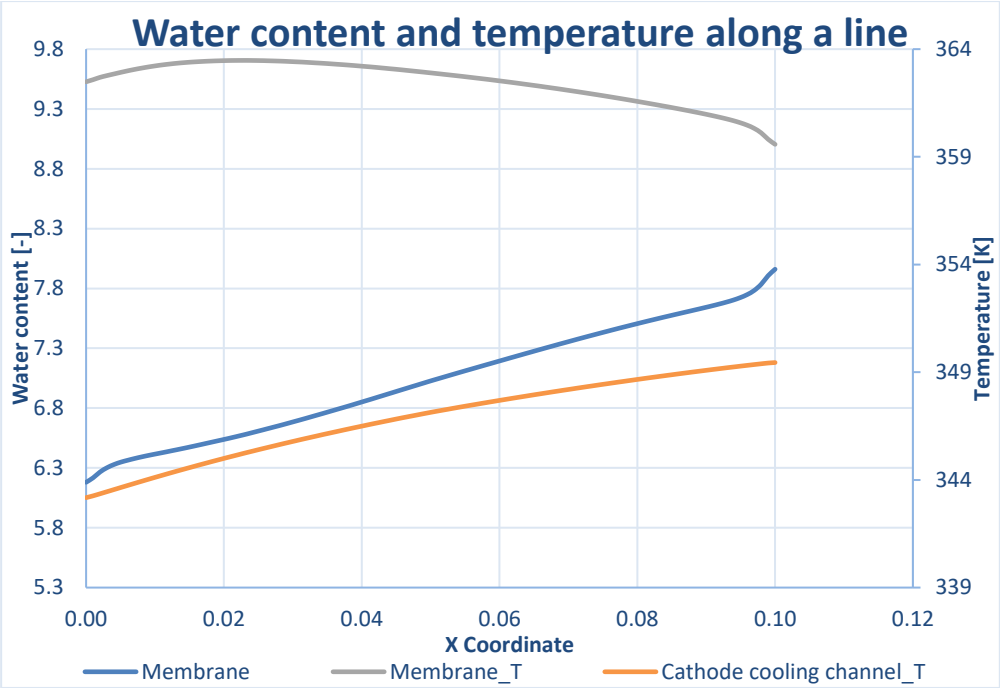

Figure 6-47 SIGRACET 34BC without MPL low voltage water content and temperature along a line

In Figure 6-47 it is represented the water content and temperature evolution in the membrane and cathode cooling channel evolution along the X coordinate at low voltage for the SIGRACET 34BC without MPL case.

The water content has the same behaviour as the other case without MPL in Figure 6-31, with a more stable slope than the medium voltage cases in Figure 6-30 and Figure 6-46. It starts increasing a high slope, then quickly changing to a constant and lower one, to return to the higher one at the end. It goes from 6.18 to 7.96, increasing a 22.4%. The increase is smaller than in the medium voltage case, but the values are between 12.5 and 4.5% higher than in Figure 6-46, corresponding to the beginning and the end, meaning they are converging. At higher currents more water is produced. It is between 46 and 13.1% smaller that the same case with MPL in Figure 6-39, getting closer towards the end. It is between 17.7 and 11.6% smaller than the other case without MPL in Figure 6-31. The lower electrical conductivity increases the temperature and therefore evaporates the water, having a lower amount than in cases with higher conductivities.

The cathode cooling channel temperature has a slight curvature, but is mainly linear, going from 343.2 to 349.4K, which makes a 1.8% increase, similar to what was obtained in the other case without MPL in Figure 6-31. It is between a 0.005 and 1.1% bigger than the medium voltage case in Figure 6-46, having its main differences at end, where the values diverge. The differences with the same case with MPL in Figure 6-39 are smaller, being between 0.004 and 0.7% higher. Both cases without MPL are very similar, having just between 0.003 and 0.2% decrease with respect to Figure 6-31. The temperatures have increased with the current.

The membrane temperature has the same behaviour as the other case without MPL in Figure 6-31, starting to increase, to decrease later slowly and dropping at the end more heavily. It has the highest temperatures seen going between 359.6 and 363.5K, ranging a 1.1%, only having other case above 360K in Figure 6-31. It is between a 3.4 and 2.2% higher than the medium voltage case in Figure 6-46, the highest increase yet seen because the low electrical conductivity makes it more sensitive to current changes, not conducting. It is between 3 and 1.3% bigger than the case with MPL in Figure 6-39, being affected by the absence of the MPL, which improves hydration, reducing the temperatures. The effect has been magnified by the effect of the conductivity. It presents less differences with the other case with MPL, having an almost constant 1% difference, which varies occasionally ±0.1, which could make them parallel. An electrical conductivity 4.4 times bigger translates in just a 1% difference in the temperatures. Since it has been seen that the cathode cooling channel curves remain in a certain range, and the membrane ones increase their values, the difference among them has increased, being between 5.3 and 2.8%.

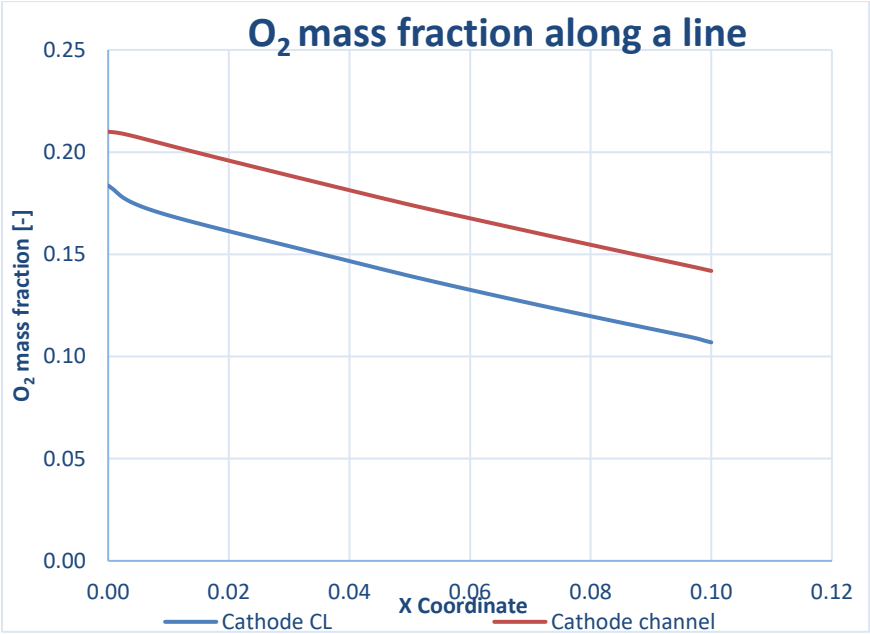

Figure 6-48 SIGRACET 34BC without MPL medium voltage oxygen mass fraction along a line

In Figure 6-48 it is represented the oxygen mass fraction in the cathode CL and channel evolution along the X coordinate at medium voltage for the SIGRACET 34BC without MPL case. The oxygen mass fraction in the cathode channel decreases linearly from 0.21 to 0.142, a 32.4%, more than in the case with MPL. It starts having the same values, just 0.002% smaller, as in the case with MPL in Figure 6-40, but diverges, ending a 6.7% smaller. The MPL has a smaller porosity and permeability, allowing less diffusion. Without it, the diffusion is not hindered anymore, going to other layers and therefore having less. It starts at the same values as the other case without MPL in Figure 6-32, but ends up a 10.8% bigger, distancing each other as it advanced along the channel and is consumed. The AvCarb P-75 case has a porosity a 11.8% bigger than the SIGRACET 34BC case, whereas the permeability is a 34.6% smaller. A higher permeability promotes diffusion, having less oxygen. The higher difference in the permeabilities has made it dominant over the other property.

The oxygen mass fraction in the cathode CL is not as linear. It goes from 0.184 to 0.107, decreasing a 42.8%. It is between a 0.5 and 13.3% smaller than the case in Figure 6-40 and between 3.3 and 17.8% bigger than Figure 6-40, showing what was stated before. It is between a 12.5 and 24.6% smaller than the cathode channel curve, having a bigger difference than in the case with MPL in Figure 6-40.

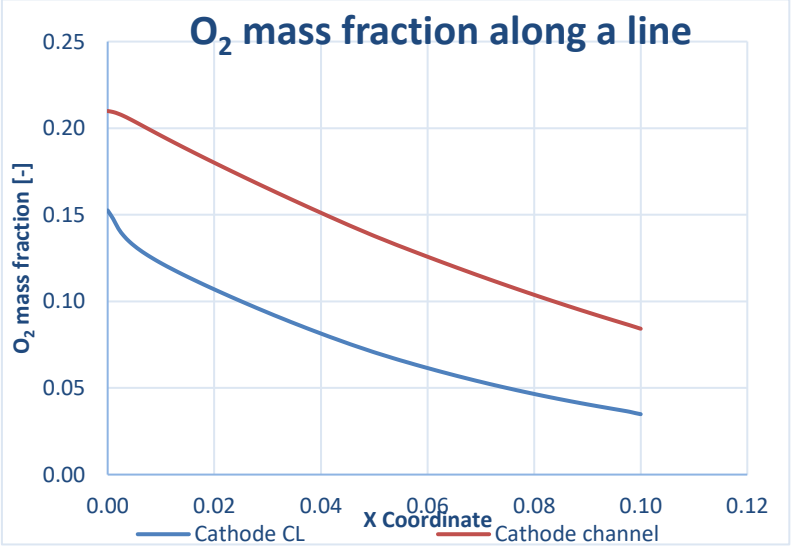

Figure 6-49 SIGRACET 34BC without MPL low voltage oxygen mass fraction along a line

In Figure 6-49 it is represented the oxygen mass fraction in the cathode CL and channel evolution along the X coordinate at low voltage for the SIGRACET 34BC without MPL case. The behaviour is similar to the other case without MPL in Figure 6-33, where the decrease is pronounced, and the cathode CL has an abrupt drop to continue as a curve and not a line. The oxygen mass fraction in the cathode channel goes from 0.21 to 0.084, decreasing a 59.9%, which is closer to the differences found in the other case without MPL in Figure 6-33. It is between 0.02 and 68.5% smaller than the case with medium voltage, diverging towards the end, having a steeper slope. Something similar happens with the case with MPL in Figure 6-41, which started being 0.02% smaller and ending with a 51.4% decrease, which is caused by the higher permeability and porosity of the GDL, which is enhanced at high voltages. The difference with the other case with MPL in Figure 6-33 is smaller, being between 0.01 and 14.3% bigger.

The cathode CL oxygen mass fraction goes from 0.153 to 0.035, decreasing 44.8%, which is less than in Figure 6-33 or Figure 6-41, but it is because it starts at a value a 20% smaller than usual, ending at approximately the same value as in Figure 6-33. It is between 16.5% and 2.6 times smaller than the case with MPL in Figure 6-41. It presents less differences with the other case without MPL being just between 9.9 and 18.9% bigger than Figure 6-33. The cathode CL curve between 27.3 and 58.6% smaller than the cathode channel, being the biggest difference seen.

The only curve that can be clearly distinguished and whose value is not zero in the SIGRACET without MPL medium voltage anode liquid saturation along the line is the under-rib anode GDL CL side liquid saturation, that around 0.04m starts to detach from the other null curves and stays around a constant 0.0011% value, which is why this figure has not been shown. The case with MPL in Figure 6-42 has its maximum at the beginning and at the end it decreases asymptotically while here its value is zero at the start and at the end it has that asymptotical value. It is several orders of magnitude smaller than the other case without MPL in Figure 6-34, but it finishes again in values close to that asymptotical value (2 times smaller) it ends with.

The anode GDL channel side liquid saturation are directly zero or raised to tenth power, considering them negligible, which are also the values found in Figure 6-42, Figure 6-34 or Figure 6-26.

The anode GDL CL side under-channel liquid saturation ends with values raised to the sixth power, which is the asymptotical values Figure 6-42 and Figure 6-34 finish with, while it starts with zero, contrary to the other cases. Having no MPL there are higher temperatures, that evaporate the water, having less. The increases porosity and permeability make that the water diffuses to other layers, not staying there. The side closer to the CL has more water because it is produced there. The under-rib also has more water because since it is a colder zone, the water condensates, having more.

It has not been shown the figure corresponding to the SIGRACET without MPL low voltage anode liquid saturation along a line because the values of all the curves were zero or negligible, not being able to see anything. The highest value is found in the anode GDL CL side under-rib, which is similar to **¡Error! No se encuentra el origen de la referencia.**, but that constant value is one order of magnitude smaller. Figure 6-43, Figure 6-35 and Figure 6-27 tend asymptotically at the end towards that low value, but at the beginning they had a peak or maximum, while here is zero. The rest of the variables are zero or raised to the ninth-tenth power. At lower voltages more water is being produced, but since the temperatures are so high as it could be seen in Figure 6-47, it evaporates, ending with the opposite effect.

In Figure 6-50 it is represented the cathode liquid saturation in different points of the GDL evolution along the X coordinate at medium voltage for SIGRACET 34BC case. It has two clearly differentiated zones: the upper part corresponds to the under-rib and the lower to the under-channel. The under-rib has higher values because since it is a colder zone, more water condensates. The curves are similar to the other case without MPL in Figure 6-36, but here they take longer to start, staying longer in null values.

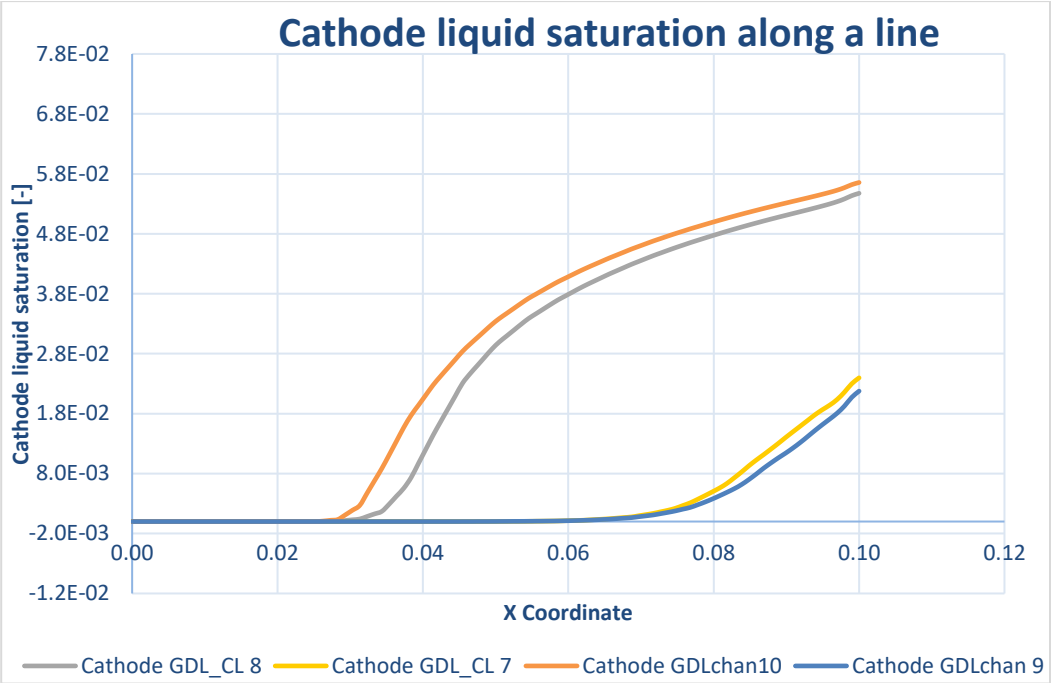

Figure 6-50 SIGRACET 34BC without MPL medium voltage cathode liquid saturation along a line

There are opposite effects taking place here. The zone closer to the CL has more water because it is being produced there, but is also where the highest temperatures are, evaporating the water. The effect of the colder zone that is the under-rib is magnified. The zone closer to the channel has less water but lower temperature, condensing it, ending up with a higher amount.

The under-rib curves start at null values and then grow parallelly, with a first and short stage of linear growth, to then do it almost vertically, leading to a less steep curve. The side closer to the channel leaves the zero values at 0.029m, while the side closer to the CL does it at 0.032m. The first one ends at a maximum of 5.7%, while the later does it at 5.5%. The one closer to the channel starts being 85.3% bigger, but it ends being just 3.5%, remaining at around a 5% in the last third of the length, reiterating the parallelism of the curves. In the other case without MPL in Figure 6-36, this difference was smaller. If both curves are compared starting where they both take off, they are between 50 and 40 times smaller than Figure 6-36, but end up with a difference of 14.5 and 13% for the CL side and the channel side respectively. These differences are because the start is delayed in this case, having small differences when both growths have arrived at the same stage. The values are one order of magnitude bigger than the case with MPL in Figure 6-44, being between around 17 and 13 times bigger.

The under-channel curves take longer to start growing, commencing both at 0.067m, but they do not take different paths until 0.076m, having the one closer to the CL a higher value. The cathode GDL CL side liquid saturation in the under-channel reaches a maximum of 2.4%, while the channel side arrives to 2.2%. The CL side is between 25.3 and 9.2% bigger than the channel side, having around a 20% constant difference in the last fifth of the length to reduce it at the end, being parallel in that zone. Since these curves take off much later than the ones seen in the other case without MPL in Figure 6-36, they are not really comparable until the end, being a 50% smaller than the later. It cannot be compared with the case with MPL in Figure 6-44, since they were 3 orders of magnitude smaller. If the not null values are considered when comparing the under-rib and under-channel values of the different zones, there is between a 96.4 and 56.2% increase in the CL side and between 95.7 and 61.5% in the channel side, which are bigger differences than in the other case without MPL because the delay on the under-channel growth increases the variance. These differences show the anomaly commented where the roles of the CL and channel side were inverted depending if they were on the under-rib or under-channel. The lower values than in the AvCarb P-75 case in Figure 6-36 are because the higher temperatures evaporate the water, reducing its amount.

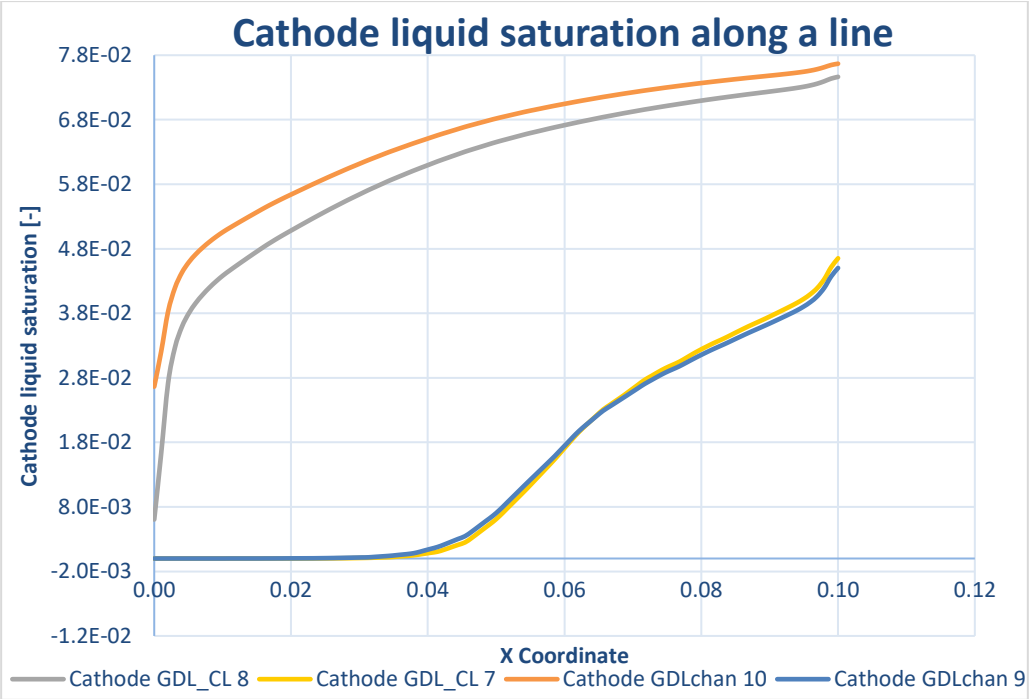

Figure 6-51 SIGRACET 34BC without MPL low voltage cathode liquid saturation along a line

In Figure 6-51 it can be seen the cathode liquid saturation in different points of the GDL evolution along the X coordinate at low voltage for the SIGRACET 34BC without MPL. This case has a low electrical conductivity that it is reflected on the increase on the temperatures that might evaporate or condensate the water present there.

It has a similar behaviour to the one seen in the other case without MPL in Figure 6-37. However, in the previous case the under-rib curves started at already high values and there was not much left to grow, here they part from lower values, having a vertical growth. Since lines are parallel, the one closer to the channel starts higher, at 2.7%, while the one closer to the CL starts below at 0.6%. In the previous case the main development was constant and horizontal because there was no more room to growth, but it has a certain slope. The cathode GDL CL side liquid saturation under-rib has a maximum at 7.7%, while the channel side has it at 7.5%. The differences between them are 77.3% at the beginning that is quickly reduced to values between 13 and 2.7%, remaining more or less constant around a 6% difference. This is a bigger variation than in the previous case because they were between 5 and 2% only. Even if the evolution had lower values than Figure 6-37, the maximums reached just at the last points are between 1.3 and 2.2% higher. The differences with the medium voltage case shown in Figure 6-50, end up being of 26.4%, while at the beginning there were several orders of magnitude of difference since they started at null values. Here the difference in temperature caused by the under-rib is more accused because of the higher temperatures, while the under-channels have significatively lower values. The case with MPL in Figure 6-45 had its values several orders of magnitude smaller than here except for the cathode GDL channel side liquid saturation in the under-rib, ending at a value that is 39% less.

The cathode GDL liquid saturation in the under-channels starts to rise at 0.039m. The effect of the low electrical conductivity is seen here in the intertwining of both curves. The channel side starts having a higher value, but at 0.063 both curves intersect, taking the CL side the lead. This is because both values are so close because of the evaporation and condensation. It could be said that the changes on the slope and curvature are almost the same as in Figure 6-37, but condensed because here it starts later and closer because they intersect. The CL side maximum is 4.7% and the channel side is 4.5%. There is just between a 2 and 3% difference among the curves, which was higher before they intersected. If the curves are compared with the medium voltage case when both have taken off, there is between 91.1 and 48.5% increase in the CL side and between 92.7 and 51.7% in the channel side. There is more water at higher currents because more water is being produced. If it is compared with the other case without MPL in Figure 6-37, starting where both curves have

already taken off, they start an order of magnitude smaller, but end up just a 9.1% smaller in the CL side and 5.8% in the channel side. This could mean that when the transitory period finishes, they both tend to the same values.

6.4. Mid-plane contours

6.4.1. AvCarb P-75

The properties shown on the mid-plane contours will be shown at the same time, having a figure that depicts the temperature, water content and through-plane current density. Low and medium voltage images will be shown at the same time in order to facilitate the comparison and see clearly the differences. The legends used and ranges are the same for both cases to simplify comparison. The temperature is between 345 and 352K, the water content is between 0 and 10.1 and the Z current flux density is between 8100 and 12450 A/m^2, which is equivalent to 0.81-12.5A/cm^2.

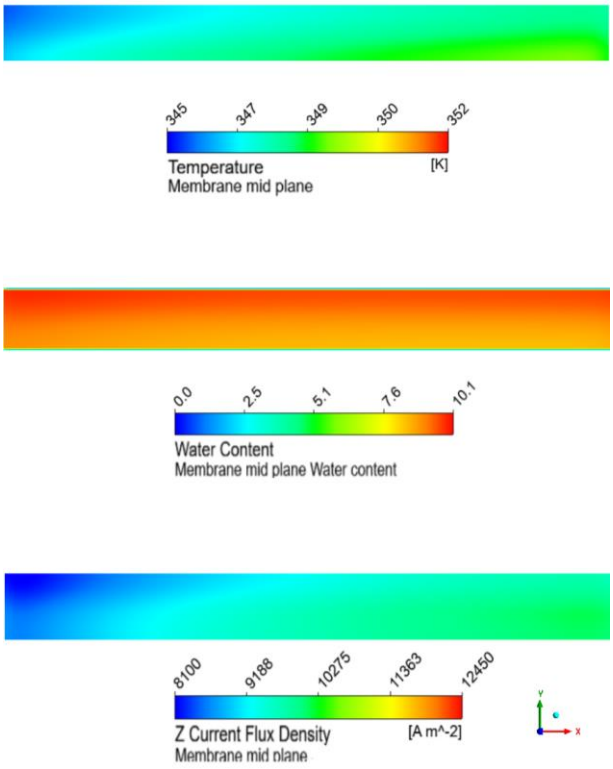

Figure 6-53 AvCarb P-75 medium voltage membrane mid-plane temperature, water content and through-plane current density

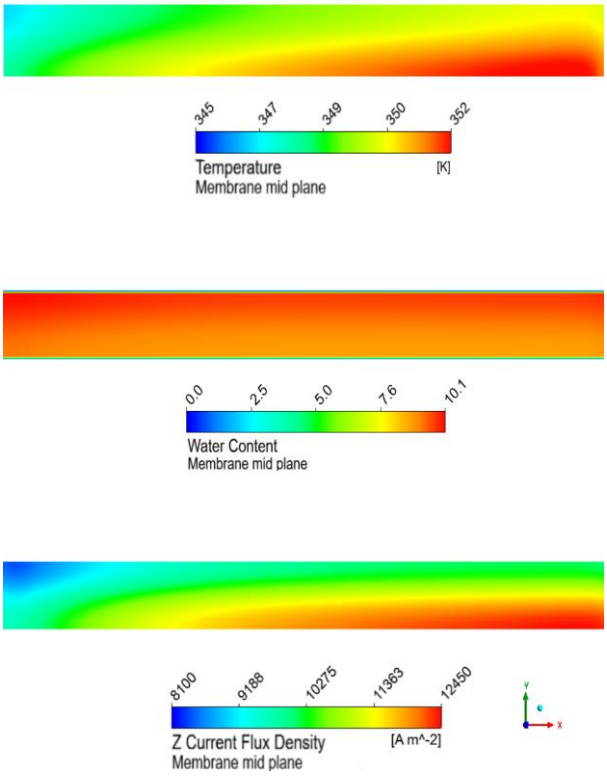

Figure 6-52 AvCarb P-75 low voltage membrane mid-plane temperature, water content and through-plane current density

In Figure 6-53 AvCarb P-75 medium voltage membrane mid-plane temperature, water content and through-plane current densityit can be seen the membrane mid-plane temperature, water content and through-plane current density at medium voltage for the AvCarb P-75 case. Opposite to it, it can be seen Figure 6-52, which is the same but at low voltage. Increasing the current increases the temperature, which makes sense, because the reaction consumes and produces more at high currents and since it is exothermic it also produces more heat. The oxidizer exits from the lower right side, that is where there are higher temperatures because the oxygen has already been consumed and there is less left. The coolant exits through the right side, so at the end the temperatures are higher because it has already been used to cool, having increased its temperature. In the opposite side is where the coolant and the oxidizer are introduced, which is why there the temperatures are lower.

There is a strange behaviour in the water content because the lower values are just in the borders, starting in very low ones. In the centre there is an almost homogeneous red colour, pointing to high values. In the

medium voltage case a more yellowish, orange colour can be seen in the lower part, indicating lower values. There is more water at lower voltages because more water is being produced.

The through-plane current density is notably bigger at lower voltages. It has a similar distribution as the one commented in the temperature, taking into account where each flow enters and exits. Where more water is being produced and oxygen consumed, would be when the oxidizer exits because more would have been consumed. At medium voltages there is not a clear separation between the upper and lower part, but between the left and right part.

6.4.2. AvCarb P-75 without MPL

The scale used in this case are not the same as on the previous case because the differences between Figure 6-53 and Figure 6-52 would not be seen due to the higher values seen mainly in Figure 6-54, that would make everything blue. The temperature goes from 348 to 364K and the water content from 5.7 to 9. The Z current flux density have different axis in order to be able to see some change on them because the low voltage case in Figure 6-54 is notably higher and the change range in Figure 6-55 is small. The medium voltage case goes from 12697 to 16415A/m^2, having a 22.7% variation, while the low voltage goes from 8689 to 34205A/m^2, having a 74.6% variation, which is much bigger.

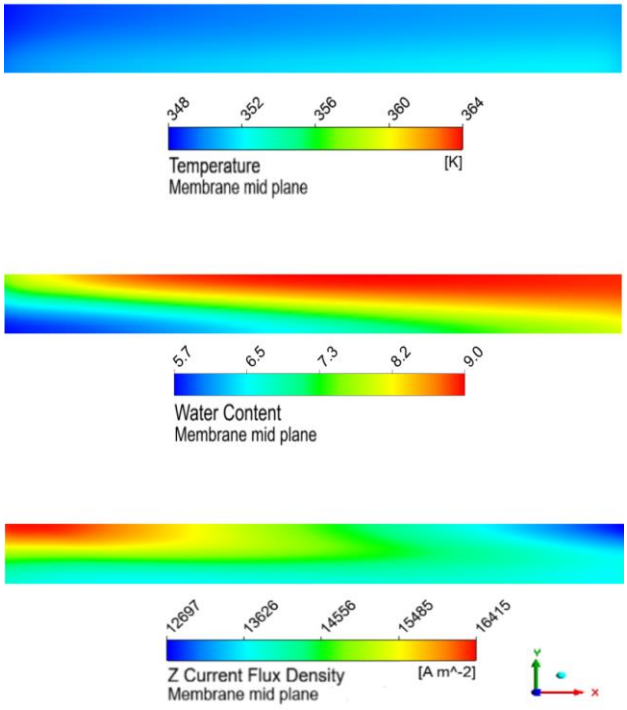

Figure 6-55 AvCarb P-75 without MPL medium voltage membrane mid-plane temperature, water content and through-plane current density

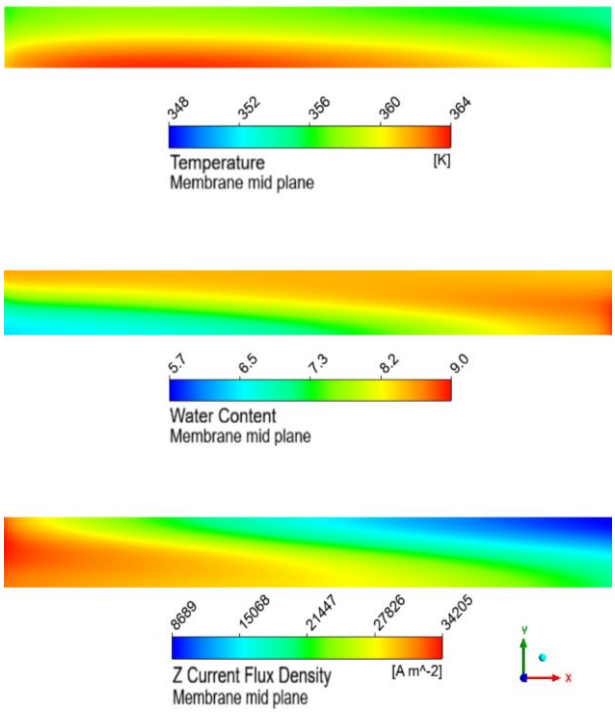

Figure 6-54 AvCarb P-75 without MPL low voltage membrane mid-plane temperature, water content and through-plane current density

In Figure 6-55 it can be seen the membrane mid-plane temperature, water content and through-plane current density at medium voltages for the AvCarb P-75 case. In Figure 6-54 the same variables for the same case are seen, but at low voltage. The difference between the temperatures is important because the medium voltage case is monochromatic, remaining in a small span. While in the medium voltage one the maximum values could be seen in the lower right side, in the low voltage case are in the lower left-centre and in the upper right are the minimums. These temperatures and ranges are higher than the ones seen in Figure 6-52 and Figure 6-53 because the MPL improves the hydration of the cell, reducing its temperature. The green zone corresponds to where the coolant travels. Being the temperatures higher and having a higher difference among them makes that the contrasts are magnified.

Here the water content does not suffer the anomaly seen in Figure 6-52 and Figure 6-53, where the lower values were concentrated in the borders making everything in the centre completely red since the scope was

bigger. What should happen is that when the current increases, more water is being produced, but the temperatures are also higher, reaching a point where it evaporates. If the temperature and water content in Figure 6-54 are compared, it can be seen that where the highest temperatures are is where there is less water and the opposite. In the medium voltage it is associated to the entrance and exits of the different fluxes, having a higher amount where the coolant is exiting and a lower one where the fuel enters because no water has been formed yet.

The Z current flux densities were so different that it was not possible a comparison with the same axis. Were there was less water is where there is a higher current because the current increases as a by-product of producing water, later there is more water, the fuel is finishing, not being able to react more.

6.4.3. SIGRACET 34BC

The SIGRACET 34BC case has a low electrical conductivity, what will be displayed on the results. Different measurement legends from the ones before, are used here. The temperature goes from 348 to 359K and the water content from 0 to 9.4. The through-plane currents are seen in different axis because the medium voltage goes from 9402 to 11004A/m^2, which is a 14.6% difference, while in the low voltage case the difference is bigger, a 42.6%, going from 10211 to 17798 A/m^2.

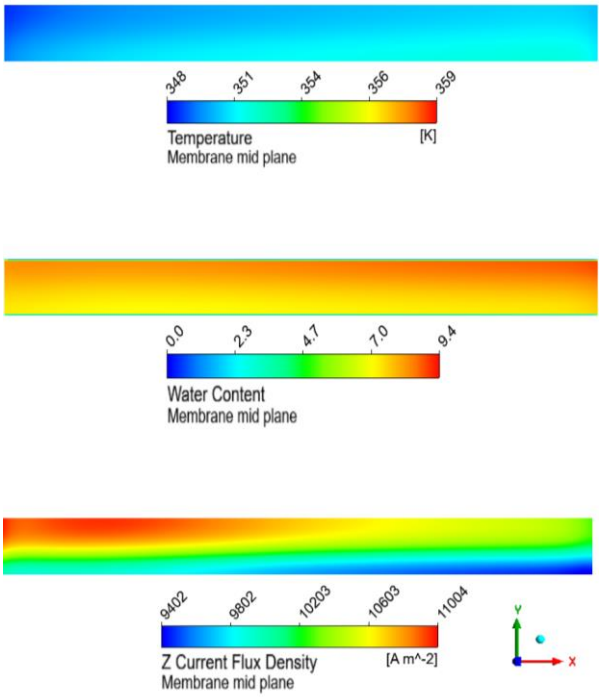

Figure 6-56 SIGRACET 34BC medium voltage membrane mid-plane temperature, water content and through-plane current density

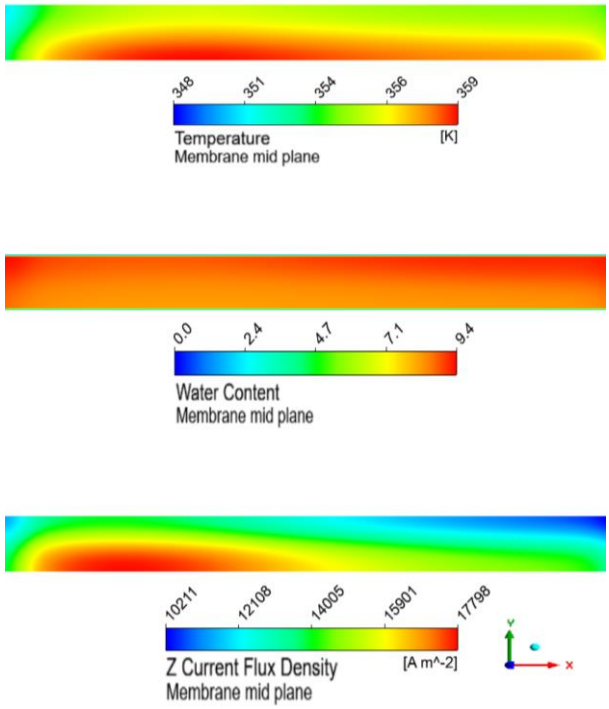

Figure 6-57 SIGRACET 34BC low voltage membrane mid-plane temperature, water content and through-plane current density

In Figure 6-56 it is represented the membrane mid-plane temperature, water content and through-plane current density at medium voltage for the SIGRACET 34BC case, while Figure 6-57 represents them at low voltage. The differences between the medium and low voltage case will be magnified by the low conductivity. The temperature range is not only 30% bigger than in the AvCarb P-75 case in Figure 6-52 and Figure 6-53, but the values are also higher, which is caused by the lower conductivity that heats up the cell. Increasing the range leads to more differences between the medium and low voltages. The medium voltage is monochromatic, meaning its temperatures are lower and have a small span. The highest temperatures are found in the oxidizer exit because more has reacted, releasing more heat. The low voltage in Figure 6-57 shows a wider range of temperatures, going from the highest found in the medium voltage, to the highest in the range. The distribution of the temperatures is similar to what happened in Figure 6-54, where there was a hotter cell. The highest temperatures are found in the lower centre-left, while in the medium voltage in Figure 6-56 that happened in

the lower right side. The effect of the coolant exit in the upper right side is magnified by the increase on the temperatures. A decrease on the voltage leads to an increase on the temperatures because the reaction is more active, producing more heat.

The water content suffers again the anomaly seen in the AvCarb P-75 case in Figure 6-52 and Figure 6-53. Both cases with MPL show the lowest values close to zero in the very thin borders and in the whole bulk of the geometry there is a higher water content. A clearer difference between the medium and low voltage cases than in the AvCarb P-75 can be seen. The medium voltage is not monochromatic but goes from an obvious limpid yellow to a dark orange in the upper part, going from 7 to 9, not reaching the maximum. The low voltage is mainly red but is orangish in the lower part, where there were higher temperatures, making the water evaporate. There are unequivocal differences between them because the lower conductivity accentuates it. It leads to higher temperatures which makes the water evaporate, having less water than the AvCarb P-75 case, which has a 7% higher maximum. If both medium voltages cases in Figure 6-53 and Figure 6-56 are compared, the extent that the SIGRACET 34BC has is 75% higher than the AvCarb P-75 case, which happens because of the higher temperatures.

The difference between the Z current flux densities was so high that it was necessary that they had different axis. Comparing the average of the ranges, the low voltage is 27% higher. The lower the voltage, the higher the current. If through-plane current is compared to the temperature contour, they have similar behaviours: where there are the highest temperatures, is where there are the highest currents. The current is higher because the reaction is happening more intensely, which means there is also more heat produced.

6.4.4. SIGRACET 34BC without MPL

The absence of the MPL and the low electric conductivity make these results extreme. The temperature axis goes from 360 to 366K and the water content goes from 5 to 8.1. The through-plane current density has completely different ranges, opting for individual axis in order to see some variation. The medium voltage case goes from 10420 to 12989A/m^2 and the low voltage goes from 10116 to 27653A/m^2.

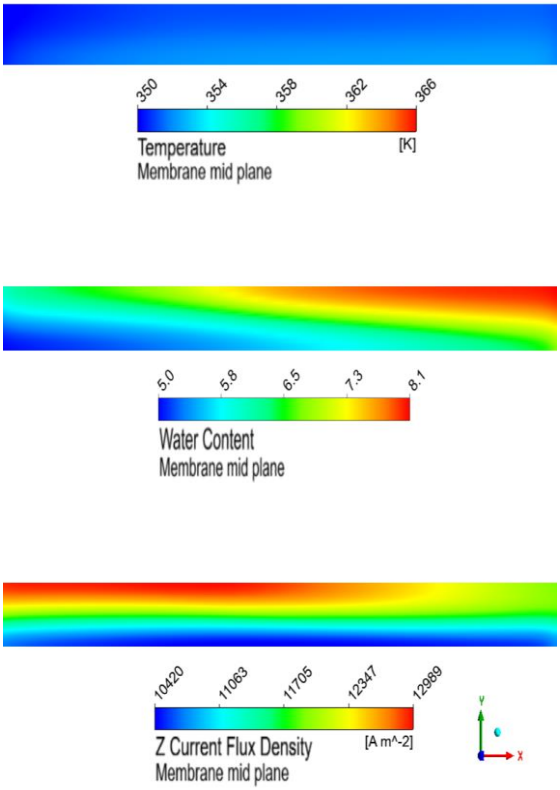

Figure 6-59 SIGRACET 34BC without MPL medium voltage membrane mid-plane temperature, water content and through-plane current density

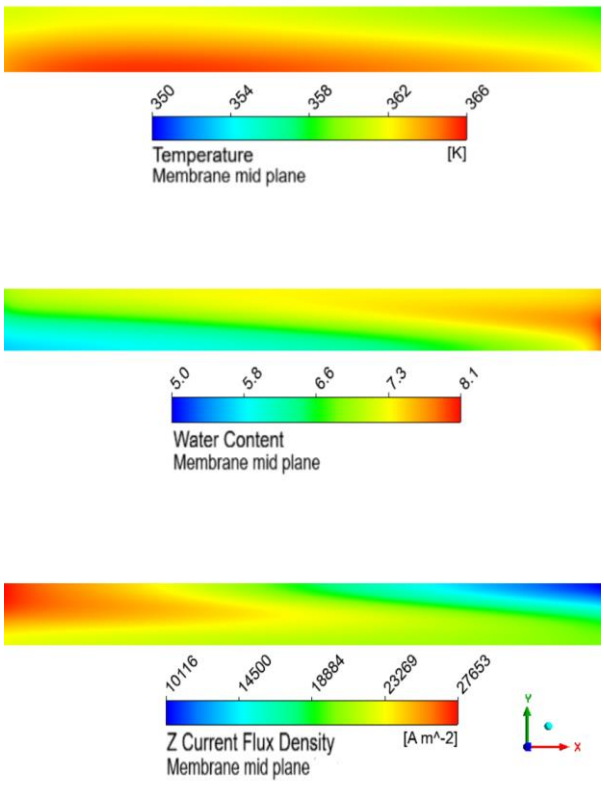

Figure 6-58 SIGRACET 34BC without MPL low voltage membrane mid-plane temperature, water content and through-plane current density

It can be seen the membrane mid-plane temperature, water content and through-plane current density at medium voltage in Figure 6-59 and at low voltage in Figure 6-58 for the SIGRACET 34BC without MPL case. The difference among them is of 16K, the same as the other case without MPL in Figure 6-54 and Figure 6-55, but a 37.5% higher than the case with MPL in Figure 6-56 and Figure 6-57. The medium voltage seems to be monochromatic, remaining in the lower values of the range. There are higher values in the lower right side, as seen in Figure 6-56 and Figure 6-55, but hear is less crystalline the difference. Its range is only between 350 and 352K, which makes the differences not appreciable in that scale. The huge difference between the medium and low voltage is accentuated by the low electrical conductivity, which makes that at high current there are higher temperatures, reaching dangerous temperatures of almost 100ºC. The behaviour in low voltage case is similar to the one seen in the other case without MPL in Figure 6-54, whereas here the higher temperature zone extends to the left also and there is less green or medium temperature zone. These slight differences emphasize the high temperatures caused by the low conductivity and absence of the MPL.

The water content does not show the anomalies the cases with MPL presented, nevertheless it bears similarities with the other case without MPL in Figure 6-54 and Figure 6-55. If the averages of the ranges in both cases without MPL are compared, this case is 12.2% smaller than the AvCarb P-75 without MPL case. The lower conductivity raises the temperatures, evaporating the water, having therefore less of it. The medium voltage has a higher water content because the temperatures are lower, having the water condensed. It can be seen clearly in the low voltage Figure 6-58 that where the temperature is highest is where there is a lower water content, being both figures opposites.

The Z current flux density are completely different. The range of the medium voltage is just of 19.8%, while the low voltage varies a 63.4%, which is a notably higher difference. The cases without MPL have higher values than without it. This difference is mainly seen at low voltages because everything is magnified there. Just the low voltage in AvCarb P-75 without MPL in Figure 6-54 had higher values, but its case with MPL in Figure 6-52 lower values not being comparable, being in the same range as the medium voltages in the cases with MPL. Not having MPL seems to increase the current density and therefore increase its range.

6.5. Discussion of the results

A lower thermal conductivity leads to lower water saturation and membrane hydration because the PEMFC heats up more significantly, which leads to the evaporation of water. The cases that had MPL have been compared among them, because its presence increase the water saturation since it improves the hydration. In the cases with MPL, a thermal conductivity 3.6 times smaller leads to 7% less water saturation. The differences when there is no MPL are more noticeable. The SIGRACET cases have between 3.2 and 3.6 times smaller thermal conductivities, which translates to around 20% less water saturation than in the AvCarb P-75 without MPL and around 40% less than the TORAY TGP-H-090. The main difference between both cases are permeability and the hydrophobic angle. It is considered that a higher PTFE amount is beneficial [1] [23] since it leads to higher hydrophobic angles, even if it is not the only thing it affects it [43]. An increase of 30% on the hydrophobic angle leads to 15% higher water saturations, confirming the positive effect. The SIGRACET case without MPL with a higher thermal conductivity is also the one which had the lowest electrical conductivity, what seems to also affect and be dominant since it results in lower water saturations. The thermal conductivity is not the only property that affects the water saturation, being able to see that higher one does not immediately lead to a higher hydration, but depends also on the electrical conductivity, that since it is smaller it inverses the effect. A 12.5% difference in both properties result in 5% lower water saturation because of the lower electrical conductivity, even if the thermal one was higher. The water saturation increases with the current density because more water is being produced, but it reaches a point where the temperatures are so high that they evaporate the water, decreasing its value.

Higher temperatures and temperatures gradients are found in the cases with lower thermal and electrical conductivities. These cases have temperatures above the safety limit of 90-100ºC and their temperature differences in the MEA are above 5K at high current densities. The simulations are suitable to foresee these problems and avoid degradation to the actual PEMFC. Cases with higher conductivities do not present the

gradient issues but are close to 90ºC when there is no MPL. The presence of the MPL is clearly seen, as in the water saturation because they are related; higher temperatures achieved without MPL result in lower water saturations. However, the maximum water saturation was achieved in the TORAY TGP-H-090, which is not the case with the lowest temperatures. It seems the temperatures are affected by the conductivities and the MPL, but the water saturation is also affected by the hydrophobic angle. The temperatures increase with the current density, because being an exothermic reaction where more products are being produced, also heat is produced. The absence of the MPL reduces the hydration and increases the temperatures in the membrane, which should not be much of a problem if the conductivities are high but lead to serious problems for lower values.

These temperatures and conductivities affect the water saturation in other layers, such as the MPL and GDL. This is seen more clearly in the cases without MPL where there was a GDL layer closer to the channel and other closer to the CL. The water saturation increases with the current density until it reaches the high current values where the temperatures are higher, making the liquid water evaporate and thus decrease. They start at almost zero values because at the beginning there is very little water in those layers. The one closer to the CL should have a higher amount because it is closer to the CL where it is being produced and it later diffuses to other layers. However, this is not what happened in the cases with low electrical and thermal conductivities because the zone closer to the CL presented a temperature that high, that the water evaporated and in the zone that is further, there was less water but more of it had condensed because the temperatures there were lower, having at the end more water in that layer. This is an atypical phenomenon caused by the low values of those properties.

The oxygen concentration decreases with the current because more O_2 is being consumed. Higher permeabilities seen in cases with no MPL lead to lower concentrations because the diffusion has not as many impediments as with the permeabilities and porosities of the MPL, which are two orders of magnitude and 2.5 times smaller than the GDL case respectively. The zone closer to the channel has the highest amount since it is closer to where the oxidizer enters and further from the CL where it is consumed. The difference between having MPL or not in the AvCarb P-75 case is being reduced to half its initial value. The difference between both SIGRACET 34BC cases was of just a 20%, having the cases without MPL the same values with small percentage differences. Not just the porosity and permeability affect the oxygen concentration because both cases with MPL had similar values in those properties and the one with the lower conductivities had values closer to the cases without MPL, maybe affecting also to the oxygen concentration.

Cooling produces a higher water saturation in the under-rib locations, locally leading to a minor oxygen diffusion capability. These differences could be clearly seen in the cathode water saturation in both cases without MPL. The case with higher conductivities has higher liquid saturation because the temperatures there are also smaller. The changes in lower voltages are more accentuated, leading to higher temperature and lower water saturations.

The MPL avoided that the water produced in the membrane arrived to the GDL, which is why it could be seen almost no water in that layer in the cases with MPL. This could be a problem in the cases without MPL because the suffer the risk of flooding.

7. CONCLUSIONS

The aim of this work was to study how the different properties of a set of commercial GDLs affected the behaviour of the PEMFC. The Computational Fluid Dynamics (CFD) ANSYS-FLUENT software was used for the simulations. First it was simulated a base case using ANSYS default variables and properties to check everything ran correctly and understand the basics of the software and PEMFC modelling. Four different commercial GDLs were then used for the study. Two of them had MPL and the two others did not. The cases with MPL were also simulated without the MPL, by modifying the properties of that layer to be the ones of the GDL, in order to analyse the effect of the presence of the MPL. The cases studied were: AvCarb P-75, SIGRACET 34BC, SIGRACET 34BA and TORAY TGP-H-090, being the first two the ones that had MPL.

First the polarization curves, the power vs. current density and electric efficiency vs. current density curves were obtained from the simulation results. Then a thorough postprocessing were carried out. A series of graphs were developed including the average in the volume of the anode and cathode GDL, MPL, CL and channels and membrane for key variables such as water saturation, temperatures, oxygen mass fraction and water content. This was done for all the commercial cases, taking the values for each cell voltage.

An additional set of graphs were prepared that included the distribution of the liquid saturation, temperature, water content and oxygen mass fraction along the length of the PEMFC (X coordinate). Such distributions were studied in the membrane, cathode CL, oxidizer and cooling channel, MPL and GDL. In the last two layers two different locations were analysed, one corresponding to the under-rib and the other to the under-channel, to study the effect that those zones had. They were studied for the cases that had MPL and their modifications without it, for medium and low voltages.

The final set of results obtained were contour plots of the membrane mid-plane evolution of the temperature, water content and through-plane current density. They were also studied just in the cases with MPL and their counterparts without it, at medium and low voltage.

The study of the cases without MPL was included in the I Meeting on Electrochemical Energy Conversion and Storage Devices, which abstract is included in Annex.

The main conclusions obtained during the study can be summarized as follows:

A higher GDL electrical conductivity reduces de Ohmic losses, increasing the power output up to a 25%. The positive effect that a higher thermal conductivity may have, is overpowered by the negative one that a low electrical conductivity has.

Lower thermal conductivities result in less water saturation and less membrane hydration, being reduced by 20%.

Cooling produces a higher water saturation under the rib, locally leading to a minor oxygen diffusion.

High temperatures and temperature gradients are identified in the membrane, for GDLs with low thermal conductivities.

A higher permeability increases the output power and cell performance.

The presence of the MPL has positive aspects if the temperatures and hydration of the layers and specifically of the membrane are taken into account, because its absence leads to temperatures that can trigger degradation. However, if the performance and power produced is considered, its effect is detrimental, having an 85% and a 30% less power than the AvCarb P-75 and SIGRACET 34BC cases without MPL respectively.

Overall, it can be concluded that CFD is a powerful tool to better understand the different phenomena affecting the performance of PEM fuel cells, and thus better design the different cell components in order to optimize the final cell performance.

REFERENCES

[1] S. PARK, L. JONG-WON and B. K. POPOV, "A review of gas difussion layer in PEM fuel cells: Materials and designs," *International Journal of Hydrogen Energy,* no. 37, 2012.

[2] M. S. ISMAIL, D. BORMAN, T. DAMJANOVIC, D. B. INGHAM and M. POURKASHANIAN, "On the through-plane permeability of microporous layer-coated gas diffusion layers used in proton exchange membrane fuel cells," *Inernational Journal of Hydrogen Energy,* no. 36, p. 11, 2010.

[3] R. OMRANI and B. SHABANI, "Gas diffusion layer modifications and treatements for improving the performance of proton exchanfe membrane fuel cells and electrolysers: A review," *International Journal of Hydrogen Science,* no. 42, p. 22, 2017.

[4] A. OZDEN, S. SHAHGALDI, X. LI and F. HAMDULLAHPUR, "A review of gas diffusion layers for proton exchange membrane fuel cells- With a focus on characteristics, characterization techniques, materials and designs," *Progress in Energy and Combustion Science,* no. 74, p. 53, 2019.

[5] E. CARCADEA et al., "PEM fuel cell performance improvement through numerical optimization of the parameters of the porous layers," *International Journal of Hydrogen Energy,* no. 35, p. 13, 2019.

[6] O. S. BURHEIM, J. G. PHAROAH, H. LAMPERT, P. J. VIE and S. KJELSTRUP, "Through-Plane Thermal Conductivity of PEMFC Porous Transport Layers," *Journal of Fuell Cell Science and Technology,* vol. 8, p. 11, 2011.

[7] A. CASALEGNO, "Lesson 1-Introduction 2020," in *Electrochemical Energy Conversion and Storage*, Politecnico di Milano, 2020.

[8] A. CASALEGNO, "Lesson 5 PEMFC Technology," in *Electrochemical Energy Conversion and Storage*, Politecnico di Milano, 2020.

[9] H. LI and et al., "A review of water flooding issues in the proton exchange membrane fuel cell," *Journal of Power Sources,* vol. 178, no. 1, p. 15, 2008.

[10] A. CASALEGNO, "Lesson 6-Electrolyser technology," in *Electrochemical Energy Conversion and Storage,* Politecnico di Milano, 2020.

[11] M. CARMO, D. L. Fritz, J. MERGEL and D. STOLTEN, "A comprehensive review on PEM water electrolysis," *International Journal of Hydrogen Energy,* vol. 38, no. 12, p. 33, 2013.

[12] C. LEFROU, P. FABRY and J.-C. POIGNET, Electrochemistry The Basics, With Examples, Springer-Verlag Berlin Heidelberg, 2012.

[13] Hydrogen Roadmap Europe team, "Hydrogen Roadmap Europe: A sustainable pathway for the energy transition," 6 February 2019. [Online]. Available: https://www.fch.europa.eu/sites/default/files/20190206_Hydrogen%20Roadmap%20Europe_Keynote_Final.pdf. [Accessed 31 December 2020].

[14] L. N. CLEEMANN, “Section for Electrochemistry. Department for Energy Conversion and Storage,” DTU, 2 February 2019. [Online]. Available: https://www.ele.energy.dtu.dk/Research/Fuel-cells. [Accessed 21 December 2020].

[15] L. CINDRELLA and et al., “Gas diffusion layer for proton exchange membrane fuel cells- A review,” *Journal of Power Sources,* no. 1, p. 14, 2009.

[16] A. P. MANSO, F. MARZO, J. BARRANCO, X. GARIKANO and M. GARMENDIA-MUJIKA, “Influence of geometric parameters of the flow fields on the performance of a PEM fuel cell. A review,” *International Journal of Hydrogen Energy,* vol. 37, no. 20, p. 36, 2012.

[17] A. JENKINS, P. KRATOCHVIL, R. STEPTO and U. SUTTER, “Glossary of basic terms in polymer science (IUPAC Recommendations 1996),” *Pure and Applied Chemistry,* vol. 68, no. 12, p. 24, 1996.

[18] A. CASALEGNO, “Lesson 8-PEMFC Issues,” in *Electrochemical Energy Conversion and Storage,* Politecnico di Milano, 2020.

[19] US Deparment of Energy, “DOE hydrogen and fuel cells program record (2016),” 30 September 2016. [Online]. Available: parameter values except for the Q/□T parameter which only occurs in single variable analysis.. [Accessed 29 December 2020].

[20] R. BORUP and et al., “Scientific Aspects of Polymer Electrolyte Fuel Cell Durability and Degradation,” *Chemical Review,* no. 107, p. 47, 2007.

[21] J. KIM and et al., “Effects of Cathode Inlet Relative Humidity on PEMFC Durability during Startuo-Shutdown Cycling,” *Journal of Electrochemical Society,* vol. 157, no. 5, 2010.

[22] A. BARICCI, “Lesson 9- PEMFC modelling and BoP,” in *Electrochemical Energy Conversion and Storage,* Politecnico di Milano, 2020.

[23] M. S. ISMAIL and et al., “Through- Plane Permeability for Untreated and PTFE-Treated Gas Diffusion Layers in Proton Exchange Membrane Fuel Cells,” *Journal of Fuel Cell Science and Technology,* vol. 7, p. 7, 2010.

[24] T&D India, “E-mobility. NTPC Invites EOIs For Supply Of Fuel-Cell Electric Vehicles,” 26 April 2020. [Online]. Available: http://www.tndindia.com/ntpc-invites-eois-supply-fuel-cell-electric-vehicles/. [Accessed 31 December 2020].

[25] A. CASALEGNO, “Lesson 19-Automotive application,” in *Electrochemical Energy Conversion and Storage,* Politecnico di Milano, 2020.

[26] Toyota, “Toyota's strategies for Environmental Technologies,” [Online]. Available: http://www.toyota.com.cn/innovation/environmental_technology/strategy_environmental_tech.html. [Accessed 31 December 2020].

[27] Sylfen, “The reversible electrolyser,” 2021. [Online]. Available: https://sylfen.com/en/technology/. [Accessed 13 January 2021].

[28] COMMISSARIAT A L'ENERGIE ATOMIQUE ET AUX ENERGIES ALTERNATIVES, “Reversible solid oxide Electrolyzer and Fuel cell for optimized Local Energy miX,” CORDIS. European Comission, 25 November 2019. [Online]. Available: https://cordis.europa.eu/project/id/779577/reporting/es. [Accessed 13 January 2021].

[29] M. ZAGO and M. MERLO, “Lesson 21- Aplications for energy storage,” in *Electrochemical Energy Conversion and Storage*, Politecnico di Milano, 2020.

[30] E. WEIDNER, R. ORTIZ-CEBOLLA and J. DAVIS, "Global deployment of large capacity stationary fuel cells," European Union, 2019. [Online]. Available: https://publications.jrc.ec.europa.eu/repository/bitstream/JRC115923/jrc115923_stationary_fuel_cells_16042019_final_pubsy_online.pdf. [Accessed 13 January 2021].

[31] AkzoNobel, "Successful Launch for Pilot Plant," 21 January 2005. [Online]. Available: https://www.akzonobel.com/en/for-media/media-releases-and-features/successful-launch-pilot-plant. [Accessed 13 January 2021].

[32] Y. WANG, K. S. CHEN, J. MISHLER, S. C. CHO and X. CORDOBES-ADROHER, "A review of polymer electrolyte membrane fuel cells: Technology, applications, and needs on fundamental research," *Applied Energy,* no. 88, p. 27, 2011.

[33] E4tech, "The Fuell Cell Industry Review 2019," 2019.

[34] Fuel Cell Works, "Daesan Hydrogen Fuel Cell Power Plant Completed with Help of Doosan Fuel Cells," Fuel Cell Works, 31 July 2020. [Online]. Available: https://fuelcellsworks.com/news/daesan-hydrogen-fuel-cell-power-plant-completed-with-help-of-doosan-fuel-cells/. [Accessed 13 January 2021].

[35] Fuel Cells Bulletin, "FCE power plants in world's largest fuel cell park, running in Korea," *Fuel Cells Bulletin,* vol. 2011, no. 12, p. 6, 2011.

[36] Fuel Cells Bulletin, "Martinique is next port of call for 1 MW PEM fuel cell power plant," *Fuel Cells Bulletin,* vol. 2016, no. 2, p. 5, 2016.

[37] DEMCOPEM, "Launching Ceremony in China of the World's first 2MW PEM fuel cell power plant," DEMCOPEM 2MW, October 2016. [Online]. Available: https://demcopem-2mw.eu/worlds-first-2mw-pem-fuel-cell-power-plant/. [Accessed 13 January 2021].

[38] A. BARICCI, "Lesson 7- Detailed analysis of PEMFC components," in *Electrochemical Energy Conversion and Storage*, Politecnico di Milano, 2020.

[39] A. IRANZO, J. M. GREGORIO, P. BOILLAT and F. ROSA, "Bipolar plate research using Computational Fluid Dynamics and neutron radiography for proton exchange membrane fuel cells," *International Journal of Hydrogen Energy,* no. 45, p. 11, 2020.

[40] A. IRANZO, M. MUÑOZ, F. ROSA and J. PINO, "Numerical model for the performance prediction of a PEM fuel cell. Model results and experimental validation," *International Journal of Hydrogen Energy,* no. 35, p. 18, 2010.

[41] Fuel Cell Store, "SIGRACET GDL 34 & 35 Series Gas Diffusion Layer," SIGRACET, 2009. [Online]. Available: https://www.fuelcellstore.com/spec-sheets/SGL-GDL_34-35.pdf. [Accessed 29 October 2020].

[42] Fuel Cell Store, "Toray Carbon Fiber Paper "TGP-H"," TORAY, [Online]. Available: https://www.fuelcellstore.com/spec-sheets/toray-carbon-paper-data-sheet.pdf. [Accessed 3 November 2020].

[43] Q. CHEN, Z. NIU, H. LI, K. JIAO y Y. WANG, «Recent progress of gas diffusion layer in proton exchange membrane fuel cell: Two-phase flow and material properties,» *International Journal of Hydrogen Energy* , p. 32, 2020.

[44] H. SADEGHIFAR, N. DJILALI and M. BAHRAMI, "Effect of Polytetrafluoethylene (PTFE) and micro porous layer (MPL) on thermal conductivity of fuel cell gas diffusion layers: Modelling and

experiments," *Journal of Power Sources,* no. 248, p. 10, 2014.

[45] A. IRANZO, Tesis Doctoral: Desarrollo y validación experimental de un modelo computacional de pila de combustible tipo PEM y su aplicación al análisis de monoceldas, Sevilla: Departamento de Ingeniería Energética-Grupo de Termotecnia. Escuela Superior de Ingenieros, 2010.

[46] E. C. KUMBUR, K. V. SHARP and M. M. MENCH, "Liquid droplet behavior and instability in a polymer electrolyte fuel cell flow channel," *Journal of Power Sources,* no. 161, p. 13, 2006.

[47] ANSYS, «Tutorial: The New PEMFC Model,» 2019.

[48] ANSYS, «Chapter 25. Modelling PEMFC,» de *ANSYS Fluent Theory Giude. Fluent 2021 R1*, 2021, p. 14.

[49] G. CHEN, G. ZHANG, L. GUO and H. LIU, "Systematic study on the functions and mechanisms of micro porous layer on water transport in proton exchange membrane fuel cells," *International Journal of Hydrogen Energy,* no. 41, p. 11, 2016.

[50] K. JIAO and X. LI, "Water transport in polymer electrolyte membrane fuel cells," *Progress in Energy and Combustion Science,* no. 37, p. 71, 2011.

[51] Y. WANG and et al., "Three- dimensional simulation of a PEM fuel cell with experimentally measured through-plane gas effective difusivity considering Knudsen diffusion and the liquid water effect in porous electrodes," *Electrochimica Acta,* no. 318, p. 13, 2019.

ACRONYMS AND GLOSARY

CCL: Cathode catalyst layer 8, 10
CHP: Combined heat and power 12
CL: Catalyst Layer ..... passim
ECSA: Electrochemically Active Surface Area 5, 8, 9, 10
EES: Electric Energy Stored 11
FCEV: Fuel Cell Electric Vehicle 10, 11
GDL: Gas Diffusion Layer ..... passim
LHV: Low Heating Value 28
MCFC: Molten Carbonate Fuel Cells 30
MEA: Membrane Electrode Assembly 5, 10
OCV: Open Circuit Voltage 5, 9, 10
PEMFC: Proton-Exchange Polymer Electrolyte/Membrane Fuel Cell ..... passim
PTFE: Polytetrafluoroethylene ..... passim
RH: Relative Humidity 6, 7, 10
SOFC:Solid Oxide Fuel Cell 11, 12

ANNEX

The results obtained during the development of this work were presented at the I Meeting on Electrochemical Energy Conversion and Storage Devices (ECHEMCONSTORE I, January 28th-29th, 2021, Leganés, Spain).

The book of abstracts of EChemCONSTORE I has been edited and published at the UC3M institutional repository, with ISBN 978-84-16829-60-6

https://e-archivo.uc3m.es/handle/10016/31914

EChemCONSTORE

uc3m | Universidad Carlos III de Madrid

Computational Fluid Dynamics modelling and simulation of a fuel cell: Influence of the Gas Diffusion Layer design on the water management and cell performance

Laura González-Morán[1], Alfredo Iranzo[1,2], José Guerra[1]

[1] *Thermal Engineering Group, Energy Engineering Department, University of Seville, Camino de los Descubrimientos, s/n, 41092, Sevilla, Spain*
[2] *AICIA - Thermal Engineering Group, Camino de los Descubrimientos, s/n, 41092, Sevilla, Spain*

The main objective of this work is to study the influence of different parameters of the Gas Diffusion Layer (GDL) on the performance and operation of a Proton-Exchange Polymer Electrolyte Fuel Cell (PEMFC). In order to do so, several CFD simulations have been carried out with the ANSYS-Fluent PEMFC model, comparing real commercial GDLs with different properties, and observing their influence on their performance. The effect of the presence of the Microporous Layer (MPL) has been studied by simulating the same GDL with and without the MPL. All the GDLs studied had approximately the same thickness range of 285± 30μm. Four commercial GDLs have been singled out (AvCarb P-75, SIGRACET 34BC, SIGRACET 34BA and Toray TGP-H-090), two of them including MPL, with a total of 6 cases. The simulations were carried out varying the voltage between 1.05 and 0.35V to a have a set of eight representative IV points to obtain the polarization curve.

The analysis of the results was carried out based on four different kind of curves. The first set of curves was obtained directly from the simulation data, obtaining the polarization curves (voltage vs. current density), power and electrical efficiency; all against the current density for all the 6 cases. Secondly, the next set of curves was obtained for all the commercial GDLs, measuring for each voltage the water content, liquid saturation, O_2 mass fraction, average and maximum temperatures in the volume of certain cell components (membrane, catalyst layer, GDL, MPL). They were grouped in sets of similar properties to simplify them. For an additional set of results, the evolution of different variables along the axial coordinate of the PEMFC was drawn in 12 strategic locations, obtaining the longitudinal evolution of temperature, O_2 mass fraction, liquid saturation and water content along the cell. This was studied for the cases of the GDLs with and without MPL, and for low voltage (0.45V) and medium voltage (0.65V). Finally, contour plots were created at the membrane mid-plane (through-plane direction) on the PEMFC representing the distributions of temperature, water content and through-plane current flux.

It can be concluded that higher electrical conductivity and higher permeability lead to a better cell performance. The MPL features a lower permeability, and therefore results in a worse performance, but the lack of it may create cell flooding issues.

On the figures shown, different through-plane key variables on the membrane mid-plane for different voltages of the same commercial GDL can be observed.

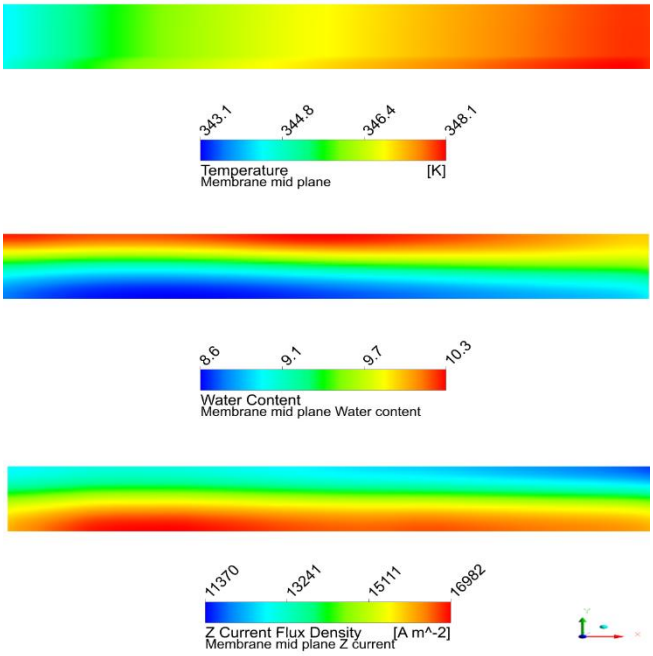

Fig.1 – Membrane midplane Temperature, Water Content and through-plane Current Density at 0.45V for AvCarb P-75 with MPL

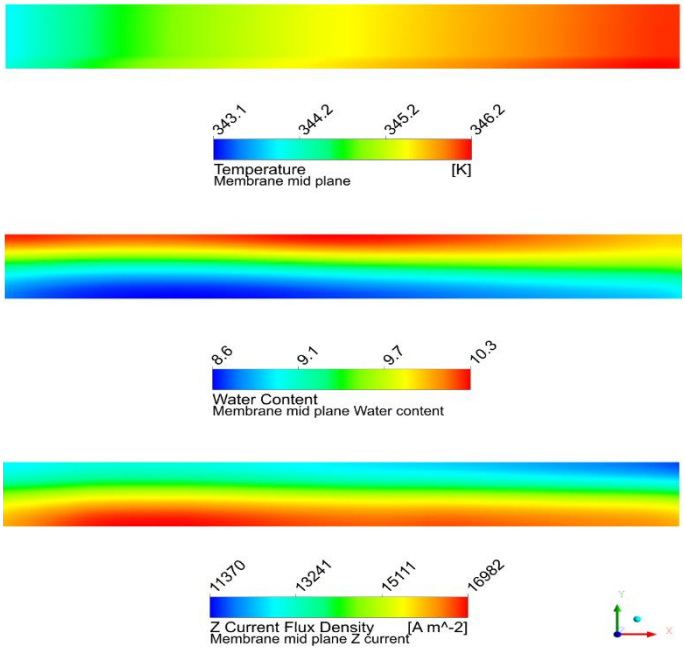

Fig.2 Membrane midplane Temperature, Water Content and through-plane Current Density at 0.45V for AvCarb P-75 with MPL

Acknowledgements

Consejería de Economía, Conocimiento, Empresas y Universidad, PAIDI 2020 (IE18_0057_AICIA; PY20 RE026 AICIA) co-funded with ERDF funds. Ministerio de Ciencia, Innovación y Universidades (EQC2018- 004258-P), funded by AEI/FEDER UE.

References

[1] R. Omrani and B. Shabani, "Gas diffusion layer modifications and treatements for improving the performance of proton exchanfe membrane fuel cells and electrolysers: A review," *International Journal of Hydrogen Science*, **42**, p. 22, 2017.

[2] C. Lefrou, P. Fabry and J.C. Poignet, Electrochemistry The Basics, With Examples, Springer-Verlag Berlin Heidelberg, 2012.

[3] M. S. Ismail, D. Borman, T. Damjanovic, D. B. Ingham and M. Pourkashanian, "On the through-plane permeability of microporous layer-coated gas diffusion layers used in proton exchange membrane fuel cells," *Inernational Journal of Hydrogen Energy*, **36**, p. 11, 2010.

Trabajo Fin de Máster
Máster en Ingeniería Industrial

Modelado de Dinámica de Fluidos Computacional y simulación de una pila de combustible: Influencia del diseño de la capa de difusión gaseosa en el tratamiento del aguay rendimiento de la pila

Autor: Laura González Morán
Tutor: José Alfredo Iranzo Paricio

Dpto. de Ingeniería Energética
Escuela Técnica Superior de Ingeniería
Universidad de Sevilla

Sevilla, 2021

Resumen

El objetivo principal de este trabajo ha sido estudiar la influencia que tienen distintos parámetros de la capa de difusión de gases (GDL) en la rendimiento y operación de una pila de combustible de membrana de intercambio protónico (PEMFC). Para ellos se han desarrollado una serie de simulaciones CFD con el modelo ANSYS-Fluent PEMFC, comparando GDLs comerciales con diferentes propiedades, observando su influencia en el desempeño final. Se ha estudiado el efecto de la presencia de la capa microporosa (MPL), simulando las GDL con y sin ella. Todas las GDLs estudiadas se encuentran en el mismo rango de grosor 285±30μm, siendo este uno de los criterios para su elección. Se han considerado cuatro GDLs comerciales (AvCarb P-75, SIGRACET 34BC, SIGRACET 34BA y TORAY TGP-H-090), donde los dos primeros incluyen MPL, creando un total de 6 casos. Se ha hecho también un estudio de los datos base que aportaba ANSYS con y sin MPL para comprobar que todo funcionara adecuadamente, añadiendo dos casos más. Las simulaciones se llevaron a cabo variando los voltajes entre 1.05 y 0.35V para tener una serie de ocho puntos IV representativos para crear la curva de polarización.

El análisis de los resultados se basó en cuatro tipos diferentes de curvas. El primer tipo se obtuvo directamente de los datos proporcionados por la simulación, creando las curvas de polarización (voltaje vs. densidad de corriente), potencia y eficiencia eléctrica; todas ellas contra la densidad de corriente para todos los casos. La siguiente serie de curvas se obtuvo para todas las GDLs comerciales, midiendo para cada voltaje el contenido el agua, saturación del líquida, fracción másica de oxígeno, temperaturas máximas y medias en el volumen de ciertos componentes de la célula, como son la membrana, GDL, MPL y capa catalítica. Fueron agrupadas en propiedades afines para simplificar la representación. Otra serie de curvas fue creada estudiando la evolución de diferentes variables a lo largo de la coordenada axial de la PEMFC, dibujando dichas líneas en 12 puntos estratégicos, obteniendo la evolución longitudinal de la temperatura, fracción másica de oxígeno, saturación líquida y contenido de agua a lo largo de la célula. Esto fue estudiado para los casos de las GDLs con MPL y sus variaciones sin ésta, para voltaje bajo (0.45V) y medio (0.65V). Finalmente, se crearon una serie de mapas de contorno, creado en plano medio (en la dirección a través del plano) in la PEMFC, representando las distribuciones de temperatura, contenido de agua y el flujo de corriente a través del plano.

Se puede concluir que altas conductividades eléctricas y térmicas llevan a un mejor comportamiento de la célula. La MPL contiene permeabilidades más bajas, resultando en una peor actuación, pero su ausencia lleva a problemas de hidratación y degradación.

Palabras clave: pilas de combustible, fluido dinámica, medio poroso, difusión, conductividad, modelado numérico.

1 INTRODUCCIÓN

Los conceptos fundamentales estudiados en este trabajo son las pilas PEM, sus partes, componentes, funcionamiento, problemática y aplicaciones. Se comenta también brevemente las distintas partes de la curva de polarización para entender sus cambios. Se ha utilizado una herramienta CFD (Computational Fluid Dynamics en inglés) para la simulación y modelado de la pila. Se ha profundizado en las distintas propiedades de la GDL (Gas Diffusion Layer en inglés) para ver cómo afectan a las prestaciones de la pila

1.1. Pila PEM

Las pilas de combustible de membrana de intercambio protónico (PEM), convierten directamente el fuel (H_2) en energía eléctrica sin pasar por el calor de un ciclo directo. Se alimenta el fuel al ánodo y el oxidante (aire) al cátodo, obteniendo las siguientes expresiones:

$$H_2 \rightarrow 2H^+ + 2e^- \text{ Ánodo}$$

$$2H^+ + \frac{1}{2}O_2 + 2e^- \rightarrow H_2O \text{ Cátodo}$$

$$H_2 + \frac{1}{2}O_2 \rightarrow H_2O \text{ Reacción total}$$

Si las reacciones fueran en el sentido contrario, sería un electrolizador, siendo un proceso similar a la carga de una batería, siendo usado para el almacenaje.

Entre las características más importantes de esta tecnología se encuentra que necesita hidrógeno puro (CO < 10 p.p.m.) porque a bajas temperaturas puede producirse envenenamiento. Tiene una alta densidad de potencia, mayor a 3kW/dm^3. Trabaja a bajas temperaturas, proporcionando rápidas dinámicas para el arranque. El agua debe ser correctamente administrada para evitar deshidratación e inundaciones, donde la formación de líquido bloquea la capa de difusión o la catalítica. Sus principales problemas son el coste y durabilidad.

1.2. Componentes

Esta tecnología está caracterizada por su membrana, que es un electrolito sólido que permite la transferencia de protones, siendo la capa activa donde tienen lugar las reacciones. Las temperaturas de operación se encuentran entre 40 y 90ºC, por lo que se requiere un catalizador muy efectivo, como

platino en ambas caras. Encima de esta capa catalítica se encuentra una capa de difusión (GDL) que es necesaria para la distribución uniforme del reactante en la capa catalítica. En algunos casos hay una capa microporosa (MPL) entre las capas catalíticas y de difusión, más hidrófoba. Luego hay unas juntas para evitar fugas. Después hay unos campos de flujo que es donde se encuentran los canales que alimentan los reactantes. Finalmente se emparedan de manera simétrica.

1.3. Principios de operación y funcionamiento

La capa catalítica está compuesta por partículas de carbono que tienen adheridas partículas de catalizador. El ionómero conecta ambas partículas con la membrana, creando por lo tanto una barrera trifásica.

En el cátodo el aire es introducido con una humedad relativa de 30-50%, saliendo con casi 100% porque se produce la electro-osmosis. En el ánodo ocurre lo contrario, el hidrógeno entra con una humedad del 30-50%, saliendo con humedades muy altas. El agua se transporta de donde está más a menos hidratado.

1.4. Problemática

Los principales problemas para su despliegue son su coste y durabilidad, gravemente afectados por la degradación. En algunos casos la degradación es producida por altas temperaturas, que podría evitarse conociendo dónde sucederían gracias a las herramientas CFD.

La disolución del platino lo lleva de un estado metálico a iones y protones. Se pueden producir dos mecanismos diferentes que serían la formación de una banda de Pt o pérdida de la carga de Pt por una parte o la maduración de Ostwald, también conocida como la redeposición o crecimiento del tamaño.

Se produce la pérdida de área efectiva activa del catalizador (ECSA en inglés) del cátodo debido a la degradación. El platino es un elemento que encarece en gran medida esta tecnología, por lo que hay que optimizar su uso y volumen, siendo dramática su pérdida.

Se producen cambios en la estructura debido a estrés térmico y mecánico, llevando al deterioro de la MPL, GDL y membrana, con el consecuente cambio en las propiedades. Ataques químicos también afectan a la membrana.

Estas degradaciones llevan también a la disminución de la difusividad de GDL y MPL.

Se incrementan las pérdidas, llevando a un incremento de la resistencia de la membrana.

Se produce un descenso de la conductividad protónica en la capa catalítica, debido a un cambio en la distribución.

Se produce corrosión del carbono, reaccionando con el agua, producido cuando hay un frente de H_2/O_2 en el arranque y apagado de la pila. Esto lleva a que a los 1500 arranques se vea un adelgazamiento de la capa catalítica. Se reduce la difusividad de la capa catalítica debido a esta corrosión del carbono.

1.5. Aplicaciones

Una de las aplicaciones es su empleo para la propulsión, necesitando un motor de tracción eléctrico, convertidores DC, tanques de hidrógeno y una pila de combustible. Son idóneos cuando existe un alto uso y rango de utilización, por lo tanto dependerá del rango diario de kilómetros y su tamaño, siendo usado principalmente para taxis, camiones o minería.

Se podría usar para el almacenaje de energía si se reconvirtiera en un electrolizador, algo que no es recomendable pues se tendría una pérdida de eficiencia.

Se está empleando para la distribución de energía eléctrica, empezándose a aprovechar de plantas químicas que producían como producto secundario el hidrógeno y posteriormente aprovechándose para producir energía. También existen plantas de producción de energía eléctrica a partir de pilas de combustible.

Especialmente en Japón se están empleando pilas de combustible como grupos electrógenos, siendo una micro combinación de calor y potencia.

1.6. Curva de polarización

La curva de polarización tiene primero una zona de la cinética de la reacción de reducción del oxígeno, luego una zona afectada por las pérdidas Óhmicas de la membrana y posteriormente la de transporte de masa en la GDL.

2 METODOLOGÍA

En esta sección se explica cómo se han calculado las distintas propiedades de las GDLs seleccionadas, haciendo un resumen de las más relevantes y se explica como se han llevado a cabo las simulaciones.

Se han seleccionado GDLs comerciales AvCarb P-75, SIGRACET 34BC, SIGRACET 34BA y TORAY TGP-H-090, de las cuáles las dos primeras tienen MPL, simulándose con y sin ella, haciendo una modificación dónde GDL y MPL eran solo la GDL. De esta forma se puede determinar el efecto de la presencia de la MPL, acabando con un total de seis casos de estudio, sin contar con los dos casos correspondientes a la base proporcionada por ANSYS con y sin MPL como comprobación. Se han seleccionado los casos que tuvieran un grosor de 280±30μm, para que encajara con los datos de la simulación.

Las simulaciones se han llevado a cabo variando los voltajes entre 1.05 y 0.35V, descendiendo a intervalos de 0.1V, obteniendo un total de ocho puntos representativos para crear la curva de polarización. Apareció un problema a voltajes muy bajos en los casos sin MPL, donde un error en la simulación debido a la variable del contenido en agua impedía continuar.

La permeabilidad de la MPL es dos órdenes de magnitud inferior a la de la GDL y su porosidad es casi tres veces inferior, por lo que se observa un importante efecto de la MPL en los resultados obtenidos.

3 DESCRIPCIÓN DEL MODELO CFD PEMFC

En esta sección se muestran diversos planos, geometrías y mallados que componen el modelo CFD PEMFC. Se muestran también algunas de las ecuaciones esenciales para entender el modelo. A continuación, se mostrarán las principales imágenes y dimensiones para entender cómo está compuesto el modelo.

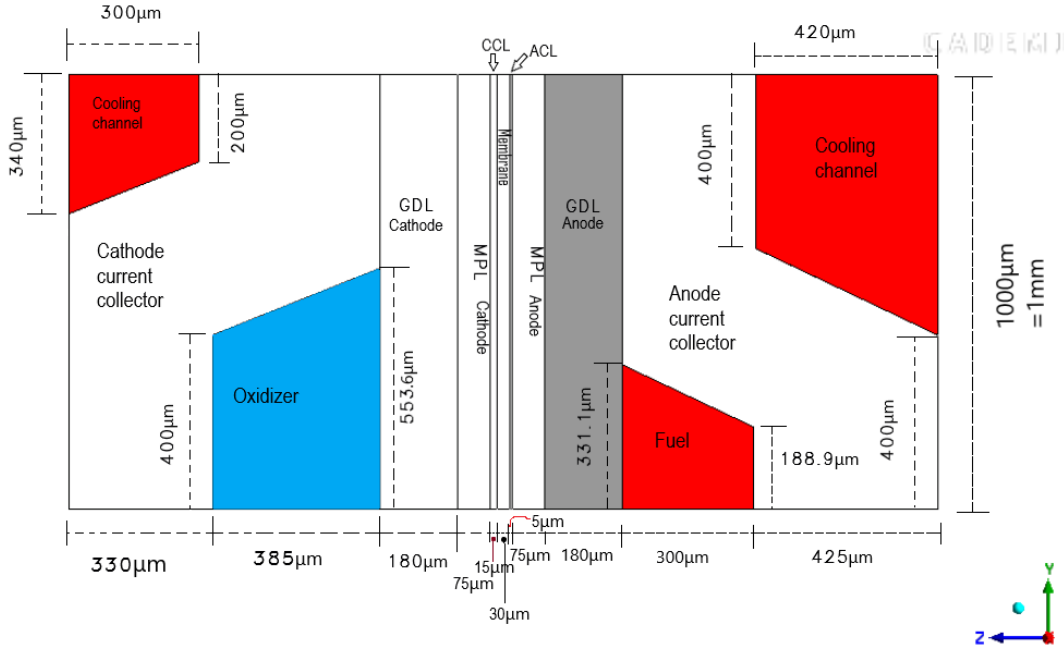

Ilustración 1 Plano ZY de las dimensiones del modelo PEMFC

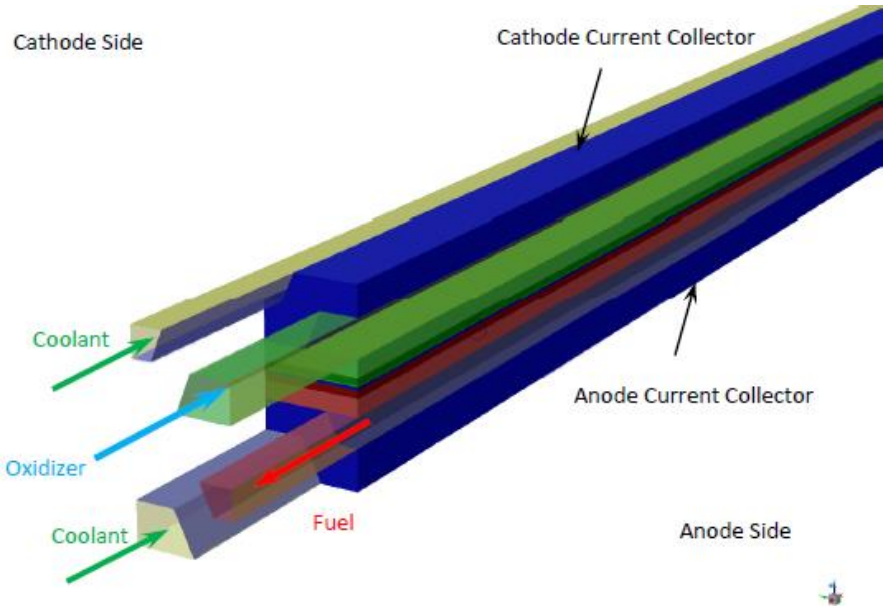

Ilustración 2 Entradas y salidas de fuel, oxidante y refrigerante en el modelo PEMFC

Se muestran las reacciones básicas que ocurren en el ánodo y cátodo. Se explican las ecuaciones que tienen en cuenta el transporte de electrones y protones en la membrana y materiales sólidos conductivos, para poder mostrar la ecuación del potencial en ánodo y cátodo. Esto ayuda a obtener una densidad de corriente de referencia, usada para la densidad de corriente dependiente de la temperatura. Se mencionan qué variables toma el programa como constantes y qué valores toman.

El transporte del agua es una parte fundamental, por lo que se explica en GDL, MPL y membrana, teniendo en cuenta los diferentes gradientes de presiones, presiones, permeabilidades relativas, velocidad de cambio de masa entre las distintas fases y la difusividad. También se aportan las ecuaciones para el transporte de agua en los canales, teniendo en cuenta principalmente las velocidades de las distintas fases.

4 RESULTADOS DE LAS SIMULACIONES

Aquí se muestran las curvas de polarización, potencia vs. densidad de corriente y eficiencia eléctrica vs. densidad de corriente. Estas gráficas son sacadas directamente de los datos brutos de las simulaciones o mediante breves cálculos, sin necesitar un post-procesado exhaustivo como posteriormente se hace. Se explican cuáles son los cálculos necesarios. Se hace un análisis de cada caso, pero por brevedad se mostrará un recopilatorio donde aparecen todas las curvas juntas y facilita la comparación de los distintos casos.

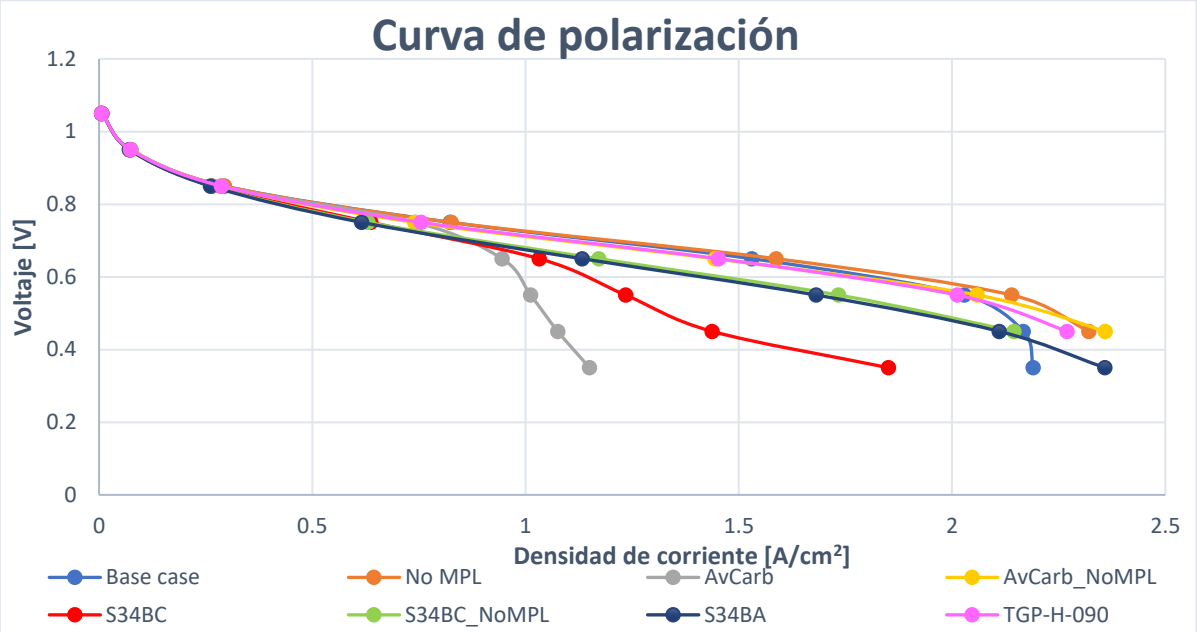

Ilustración 3 Compilación de las curvas de polarización de todos los casos

Las curvas se ven claramente separadas entre las que tienen una mayor conductividad eléctrica (AvCarb y TORAY) y las que tienen una menor (SIGRACET). Se observa que los casos con MPL tienen un comportamiento desventajoso en comparación con los que lo tienen. Las diferencias entre ambos casos de SIGRACET sin MPL, son principalmente en la conductividad eléctrica ya que, aunque sea la diferencia de tan solo un 12%, se observa un mejor comportamiento.

Las principales diferencias en los casos con alta conductividad eléctrica son la permeabilidad, porosidad y ángulo de contacto hidrofóbico. Una mayor permeabilidad y porosidad favorece la difusión, por lo que una porosidad y permeabilidad menor conlleva un peor comportamiento.

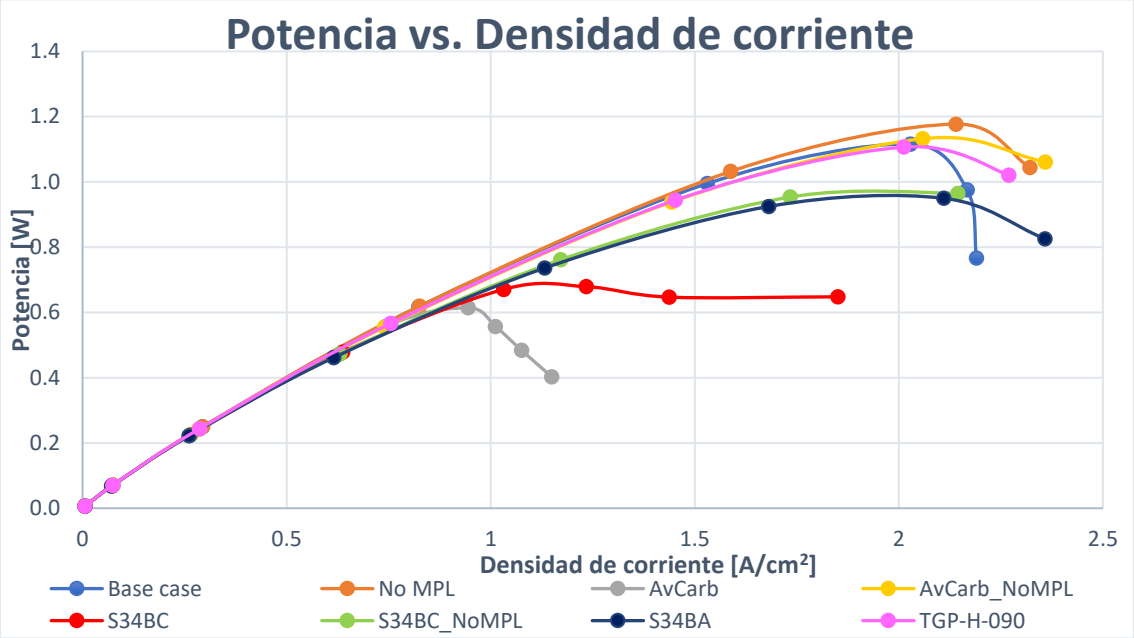

Ilustración 4 Compilación de las curvas potencia-densidad de corriente de todos los casos

Las curvas de la eficiencia eléctrica son dependientes de la corriente, por lo que se ha decidido obviarlas en el documento resumen.

Una mayor conductividad eléctrica implica una mayor potencia. Esto se cumple solo en los casos sin MPL, donde conductividades 4-5 mayores se traducen en una potencia un 15-20% mayor, por lo que no es una relación directa.

Los casos con MPL tienen una potencia mucho menor que sin él, siendo 2 veces y un 40% menor en los casos de AvCarb P-75 y SIGRACET 34BC respectivamente.

La permeabilidad y porosidad tienen un efecto en la potencia final. Una permeabilidad un 20.5% mayor y una porosidad un 8.2% mayor llevan a un incremento del 2.5% en la potencia.

En el caso de SIGRACET, una conductividad eléctrica un 11.1% mayor y una conductividad térmica un 12.4% menor llevan a una potencia un 1.6% mayor. Una mejor conductividad térmica debería llevar a un mejor comportamiento, pero como se encuentran efectos contrapuestos, se ve que el efecto de la conductividad eléctrica prevalece y es dominante sobre la térmica.

5 ANÁLISIS DE LOS RESULTADOS

En esta sección se analiza cómo se han calculado las distintas propiedades de las GDLs seleccionadas, haciendo un resumen de las más relevantes y se explica cómo se han llevado a cabo las simulaciones. Se mostrarán los casos más representativos.

Las gráficas de la media en el volumen están hechas para la saturación líquida en canales, MPL y GDL del ánodo y cátodo; fracción másica de oxígeno en MPL, GDL y capa catalítica del cátodo; temperatura máxima y media y contenido de agua en la membrana.

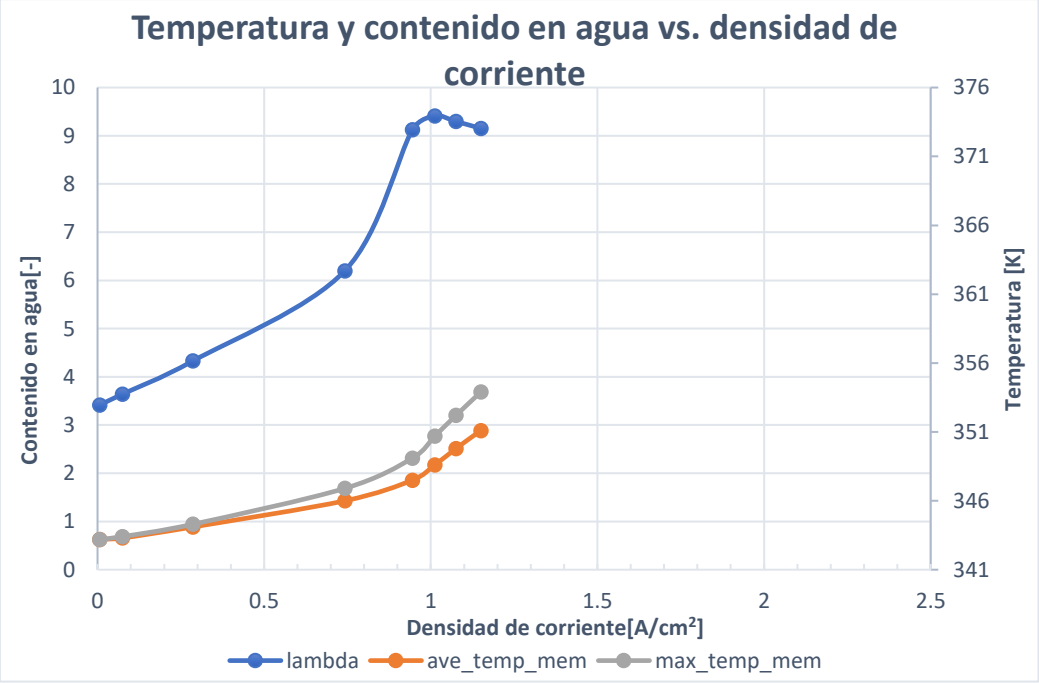

Ilustración 5 AvCarb P-75 Temperatura y contenido en agua vs. densidad de corriente en la membrana

Se han agrupado las variables que se medían en la media en la membrana. Se puede ver que en el caso de AvCarb P-75, las temperaturas no son demasiado altas, debido a su buena conductividad eléctrica que facilita el transporte de electrones y evitando su recalentamiento. Esto hace que el contenido en agua también sea mayor porque incrementa con la corriente, pero llega un punto que empieza a decrecer debido que se empieza a evaporar por las altas temperaturas alcanzadas. Si su conductividad

eléctrica fuera menor, se alcanzarían temperaturas más altas, evaporando el agua, evitando obtener valores mayores.

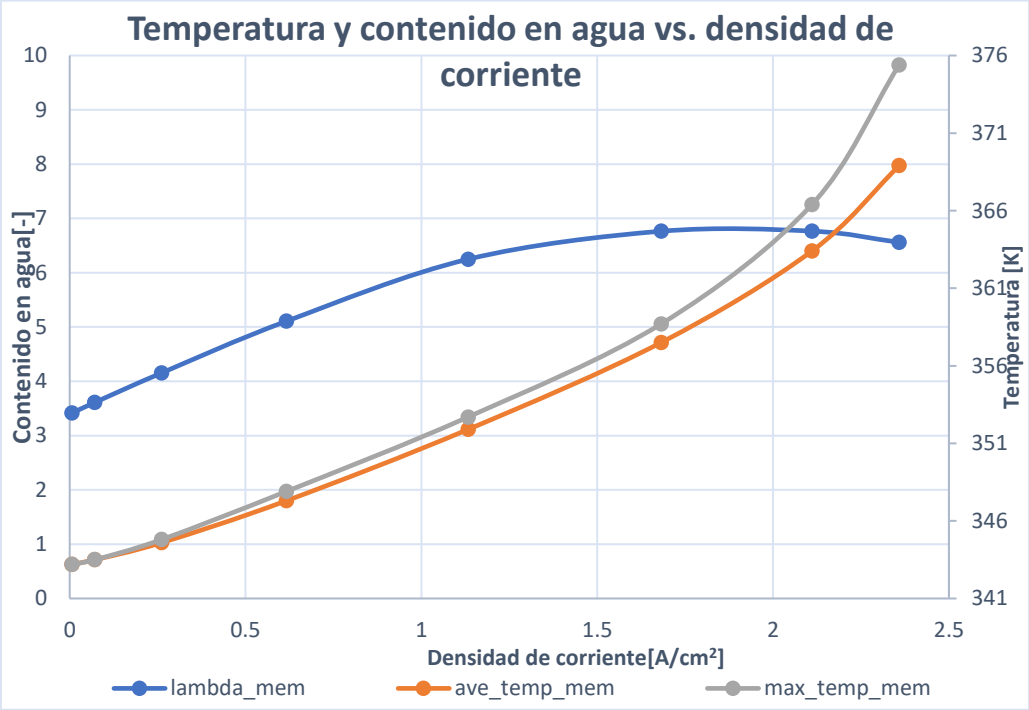

Ilustración 6 SIGRACET 34BA temperatura y contenido en agua vs. densidad de corriente en la membrana

Esto es lo que sucede en el caso de SIGRACET 34BA, que al ser el que menor conductividad eléctrica tenía aumenta su temperatura, deshidratando la membrana. Se alcanzan temperaturas superiores a los 90-100ºC puestos como seguridad a partir de los cuales se produce degradación. También existe un gradiente térmico mayor al límite de 5K. El caso de AvCarb P-75 se encontraba lejos de estos límites.

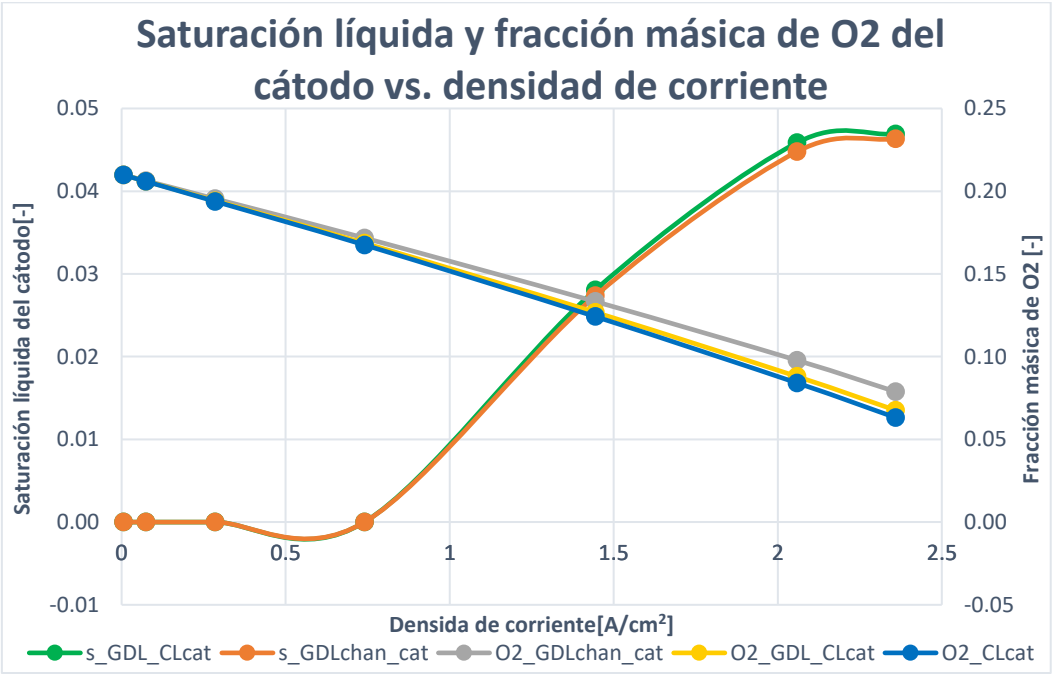

Ilustración 7 AvCarb P-75 sin MPL saturación líquida y fracción másica de O_2 vs. densidad de corriente del cátodo

La saturación de agua líquida y fracción másica de oxígeno se han agrupado, ya que ambas variables se estudian en el cátodo. La saturación de agua líquida aumenta con la corriente, pero llega un punto que este crecimiento llega a una meseta debido a que las altas temperaturas evaporan parte del agua generada. En la Ilustración 7 de AvCarb P-75 sin MPL se ve un comportamiento típico en el que la zona más próxima al catalizador, que es donde se produce el agua, tiene un mayor contenido de agua líquida. En la otra zona, la saturación es menor, ya que se va difundiendo a desde el catalizador a las otras capas cada vez habiendo menos. Sin embargo, en el caso de SIGRACET 34BC sin MPL en la Ilustración 8, se observa que sucede lo contrario. La zona más cercana a la capa catalítica es la que tiene una mayor saturación de agua líquida, pero a su vez es la que tiene una temperatura mayor al producir la reacción calor. Se ha visto que en SIGRACET las temperaturas son muy altas debido a la baja conductividad eléctrica, haciendo que el agua se evapore en la zona más próxima a la reacción y condensándose cuando alcanza otra capa más fría, invirtiendo ambas curvas.

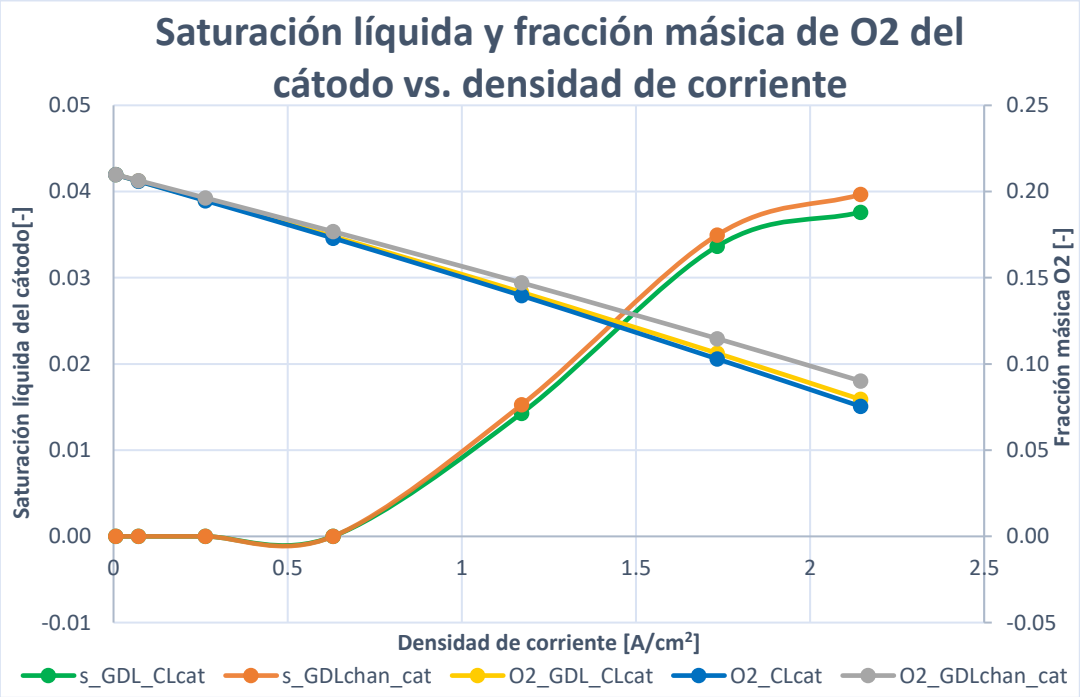

Ilustración 8 SIGRACET 34BC sin MPL saturación líquida y fracción másica de O_2 vs. densidad de corriente del cátodo

La fracción másica de oxígeno se va reduciendo con el aumento de la corriente generada, ya que cada vez más está siendo consumido en mayor cantidad por la reacción electroquímica. Dónde habrá menos será lo que esté más próximo a la reacción, difundiéndose y habiendo más en la zona más lejana.

La saturación líquida del ánodo se muestra junto con la de los canales. TORAY TGP-H-090 tiene una alta conductividad eléctrica frente a SIGRACET 34BC que tiene una cuatro veces menor. Esa diferencia se ve en que en el primer caso se ven mayor cantidad de líquido porque no se ha calentado la célula. La presencia de la MPL hidrata y enfría la célula, algo que se ve más afectado por la conductividad eléctrica por los menores valores de la Ilustración 10.

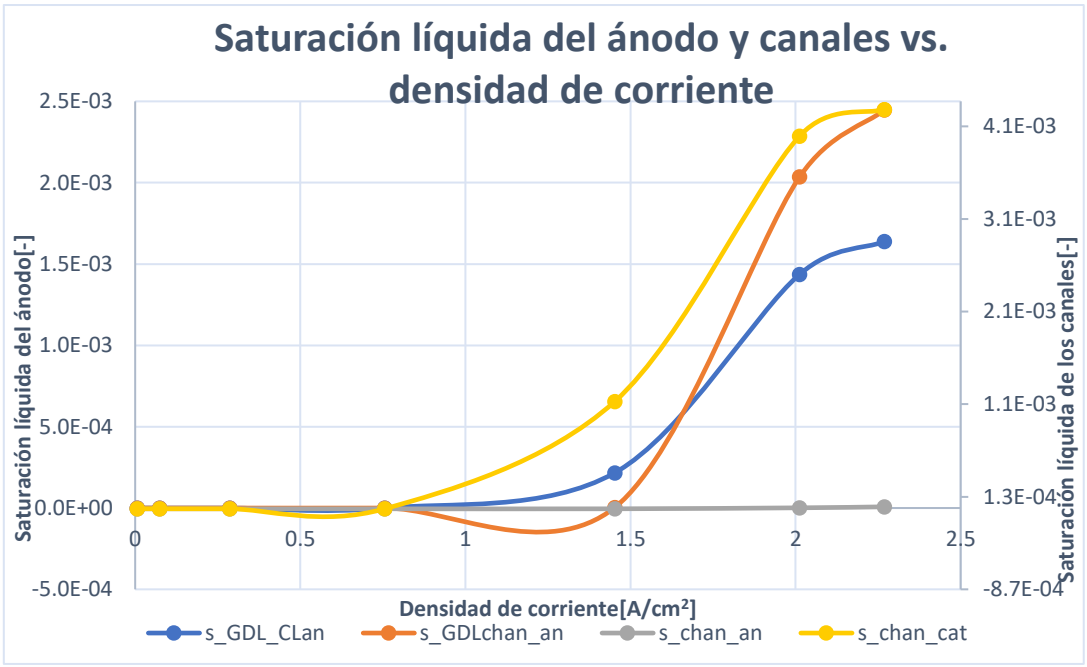

Ilustración 9 TORAY TGP-H-090 Saturación líquida vs. densidad de corriente del ánodo y canales

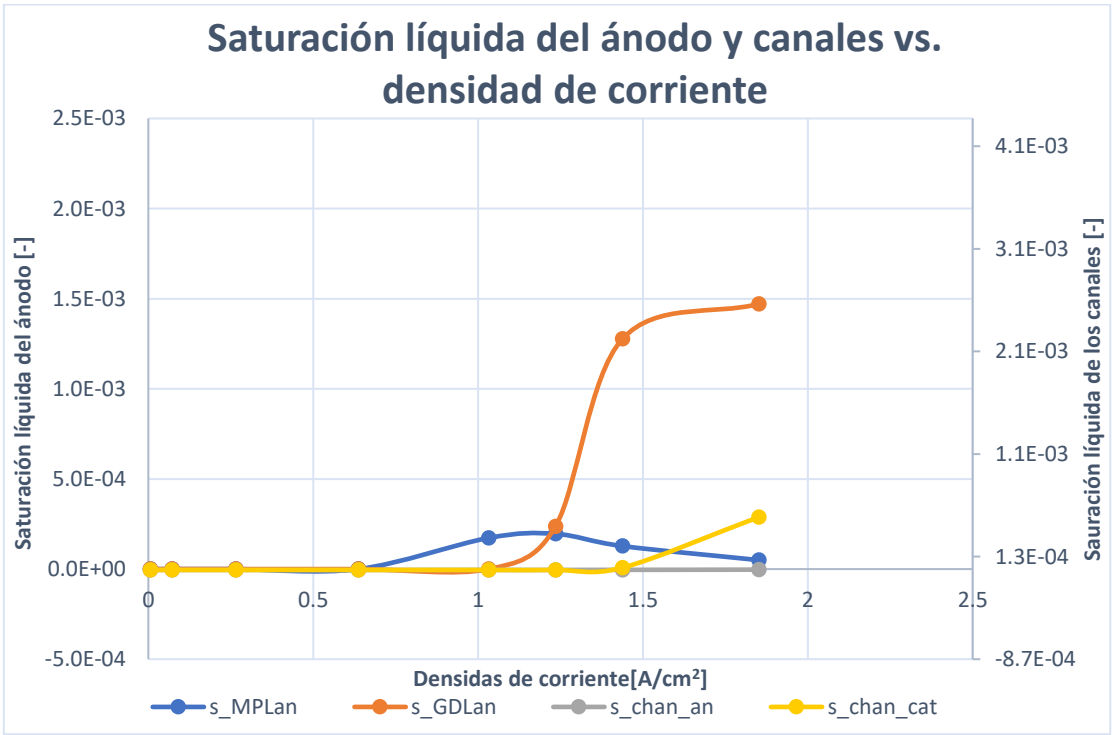

Ilustración 10 SIGRACET 34 BC saturación líquida vs. densidad de corriente del ánodo y canales

La siguiente serie de gráficas corresponde con la evolución a lo largo de la coordenada X o longitud, midiendo la evolución de una serie de variables en las líneas trazadas a partir de los siguientes puntos:

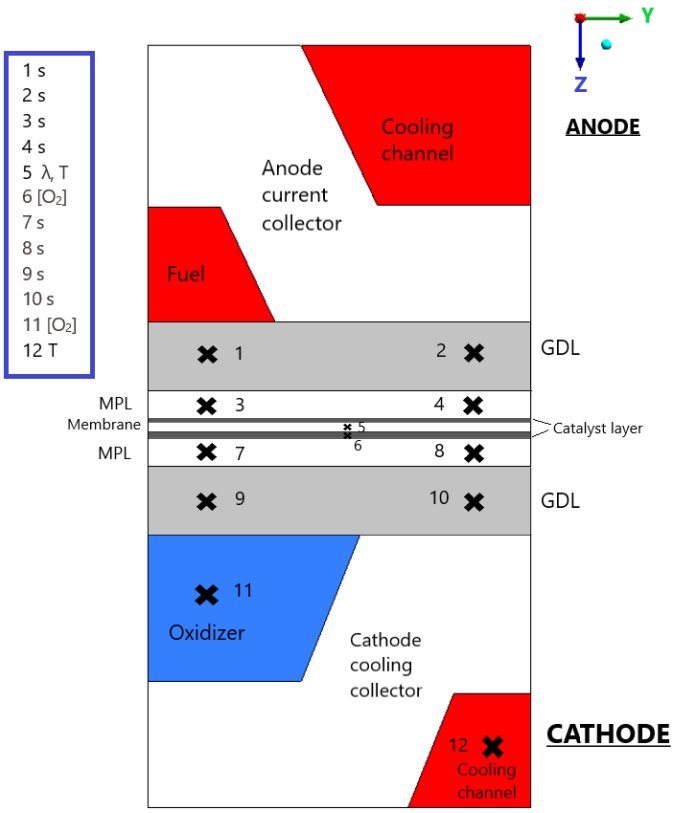

Ilustración 11 Plano ZY del modelo PEMFC y la posición de los puntos

Se observa sobre todo el efecto del bajo canal y bajo costilla en los casos sin MPL porque la MPL es una capa hidrófoba impidiendo que le llegue a la GDL más agua. En la zona bajo costilla hay mayor concentración de agua líquida debido a que es una zona más fría (debido a la refrigeración líquida) por lo que el agua condensa en mayor cantidad.

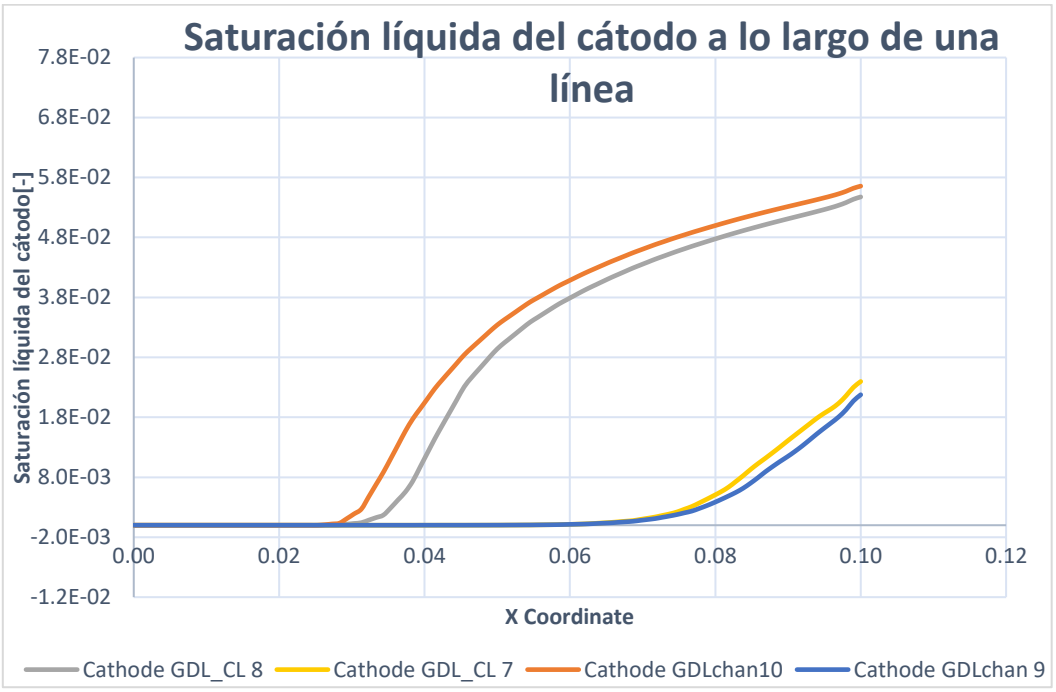

Ilustración 12 SIGRACET sin MPL 0.65V saturación líquida a lo largo de la línea longitudinal

Estas gráficas se han obtenido para medio y bajo voltaje (0.45V). A bajos voltajes hay una densidad de corriente mayor, por lo que más agua está siendo producida, siendo los valores mayores.

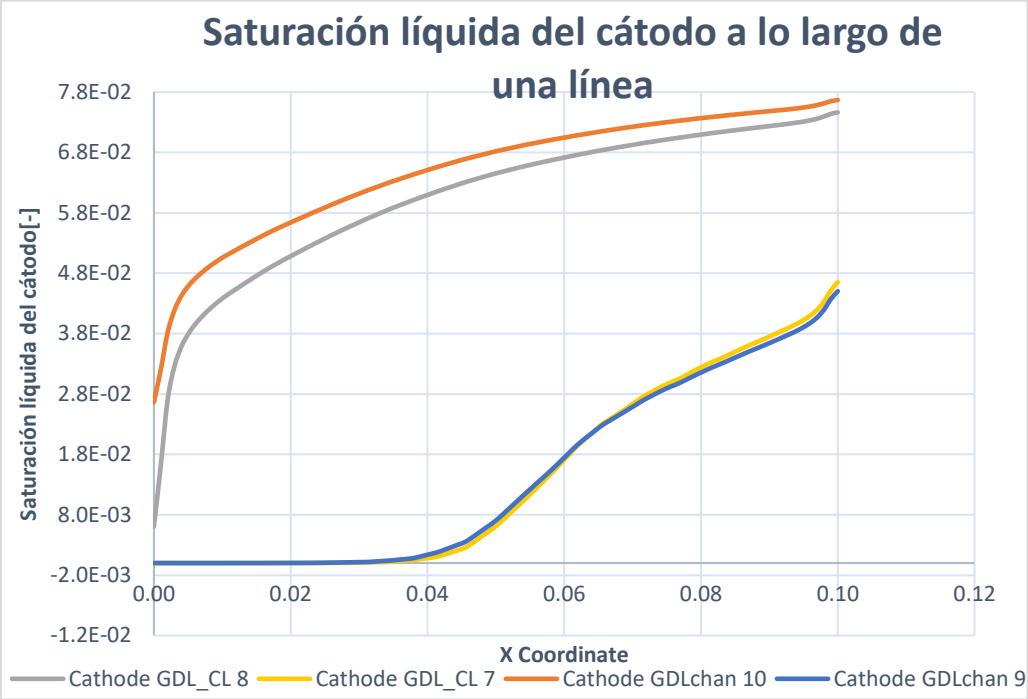

Ilustración 13 SIGRACET sin MPL 0.45V saturación líquida del cátodo a lo largo de la línea longitudinal

Se supone que debería haber más agua en la zona cercana a la capa catalítica porque es donde se produce el agua. Esto sucede en la zona bajo canal, pero en la zona bajo costilla es tal la cantidad que se condensa que ambas gráficas se ven invertidas. La cantidad de agua que hay a bajos voltajes mayor y empieza a crecer antes.

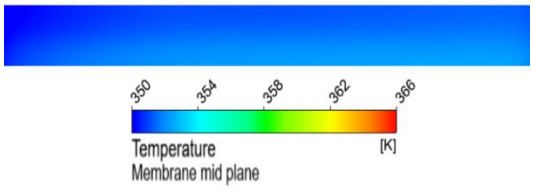

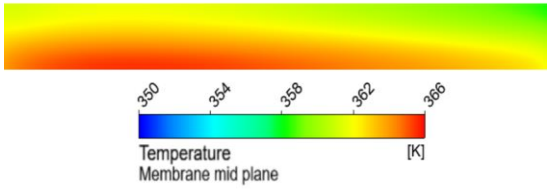

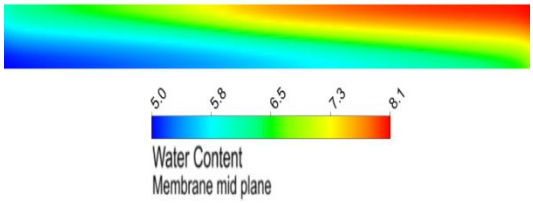

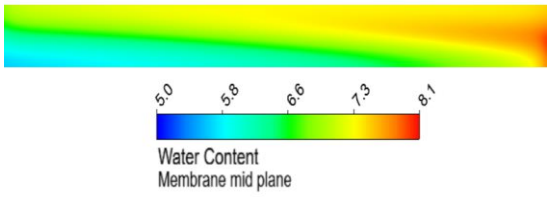

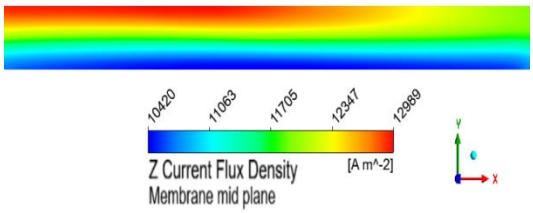

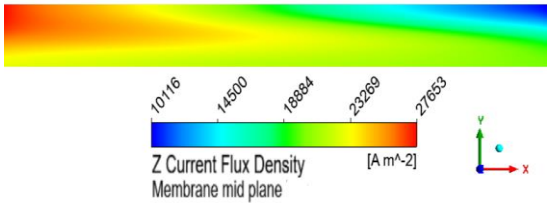

Ilustración 15 SIGRACET sin MPL medio voltaje: distribuciones de temperatura, contenido en agua y densidad de corriente perpendicular al plano medio de la membrana

Ilustración 14 SIGRACET sin MPL bajo voltaje: distribuciones de temperatura, contenido en agua y densidad de corriente perpendicular al plano medio de la

La última serie de figuras se muestra en Ilustración 15 y Ilustración 14. Son curvas de contorno del plano medio de la membrana, mostrando el desarrollo de la temperatura, el contenido en agua y el flujo de densidad de corriente transversal al plano. Se observa que la temperatura a bajos voltajes es mayor que a medios voltajes, ya que cuanto mayor sea la densidad de corriente, mayor es la temperatura porque la reacción está más activa porque se tiene más oxígeno para reaccionar, por lo tanto más agua y calor se está produciendo al ser una reacción exotérmica. Las figuras de agua y temperatura son opuestas, mostrando menos agua donde las temperaturas son mayores, debido a la evaporación. Incluso aunque se esté produciendo más agua a mayores voltajes, a partir de cierto de valor de densidad de corriente el contenido en agua comienza a descender debido a la evaporación ocasionada por las altas temperaturas alcanzadas.

6 CONCLUSIONES

El objetivo de este trabajo es estudiar cómo las diferentes propiedades de una serie de GDLs comerciales afecta el comportamiento de las pilas PEM. El software de fluido dinámica computacional (CFD en inglés) ANSYS-Fluent fue utilizado para las simulaciones. En primer lugar se simuló un caso base con las variables y propiedades por defecto de ANSYS para verificar el funcionamiento correcto y facilitar la comprensión de los fundamentos del software y modelado PEMFC. Se utilizaron posteriormente cuatro GDLs comerciales para el estudio, de las cuáles dos tenían MPL y las otras no. Los casos con MPL fueron también simulados sin MPL, modificando las propiedades de la capa para que correspondieran con las de la GDL, para analizar el efecto de la presencia de la MPL. Los casos estudiados son: AvCarb P-75, SIGRACET 34BC, SIGRACET 34BA y TORAY TGP-H-090, donde las dos primeras son las que tienen GDL.

Se obtuvieron las curvas de polarización, curvas potencia vs. densidad de corriente y eficiencia eléctrica vs. densidad de corriente, directamente de los resultados de las simulaciones. Posteriormente se llevó a cabo un postprocesado detallado de los resultados, generando tres tipos diferentes de curvas. Se desarrollaron una serie de curvas estudiando la media en el volumen de GDL, MPL, membrana, canales y capa catalítica en ánodo y cátodo, de variables clave como son la temperatura, saturación del líquido, contenido en agua y fracción de oxígeno. Se realizó para todos los casos comerciales, tomando valores para cada voltaje.

Una serie adicional de gráficos se creó incluyendo la saturación líquida, temperatura, contenido en agua y fracción de oxígeno a lo largo de la longitud de la pila PEM (coordenada X). Estas distribuciones se estudiaron en la membrana, capa catalítica, canal de oxidante y refrigerante del cátodo, MPL y GDL de ánodo y cátodo. En las dos últimas capas se estudiaron dos puntos diferentes, uno bajo costilla y otro bajo canal, para estudiar el efecto que tienen esas zonas. Se ha estudiado para los casos con MPL y sus modificaciones sin ella, a medio (0.65V) y bajo (0.35V) voltaje.

La última seria de curvas está compuesta por mapas de contorno en el plano medio de la membrana, estudiando la evolución de la temperatura, contenido en agua y flujo de corriente perpendicular al plano. Fueron también estudiados solo en los casos con MPL y sus modificaciones sin ésta para medio y bajo voltaje.

El estudio de los casos sin MPL se presentó en forma de ponencia oral en el I Meeting on Electrochemical Energy Conversion and Storage Devices (ECHEMCONSTORE I, 28-29 enero, 2021, Leganés, España). Aparece en el repositorio institucional de UCM3, con ISBN 978-84-16829-60-6.https://e-archivo.uc3m.es/handle/10016/31914

Las principales conclusiones obtenidas durante el estudio se resumen a continuación:

Una mayor conductividad eléctrica de la GDL reduce las pérdidas Óhmicas, incrementando la potencia hasta un 25%. El efecto positivo que pueda tener una mayor conductividad térmica es sobrepasado por el efecto negativo que tienen una menor conductividad eléctrica.

El enfriamiento produce una mayor saturación del líquido bajo costilla, llevando localmente a una menor difusión del oxígeno.

Una mayor permeabilidad aumenta la potencia y rendimiento de la célula, pero afecta negativamente a la cantidad de oxígeno.

La presencia de la MPL tiene aspectos positivos si se tiene en cuenta la temperatura e hidratación de las distintas capas, y específicamente la de la membrana, porque su ausencia dispara las temperaturas y reduce la cantidad de agua, llevando a problemas de degradación. Sin embargo, si los que se tiene en cuenta es meramente la potencia producida, su efecto es perjudicial, ya que se obtiene una potencia un 85% y 30% menor cuando está presente en los casos de AvCarb P-75 y SIGRACET 34BC que cuando está ausente.

En general se puede concluir que el modelado y simulación CFD es una herramienta con capacidades muy avanzadas para entender los distintos fenómenos que afectan al rendimiento y actuación de las pilas de combustible PEM, por lo tanto mejorando los diferentes componentes de la pila para optimizar las prestaciones y rendimiento final.